TORQUE RIPPLE MINIMIZATION IN PERMANENT MAGNET SYNCHRONOUS MOTOR DRIVE

Thesis submitted to the

Delhi Technological University

For the award of the

Doctor of Philosophy

by

SURYA KANT
(2K16/PhD/EE/08)

Under Supervision of

PROF. MINI SREEJETH
&
PROF. MADHUSUDAN SINGH

DEPARTMENT OF ELECTRICAL ENGINEERING
DELHI TECHNOLOGICAL UNIVERSITY
DELHI-110042, INDIA

JULY 2021

CERTIFICATE

This is to certify that the thesis entitled "**Torque Ripple Minimization in Permanent Magnet Synchronous Motor Drive**" which is being submitted by **Mr. Surya Kant** for the award of degree of **Doctor of Philosophy in Electrical Engineering**, Delhi Technological University, Delhi, is a record of student's own work carried out by him under our supervision and guidance. The matter embodied in this thesis has not been submitted in part or full to any other University or Institute for award of any degree or diploma.

Date: **28/07/2021**

(Prof. Mini Sreejeth)
Professor
Department of Electrical Engineering
Delhi Technological University
Delhi-110042, India

(Prof. Madhusudan Singh)
Professor
Department of Electrical Engineering
Delhi Technological University
Delhi-110042, India

ACKNOWLEDGEMENT

I would like to express my sense of gratitude and indebtedness to my supervisors **Prof. Mini Sreejeth** and **Prof. Madhusudan Singh**, Electrical Engineering Department, Delhi Technological University for their inspiring guidance, valuable suggestions, encouragement, untiring effort throughout the course of this work and help in providing necessary facilities and resources during the entire period of my research work timely. Working under them have been a wonderful experience, which has provided a deep insight to the world of research. Their wide knowledge and logical way of thinking have helped me to complete my research work. They always made themselves available for me despite of their busy schedules and I consider it as a great opportunity to carry out my research work under their guidance and to learn from their research expertise.

My sincere thanks and deep gratitude are to **Prof. Mukesh Pathak, Prof. Narendra Kumar**, and all SRC members for their valuable guidance and consistent support during my research work. I would like to thank **Dr. R.K. Jarial**, Associate Professor, NIT, Hamirpur for his belief in me, constant support and encouragement.

I would like to convey my unbounded love to my grandfather late **Mr. Ravi Prakash Shukla** and my grandmother **Mrs. Krishna Devi** for showering their blessings on me. A great deal of effort, endurance, encouragement and blessings of my parents **Mrs. Adesh Shukla** and **Mr. Durgesh Shukla**. I would like to express my greatest admiration to all my family members and relatives for their positive encouragement that they showered on me throughout this research work.

I extend my personal thanks to all my friends, seniors and juniors **Hemant Saxena, Astitva Kumar, Ajishek Raj, Pallavi Verma, Dr. Ambrish Devanshu, Dr. Prakash Chittora, Saket Gupta, Akash Seth, Amarendra Pandey, Kamakshi Rautela, Nikhil Kushwaha, Ritu Kandari**

and Dr. Hasmat Malik for their valuable support and reminding me to complete my work at the earliest. I would also like to thanks to faculties and staff of Delhi Technological University faculties and authorities for providing me necessary facilities for the smooth completion of my work.

Above all, I would like to thank The Almighty God, who has blessed me strength and support throughout my life and always provides me with a path to acquire knowledge and learning.

SURYA KANT

(2K16/PhD/EE/08)

ABSTRACT

Use of permanent magnets made of rare earth materials such as samarium cobalt and neodymium-boron-iron in Permanent Magnet Synchronous Motor (PMSM) drives has resulted in high flux density and improved performance of the drive. Field Oriented Control (FOC) has become one of the most popular speed and torque control techniques for AC motors. In PMSM drive detection/computation of rotor position is crucial for ensuring high performance during FOC. Rotor position is often sensed by incremental encoders or resolvers. The use of positon sensors in motor speed control increases the cost, size, weight and wiring complexity, and reduces the mechanical robustness and reliability of the PMSM drive systems. Sensor-less speed control techniques overcome these drawbacks related to estimation of speed and rotor position. The PMSMs are generally employed in industrial servo applications because of their fast dynamic performance. However, PMSMs suffers from ripples in the torque produced. Torque ripples in PMSM are produced because of cogging, current measurement error, switching of inverter and harmonics in magnetic flux. Torque ripples also leads to fluctuations in speed thus limiting the use of PMSM in several servo applications. Torque ripples could be minimized in applications that demand accurate speed/position tracking.

The present work aims to explore use of different modern control techniques to minimize torque ripples in the operation of PMSM drives in comparison to previously reported control techniques. The objectives of the research include –

a) modelling, design and development of laboratory prototype of PMSM drive,

b) design and implementation of improved artificial neuro fuzzy inference system (ANFIS) based model reference adaptive control (MRAC) observer for sensor-less control of PMSM,

c) minimization of stator current ripples and torque ripples in PMSM drive using advanced predictive current controller (APCC) based on Dead Beat (DB) control theory

d) minimization of torque ripples using intelligent hybrid controller (IHC) and

e) torque ripple minimization by model predictive control of PMSM using proportional-plus-integral resonant (PI-RES) controller.

The strategies to reduce torque ripples, that have been reported in the literature, may be classified into a) approaches based on the design improvement of the motor, b) methods based on control techniques or c) a combination of these two. The most critical aspect in high performance drive is the choice of the control algorithm that minimizes the torque ripples effectively for a given application.

In this research work, a laboratory hardware prototype is designed and developed for real time analysis of PMSM drive based on sensor-less field-oriented control. An experimental setup is developed for implementation of FOC on PMSM using dSPACE DS1104 controller and performance of the drive is analysed using different control techniques.

An improved ANFIS based MRAC observer is designed and implemented for FOC of PMSM with space vector PWM (SVPWM). In the proposed method adaptive model and adaptive mechanism are replaced by an improved ANFIS controller, which neutralize the effect of parametric variation and results in improved performance of the drive. The required rotor position and speed are estimated using the proposed MRAC observer. Simulation studies using MATLAB/Simulink and comparative analysis of the conventional MRAC based observer with improved ANFIS based MRAC observer show that better dynamic performance of the PMSM drive is achieved using the improved ANFIS based MRAC.

An advanced predictive controller (APCC) based on deadbeat (DB) control theory is also developed and analysed for reduction of torque ripples in PMSM. The performance of the proposed APCC based on DB control theory are compared with hysteresis based direct current controller (DCC) and duty cycle-based model predictive controller (Duty-MPCC) under different operating condition through simulation studies using MATLAB/Simulink. It is observed that the implementation of proposed APCC results in better dynamic performance with less ripples in torque and stator currents, and lesser THD in stator current as compared to DCC and Duty-MPCC.

An intelligent hybrid controller (IHC) has also been developed and implemented for FOC of PMSM to minimize torque ripples for constant torque operation. The proposed IHC is designed by combining a fuzzy logic controller (FLC) with PI controller with a novel switching capability. The intelligent switching decision of the developed IHC is based on overshoots, undershoots and oscillations observed in the system. Simulation studies for the FOC of PMSM using the proposed IHC indicates better dynamic performance with lesser torque ripples and lower THD in stator current in comparison with conventional PI controller.

In addition, a proportional-plus-integral resonant (PI-RES) controller is designed and implemented for FOC of PMSM with model predictive controller (MPC) to minimize torque ripples for constant torque operation. The MPC is designed to provide the optimal voltage vector by minimizing the objective function calculated from stator current prediction for k^{th} instant. The PI-RES controller is developed by combining a resonant controller with PI controller. Due to the compensating torque current produced by the resonant controller and reference current from the PI controller, ripples in the speed response are minimized. A PI-RES controller generates the reference pulsating torque current, which counteracts the ripples

in load torque. The FOC of PMSM with MPC using PI-RES is simulated in MATAB/Simulink and the performance of the drive is compared with MPC using PI controller. The proposed FOC of PMSM with MPC using PI-RES demonstrate better dynamic performance, lower torque ripples and lower THD in stator current in comparison with conventional PI controller based MPC.

Table of Contents

List of Abbreviations and Symbols

The list of abbreviations and symbols used in this dissertation are given below. Some other abbreviations / symbols, which are not mentioned here are described locally.

AF	:	Axial-Flux
AFFSPMM	:	Axial-Field Flux Switching PM Machine
AICF	:	Advanced Inverse Cosine Function
AILC	:	Adaptive Iterative Learning Control
ANFIS	:	Artificial Neuro Fuzzy Inference System
ANN	:	Artificial Neural Network
APCC	:	Advanced Predictive Current Controller
APCC	:	Advanced Predictive Current Controller
APID-SMC	:	Adaptive PID based Sliding Mode Control
ARO	:	Angle-Based Repetitive Observer
BLDC	:	Brushless DC
BVVs	:	Best Voltage Vectors
CCS-MPCs	:	Continuous Control Set-MPCs
CM	:	Common Mode
CSI	:	Current Source Inverter
DB	:	Dead Beat

DCC	:	Direct Current Controller
DFOC	:	Direct FOC
DPC	:	Direct Predictive Control
DTC	:	Direct Torque Control
Duty-MPCC	:	Duty Cycle-based Model Predictive Current Controller
ECS	:	Extended Control Set
EMF	:	Electromotive Force
EMI	:	Electromagnetic Interference
FCS-MPCs	:	Finite Control Set-MPCs
FE	:	Finite-Element
FEA	:	Finite Element Analysis
FLC	:	Fuzzy Logic Controller
FOC	:	Field Oriented Control
FOVR	:	Fractional Order Vector Resonant
FSCW	:	Fractional-Slot, Concentrated Wound
HCC	:	Hysteresis Current Control
HF	:	High Frequency
ICF	:	Inverse Cosine Function
IFOC	:	Indirect FOC

IHC	:	Intelligent Hybrid Controller
ILC	:	Iterative Learning Control
IM	:	Induction Motor
INFORM	:	Indirect Flux detection by on-line Reactance Measurement
IPMSMs	:	Interior PMSMs
LM	:	Loss Minimization
MF	:	Membership Function
mmf	:	Magneto-Motive Force
MOES	:	Multi-Objective Extremum Seeking
MPC	:	Model Predictive Controller
MPCs	:	Model Predictive Controllers
MPTC	:	Model Predictive Torque Control
MRAC	:	Model Reference Adaptive Control
MRAS	:	Model Reference Adaptive System
MRF	:	Multiple Reference Frame
ms	:	Millisecond
MTPA	:	Maximum Torque Per Ampere
NeFeB	:	Neodymium-Iron-Boron
op-amp	:	Operational Amplifier

PALC	:	Periodic Adaptive Learning Control
PI-RES	:	Proportional-plus-Integral Resonant
PM	:	Permanent-Magnet
PMSM	:	Permanent Magnet Synchronous Motor
PR	:	Proportional Resonant
PSO	:	Particle Swarm Optimization
PTC	:	Predictive Torque Control
PWM	:	Pulse Width Modulation
qZS	:	Quasi-Z-Source
RCP	:	Rapid Control Prototyping
Robust-IMC	:	Robust Internal Model Control
RTI	:	Real-Time Interface
RTW	:	Real-Time Workshop
SMC	:	Sliding Mode Control
Sm-Co	:	Samarium-Cobalt
SMO	:	Sliding Mode Observer
SNR	:	Signal-to-Noise Ratio
SPMSMs	:	Surface Mounted PMSMs
SPWM	:	Sinusoidal PWM

SVM	:	Space Vector Modulation
SVPWM	:	Space Vector PWM
THD	:	Total Harmonic Distortion
TRF	:	Torque Ripple Factor
TS	:	Takagi-Sugeno
TTL	:	Transistor-Transistor Logic
UMP	:	Unbalance Magnetic Pull
VFDs	:	Variable Frequency Drives
VSI	:	Voltage Source Inverter
ZVV	:	Zero-Voltage Vector
ns	:	linguistic variable of IHC - negative small
nm	:	linguistic variable of IHC - negative medium
nmh	:	linguistic variable of IHC - negative medium high
nh	:	linguistic variable of IHC - negative high
ps	:	linguistic variable of IHC - positive small
pm	:	linguistic variable of IHC - positive medium
pmh	:	linguistic variable of IHC - positive medium high
ph	:	linguistic variable of IHC - positive high
ze	:	linguistic variable of IHC - zero

Symbols

V_s^*	:	Reference Voltage
f^*	:	Reference Frequency
v_{sa}, v_{sb}, v_{sc}	:	Stator winding voltages
i_{sa}, i_{sb}, i_{sc}	:	Stator winding currents
$\phi_{sa}, \phi_{sb}, \phi_{sc}$	:	Stator winding flux linkages
L_{0s}	:	stator winding fundamental magnetizing inductance
L_{ls}	:	stator winding leakage inductance
L_{ms}	:	stator winding inductance which depends on the rotor position.
$L_{ab}, L_{ba}, L_{ac}, L_{ca}, L_{bc}, L_{cb}$	:	Mutual inductances
ϕ_m	:	Permanent Magnet Flux Linkage
θ_r	:	Rotor Position
v_{sd}, v_{sq}	:	Stator voltage components in dq axis
i_{sd}, i_{sq}	:	Stator current components in dq axis
ϕ_{sd}, ϕ_{sq}	:	Flux linkage components in dq axis
L_d, L_q	:	dq axis inductances
R_s	:	Stator resistance

ρ	:	Derivative operator
ω_r	:	Electrical Speed
T_e	:	Electromagnetic Torque
ω_m	:	Mechanical Speed
P	:	Number of poles
T_l	:	Load Torque
B	:	Friction coefficient
J	:	Inertia constant
$v_{s\alpha}, v_{s\beta}$	:	Stator voltages in αβ axis
$i_{s\alpha}, i_{s\beta}$	:	Stator currents in αβ axis
I_s	:	Stator current
α	:	Torque angle
$i_{sa}^*, i_{sb}^*, i_{sc}^*$	:	Stator reference currents
$v_{sa}^*, v_{sb}^*, v_{sc}^*$	:	Stator reference voltages
ω_r^*	:	Reference speed
T_e^*	:	Reference Torque
e_α, e_β	:	Back emf in αβ axis
$\phi_{s\alpha}, \phi_{s\beta}$	:	Stator Flux Linkages in αβ axis

$\phi_{r\alpha}, \phi_{r\beta}$	:	Rotor Flux Linkages in αβ axis
$\widehat{\omega}_r$	:	Estimated speed
$\hat{\imath}_{sd}, \hat{\imath}_{sq}$	:	Estimated currents in dq axis
$\hat{v}_{sd}, \hat{v}_{sq}$	:	Estimated voltages in dq axis
K_p	:	Proportional gain
K_i	:	Integral gain
θ_{est}	:	Estimated rotor position
$e(k)$	:	Speed error of FLC
$\Delta e(k)$	:	Change in speed error of FLC
$\Delta T_e^*(k)$	:	reference torque inferred by FLC at the k^{th} sampling time
μ	:	FLC gain factor of IHC
$\overrightarrow{v_s^*}$	:	An arbitrary non zero voltage vector
i_{sd}^*, i_{sq}^*	:	Reference stator currents in dq axis
v_{sd}^*, v_{sq}^*	:	Reference stator voltage in dq axis
V_{dc}	:	DC link voltage
T_{est}	:	Estimated torque of the motor
K_{ir}	:	Resonance coefficient

List of Figures

Chapter 1

Chapter 2

Chapter 3

Chapter 4

Chapter 5

Chapter 6

Chapter 7

List of Tables

Chapter 3

Chapter 4

Chapter 5

Chapter 6

CHAPTER 1

INTRODUCTION

1.1. GENERAL

In today's world, variable torque and speed drives are required for industrial applications such as robotics, computer numeric control systems, electrical vehicles, etc. Permanent magnet synchronous machines (PMSMs) are widely used in variable speed industrial drives for high performance applications. Use of improved rare earth magnetic materials has increased the usage of PMSM in a wide variety of applications. While the analysis and design techniques of traditional AC electrical machines are becoming mature, extensive research is required to develop a systematic methodology for the analysis, design and control of PMSMs. The recent developments in power electronics and microelectronics have expanded the motor control techniques of PMSM drives.

1.2. ELECTRIC AC DRIVES

Drive refers to the mechanism that is used to control motion, and electric drives refers to the system that uses an electric motor to control motion [1],[2]. Electric drives are classified [3] into: DC and AC drives. Due to their inherent limitations in terms of commutators and brushes, DC drives are not widely used nowadays and are being replaced by AC drives. Based on control strategy, AC drives can be classified into either scalar or vector-controlled AC drives. Scalar control is simple and easy-to-implement. In scalar control the magnitude of the control variable is adjusted to change the motor speed. It gives poor dynamic response but performs well under the steady state operation. The air gap flux is always retained at the desired value

in this scheme. In comparison to scalar control, vector control provides more precise control of AC motors. It allows the torque producing component of the current to be decoupled from the flux producing component of the current using co-ordinate transformation, resulting in a fast transient response of the drive. To obtain the desired mechanical output, electric drive supplies the motor with the necessary voltage, current, and frequency from the main supply. The basic structure of modern AC drive system in shown in Fig. 1.1.

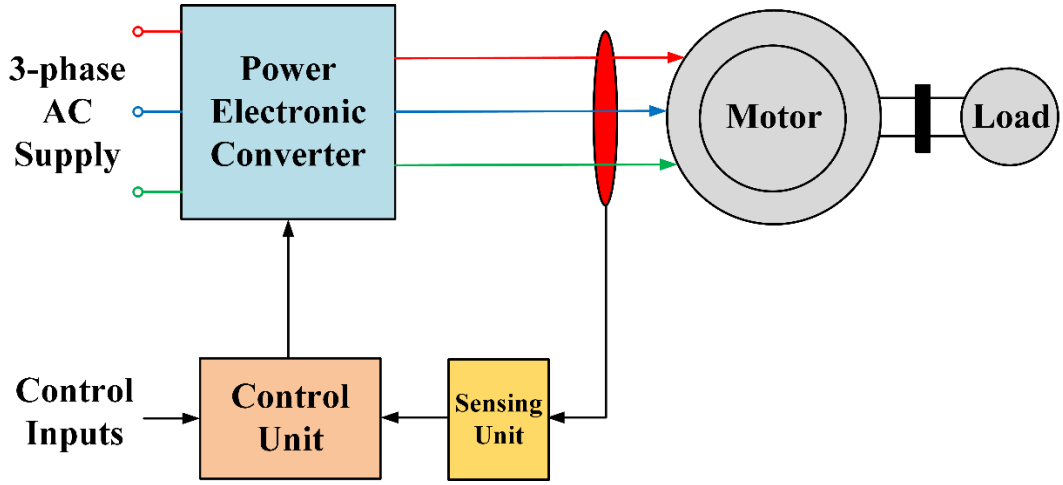

Fig.1.1. Basic Structure of Modern AC Drives

The basic components of a modern AC electric drive system are listed below.

i. Power Supply

The power supply deliver power required for the power converter. It is 3-phase/1-phase AC supply. Batteries, photovoltaic, and fuel cells of sufficient capacity.

ii. Converter

In drive system, converter is used to provide the required power in a controlled manner to the electric motor. Different types of control algorithms to control the power being fed to the motor through power electronic converters have been reported in the literature. There are several kinds of power converters, such as current source inverter (CSI), cyclo-converter, voltage

source inverter (VSI), multilevel bridge inverter, etc., and each of these may be used depending on the type of applications.

iii. Motor

The electric motor transforms electrical energy into mechanical energy in the form of motion, which can then be transferred to the load attached to the motor's shaft. Depending on the application, the motor used can be DC motor, synchronous motor, Induction motor (IM), etc.

iv. Sensing Unit

Sensing unit is generally required for closed loop operation of the drives. Different types of sensors are used for sensing electrical and mechanical quantities such as voltage, current, rotor position, torque, temperature and speed. The sensed signal provides feedback to the control unit and are used to equate actual performance to the desired performance, thereby ensuring proper operation of the drive. Encoders and resolvers are generally used to measure the rotor position and motor speed and hall sensors are generally used to sense the voltage and current.

v. Control Unit

Generally, microcontroller/DSP based controllers are used in the control unit to implement control techniques. This processes the control algorithms and provides the necessary control signals to the converter using the feedback signal and reference input.

1.3. CLASSIFICATIONS OF ELECTRIC AC DRIVES

Variable frequency drives (VFDs) are becoming increasingly common in high-performance applications, which provides a controlled voltage and frequency to the motor to obtain the desired motor performance [4]-[5]. Classification of VFDs is shown in Fig.1.2.

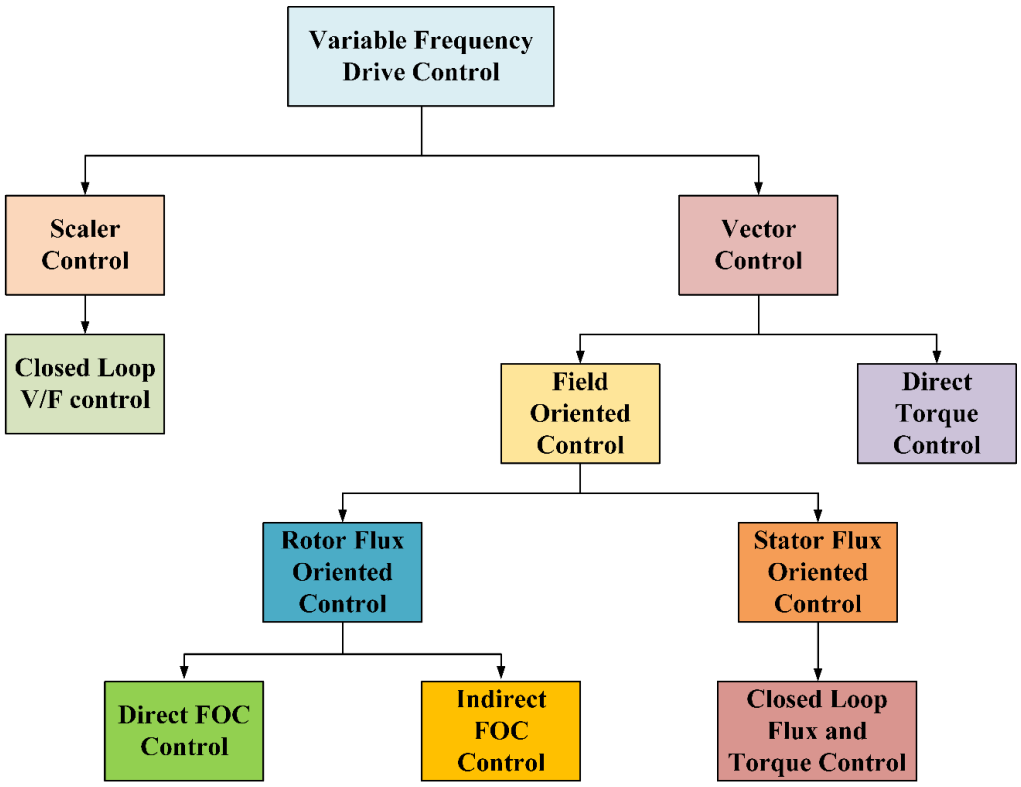

Fig.1.2. Types of Variable Frequency Drive Control

In comparison to a traditional DC electric drive system for variable speed applications, an AC drive system is smaller, cheap, more compact, more reliable, needs less maintenance, and can be used for high-speed operation. Previously, variable speed applications were controlled by DC drives, while constant speed applications were controlled by AC drives but nowadays AC drive system becomes more popular for variable speed applications due to development of power electronics converter circuits for AC drives. However, due to the inherent coupling between the torque and flux producing current components of motor current, AC motor application were limited to constant speed applications. With the advent of field-oriented control scheme and reduction in the cost of semiconductor components, modern AC electric drive systems have become more attractive than DC drives for high-performance applications.

Use of rare earth magnetic materials in motors has increased the popularity of permanent magnet machines in AC drives.

1.4. PERMANENT MAGNET MACHINES

In traditional doubly excited electric machines, the excitation sources are electric windings in the armature and field, which are coupled to external sources of electric energy. However, in Permanent-magnet (PM) machines, PMs produce the necessary magnetic field, thus removing the need for field windings and an external electrical source for their excitation.

In comparison to traditional doubly excited electric machines, PM machines do not have the copper loss associated with field windings, improving the machine's performance. Furthermore, as PMs are used to produce the field, these machines are lighter in weight and smaller in size. However, permanent magnets produce a continuous field flux in PM electric machines, which cannot be regulated as effectively as the field current of traditional doubly excited electric machines.

The use of permanent magnets in the rotor circuit has the advantage of simplifying system design and practically eliminating rotor circuit losses because the rotor is (ideally) free of currents. Since it reduces losses, it is very attractive for the designers of electrical machines for EV applications because it gives higher efficiency and high speed capabilities.

1.4.1. Classifications of PM Machines

PM machines can be classified as shown in Fig.1.3. PM machine are categorized into two types according to the excitation, namely, PMDC and PMAC machines. PMDC machines have a configuration similar to DC commutator machines except for having PMs in place of field windings [6]-[7].

PMAC machines are synchronous machine in which permanent magnet in the rotor is used to produce the magnetic field. The structure of these machines is very simple due to absence of commutator and brushes. PMAC machines are further categorized into trapezoidal type and sinusoidal type on the basis of stator windings. They are also called Brushless DC (BLDC) motor and PMSMs respectively. BLDC motors have trapezoidal emf and wound stator windings and should be fed with square currents to create a smooth torque. PMSMs have sinusoidal emf distributed stator windings and a permanent magnet rotor configuration.

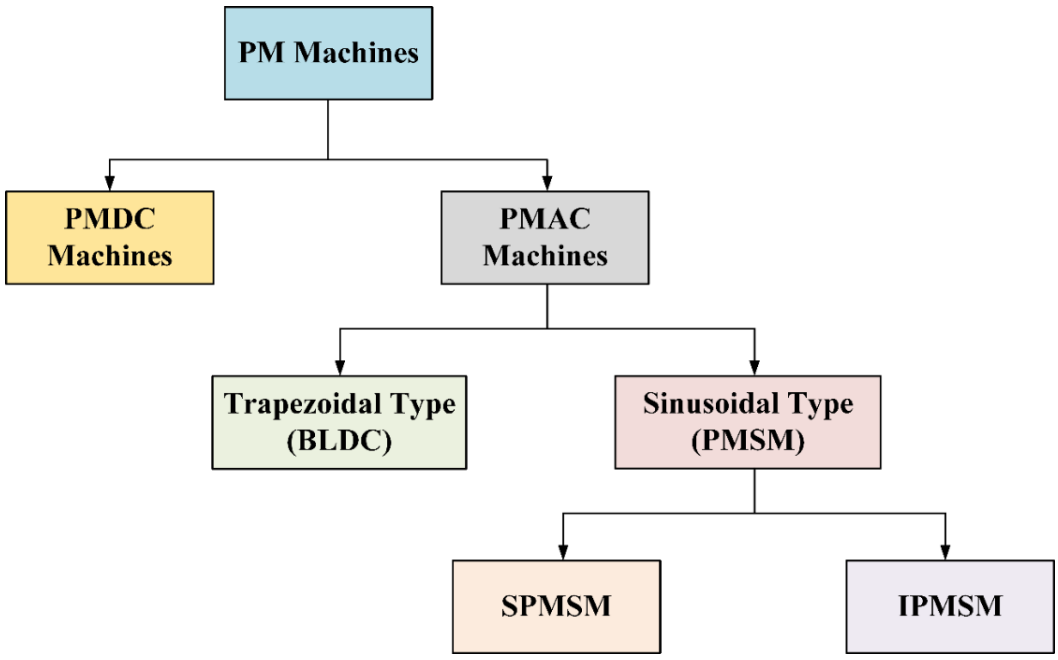

Fig.1.3. Types of PM Machines

The BLDC machines were the first to be developed due to their ease of control but were not found suitable for high performance and high speed applications due to the presence of torque ripples. PMSMs were developed in the late 1970s and 1980s and are proving their suitability in drive applications over IM and getting attention of the researchers and manufacturers. PMSMs have different rotor configurations depending on how the magnets are mounted on the

rotor. There are two common rotor configurations which are shown in Fig.1.4. i.e surface mounted magnet type and interior magnet type. In Surface mounted PMSMs (SPMSMs) the magnets are attached on the surface of the rotor core, while in interior PMSMs (IPMSMs) the magnets are located inside the rotor core.

The PMSM is usually operated by a VSI and is used for high-performance applications [8]. Samarium-Cobalt (Sm-Co) or Neodymium-Iron-Boron (NeFeB) are the most widely used materials for the PM. The magnets made of NeFeB have a high flux density and a strong coercive power. Unfortunately, these motors are still very costly compared to IMs, but the cost has decreased over the last decade[9].

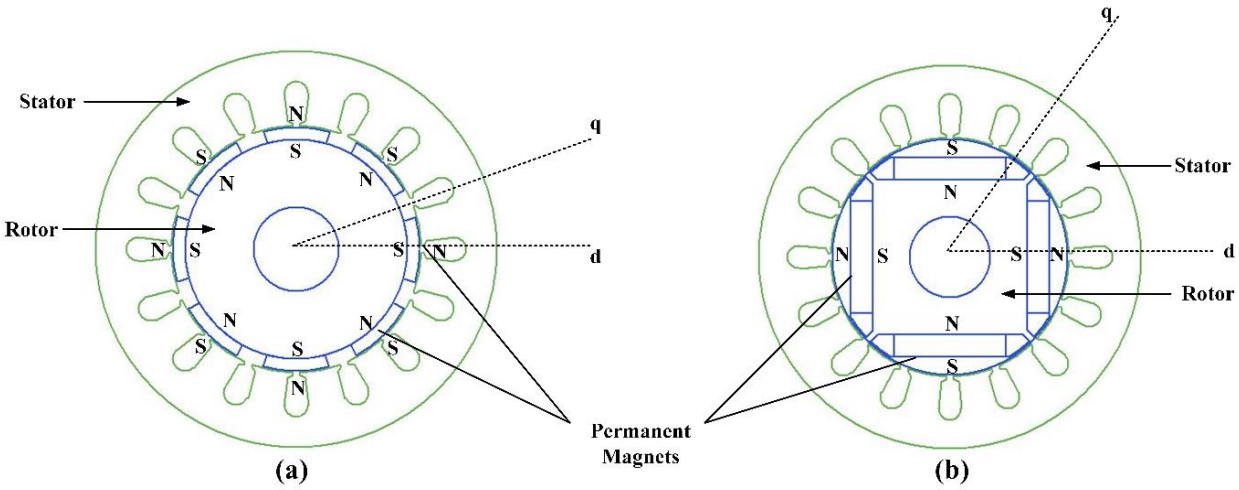

Fig.1.4. Rotor configuration of PMSMs: (a)Surface mounted magnet type (b) Interior magnet type

1.4.2. Torque Ripples in PMSM

PMSMs provide a number of benefits, including high performance, low inertia, and a high torque-to-volume ratio; however, the ripple in the induced torque is the main disadvantage of the PMSMs. Torque ripple sensitivity is dependent on the application. In applications like

water pumping, the effect of torque ripple is insignificant, however, the value of torque ripples is critical in other applications such as electric vehicle. Torque ripple may be a source of friction or noise in a hybrid vehicle application, and in the worst-case scenario, it can impact the vehicle's active parts' fatigue.

One of the major sources of torque ripple in PMSM is cogging torque, which is produced by the angular variations in the stator magnetic reluctance and the rotor magnetic flux. There are many methods for minimizing cogging torque, the majority of which depend on improvements to the machine's configuration [10]. Skewing is a popular method in design of machine that can be used on both the rotor and stator. Skewing can effectively minimize cogging torque, but the manufacturing process is difficult, which raises the cost of the machine [11]-[12]. Another disadvantage to skewing is that it reduces the machine's average torque [13]. Shifting PMs, notching stator teeth, and using separate pole arc widths are some other construction techniques for eliminating cogging torque [14].

Torque ripple is also produced by the interaction of rotor magnetic field and stator current magneto motive forces. This torque depends on construction of stator and rotor field. Torque ripple can be reduced by using different winding methods such as fractional slot-pitched windings or short-pitched windings [15]-[16]. The rotor field formed by the magnets must be sinusoidal in order to reduce torque ripple. Unfortunately, a sinusoidal field is difficult to produce due to the complicated configuration of the rotor magnets, which increases the machine's cost.

Another method to reduce torque ripples in PMSMs is to implement control schemes with purpose of controlling stator current to cancel out the ripples. A detailed review has been

carried out in chapter 2 of this dissertation on different types of control schemes to minimize torque ripples.

1.5. CONTROL OF PMSM

PMSMs can produce the desired torque only if the AC excitation frequency is exactly matched with the rotor frequency. Therefore, the guarantee of accurate synchronization of the machine's excitation with the rotor frequency is necessary for the control of PMSMs. This requirement can be fulfilled through continuous measurement of rotor position and corresponding excitation of the machine windings. PMSMs can be controlled with different methods according to the needs of each application.

1.5.1. V/f Control

V/f control methods are used in drive systems where easy, low-cost control is required in applications like pumps and fan drives [17]-[18]. The performance of V/f method depends on load conditions and motor parameters. V/f control at times suffers power fluctuations at particular speed ranges, which may cause the motor to lose synchronism. Squirrel cage windings can be used in the construction of IPMSMs (damper windings) to overcome this. When the IPM rotor does not rotate at synchronous speed, these squirrel cage rotor windings generate asynchronous torque, comparable to induction machine squirrel cage rotor windings. Open loop V/f control scheme is shown in Fig.1.5.

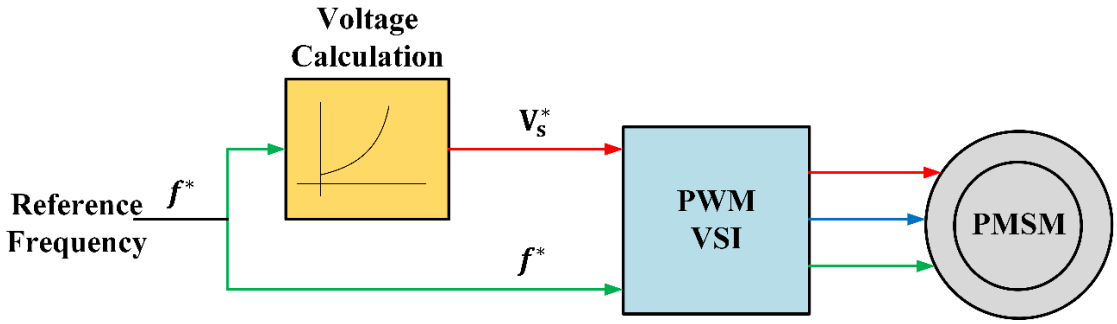

Fig.1.5. Open loop V/f control scheme of PMSM

One benefit of this control scheme is that the rotor speed is solely determined by the machine's excitation frequency, and no slip correction is needed, unlike induction machine drives. However, complexity can be faced in the control of PMSMs which do not have rotor cage windings. Hence the V/f control scheme for PMSMs without having rotor cage windings requires the information of rotor speed (rotor frequency) in order to attain the synchronization between AC excitation frequency and rotor frequency. For this purpose, closed loop V/f control scheme is useful as shown in Fig.1.6.

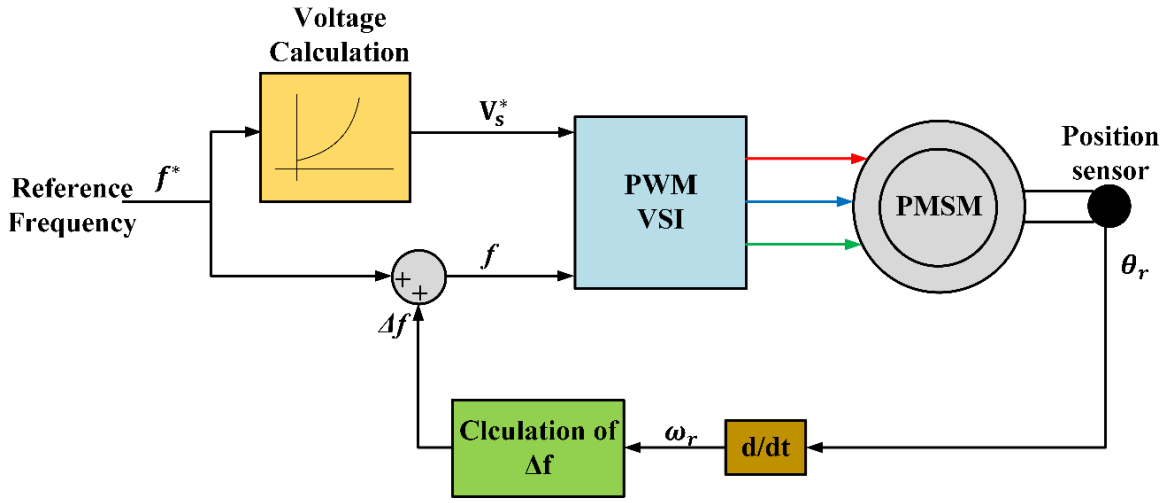

Fig.1.6. Closed loop v/f control scheme of PMSM

1.5.2. Vector Control

Vector control is the most advanced method of controlling electrical machines [19]-[20]. Vector control consists of different control techniques that use different types of feedback mechanisms for improved control. A basic configuration of vector controlled PMSM is shown in Fig.1.7. The VSI, which is powered through an AC-DC converter, feeds the PMSM. In the hybrid electric vehicle cases, the VSI is powered by the battery. The voltages in the three phases of the PMSM are regulated using a DSP. The feedback device includes current measurement devices and rotor position detectors. Encoders or resolvers are commonly used to detect the rotor position.

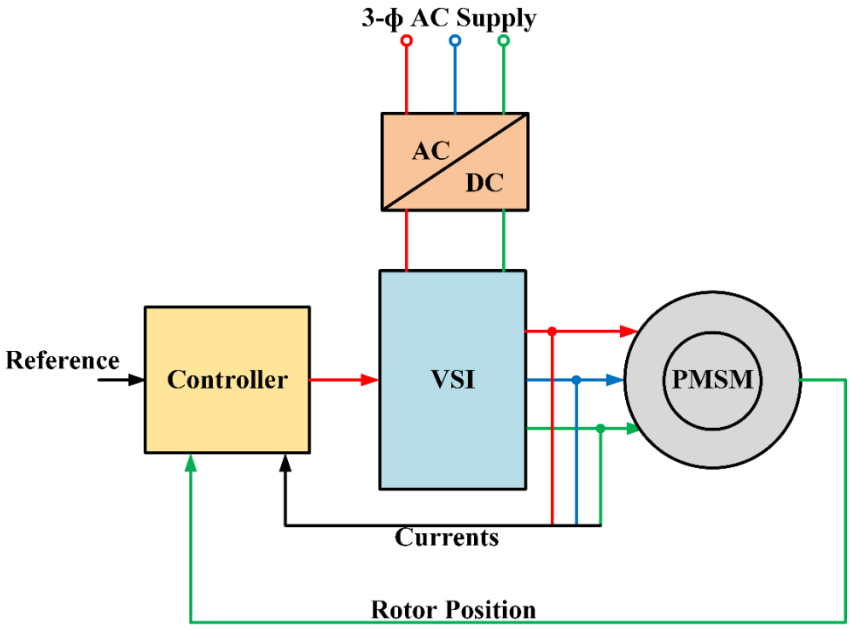

Fig.1.7. Basic Configuration of vector control scheme of PMSM

In sensor-less control, rotor speed and/or rotor position are/is estimated from the motor voltage and current [21]. The performance of PMSM such as rotor speed, shaft torque and angular position can be controlled by implementing vector control scheme. In the vector control scheme, the flux and torque of PMSM can be controlled independently similar to a separately

excited DC machine. To operate PMSMs above its rated speed, field-weakening algorithms are generally implemented with vector control schemes [22], [23], [24].

1.6. OBJECTIVES OF THE PRESENT WORK

The aim of this research is to analyse and propose different control techniques to minimize torque ripples to enhance the performance of PMSM drives. The new control methods are used to reduce the torque ripples in PMSM significantly in comparison to previously reported control techniques. The objectives identified for the present research work are as follows:

I. Modelling, Design and Development of Laboratory Prototype of PMSM Drive

II. Design and Implementation of Improved artificial neuro fuzzy inference system (ANFIS) based Model Reference Adaptive Control (MRAC) Observer for Sensor-less Control of PMSM.

III. Minimization of Stator Current Ripples and Torque Ripples in PMSM Drive using Advanced Predictive Current Controller (APCC) based on Dead Beat (DB) Control Theory

IV. Minimization of Torque Ripples using Intelligent Hybrid Controller (IHC)

V. Torque ripple minimization by Model Predictive Control of PMSM using Proportional-Plus-Integral Resonant (PI-RES) Controller

1.7. OUTLINE OF THE THESIS

Fig.1.8. shows the layout of thesis organisation.

The research work reported in this thesis has been divided into the following chapters: -

Chapter-1: This chapter presents the introduction and background of PMSM Drive, causes of torque ripples and its possible solutions.

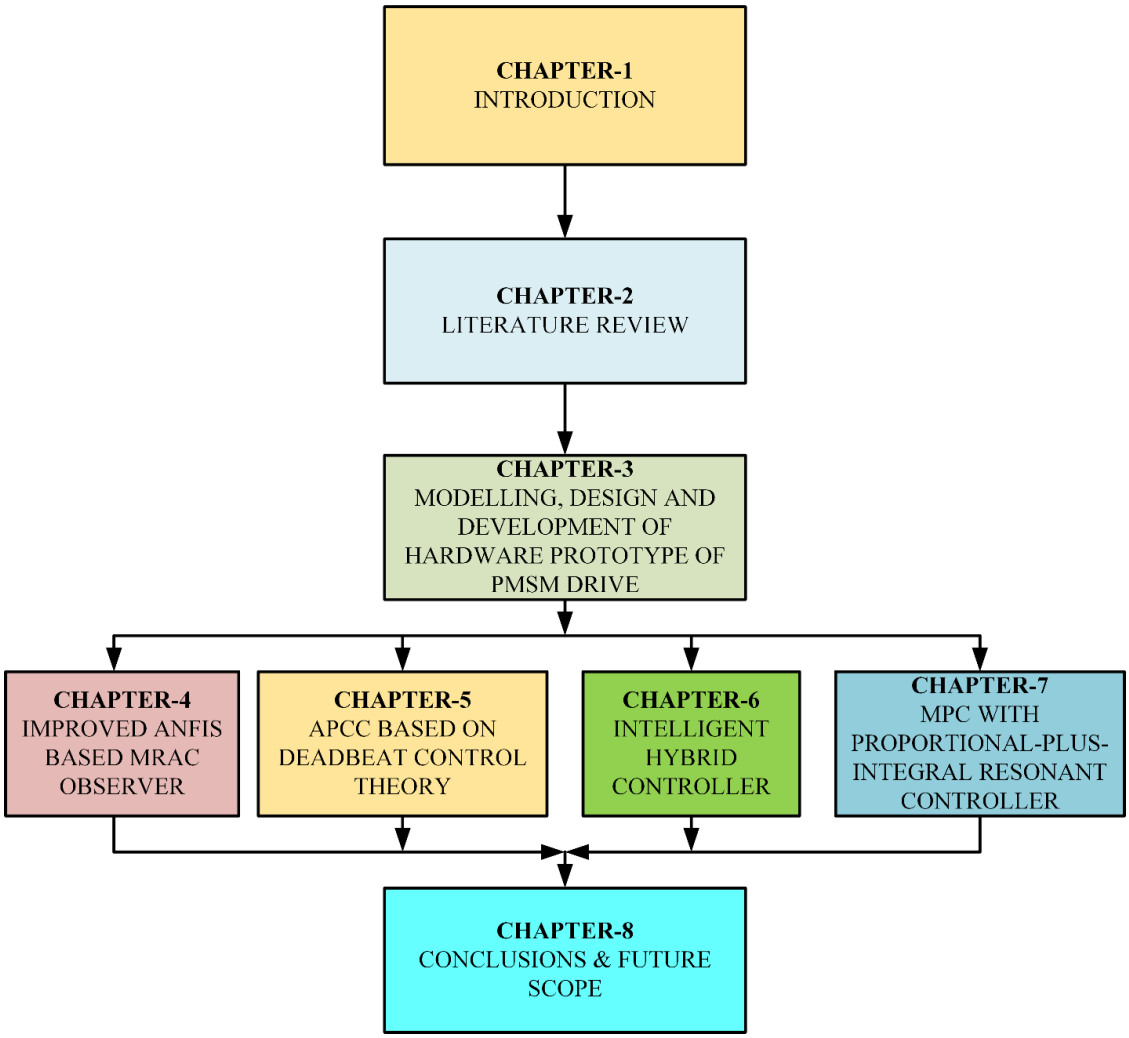

Fig.1.8. Layout of Thesis Outlines

Chapter-2: This chapter includes reported literature review on modelling of PMSM, field-oriented control of PMSM, sensor-less control techniques and torque ripple minimization techniques for PMSM.

Chapter-3: This chapter describes the modelling, design and development of laboratory prototype of the PMSM Drive. The PMSM is modelled in both stationary and rotating reference frames and field-oriented control with voltage and current control methods are

implemented for PMSM drive. A hardware prototype of PMSM drive developed in the laboratory to validate the control schemes in real time. This experimental setup consists of a DSPACE ds1104 controller, 3-Phase Diode Rectifier, 3-Phase PWM Inverter, Voltage / Current Sensors and PMSM with encoder. The performance of FOC of PMSM drives using hysteresis controller and PWM current controller are analysed through simulation studies. The dynamic performance of PMSM under constant torque operation for different operating conditions are presented with both different controllers.

Chapter-4: Detection of rotor position is an important prerequisite for controlling the speed and developed torque in PMSM. Though use of incremental encoder and resolver is one of the popular schemes for sensing the rotor position in a PMSM drive, it increases the size and weight of the drive and reduces its robustness and reliability. The sensor-less speed control of PMSM are more reliable and cost effective. The sensor-less control algorithms use machine parameters like torque constant, stator inductances and stator resistance for estimating the rotor position and speed. However, accuracy of such estimation and the performance of the motor degrades with variation in motor parameters. MRAC provides a simple solution to this issue. An improved ANFIS based MRAC observer for speed control of PMSM drive is presented in this chapter. In the proposed method adaptive model and adaptive mechanism are replaced by an improved ANFIS controller, which neutralize the effect of parametric variation and results in improved performance of the drive. The modelling equations of PMSM are used to estimate the rotor position for speed and torque control of the drive. A comparative analysis of the conventional MRAC based observer and improved ANFIS based MRAC observer for sensor-less speed control of PMSM is carried out an it is observed that the proposed method results in better performance of the PMSM drive.

Chapter-5: An APCC based on DB control theory for PMSM drives is proposed in this Chapter, where the optimum voltage vector is computed offline by solving an optimization problem. The optimum voltage vector along with a zero-voltage vector (ZVV) is applied to the motor under steady state condition to minimize ripples in the stator current. To achieve a fast dynamic response during the transient state, the voltage vector having the largest magnitude is applied for the complete duration of the control cycle. The phase of the voltage-vector is synchronized to control the components of the stator-current in a DB manner. In previously reported control methods, the two best voltage vectors (BVVs) are selected through enumeration and two independent duty ratios are calculated. However, this increases the computation complexity and computational time. The proposed APCC employs a novel approach in calculating the stator current references of PMSM using maximum torque per ampere (MTPA) control. The effectiveness of the proposed APCC is investigated and compared with direct current controller and MPCC. The APCC improves the performance of PMSM drive under steady and transient operation with lower THD in the stator current and with better torque dynamics.

Chapter-6: The switching of voltage source inverter in PMSM drives causes ripples in motor current and torque and hence mechanical vibrations. Torque ripples in PMSM can be minimized by keeping the switching frequency of the inverter constant. The performance of vector controlled PMSM is affected by the choice of the controller in the outer speed loop. This Chapter elucidates the design and implementation of IHC speed controller for vector controlled PMSM drive based on a novel torque estimation technique. FLC performs superiorly under transient conditions and PI controller under steady state condition. The developed IHC combines the FLC and PI controllers with a switching unit capable of

intelligently switching between the two controllers depending on operating conditions. Novelty has been achieved in the design of FLC through optimization of universe of discourse by fine-tuning the membership functions at the centre to provide greater sensitivity in the region around rated speed. Enhancement in performance of the drive is also achieved through fine tuning of the membership functions in accordance with the variations in input and output variables. The effectiveness of IHC is investigated through simulation study and improved transient and steady state performance of PMSM drive is analysed. It is observed that THD in stator currents and torque ripples are considerably reduced by introducing the IHC as speed controller in PMSM drive.

Chapter-7: This chapter presents the design and implementation of a PI-RES controller, which is implemented in outer speed loop of the drive to generate reference torque current for MPC in PMSM drive system. The PI-RES controller is designed by connecting a variable frequency resonant controller with PI controller in parallel. The resonant controller generates the compensating torque current while PI controller delivers reference current and both together establish the reference torque current. The speed ripples are reduced as the electromagnetic torque tracks the load torque precisely due to the presence of compensation torque current. A comparative study of the MPC based PMSM drive using classical PI controller and PI-RES controller are presented and the simulation study in MATLAB/Simulink platform shows improved performance of PMSM drive using the proposed technique.

Chapter-8: This chapter summarizes the scope of present research work and lists the scope for future work in this area of research.

CHAPTER 2

LITERATURE REVIEW

2.1. GENERAL

Electric motors are electromechanical machines used for the conversion of electrical energy into mechanical energy. Asynchronous and Synchronous motors are most popular in the category of AC motors. The Asynchronous motors are termed as singly excited machines where power supply is connected to the stator windings the machine. Mutual electromagnetic induction phenomenon is responsible for the transfer of the power from the stator to the rotor.

In synchronous machines, stator winding requires AC supply while DC supply is given in field winding on the rotor. The speed of the motor is dependent on the number of poles and frequency of the power supply given to the stator winding; and the rotor rotates at synchronous speed. The mechanical load variations do not impact the speed of the motor.

PMSM is a type of synchronous motor, which consists of three phase windings in the stator and PM on the rotor. As the field windings are replaced by PMs, there is no need of an additional DC power supply for field excitation in PMSM, whereas conventional synchronous machine needs both AC and DC power supply.

In this chapter, an extensive literature review is presented on the mathematical modelling of PMSM, field-oriented control, sensor-less control techniques and torque ripple minimization of PMSM. Further, the research gaps have been identified.

2.2. LITERATURE SURVEY

To identify the gap existing in contemporary research work an extensive literature review has been carried to facilitate the identification and formalisation of the research objective. The details of which are given herein.

2.2.1. Mathematical Modelling of PMSM Drive system

A mathematical modelling of the PMSM drive system is necessary required for analysis and control the drive system**.** Modelling and simulation study are utilized in the improvement of existing design of PM drives prior to creating system prototypes and reduce wasteful expenses.

T. Sebastian, et.al.[25] evaluated permanent magnet synchronous motor developments in 1986 and offered electric circuit models for such motors, comparing calculated and observed characteristics.

Pillay, P. et.al [26] presented comprehensive modelling, simulation, and analysis of the PMSM drive system for vector control applications. The wound rotor type synchronous motor model was used to derive the model for the PMSM. The analogous circuit was given without damper windings and the modelling equations were obtained in the rotating frame of reference. The performance of motor was investigated by using hysteresis and PWM current controllers.

Wijenayake, A.H. et.al. [27] reported the design of a two-axis circuit model for PMSMs, that accounted for machine magnetic parameter changes and core losses. To enhance the model, a strategy for on-line parameter detection based on saturation level and no-load parameters was briefly addressed. Additional test techniques were described for measuring equivalent circuit parameters and calculating saturation constants that regulate parameter changes.

B. K. Bose [28] described many types of synchronous motors and compared them to IMs. The salient pole synchronous motor model was used to create the PM motor model. All modelling equations were calculated in a synchronously rotating reference frame and presented as a matrix.

Bowen, C. et.al [29] used the state space technique to model and simulate a PMSM powered by a six-step inverter. Park transformation was used to create the motor model in the stationary frame of reference and subsequently in the rotating frame of reference. The simulation results showed that the approach for determining initial states was quite successful.

Kayhan Gulez, et.al. [30] proposed a high-frequency common-mode modelling of PMSM with wide range of frequency that can be beneficial to observe electromagnetic interference (EMI) noise. Common mode (CM) or differential mode-based EMI filters were employed in model to reduce the noise. The suggested modelling approach required a series of tests at various frequencies to get the impedance of CM path by allowing the possibility of high-frequency signals entering the motor frame and windings.

Silverio Bolognani, et.al [31] presented a precise model of PMSM to estimate motor torque by measuring voltage and current. The model accounts for all motor losses to improve overall accuracy and reaction time. A novel commissioning process and a simple torque estimation scheme were suggested for PMSM drive. The commissioning method was used to acquire the motor parameters utilized in the estimation model.

Paavo Rasilo, et.al. [32] in 2014, presented a combined analytical-numerical approach for the modelling of IPMSM, in which static finite-element (FE) analysis was used to link the stator currents and flux linkages. Flux-linkage space vector was also used to develop new models,

allowing for more appropriate time-integration of the voltage equations. The zero-sequence current effect on the torque ripple was also discussed in a delta-connected stator winding.

Wei Yu, et.al. [33] developed fractional-order model of PMSM in frequency domain by extending conventional integer order model to fractional order one which improves the accuracy of the model. The parameters used in fractional order model were identified using a weighted augmentation of the standard Levy identification approach.

Alejandro J. Pina,et.al.[34] developed an analytical model of IPMSM including fundamental as well as harmonics of flux linkage. The harmonics in the d−q axes flux linkages were discussed to improve the traditional model and for improving the performance of torque transients in an IPMSM. Finite element analysis (FEA) was used to validate the analytical model by isolating flux linkages using frozen permeability. In addition, saturation and cross-magnetization were investigated for different PM flux linkages and currents in d−q axes.

Abraham Gebregergis, et.al.[35] proposed modelling of PMSM with electromagnetically produced torque ripple. A method for quantifying the various causes of torque ripple was presented, which improved the modelling capabilities of both surface-mount and interior PMSMs by modifying the existing dq-model.

Guangzhao Luo, et.al. [36] described a field-circuit-coupled parameter adaptive model for a PMSM by including the qualities of mathematical model and a magnetic field model. Three modelling approaches were compared in an offline simulation to evaluate the efficacy of the suggested model and it was found that the suggested model closely resembles the actual machine and can be easily modified to meet various requirements.

Sergio Zarate, et.al. [37] presented an adapted dynamic vector model of a PMSM. A high-fidelity and computationally efficient model was developed to simulate PMSM comprising all torque ripples based on a hybrid abc + dq reference frame. The suggested model estimates the torque ripple at each working point more precisely than a FEM simulation, saving time when assessing the performance of electrical drives. The model allowed to determine the total torque *term by term* and assessed the influence of imbalanced linkage fluxes.

Roser A. Ordonez, et.al.[38] presented the model of PMSM including torque conditions and variable speed using mathematical Parks Transformation. The behaviour of model is analysed using MATLAB/Simulink. Different PID control models are implemented with various reference values to bring its behaviour to reality.

2.2.2. Field Oriented Control of PMSM

FOC was first introduced for controlling an IM by F. Blaschke in 1972 and it was established that using the orientation of stator magneto-motive force (mmf) or of current vector with regard to rotor flux, it is possible to control an IM or synchronous motor similar to a separately excited DC motor [39]. Due to recent advancements in power electronics, microprocessors and computers, now FOC is widely used in the industry. With FOC it is possible to control PMSM like a DC motor. The information of instantaneous rotor flux and position of the rotor is required to control the PMSM like a DC motor. For this purpose, an absolute optical encoder or resolver is attached to the shaft of the motor. An inverter develops a variable voltage with variable frequency, which is supplied to the stator windings of the motor. The frequency and the phase angle of the output wave is controlled using a position sensor rather than independently controlling the frequency of the inverter.

Based on the way that the rotor position is obtained, FOC can be classified into Indirect FOC (IFOC) or Direct FOC (DFOC). The most popular method is IFOC, which uses a mechanical sensor attached to the motor shaft to detect the position of the rotor. In DFOC the rotor position is calculated from the flux or back electromotive force (EMF) vector [40].

A. Benchaib, et.al. [41], presented a discrete-time FOC for a SPMSM. One of the most vital problems is to deal with the voltage and / or current limiting constraints. As a consequence of taking these restrictions into consideration a priori, the suggested controller produced optimum torque dynamics across the whole range of operating speed.

Mohamed Rashed, et.al. [42] presented an indirect rotor field-oriented control of PMSM, which is unaffected by mismatch in stator resistance. The stator resistance, rotor flux magnitude and rotor speed were estimated using three Model Reference Adaptive System (MRAS) estimators. Estimating the stator resistance and rotor-flux magnitude at the same time was impossible, hence, two distinct techniques for estimation were presented. In first technique, rotor speed and stator resistance were estimated using MRAS estimator by setting the magnitude of rotor flux to its minimal value. In second technique, the magnitude of the rotor flux and the rotor speed were adaptively calculated using MRAS estimators by setting the stator resistance to its minimal value. The MRAS estimators were developed for an error model of PMSM in a rotating frame of reference.

Wonhee Kim, et.al.[43], presented a simple FOC without using *dq* transformation to track the rotor position of PMSMs. A PID controller with velocity feedforward was proposed to get the desired torque modulation for exact position tracking. A novel commutation method was also implemented that produced necessary currents with torque modulation.

Dmitry V. Lukichev, et.al.[44], described the methodology for tuning of controllers in two FOC techniques based on current control mode and voltage control mode. The type of inverter and the layout of the control scheme are determined by each algorithm. A simplified model of the motor and plant was used in certain techniques to tune the controllers.

Zheng Wang,et.al.[45], proposed three control methods with variable switching frequencies for paralleled VSIs supplied PMSM drive during low speed and high power operation. The FOC with phase-shifted chaotic space vector modulation (SVM) under rotating frame of reference and the FOC with phase-shifted chaotic sinusoidal pulse width modulation under stationary frame were developed for the paralleled VSIs fed PMSM drive. The suggested phase-shifted chaotic PWM methods suppressed all remaining switching harmonic peaks in the spectrum while also fully eliminating particular switching harmonics. In developing these two systems, the avoidance of intrinsic circulating current was also taken into account. In addition, using circulating current suppression, a direct torque control (DTC) for paralleled VSIs fed PMSM drive was presented.

Pradeep Kumar, et.al. [46], provided comparative study of two control schemes of FOC with and without MRAS. PMSM speed control is done without the need of sensors by using estimated speed deviation as a feedback signal for the PI controller.

Ping Zhang, et.al [47], presented two methods of FOC for dual three phase PMSM. The first method was based on vector space decay, which analysed the influence of current harmonics on electromechanical energy conversion. And the second method provided coupling between two sets of windings with d-q transformations.

Jorge Lara, et.al. [48], presented the study of the effect of error of rotor position on performance of FOC in PMSM drive for application of electric vehicle traction. The torque ripple induced

along the typical trajectories in the different operating zones of the PMSM was given specific attention. Analytical derivation of an expanded and generalized model of the torque ripple produced by the PMSM as an error function of rotor position has been presented.

Literature survey revealed that the best control for the PMSM is vector control or field-oriented control in which the PMSM performs like a DC motor using decoupling control. There are various control approaches which is used in FOC of PMSM, which are summarised below.

Unity power factor approach [49],[50] aims to achieve unity power factor by controlling stator currents in d-q axes in such a way that stator currents and voltages are in phase. The reactive power will be zero if power factor is unity. The VA ratings of VSI is thus reduced as the input power of motor is active power.

In **Constant stator flux approach** [51] the magnitude of stator flux can be controlled by controlling the required stator voltage. The torque producing ability of the motor can also be controlled by controlling stator flux. The magnitude of the stator flux is usually kept constant and equal to the PM flux linkage in the case of stator flux regulation for the motor. The torque producing ability is not worsened if the required stator voltage of the motor is reduced using this approach.

In **Maximum torque per ampere approach** [52]**,** [53]**,** [54] the torque producing ability of the motor is maximized by keeping the magnitude of stator current minimum, which is fed to the motor for a desired motor torque. This results in reduction of copper losses. Thus, the maximum efficiency of PMSM is achieved. This approach will be same as constant torque angle approach for SPMSM because the d-q axes inductances are of same value.

Constant torque angle approach [55]**,** [56] is one of the most common and easiest approach to implement because the d-axis reference current is fixed as zero in this approach. The aim of this control approach is to keep the electrical angle between the current space vector and the PM flux axis at 90°. The whole current is anticipated on the q axis in this manner. Since the reluctance torque is almost non-existent in an SPMSM, this control approach is suitable.

Control of a PMSM requires the knowledge of the shaft position and rotor speed. These can be measured using the sensors attached to the shaft of the motor. There are many position sensors available in market like encoder and resolver. However, use of position sensors may not be practically feasible for many applications. Moreover, use of position sensors increase the overall cost of the system and vulnerability due to physical wires used to connect these sensors. In addition, physical wires also produce EMI. These factors led to the use or introduction of sensor-less algorithms for control, which handles the control action without explicitly detecting position and speed.

In the recent times, sensor-based rotor position determination has been replaced by sensor-less control, eliminating the need for mechanical sensors, thereby reducing the total cost of the drive system. Without position sensors, the rotor position can be measured using electrical quantity such as voltage at motor terminals, motor currents, DC link voltage of inverter, etc.

2.2.3. Sensor-less Control Techniques

To facilitate the analysis and better understanding of the problems faced with control of motors at low speed, sensor-less FOC techniques can be classified in various types. Fig.2.1. shows various types of sensor-less techniques. Sensor-less control of motors can be broadly classified into model-based techniques and saliency-based techniques. Model based techniques are

commonly used at high operating speed, while saliency-based techniques are preferred for low operating speed for better overall performance [57], [58], [59].

2.2.3.1. Model Based Sensor-less Control Technique

The model-based technique was the first to be evolved and promoted; but was limited to low-speed operation because of poor signal-to-noise-ratio (SNR) caused by error in modelling, nonlinear behaviour of inverter, etc. The model based technique mostly use back-EMF or flux linkage estimation that can be measured at zero currents [60], [61], [62]. These methods can be implemented in rotating or stationary reference frame. The major disadvantage of these methods is that at zero speed there is no back-EMF, which results in discontinuity in control action. This disadvantage can be overcome by using back-EMF or flux linkage estimation at low operating speeds or by limiting their uses only at high operating range of speeds. Model based techniques are divided in two categories, namely – open loop estimation and closed loop observer.

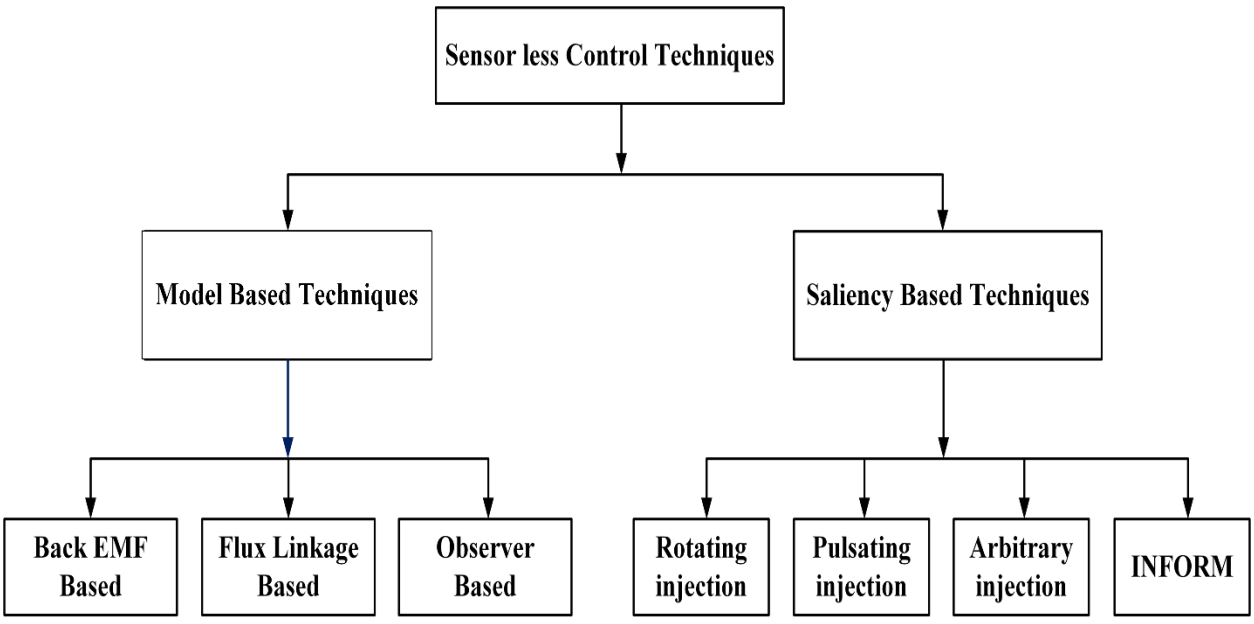

Fig.2.1. Sensor-less Control Techniques of PMSM

The open loop estimation of speed/position is simple and easy to implement. The back EMF, stator inductance and rotor flux can be estimated using dynamic modelling equations of PMSM and rotor position and motor speed can be computed from the back EMF and rotor flux.

In a closed-loop observer method, the inputs to the observer are generally defined by the error of the plant output and observer and control inputs of the plant. The gains of the observer are meant to force the observer output into the output of the plant. Therefore, the estimated values of the states of interest must meet with their true values. From this characteristic, an adaptive filter with a good disturbance rejection property and good robustness can be realized as the closed loop observer in current/voltage measurements with variations in machine parameters and noises. Many rotor position/speed estimation observers, like perturbation observers, sliding mode observer (SMO), extended Kalman filters, and others have been proposed in the literature.

Back EMF based Techniques: The back EMF components can be calculated from the measured voltages and measured stator phase current of PMSM based on machine model. This technique is simple and can be implemented without using complex observer. However, the performance of this technique is dependent on the precise measurement of the sensed current/ voltage and machine parameters.

Flux Linkage based Techniques: The vector components of stator flux and rotor flux of the motor rotate synchronously at steady state condition where $\frac{di_{s\alpha}}{dt} \approx \frac{di_{s\beta}}{dt} \approx 0$. Consequently, if the stator flux angle can be found, angle of rotor flux can also be calculated and that will be the same as angle of rotor position [63], [64]. The effectiveness of this method relies on the quality and precise measurements of currents and voltages. The initial integration condition and current sensor DC offset are issues that have to be correctly managed as integrators are

required in this technique. This technique is effective during steady state condition but generally gives unsatisfactory performance during transient conditions.

Observer based Techniques: In this method rotor position and speed state observers are developed using machine model and the inputs of actual machines, such as voltages and load torque, are applied to the model [65], [66]. The error between output variables of model and actual machine is used in the state observer to correct any error between actual values and estimated values of position and speed.

A state observer for PMSM is difficult to design because of its nonlinear behaviour. Since observers are dependent on models, they are influenced by changes in parameters of PMSM. An on-line parameter estimator may be used to develop the observer-based approach. Initial rotor position cannot be detected by this method and it needs high processing power [67].

2.2.3.2. Saliency based Sensor-less Control Techniques

The model-based sensor-less techniques to estimate the rotor position and speed can provide highly precise position/speed estimates in medium and high-speed operating ranges for vector control of PMSM. However, they perform poorly in standstill and low range of operating speed, because they have low SNR of the position-related system conditions. These limitations can be overcome by using machine saliency tracking [68]. In these techniques, high frequency signals which have higher frequency than fundamental frequency is generally applied [69], [70]. The HF excitation based methods [71] can be described in accordance to the following three characteristics:-

- The rotor position of the salient pole PMSM, i.e. IPMSM, [72] can be identified by tracing the deviation of the position dependent stator inductance. The rotor position of non-salient pole PMSM, i.e. SPMSM, can be generally identified by using special

saliency related to the stator leakage flux saturation or main flux saturation and a nearly zero special variation of inductance [73].

- The methods of HF injection in both continuous [74], [75] and discontinuous [76] have been reported in literature. A PWM pattern modification or a carrier signal injection are used in different types of HF excitation. Sinusoidal waveform and square waveform are required for carrier signal injection into either rotating reference frame or stationary reference frame.
- Saliency tracking observer and signal processing method: The measured saliency related signal is different for different types of HF excitation and the methods to process these signals also differ. In recent years, closed loop saliency tracking observers [77], have been widely studied to improve the detection of position.

Rotating injection-based method: Rotating signal injection method was initially proposed for IMs [78] and later for PMSM [79] by Prof. Lorenz. In this method the machine acts as a resolver. Position and speed can be estimated using the demodulation and excitation method, which is employed in resolver for digital conversion [80]. The basic principle of this method is represented in Fig.2.2.

The outer red line and inner blue dotted-line signify the trajectory of the injected voltage signal v_c and induced current signal i_c. In the stationary reference frame, the excitation voltage signal rotates periodically at a speed of ω_c. The trajectory of i_c has been converted in ellipse in the presence of single saliency. The information of rotor position is concealed in ellipse which is decoded using demodulation methods such as observer, phase transformations and phase locked loop.

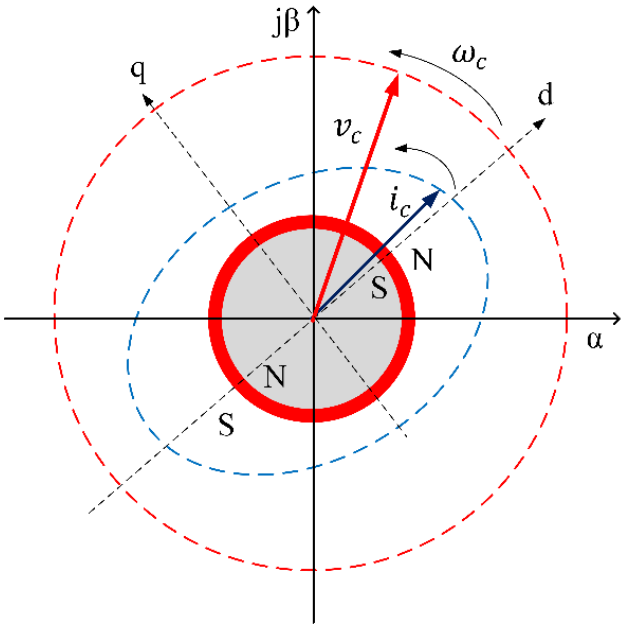

Fig.2.2. Rotating signal injection method in αβ

Pulsating signal injection method: In pulsating signal injection method [81], [82] a sinusoidal voltage signal is injected into the q-axis and a corresponding demodulation method is employed by applying *d-axis* current signal, i_{cd}. In this method, the estimated rotor position is close to actual one but torque ripples and noise are induced in the system. The estimated d-axis HF signal injection method in d- axis was presented later in [83].

Indirect Flux detection by on-line Reactance Measurement (INFORM) Method: The INFORM was developed in 1988 for PMSM [84]. Further it was improved to minimize the losses and noise by using test voltages [85]. The INFORM approach requires a disturbance of the fundamental PWM pattern for a particular time period in order to inject a manually created sequence of test voltages. This approach does not depend on the fundamental PWM pattern. The magnitude and time period of test voltages can be selected by the manufacturer on the basis of types and operation of the machine.

2.2.4. Minimization of Torque Ripples in PMSM Drive

For the past 20 years' smoothness of torque is the main concern in many applications of the PMSM. Torque ripple minimization in PMSM [13], [86] can be achieved either by (a) using proper motor design or (b) using active control techniques. The following sub-sections present a survey of these two categories. The main focus of this dissertation is the control aspects for minimizing the torque ripples in PMSM.

2.2.4.1. Design Techniques of the Motor to Minimize Torque Ripples

Accurate design of the motor is the most vital and effective approach to minimize the torque ripples that are inherently generated within the PMSM. The variance of the air gap magnetic reluctant as shown by rotor magnets should be minimized to achieve minimum cogging torque. The harmonic components of the motor back-emf also need to be reduced to a minimum in order to obtain minimum ripple torque.

Stator Slot Skewing is one of the most common methods employed for torque reduction. Studies have shown that cogging torque can be reduced to a very low level by skewing the stator slot by one stator tooth pitch [87],[88],[89]. If stator skewing presents inacceptable manufacture problems, the cogging torque can be reduced by the alternative method of skewing the magnetic field distribution by either skewing rotor magnets or mounting discrete magnet segments on the rotor. Skewing also enriches the distribution of the stator winding and reduces the harmonics in back-emf, thereby creating a more sinusoidal back-emf. The ripples in motor torque are also reduced. Skewing also has demerits, such as some loss in the average torque, requirement of a complex stator construction, production line set-up, and an increase in leakage inductance and stray losses. Several approaches have been developed to reduce the air gap magnetic reluctance by reducing the stator slot openings but these methods created

complications in stator construction. In special cases, stator configurations without any slot have been adopted. Short pitched stator windings can also be utilized to reduce the back-emf harmonics. Cogging torque is defined as sine terms in the coefficient of Fourier expansion. When the pitch of winding is reduced, the sine term changes and it eliminates a specific harmonic in cogging torque. In the method proposed [90], the cogging torque can be reduced by optimizing the distribution of the residual magnetic flux density of PM. Additional techniques are designed to minimize cogging torque by adding dummy slots or dummy teeth to the spatial air gap. The different methods employed for minimisation of torque ripples are shown in Fig.2.3.

The motor torque ripples and cogging torque can also be reduced by appropriately designing the rotor magnets. In design techniques of rotor magnet, the cogging torque is minimized by varying the magnet arc length, varying the magnet strength, shifting the magnet poles and varying the radial shoe depth. A proper configuration of the PM on the rotor provides a more sinusoidal flux distribution which results in less torque ripples.

Most of the proposed techniques involve a trade-off between reduction of torque ripples and degradation in production of average motor torque. The sensitivity to production tolerances is another important aspect that effects the practicality of motor design technology. For low-cost, large volume production it may be impractical to use techniques that involve high precise assembly, magnetization, magnet mounting or dimensions.

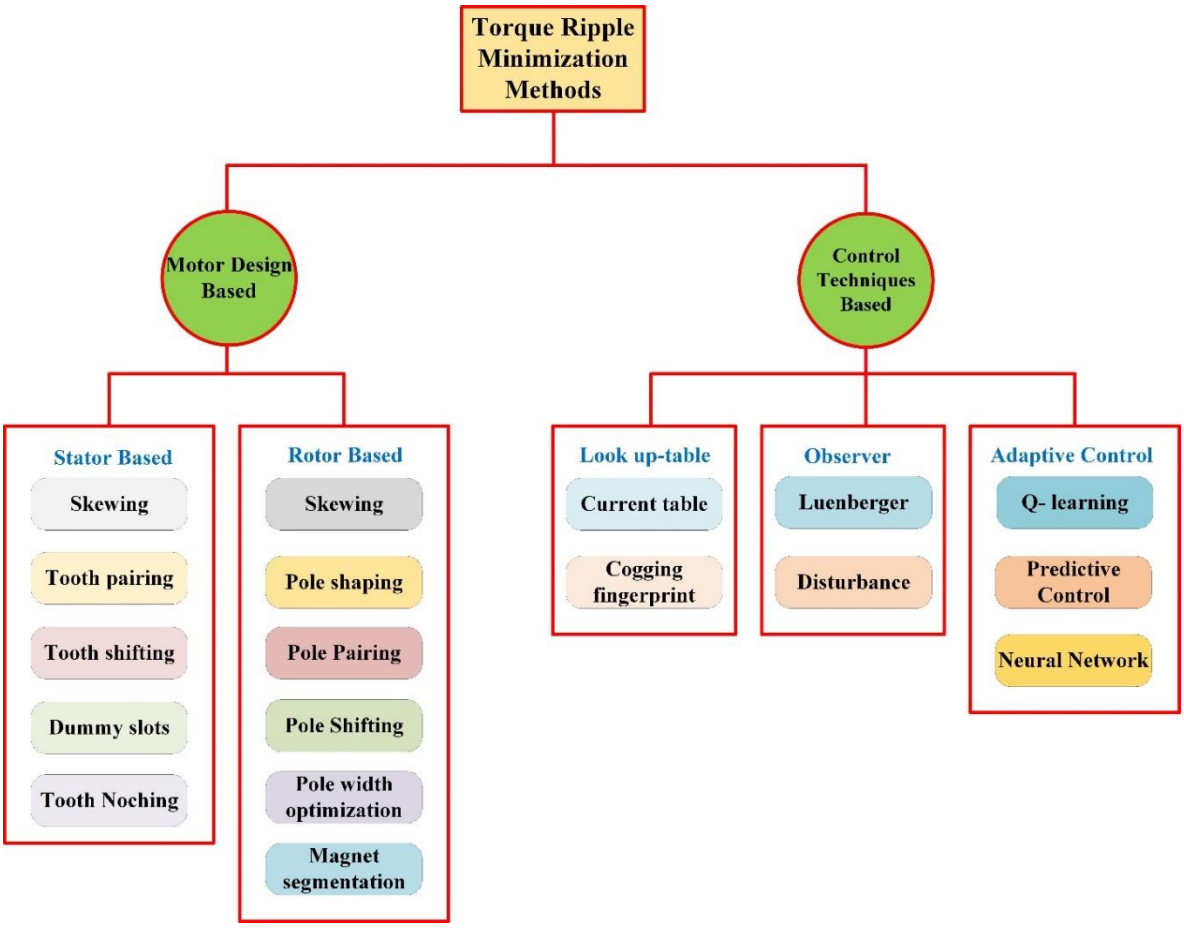

Fig.2.3. Torque ripple minimization methods

Z. Q. Zhu, et.al. [91] investigated the effect of different design factors on the cogging torque produced in PMSM. It was demonstrated that the number of pole and slot combination impacts the ideal value of both skew angle and magnet arc, as well as defining the appropriate number of auxiliary teeth/slots, and had a substantial effect on the cogging torque. A simple factor called 'goodness' proportional to the number of slot and pole and inversely proportional to their minimum common multiple, had been presented.

Metin Aydin,et.al.[92] , proposed numerous low-cost magnet-skewing methods for reducing cogging torque components in Axial-Flux (AF) PM motors with two rotors. The magnet-skewing approach to rotor side cogging torque reduction was investigated in depth, and many

cost-effective alternative skewing strategies were offered. Based on the studies, a prototype AFPM motor with various rotor structures was developed. The results verified that, when compared to a reference AFPM motor with unskewed magnets, the suggested magnet-skewing techniques may considerably minimize cogging and enhance the torque quality of disc motors.

Kyung-Sik Seo, et.al. [93] presented the design technique of the shape of stator teeth in SPMSM for minimization of torque ripple. To investigate the influence of stator teeth shape on torque ripple, three SPM motor models with varied stator teeth forms were chosen, and FEM analysis was performed to compare their features. Then, a technique for identifying a design parameter was developed to reduce torque ripple efficiently.

L. Hao, et.al. [94], investigated reduction method of cogging torque in axial-field flux switching PM machine (AFFSPMM). The expression of cogging torque of AFFSPMM is calculated theoretically. A 3-D FEM technique was applied to analyse the effects of stator and rotor tooth arc, stator and rotor axial length, stator PM thickness, stator yoke width and rotor tooth form on cogging torque.

X. Wang, et.al.[95], proposed a scheme for analytically calculating the cogging torque and presented a useful tool for the study of cogging torque. The researchers believe that the air gap varies from tooth to tooth on a regular basis.

L. Zhu,et.al. [96], presented an investigation on the impact of machine design parameters on cogging torque analytically and determined their ideal values for the lowest cogging torque. A general analytical formula for the cogging torque was developed using the energy technique and Fourier series analysis of the air gap existence and air gap flux density in comparable slot-less machines. The best design parameters were found, including skewing, slot opening and ratio of pole-arc to pole-pitch based on FEA.

Seok-Hee Han, et.al. [97] presented analytical principles for reducing ripples in torque of IPMSM. The importance of slot harmonics was discussed, along with the advantages of stators with an odd number of slots per pole pair. The synchronization of the selection of stators with odd numbers of slots per pole pair with IPM rotors with several layers of flux barriers was recommended to minimize torque ripple. A finite-element-based Monte Carlo optimization method was applied to four IPM machine topologies which verified the value of using stators with odd number of slots per pole pair in reducing torque ripple. Torque ripple can be minimized by choosing a stator with an odd number of slots per pole pair and the IPM rotor with optimized barrier design, without rotor pole shaping and stator/rotor skewing.

W. Fei, et.al. [98] presented a different axial pole-pairing technique to minimize the cause of cogging torque in PM brushless machine. The back-EMF can be improved by using unequal stator poles. According to the FEA results presented, the proposed technique not only reduced cogging torque successfully, but also improved the harmonic content of the back EMF. To minimize total torque ripple, the importance of improving both load-independent machine design approaches and load-dependent driving strategies were highlighted.

Rukmi Dutta, et.al. [99] proposed multi-objective design optimization of the fractional-slot, concentrated wound (FSCW) PMSM using finite-element methods. These multi-objectives included low ripple, cost reduction, and maximization of efficiency without the loss of torque density and wide range of constant power speed. In order to integrate the benefits of both V- and spoke-type rotors in an FSCW stator, a unique internal PM rotor topology known as Y-type was developed. In the suggested Y-type FSCW IPMSM, the objectives of maximum efficiency, lowest cost, and broad range of constant power speed are met.

Daohan Wang, et.al. [14] provided a study of simple technique for reducing cogging torque while also reducing operating torque ripple. A magnet of varying width is utilized to significantly modify the flux density distribution in the machine. An analytical model is used to determine the magnet widths for reducing cogging torque. The effect of magnet widths on torque ripple and average torque operation was investigated using FEA. Unequal distribution of magnets can significantly enhance the Unbalance Magnetic Pull (UMP).

Y. H. Jung, et.al. [100] presented a novel numerical formula and design approach for reducing torque ripple and increasing the efficiency and control performance of an IPMSM. The inverse cosine function (ICF) had been developed in earlier research to reduce torque ripple by keeping the air gap flux density distribution sinusoidal at no-load conditions. The advanced inverse cosine function (AICF) based on the ICF was proposed later. It defined an unequal rotor shape to represent the air gap flux density distribution sinusoidal at a load condition. In comparison to other traditional techniques, the AICF may also achieve lower peak values, reduced iron loss and THD of the induced voltage.

Zhentao S. Du, et.al. [101] proposed axial pole shaping method and compared it with several design methods such as the conventional skewing, radial pole shaping for torque ripple reduction in IPMSM. By radially and axially manipulating the pole arc, the axial pole shaping approach produced a certain flux concentration design on the rotor surface in the axial direction. The differential evolution method was used to optimize the flux concentration pattern.

2.2.4.2. Torque ripple minimization based on control techniques

The motor design techniques are not able to reduce torque ripples in PMSM for many high-performance applications. In certain cases, the developed motor design techniques may not be

economical to manufacture in large volumes. Furthermore, several factors such as load, running speed and the normal frequency of the system decide the impact of the torque ripples on the system. In order to reduce torque ripples, researchers have put greater focus on the control techniques because of the limitations of the motor design techniques.

Vladan Petrovic, et.al. [102] addressed an adaptive control technique for reducing torque ripple in PMSM drives, as well as presented controller implementation and relevant experimental constraints. The electrical subsystem provided information on torque ripple harmonics, which was employed in adaptation, and a current controller was intended to minimize ripples in motor torque.

Bojan Grcar, et.al. [103] presented an estimator-based control technique for reducing torque ripple in PMSM. Lyapunov's direct technique was employed to design the flux Fourier's coefficients estimator which ensured parameter convergence. A nonlinear torque controller based on flux/torque estimation was presented to decrease the effect of flux harmonics.

Kayhan Gulez, et.al. [104] presented a dissipative passive filter system that minimizes torque pulsation and noise of current harmonic in surface PMSM. The passive filter system made of a low pass filter cascaded with a dissipative filter. The complex filter includes two frequency setting points, one at the switching frequency of inverter and the other at a randomly chosen average frequency. The filter system affected the switching frequency of inverter in such a manner that it reduces the severity of $\frac{dv}{dt}$ on the motor while decreasing stress on the inverter switching components. The filter system employed series dissipative components to reshape the waveform of applied voltage such that the motor windings get almost semi-sinusoidal voltage.

N. Nakao, et.al. [105] proposed a control technique based on torque estimation using equation that correctly accounted for both magnetic energy and magnetic co-energy fluctuations. A feedback control and feedforward control were used in the proposed system which reduce the effective torque ripples.

Yan Yan,et.al. [106] presented a PI type iterative learning control (ILC) technique to minimize torque ripples in PMSM. The controller's tuning mechanism guaranteed system stability and convergence. In comparison to the previous ILC compensatory technique, the suggested method did not need estimation of electromagnetic torque or close loop control and it simplified the controller construction.

Zhiyong Zeng, et.al. [107] proposed a hybrid SVM technique to reduce torque ripples by alternately employing the two equivalent zero vector synthesis procedures. The position of the stator current vector determined the sector division of the proposed hybrid SVM strategy, which is significantly distinct from the approaches utilized in conventional SVM methods. A sector identification technique was also implemented to minimize the complexity of the proposed SVM strategy by eliminating the need for trigonometric function computations.

Jing Liu, et.al. [108], presented a robust iterative learning control (ILC) achieved by adaptive sliding mode control (SMC) to reduce the torque ripples, which improve the ability of anti-disturbance of a servo system. In this method ILC was employed to reduce the periodic torque ripples and the SMC was used to guarantee fast response and strong robustness. An adaptive algorithm was applied to estimate the system lumped disturbances, including parameter variations and external disturbances. These estimated values compensate the robust ILC speed controller by eliminating the effects of the disturbance, and suppress the sliding mode chattering phenomenon simultaneously.

Jinsong Kang, et,al. [109] presented an improved model predictive control of PMSM to minimize torque ripples. The best active vector was chosen from the control set to control current. An objective function of torque ripples was evaluated to determine the optimum time period of the active vector using voltage vectors and torque responses in one control cycle. The active vector and a zero vector were merged according to the ideal duration which was used to determine the control signals of inverter switching control.

Zhanqing Zhou, et.al. [110] proposed a modified predictive torque control (PTC) algorithm based on the extended control set (ECS) to minimize the steady state torque ripples in PMSM. In this method, the candidate voltage vectors were extended to develop ECS for precise control of torque and to achieve reduced torque ripples. A new voltage vector synthesis method was developed in ECS-PTC, and this approach was applied to develop the corresponding predictive model and cascaded predictive algorithm.

Hao Zhu, et.al. [111] presented a predictive control scheme to reduce the torque ripples in PMSM. In this scheme, an optimal voltage was applied in each cycle of digital signal processor and the flux and torque controllers produce the phase angle of voltage vectors. This prediction scheme made calculation simple and improved the accuracy.

Jong-Heon Lee, et.al. [112] developed a torque compensator to reduce the ripples and speed error. The proposed controller was based on conventional PI controller but the torque compensator was different from traditional differential controller and it produced a compensation torque to reduce speed ripple. Compensation was achieved from discrete activation function in the proposed control scheme.

J.Kim, et.al. [113] proposed model-based loss minimization (LM) control scheme to reduce the torque ripples and improve the efficiency of SPMSM drives. In this method, the appropriate

d-axis current value was selected by differentiating the electromagnetic torque and equating it to zero in the SPMSM drive; unlike the conventional MTPA where zero *d-axis* current was applied by neglecting the actual core loss resistance in design of the controller.

G. Feng, et.al. [114] designed a controller based on multiple reference frame (MRF) to minimize torque ripples, in which the measured speed ripple is explored as the feedback control signal. The MRF-based controller was used to find the optimal current reference with a current controller controlling the actual current so that it can follow reference optimal current. MRF was implemented to transform harmonic current control into DC current control.

Amir Ebrahimi, et.al. [115] presented a new control algorithm for reduction of torque ripples in PMSM for traction application. A voltage-based production of the electromagnetic torque was proposed and a current control approach was developed to reduce the torque ripples caused from the harmonics in flux. The principle of output active power was applied to determine the motor torque generation, and the current controller provided a smooth torque at low speeds.

S. F. Toloue, et.al. [116] developed a multi-objective extremum seeking (MOES) approach torque control and reduction of torque ripples in PMSM. It was a combination of an adaptive iterative learning control (AILC) method and an adaptive PI controller which improved the torque control performance by making the system less sensitive to load disturbances during transient state.

A smooth torque can be achieved by tracking a modified current reference which is periodic over one sixth of the electrical time period in the synchronous reference frame. The conventional controllers are not able to achieve high current loop bandwidth, which is required for accurate tracking. For that purpose, repetitive current control technique was developed

[117]. In this technique constant torque was achieved by modifying the reference current in q-axis.

Guodong Feng, et.al. [118] designed a closed-loop fuzzy logic based current controller for torque ripple reduction using speed harmonics magnitude. In this approach speed harmonics was obtained by encoder to avoid the effect of nonlinearity of machine and inverter. The speed harmonic magnitude is proportional to the same order of torque harmonic magnitude. Thus, torque harmonics magnitude can be reduced by using same order of speed harmonics magnitude in feedback signal. Torque ripples can also be minimized with the use of speed harmonic as a measure of the torque harmonic.

A torque predictive control was suggested to reduce the torque ripple [119], which was sensitive to parameter variation of machine as the torque estimator/observer requires precise machine model. Hamid Mahmoudi, et.al. [120] presented a torque ripple minimization technique for PMSM drive using a modified quasi-Z-source (qZS) inverter. The suggested modified qZS network was developed by adding an additional switching device to the traditional qZS architecture and provided a larger range of inverter input voltage. The control system used a different technique for selection of switching sequence for SVM modulation, which reduced torque ripples.

L. A. Adase, et.al. [121] developed predictive torque control algorithm with simple duty-ratio to reduce torque and flux ripples in PMSM. In this method, the error in torque was minimized using an appropriate minimization function of torque. The space vector modulation synthesized this minimization function, which reduced the induced flux and torque ripples at low operating speed.

The DC-link current and torque ripples which are produced by injection of carrier signals can be minimized using optimization of voltage and current carrier signals with conventional saliency based self-sensing control schemes for interior PMSMs [122].

Kayhan Gulez, et.al.[123] developed an active filter topology to reduce harmonic noises and torque ripples in field oriented control of PMSM. The filter topology was assembled with an insulated-gate bipolar transistor active filter and two RLC filters. One RLC filter was applied in the primary circuit and the other in the secondary circuit of the coupling transformer.

Amir Masoud Bozorgi, et.al. [124] employed a fuzzy logic controller to minimize current and torque ripples in SPMSM. The controller determined the duty cycle of voltage vectors and applied two voltage vectors instead of one voltage vector as in conventional MPCC, during a control period. The rules and inputs of the fuzzy-based modulator were designed to cater for variations in operating point of the motor and its effect on voltage vectors duty ratio.

Jian Gao, et.al. [125] designed a PI-resonance controller by connecting frequency variable resonance controller in parallel with PI controller to minimize torque ripples. The compensating torque current developed by the resonance controller and the main reference current developed by the PI controller create the reference torque current. The electromagnetic torque tracked the variation of the load torque very well due to the existing compensation torque current, thus reducing speed ripples.

Mi Tang, et.al. [126] developed an angle-based repetitive observer (ARO) to reduce torque ripples in PMSM. The suggested ARO can be quickly integrated into an existing control loop while maintaining system stability. It requires only two parameters to be adjusted and takes less than 10μs seconds to complete. For tracing the desired high frequency compensating current, the proposed ARO and many other developed compensation systems require a high

bandwidth current controller. The deadbeat current loop was chosen as it has a high bandwidth and a fixed time delay.

Mingfei Huang, et.al. [127] developed a hybrid robust resonant control scheme for the suppression of torque ripples of PMSM by combining the fractional order vector resonant (FOVR) controller and the robust internal model control (Robust-IMC). In the parameter mismatch situation, the FOVR controller was designed to guarantee that the vector resonant controller maintains appropriate resonant gain and enhanced the harmonics suppression performance. Meanwhile, the Robust-IMC was used to increase the robustness of current loop and achieve the required dynamic behaviour.

Zhanfeng Song, et.al. [128] proposed an improved two-vector-based model predictive flux control of PMSM to reduce torque ripples. In previously developed techniques, the zero or nonzero vector of voltage was employed within one sample time interval for reduction of torque ripples and on other hand the entire control duration of two voltages was limited to the constant sampling time interval which constrained future developments in performance of reference value tracking. The said technique was developed without limiting the entire control time of the active voltage vector and the zero-voltage vector. The control time of both vectors were adjusted flexibly on the basis of minimization of objective function. The torque ripples were reduced without increasing switching losses.

Guodong Feng, et.al. [129] proposed closed loop decoupled control for reduction of torque ripples in PMSM using measured speed. A decoupled method was implemented to regulate the harmonic currents. The magnitude and phase angle were controlled separately to reduce complexity in designing the controller. The decoupled technique included one control rule and two PI controllers. Both PI controllers were used to control phase angle and magnitude and the

control rule was implemented for coordination between the two PI controllers for reducing torque ripples.

Wenjing Zhang, [130] presented an adaptive compensation technique for suppression of torque ripples in PMSM with combination of adaptive PID based sliding mode control (APID-SMC) and periodic adaptive learning control (PALC). The gain of sliding mode control was improved using the particle swarm optimization (PSO) technique to attain energy efficiency for long-time operation. The ripple compensation algorithm produced an additional control effort for ripple compensation by properly approximating two prominent harmonic amplitudes in the torque ripple.

2.3. RESEARCH GAPS IDENTIFIED

A thorough analysis of the research reported in literature reveals that few gaps exist in other reported contemporary research activities, which offers the potential for further investigation and detailed study. These areas include detailed analysis of sensor-less control of PMSM drive for smooth and efficient operation, examining ANFIS based MRAC control for efficient operation of PMSM, exploring new control techniques for minimization of torque ripples and stator current ripples in PMSM drives.

2.4. CONCLUSION

In this chapter, detailed review on modelling of PMSM, field-oriented control of PMSM, various sensor-less control techniques and torque ripple minimization techniques have been carried out. The torque ripple is one of the major limitations of PMSM. Torque ripples are produced from mutual torque, reluctance torque and cogging torque. Torque ripples in PMSM can be minimized using two different techniques which are design-based techniques and

control-based techniques. There are several design techniques which have been reviewed to minimize the cogging torque. The control techniques are also presented in literature review which aims at controlling stator current to cancel out the ripples. Based on the reported research activities in literature, the existing gaps have been identified and accordingly the research objectives are proposed.

CHAPTER 3

MODELLING, DESIGN AND DEVELOPMENT OF HARDWARE PROTOTYPE OF PMSM DRIVE

3.1. GENERAL

In this chapter[1] the mathematical modelling of PMSM is carried out in stationary and rotating reference frames. The design accuracy of the controller and its parameters are determined by the precise modelling of the system. The simulation studies of the PMSM drive under various operating conditions are carried out using MATLAB / Simulink.

The development of laboratory prototype of PMSM drive is also described in this chapter. The encoder connected to the shaft of the PMSM is used to provide rotor position and speed of the motor. A dSPACE 1104 digital controller is used as processing/control unit in this prototype. The switching pulses are generated to the inverter via digital I/O of dSPACE. The Semikron make inverter with IGBT module is used for developing 3 phase VSI. This prototype consists of both software and hardware. The hardware part consists of the CPL 1104 controller with digital and analogous I/O. Digital I/Os work within the Transistor-Transistor Logic (TTL) range, while analogue I/Os can send or receive signals up to ±10 V. Real-time interface (RTI) blocks link the Simulink model of controller in MATLAB to the ds1104 digital controller boards which drives the VSI of the PMSM drive.

[1] **Paper Published**: Suryakant, M. Sreejeth and M. Singh, "Performance Analysis of PMSM Drive using Hysteresis Current Controller and PWM Current Controller", 2018 IEEE International Students' Conference on Electrical, Electronics and Computer Science (SCEECS), 2018, pp. 1-5, doi: 10.1109/SCEECS.2018.8546862.

3.2. MODELLING OF PERMANENT MAGNET SYNCHRONOUS MOTOR

The mathematical modelling of PMSM is required for controller design, simulation analysis, and implementation of digital control techniques. The transformation of variables is used to characterize the performance of the motor for time-varying inductances and coefficients of differential equations. The modelling equations of the motor are derived in two different frames of reference. In stationary reference frame the stator of the motor is fixed and rotor of the motor is fixed in rotating frame of reference. Generally, transient performance of drives is analysed in stationary frame due to simple calculation and zero speed of frame. A rotating frame of reference is used for stability analysis of small signals which provides unbalance conditions of steady state voltages and currents.

3.2.1. Modelling of PMSM in Stationary a-b-c Reference Frame

The mathematical equation for the voltages of PMSM in stationary reference frame is given as[131]

$$\begin{bmatrix} v_{sa} \\ v_{sb} \\ v_{sc} \end{bmatrix} = R_s \begin{bmatrix} i_{sa} \\ i_{sb} \\ i_{sc} \end{bmatrix} + \frac{d}{dt} \begin{bmatrix} \phi_{sa} \\ \phi_{sb} \\ \phi_{sc} \end{bmatrix} \tag{3.1}$$

Here v_{sa}, v_{sb}, v_{sc} and i_{sa}, i_{sb}, i_{sc} are stator winding voltages and current respectively. $\phi_{sa}, \phi_{sb}, \phi_{sc}$ stator winding flux linkages are defined as[132]

$$\begin{bmatrix} \phi_{sa} \\ \phi_{sb} \\ \phi_{sc} \end{bmatrix} = L_{abc} \begin{bmatrix} i_{sa} \\ i_{sb} \\ i_{sc} \end{bmatrix} + \begin{bmatrix} \cos\theta \\ \cos\left(\theta - \frac{2\pi}{3}\right) \\ \cos\left(\theta + \frac{2\pi}{3}\right) \end{bmatrix} \phi_m \tag{3.2}$$

Where inductance matric L_{abc} is expressed as [133]

$$L_{abc} = \begin{bmatrix} L_{aa} & L_{ab} & L_{ac} \\ L_{ba} & L_{bb} & L_{bc} \\ L_{ca} & L_{cb} & L_{cc} \end{bmatrix} \tag{3.3}$$

The inductances L_{aa}, L_{bb}, L_{cc} are self-inductances and inductances $L_{ab}, L_{ba}, L_{ac}, L_{ca}, L_{bc}, L_{cb}$ are mutual inductances. The magnitude of the fundamental component of PM flux linkage is denoted as ϕ_m.

It is evident from equation (3.2) that the stator winding flux linkage contains two parts one provided by the stator current and other by the PM. The components of self-inductance and mutual inductance can be further expressed by including second order harmonics and a constant DC component as:

$$\left.\begin{aligned} L_{aa} &= L_{ls} + L_{0s} - L_{ms}\cos 2\theta \\ L_{bb} &= L_{ls} + L_{0s} - L_{ms}\cos 2\left(\theta - \tfrac{2\pi}{3}\right) \\ L_{cc} &= L_{ls} + L_{0s} - L_{ms}\cos 2\left(\theta + \tfrac{2\pi}{3}\right) \\ L_{ab} &= L_{ba} = -\tfrac{L_{0s}}{2} - L_{ms}\cos 2\left(\theta - \tfrac{\pi}{3}\right) \\ L_{ac} &= L_{ca} = -\tfrac{L_{0s}}{2} - L_{ms}\cos 2\left(\theta + \tfrac{\pi}{3}\right) \\ L_{bc} &= L_{cb} = -\tfrac{L_{0s}}{2} - L_{ms}\cos 2(\theta + \pi) \end{aligned}\right\} \tag{3.4}$$

Where L_{0s} and L_{ls} are defined as fundamental magnetizing inductance and the leakage inductance of the stator winding respectively and L_{ms} is termed as inductance which depends on the rotor position. L_{ms} will be zero for SPMSM and is independent of rotor position.

Equations (3.2) and (3.4) is used to calculate derivative of flux linkage of phase A and expressed as:

$$\frac{d\phi_{sa}}{dt} = \frac{d}{dt}\left(L_{aa}i_{sa} + L_{ab}i_{sb} + L_{ac}i_{sc} + \phi_m \cos\theta\right) \tag{3.5}$$

$$= \frac{d}{dt}\left[(L_{aa} - L_{ac})i_{sa} + (L_{ab} - L_{ac})i_{sb} + \phi_m \cos\theta\right] \tag{3.6}$$

The simplified equation for $\frac{d\phi_{sa}}{dt}$ using equation (3.6) is expressed as

$$\frac{d\phi_{sa}}{dt} = Ka_1 i_{sa} + Ka_2 \frac{di_{sa}}{dt} + Ka_3 i_{sb} + Ka_4 \frac{di_{sb}}{dt} - \phi_m \omega_r \sin\theta \tag{3.7}$$

where

$$Ka_1 = 2\omega_\gamma L_{ms} \sin 2\theta - 2\omega_\gamma L_{ms} \sin 2\left(\theta - \frac{\pi}{3}\right) \tag{3.8}$$

$$Ka_2 = \frac{3}{2} L_{0s} + L_{ms} \cos 2\left(\theta + \frac{\pi}{3}\right) - L_{ms} \cos 2\theta \tag{3.9}$$

$$Ka_3 = 2\omega_\gamma L_{ms} \sin 2\left(\theta - \frac{\pi}{3}\right) - 2\omega_\gamma L_{ms} \sin 2\left(\theta + \frac{\pi}{3}\right) \tag{3.10}$$

$$Ka_4 = L_{ms} \cos 2\left(\theta + \frac{\pi}{3}\right) - L_{ms} \cos 2\left(\theta - \frac{\pi}{3}\right) \tag{3.11}$$

Similarly, derivative of flux linkage of phase B is given as

$$\frac{d\phi_{sb}}{dt} = Kb_1 i_{sa} + Kb_2 \frac{di_{sa}}{dt} + Kb_3 i_{sb} + Kb_4 \frac{di_{sb}}{dt} - \phi_m \omega_r \sin\left(\theta - \frac{2\pi}{3}\right) \tag{3.12}$$

where

$$Kb_1 = 2\omega_\gamma L_{ms} \sin 2\left(\theta - \frac{\pi}{3}\right) - 2\omega_\gamma L_{ms} \sin 2(\theta + \pi) \tag{3.13}$$

$$Kb_2 = L_{ms} \cos 2(\theta + \pi) - L_{ms} \cos 2\left(\theta - \frac{\pi}{3}\right) \tag{3.14}$$

$$Kb_3 = 2\omega_\gamma L_{ms} \sin 2\left(\theta - \frac{2\pi}{3}\right) - 2\omega_\gamma L_{ms} \sin 2(\theta + \pi) \tag{3.15}$$

$$Kb_4 = \frac{3}{2} L_{0s} + L_{ms} \cos 2(\theta + \pi) - L_{ms} \cos 2\left(\theta - \frac{2\pi}{3}\right) \tag{3.16}$$

The equations of stator voltage can be given by using equations (3.2) – (3.16)

$$v_{sa} = R_s i_{sa} + Ka_1 i_{sa} + Ka_2 . \frac{di_{sa}}{dt} + Ka_3 i_{sb} + Ka_4 . \frac{di_{sb}}{dt} - \phi_m \omega_r \sin\theta \tag{3.17}$$

$$v_{sb} = R_s i_{bs} + Kb_1 i_{as} + Kb_2 . \frac{di_{sa}}{dt} + Kb_3 i_{bs} + Kb_4 . \frac{di_{sb}}{dt} - \phi_m \omega_r \sin\left(\theta - \frac{2\pi}{3}\right) \tag{3.18}$$

Stator current derivative can be evaluated from equations (3.17) and (3.18)

$$\frac{di_{sa}}{dt} = M_a = \frac{\begin{matrix} Kb_4 v_{sa} - Ka_4 v_{sb} - [Kb_4(R_s + Ka_1) - Ka_4 Kb_1] i_{sa} - [Ka_3 Kb_4 - Ka_4(R_s + Kb_3)] i_{sb} \\ + Kb_4 \phi_m \omega_r \sin\theta - Ka_4 \phi_m \omega_r \sin\left(\theta - \frac{2\pi}{3}\right) \end{matrix}}{Kb_4 Ka_2 - Ka_4 Kb_2} \tag{3.19}$$

$$\frac{di_{sb}}{dt} = M_b = \frac{\begin{matrix} Kb_2 v_{sa} - Ka_2 v_{sb} - [Kb_2(R_s + Ka_1) - Ka_2 Kb_1] i_{sa} - [Ka_3 Kb_2 - Ka_2(R_s + Kb_3)] i_{sb} \\ + Kb_2 \phi_m \omega_r \sin\theta - Ka_2 \phi_m \omega_r \sin\left(\theta - \frac{2\pi}{3}\right) \end{matrix}}{Kb_2 Ka_4 - Ka_2 Kb_4} \quad (3.20)$$

Here $\frac{di_{sa}}{dt}$ & $\frac{di_{sb}}{dt}$ are defined in terms of M_a & M_b

The stator winding current are calculated in discrete form using forward Euler's technique from equations (3.19) and (3.20)

$$i_{sa}(k) = M_a . T_s + i_{sa}(k-1) \quad (3.21)$$

$$i_{sb}(k) = M_b . T_s + i_{sb}(k-1) \quad (3.22)$$

$$i_{sa}(k) = -i_{sa}(k) - i_{sb}(k) \quad (3.23)$$

Electromagnetic torque is given as

$$T_e = \frac{1}{2}\frac{P}{2}\, i_{cab}^T \frac{\partial L_{abc}(\theta)}{\partial \theta}\, i_{abc} + \frac{1}{2}\frac{P}{2}\, i_{abc}^T \frac{\partial}{\partial \theta} \begin{bmatrix} \cos\theta \\ \cos\left(\theta - \frac{2\pi}{3}\right) \\ \cos\left(\theta + \frac{2\pi}{3}\right) \end{bmatrix} \quad (3.24)$$

Let $$N_1 = i_{abc}^T \frac{\partial L_{abc}(\theta)}{\partial \theta} i_{abc} \quad (3.25)$$

$$N_2 = i_{abc}^T \frac{\partial}{\partial \theta} \begin{bmatrix} \cos\theta \\ \cos\left(\theta - \frac{2\pi}{3}\right) \\ \cos\left(\theta + \frac{2\pi}{3}\right) \end{bmatrix} \quad (3.26)$$

Thus, electromagnetic torque is expressed as

$$T_e = \frac{P}{4}(N_1 + \phi_m N_2) \quad (3.27)$$

3.2.2. Modelling Equations of PMSM in d-q Rotating Reference Frame

The rotor reference axis forms an angle θ_r with the stationary stator axis at any given time *t*, and the rotating stator mmf forms an angle α with the rotor *d axis* [8]. Fig.3.1. shows schematic of two-pole PMSM.

The following assumption are made for the modelling of PMSM without damper windings: -

(1) Saturation is neglected.

(2) Nature of induced EMF should be sinusoidal.

(3) Eddy current and hysteresis losses are neglected.

(4) Field current dynamics are neglected.

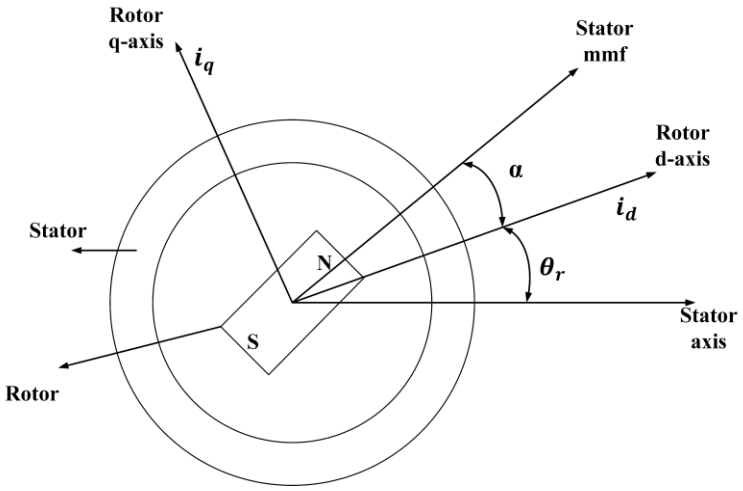

Fig.3.1. Schematic of two-pole PMSM

Modelling equation of voltages are given as: -

$$v_{sq} = R_s i_{sq} + \omega_r \phi_{sd} + \rho \phi_{sq} \tag{3.28}$$

$$v_{sd} = R_s i_{sd} - \omega_r \phi_{sq} + \rho \phi_{sd} \tag{3.29}$$

Flux linkages are given as:

$$\phi_{sq} = L_q i_{sq} \tag{3.30}$$

$$\phi_{sd} = L_d i_{sd} + \phi_m \tag{3.31}$$

By substituting equation (3.30) and (3.31) into equation (3.28) and (3.29)

$$v_{sq} = R_s i_{sq} + \omega_r (L_d i_{sd} + \phi_m) + \rho\, L_q i_{sq} \tag{3.32}$$

$$v_{sd} = R_s i_{sd} - \omega_r L_q i_{sq} + \rho (L_d i_{sd} + \phi_m) \tag{3.33}$$

Equations (3.32) and (3.33) are arranged as: -

$$\begin{bmatrix} v_{sq} \\ v_{sd} \end{bmatrix} = \begin{bmatrix} R_s + \rho L_q & \omega_r L_d \\ -\omega_r L_q & R_s + \rho L_d \end{bmatrix} \begin{bmatrix} i_{sq} \\ i_{sd} \end{bmatrix} + \begin{bmatrix} \omega_r \phi_m \\ \rho \phi_m \end{bmatrix} \quad (3.34)$$

The developed motor torque is expressed as follows:

$$T_e = \frac{3}{2}\left(\frac{P}{2}\right)\left(\phi_{sd} i_{sq} - \phi_{sq} i_{sd}\right) \quad (3.35)$$

The mechanical equation of the torque is given as:

$$T_e = T_l + B\omega_m + J\frac{d\omega_m}{dt} \quad (3.36)$$

Solved equation for rotor mechanical speed from equation (3.36) is,

$$\omega_m = \int \left(\frac{T_e - T_l - B\omega_m}{J}\right) dt \quad (3.37)$$

$$\omega_m = \frac{2}{P}\omega_r \quad (3.38)$$

3.2.3. Equivalent Circuit of PMSM

Equivalent circuit of the PMSM is derived from *d-q* modelling of motor using stator voltage.

The rotor flux in *d-axis* is represented by constant source, which is expressed as [3]:

$$\phi_m = L_d i_f \quad (3.39)$$

Fig.3.2. shows the equivalent circuit of PMSM

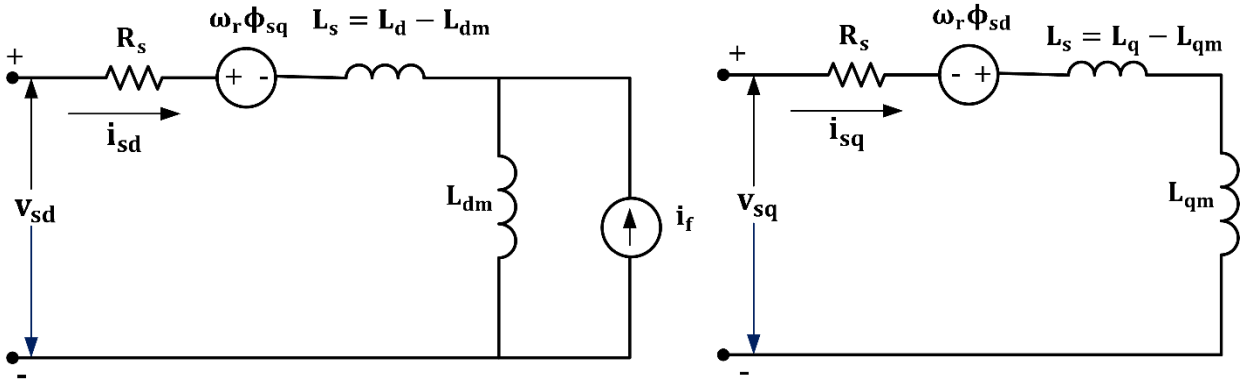

Fig.3.2. Equivalent Circuit of PMSM

3.2.4. Park's Transformation and Clark's Transformation

Previously, the voltage equations, flux linkage equations, and electromagnetic torque were used to describe the complex model of three phase AC machines. These variables are time varying in the model of PMSM. The dynamic model complexity can be reduced by Park's and Clark's Transformation as shown in Fig.3.3.

The mathematical model for Clark's Transformation is given as [134]

$$\begin{bmatrix} v_{s\alpha} \\ v_{s\beta} \\ v_0 \end{bmatrix} = k \begin{bmatrix} 1 & -1/2 & -1/2 \\ 0 & \sqrt{3}/2 & -\sqrt{3}/2 \\ 1/\sqrt{2} & 1/\sqrt{2} & 1/\sqrt{2} \end{bmatrix} \begin{bmatrix} v_{sa} \\ v_{sb} \\ v_{sc} \end{bmatrix} \tag{3.40}$$

Here k=2/3

Park Transformation is given as [135]

$$\begin{bmatrix} v_{sd} \\ v_{sq} \\ v_0 \end{bmatrix} = k \begin{bmatrix} cos\theta & \cos(\theta - 2\pi/3) & \cos(\theta - 2\pi/3) \\ sin\theta & \sin(\theta - 2\pi/3) & \sin(\theta - 2\pi/3) \\ 1/\sqrt{2} & 1/\sqrt{2} & 1/\sqrt{2} \end{bmatrix} \begin{bmatrix} v_{sa} \\ v_{sb} \\ v_{sc} \end{bmatrix} \tag{3.41}$$

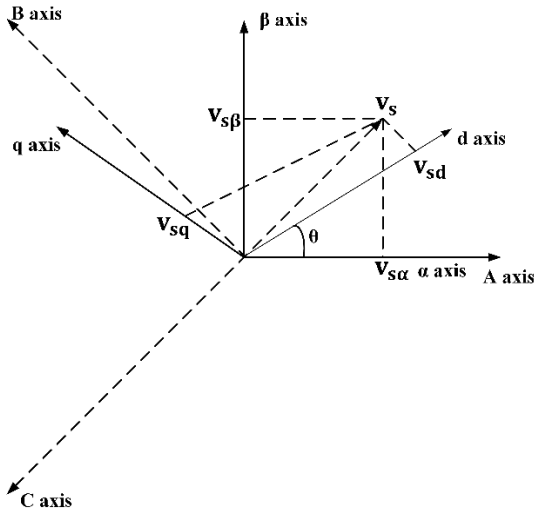

Fig.3.3. Different frames of reference

3.3. IMPLEMENTATION OF FIELD ORIENTED CONTROL FOR THE SPEED CONTROL OF PMSM DRIVE

Many applications, like factory automation and robotics, need accurate speed and position control. The drive system is designed by using a speed setting device, an inverter, a speed feedback system, a motor and a controller. The FOC technique aims to regulate the torque and magnetic field by adjusting the d and q components of the stator currents, and therefore the fluxes, respectively [136].

FOC of PMSM is obtained using the dynamic model and expressed as [8]

$$i_{sa} = I_s \sin(\omega_r t + \alpha) \tag{3.42}$$

$$i_{sb} = I_s \sin\left(\omega_r t + \alpha - \frac{2\pi}{3}\right) \tag{3.43}$$

$$i_{sc} = I_s \sin\left(\omega_r t + \alpha + \frac{2\pi}{3}\right) \tag{3.44}$$

Here α is defined as torque angle which is angle between phasor of stator current and rotor magnetic field.

The matrix equation of current using equations (3.42), (3.43), (3.44) is expressed as

$$\begin{bmatrix} i_{sa} \\ i_{sb} \\ i_{sc} \end{bmatrix} = \begin{bmatrix} \sin(\omega_r t + \alpha) \\ \sin\left(\omega_r t + \alpha - \frac{2\pi}{3}\right) \\ \sin\left(\omega_r t + \alpha + \frac{2\pi}{3}\right) \end{bmatrix} [I_s] \tag{3.45}$$

The stator currents calculated before is transformed in d and q components using Park's transformation with speed of the rotor ω_r. The stator current components in d and q will be fixed due to the fixed angle between rotor field and stator currents, α for a specified load torque. These components behave like the armature and field current of separately excited DC

machine. The torque generating component of the stator currents is the q axis current, whereas the flux generating component is the d axis current.

i_{sd} and i_{sq} currents are obtained from equations (3.41) and (3.45) in terms of I_s

$$\begin{bmatrix} i_{sd} \\ i_{sq} \end{bmatrix} = I_s \begin{bmatrix} \sin\alpha \\ \cos\alpha \end{bmatrix} \tag{3.46}$$

The electromagnetic torque is derived using equations (3.28), (3.29), (3.35) and (3.46) as

$$T_e = \frac{3}{2}\frac{P}{2}\left[\frac{1}{2}(L_d - L_q)I_s^2 \sin 2\alpha + \phi_m I_s \sin\alpha\right] \tag{3.47}$$

The torque of the motor depends on the type of rotor and inductance components in d and q axes, i.e. L_d, L_q. The rotor of the non-salient PMSM has surface mounted magnets, and the reluctance term is eliminated since L_d is equal to L_q. When permanent magnets are placed inside the rotor and the rotor saliency creates a difference in L_q and L_d, the reluctance component will also come into play in addition to the electromagnetic torque.

Most high-performance AC drives utilize current control methods for speed control of motor. The controller switches a VSI such that the motor stator currents follow a set of reference current waveforms [137]. The current controllers are classified into PWM and hysteresis controllers. PWM controllers are based on the principle of comparing a triangular wave of desired switching frequency with the error of controlled signal, where switching frequency is constant. In a hysteresis controller the current error is fed to a comparator having a hysteresis band and the switching frequency depends on the width of the hysteresis band.

In this section FOC of PMSM drive based on hysteresis current controller and Sinusoidal PWM (SPWM) current controller is described for the motor with ratings given in Appendix-1

A. Hysteresis current controller (HCC)

In high-performance vector-controlled drives, a current-control loop with a high bandwidth is required to (a) ensure accurate current tracking, (b) shorten the transient period as much as possible and (c) to force the VSI to work as a current source amplifier within the current loop bandwidth. Fig.3.4. shows the block diagram of a vector controlled PMSM Drive using HCC.

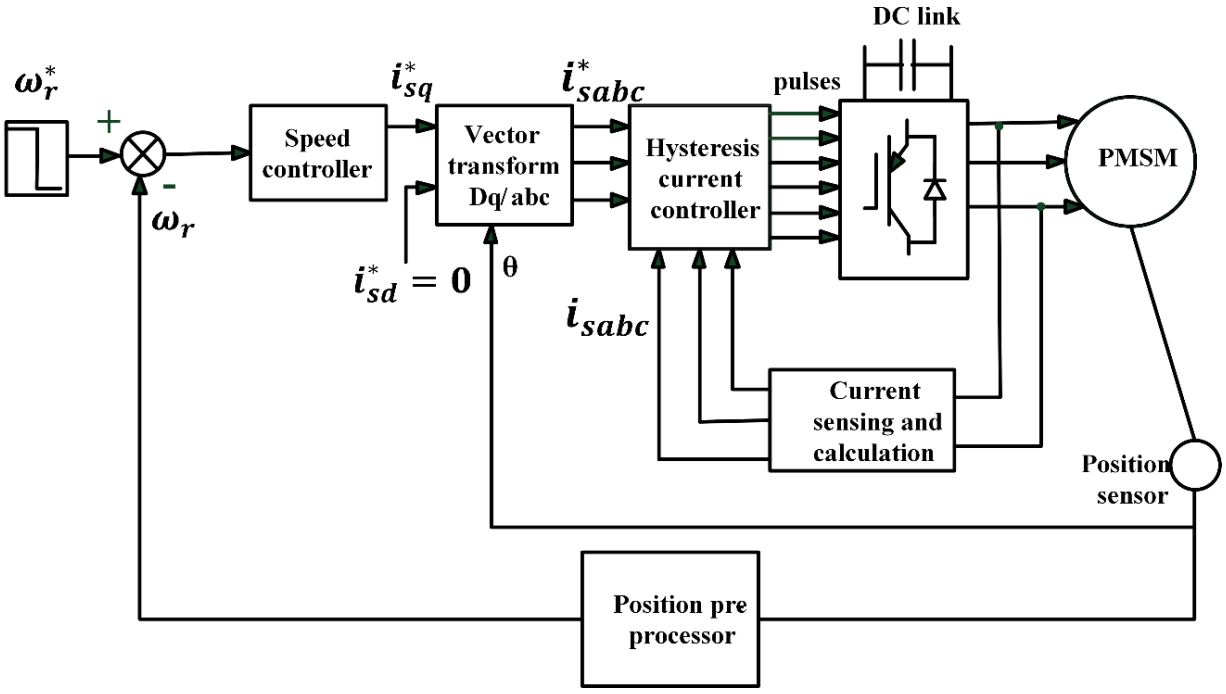

Fig.3.4. FOC of PMSM drive system with HCC

Hysteresis current control (HCC) may be employed so that a near-sinusoidal AC output current can be obtained while satisfying the torque or speed requirements [138], [139]. A hysteresis band controller is used to attain a regular switching frequency through comparison of actual stator current with desired reference current of motor while ensuring low harmonic content in stator current. The reference currents are generated by this controller with the inverter within a range fixed by width of the hysteresis band. The error between the desired current of a given phase (i_{sa}^*, i_{sb}^*, or i_{sc}^*) and the measured currents (i_{sa}, i_{sb}, i_{sc}) is fed to a comparator having a

hysteresis band. When this error exceeds the upper limit, a HIGH signal (i.e., 1‘) is generated, and when this error falls below the lower limit, a LOW signal (i.e., 0‘) is produced. This controller does not have specific switching frequency but it is related to the bandwidth and changes continuously. Speed controller calculates the error between the reference speed (ω_r^*) and the actual speed (ω_r), which is fed to the PI controller. The position feedback is obtained by a position encoder mounted on motor shaft.

B. Sinusoidal PWM (SPWM) controller

The switching signals for the inverter are generated by the SPWM controller. The state of these switching signals at any instant is determined by the rotor position, speed error and stator currents [140], [141]. The controller synchronizes the winding currents with rotor position. It has the advantage of smaller output ripple current for a given switching frequency in comparison to the hysteresis current controller. Fig.3.5. shows the block diagram of PMSM drive using SPWM controller.

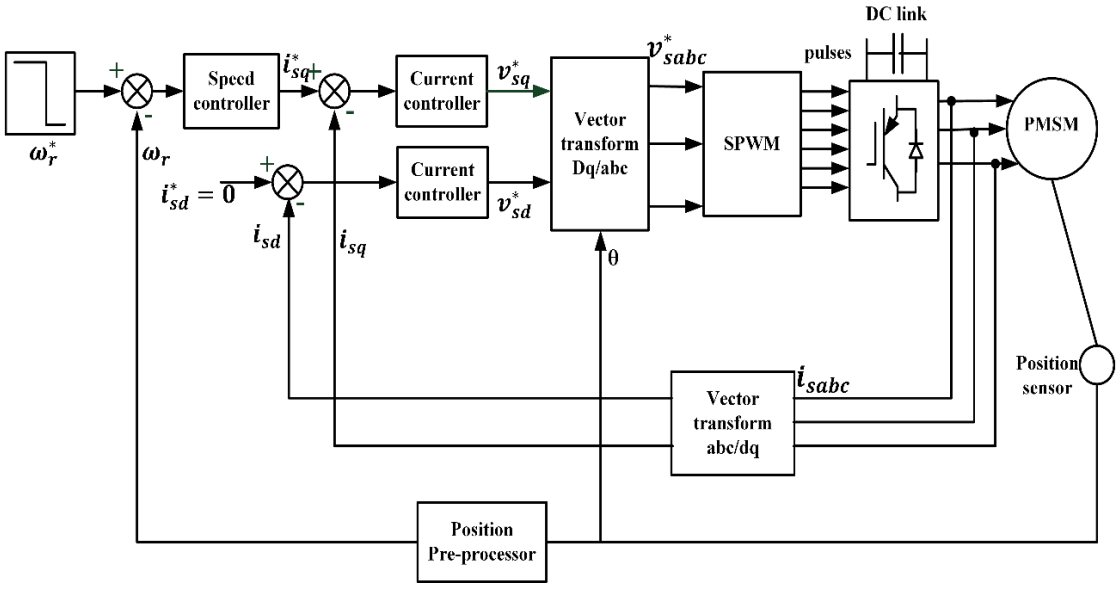

Fig.3.5. PMSM drive system with SPWM controller

The currents (i_{sa}, i_{sb}, i_{sc}) are measured with the current sensors and are transformed into dq axis currents for the decoupling of air gap flux which is fed to the current controllers. The controller output is given for the vector transformation from *d-q axes* currents into desired voltage of a given phase (v_{sa}^*, v_{sb}^*, or v_{sc}^*). Now the desired voltage fed into SPWM which gives the pulses to turn on the inverter VSI and output of inverter is given to the motor. Speed of the motor is sensed through the position sensor and fed into the speed controller.

3.4. DESIGN AND DEVELOPMENT OF LABORATORY PROTOTYPE OF PMSM DRIVE

The schematic layout and the experimental setup of PMSM drive developed for research studies is shown in Fig. 3.6 (a) and (b). It consists of 380V, 3.4kW, 8 pole, 3000rpm PMSM.

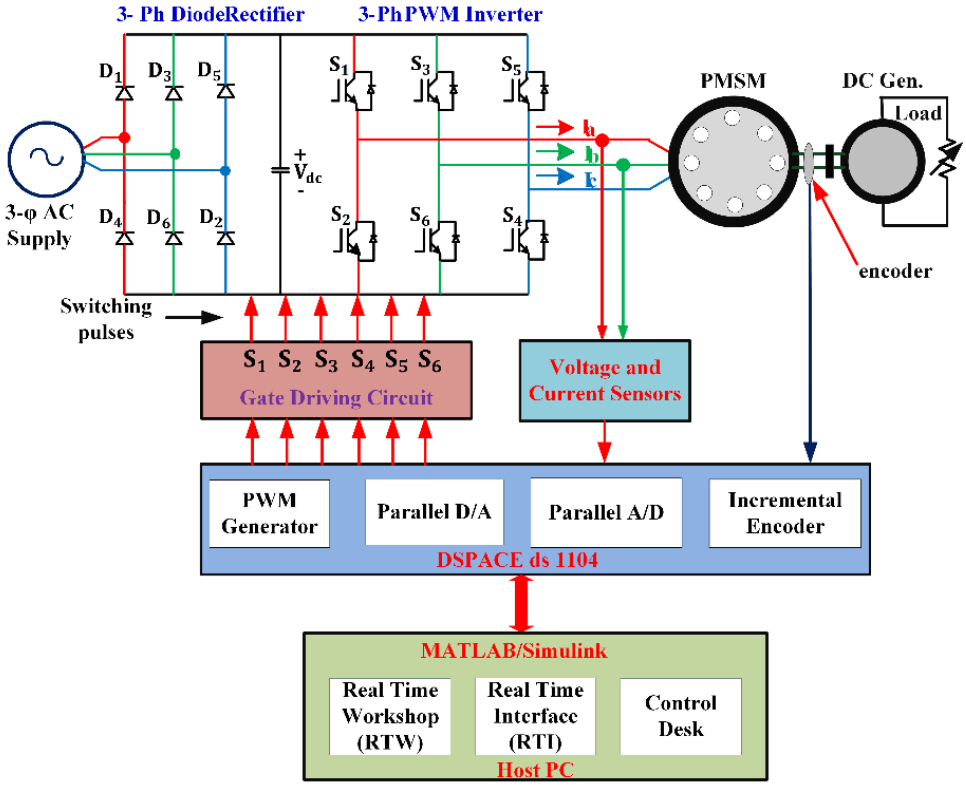

(a)

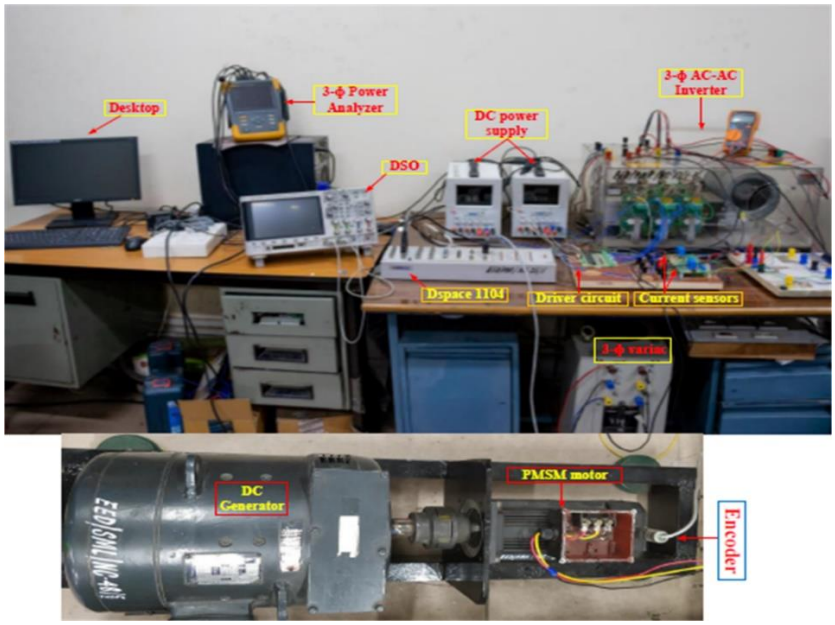

(b)

Fig.3.6. Experimental setup of PMSM Drive: (a) Schematic Layout (b) Laboratory Prototype

The major components used to develop the laboratory prototype are given below: -

1. Inverter as power module
2. Interfacing Unit
3. Measurement Unit consisting of Encoder for measuring rotor position, Current sensors and Voltage sensors

3.4.1. Inverter as power module

A 3-phase diode rectifier and 3-phase inverter are used as power module [142], [143]. The inverter is equipped with six number of high-speed, low-loss IGBTs, as well as an optimized gate drive and a protection circuit. It has an IGBT-based power module with a rating of 1200V and a current of 25A that receives gate pulses from DSP / dSPACE 1104 controller board.

3.4.2. DSP based dSPACE DS 1104

Both hardware and software are built-in in the dSPACE device, which is based on the DS1104 R&D controller board. It is intended for high-speed multivariable digital control and real-time simulation applications, that can be conveniently installed in a computer's PCI port. It is a real-time controller with a 603 PowerPC floating point processor. For advanced I/O, the board has a slave-DSP subsystem based on the TMS320F240 DSP. Rapid Control Prototyping (RCP) is enabled by the presence of unique connectors on the board, which allow access to both input and output signals. The DS1104 is the perfect hardware for developing cost-sensitive RCP applications.

In dSPACE, RTI blocks link the simulation model of controllers the hardware-implemented controller boards. Control Desk is a software that allows users to run tests, change parameters / operating points online and visualise the signal profiles.

3.4.2.1. Hardware

In dSPACE there are some other output and input connectors such as ADCs and DACs. Table.3.1 lists detailed parameters of the DS1104 controller board.

Table.3.1. Parameters of dSPACE DS 1104 Controller Board

Parameter	Description/value
Processor	• CPU (250MHz) • 33 MHz on chip PCI bridge • Floating point processor • On chip cache (2X16 KB) • MPC8240 with PPC603e core and on-chip peripherals

Parameter	Description/value
Interrupt Controller	• Two Incremental encoder index line interrupts • One Slave DSP PWM interrupt • One UART interrupt • Five timer interrupts • One slave DSP interrupt • One host interrupt • Five ADC end of conversion interrupts • Four user interrupts from the I/O connector
Memory	• 32 MB SDROM global memory • 8 MB flash memory
Power consumption	18.5 W
Power Supply	• +5 V± 5 %, 2.5 A • +12 V± 5 %, 0.3 A • -12 V± 5 %, 0.2 A
Size	185 X 106.68 mm
Cooling	Fan
Temperature	$0\text{-}55^{0}$C
Host Interface	• PCI slot (5V) • 33 MHz ± 5% • PCI host interface (32-bit)

Parameter	Description/value
Serial Interface	• 1 UART • RS232/RS422/RS485 mode selectable transceiver RS232 mode max baud rate (115.2 kBaud) • RS422/RS485 max baud rate (1 MBaud)
ADC with MUX (1 X 16 bit)	• ±10V input voltage • Four channels with one 16-bit sample and hold ADC [05 ADCs (1X16-bit+ 4X12-bit)] • resolution (16-bit) • conversion time (2μs) • off-set error (±5 mV) • gain error (±0.25%) • signal-to-noise ratio(>80 db)
ADC (4 X 12-bit)	• ±10V input voltage • Four channels with one 12-bit sample and hold ADC • resolution (12-bit) • conversion time (8 ns) • off-set error (±5 mV) • gain error (±0.25%)
DAC (8 X 16-bit)	• ±10V output voltage • resolution (16-bit) • maximum output current (±5 mA)

Parameter	Description/value
	• off-set error (±1 mV) • gain error (±0.1%) • signal-to-noise ratio(>80 db)
Slave DSP	• TI TMS320F240 DSP processor (16-bit) • clock-frequency (20 MHz) • external program memory (64k X 16) • external data memory (28k X 16) • dual port memory for communication (4k X 16) • flash memory (16k X 16) • 1 X 3-phase PWM outputs • 4 X 1-phase PWM outputs • Four Capture inputs
Digital Incremental Encoder Interface (2 X 24 bit)	• Two channels • Selectable single-ended (TTL) or differential (RS422) input • Max input frequency (1.65 MHz) • position counter (24-bit) • Reset on index • sensor supply voltage(5V/0.5A)
Digital I/O	• 20-bit parallel I/O • Single bit selectable from input or output

Parameter	Description/value
	• maximum output current (±5 mA) • TTL output/input levels

3.4.2.2. Software

In the past, assembly language was used for control software development. In recent years, industries have begun to follow a platform-based method called Real-Time Workshop (RTW) and MATLAB/SIMULINK models of controller or devices, which offers an efficient approach for developing software control. Fig.3.7 shows a platform of dSPACE for real time applications which consists of the following major components: -

- MATLAB is a popular interactive tool for modelling, simulations, and conception of real-time systems. It includes over 600 mathematical functions and supports additional toolboxes to make it more versatile.
- MATLAB has an additional software called SIMULINK that allows modelling and analysis of linear, nonlinear and hybrid structures using block diagrams.
- RTW is a tool in SIMULINK that is used to generate C or ADA code from the SIMULINK model.
- RTI is the software of dSPACE that supports libraries for DS1104 R&D controller board, I/O hardware integration and generates optimized code for the board's master and slave processors.
- The control desk software of dSPACE is used for interfacing with real-time experimental setups, allowing for simple and scalable analysis, visualization, control, data acquisition and automation.

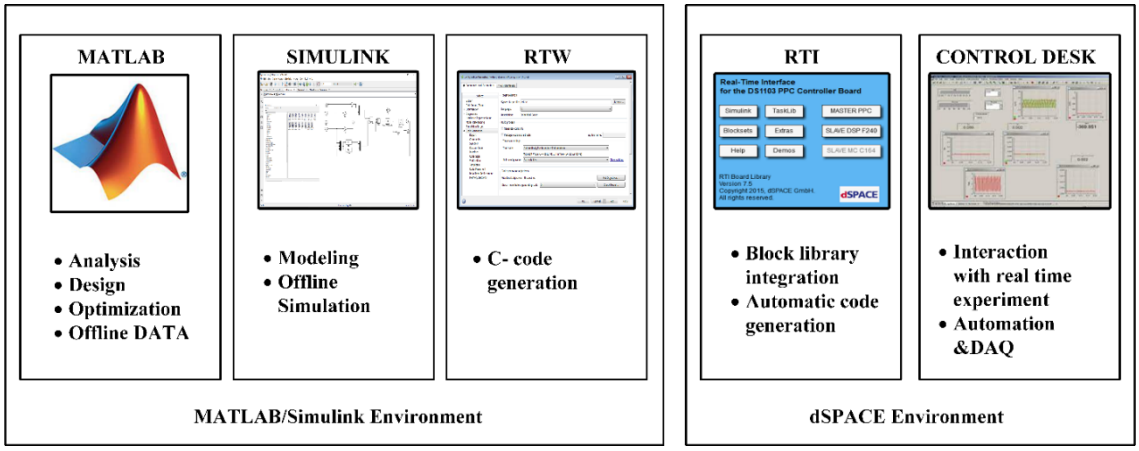

Fig.3.7. dSPACE platform for real time applications

The ADC channels are used to feed sensed currents and voltages to the dSPACE. The ADC or master bit I/O blocks are added to the SIMULINK model by dragging from the library of dSPACE and dropping to the SIMULINK model of PMSM drive. The model is connected to six master bit I/Os designed in output mode for defining six gating signals to the IGBT based inverter. A total of eight ADCs are attached to the model, providing the inputs to the DSP such as input voltage and motor phase currents.

In balanced three phase system the requirement of sensors can be reduced by using two electrical quantities and calculating the corresponding value for the third phase. The automatic generation of real-time code that can be implemented on system hardware is crucial. The RTI module in dSPACE performs this role for dSPACE-based systems. It automatically generates real-time code from SIMULINK models using RTW from Mathworks® and implements this code on dSPACE real-time prototype hardware. It saves a lot of time and effort because the MATLAB SIMULINK model does not need to be manually converted to another language like C. The RTI completes the required steps, which only require the SIMULINK model to be updated with the mandatory dSPACE blocks.

3.4.3. Measurement Unit

The measurement of various parameters, such as the input AC voltage to the motor, stator currents, and rotor position information given by the encoder attached to shaft of the motor are required for accurate and reliable close-loop operation of the drive. The measurement circuit must be precise, have galvanic isolation from the power supply and respond linearly to its input (voltage or current). To meet the above requirement of sensing circuits, hall-effect sensors and isolation amplifiers were used.

3.4.3.1. Voltage Sensor Circuit

Two voltage sensors are used to sense three phase input voltages fed to PMSM from output terminals of inverter. The LEM make LV-20-P [144] hall sensor is used to sense voltage using voltage sensor circuit. The output of voltage sensor circuit is in the form of current and it is directly proportional to input voltage. The output current is supplied to a measuring resistance, which produces an equivalent voltage of the input voltage. The output voltage is limited to 10V by an operational amplifier (op-amp)-based signal conditioning circuit [145] according to voltage limit of ADCs of the dSPACE controller. Figs.3.8 (a) and (b) shows the circuit diagram and printed circuit board (PCB) of voltage sensor.

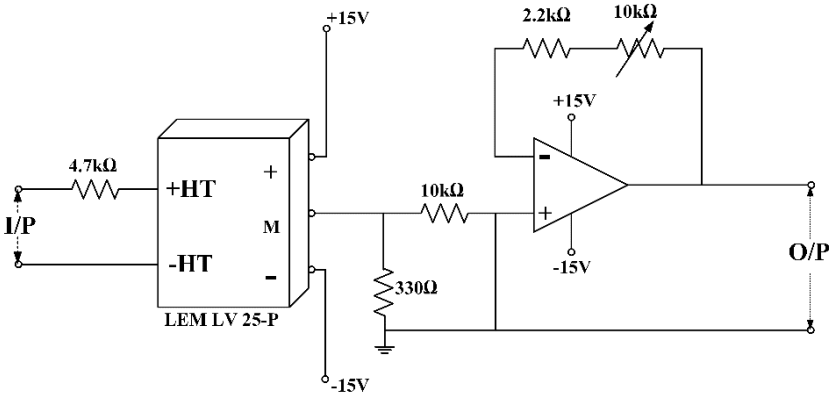

(a)

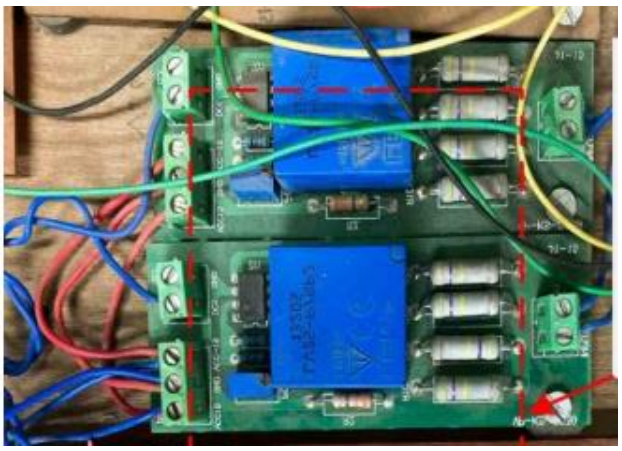

(b)

Fig.3.8. Voltage sensor: (a) Circuit; (b) PCB

3.4.3.2. Current Sensor Circuit

The currents are sensed using a Hall Effect current sensor (LEM LA 55-P) [146]. Instantaneous performance, excellent accuracy and linearity, optimum response time, large frequency bandwidth, no insertion losses, insensitivity to external interference and current overload capability are some of the characteristics. Current at the output of the sensor is directly proportional to current sensed at the input. The galvanic separation between the high power primary circuit and secondary electronic circuits is also provided by this sensor. The circuit shown in Figs.3.9. (a) and (b) is used to process its output.

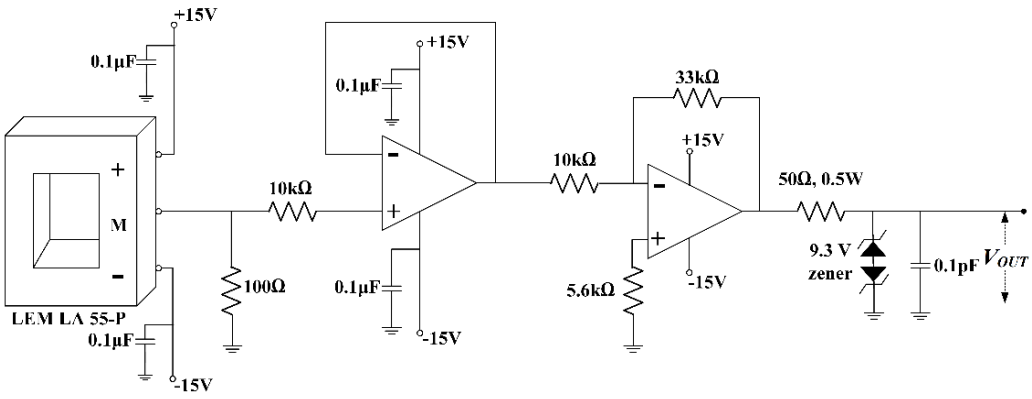

(a)

(b)

Fig.3.9. Current Sensor: (a) Circuit diagram; (b) PCB

This sensor circuit is designed to keep the output voltage within the safe range of ADC channels for input currents up to 25 A. The zener diodes are connected in anti–parallel way to limit the output current so that it cannot exceed the input current.

3.4.3.3. Position Sensors

Generally, resolvers and incremental encoders are used to sense the rotor position in PMSM. These sensors are mounted on the shaft of the motor. The PMSM used in this work is designed with incremental encoder connected to the shaft of the motor. Hollow type Autonics made E40H encoder is used as shown in Fig.3.10.

Fig.3.10. Incremental Encoder

The specification of this encoder is given in Table.3.2.

Table.3.2. Specification of Incremental Encoder (E40H12-1000-6-L-5)

Item	Description/Value
Resolution(P/R)	1000
Output Phase	A, B, Z (Line Driver $A, \overline{A}, B, \overline{B}, Z, \overline{Z}$ phase)
Phase difference of the output	Phase difference between A and B: $\frac{T}{4} \pm \frac{T}{8}$ (T=1cycle of Phase-A)
Control output	• Low –load current: Max. 20mA, residual voltage: Max. 0.5V dc • High- load current: -20mA, output voltage: Min: 2.5V dc
Maximum response frequency	300kHz
Power supply	5V DC±5%
Current Consumption	50mA
Insulation resistance	Min 100MΩ
Dielectric strength	750VAC 50/60Hz for 1 min
Connection	Cable type
Starting torque	0.005Nm
Moment of inertia	40×10^{-6} kg.m^2
Maximum allowable revolution	5000rpm
Vibration	300 m/s^2 at frequency of 10 to55Hz
Ambient temperature	-10 to 70^{o}C

Item	Description/Value
Protection	IP50 (IEC standard)

3.4.3.4. Design of amplifier and isolation circuit for gate driver of inverter

The gate driver of IGBT module are isolated from real time controller by using opto-coupler ICs (i.e. 6N136/6N137/6N139) based isolated gating circuit [147]. The controller produces 5V switching pulses while the voltage required for switching of gate driver is 15V. As a result, the voltage of gate pulses must be amplified to 15 V [148]. Figs.3.11 (a) and (b) show the circuit diagram and designed PCB of the Amplifier and Isolation Circuit.

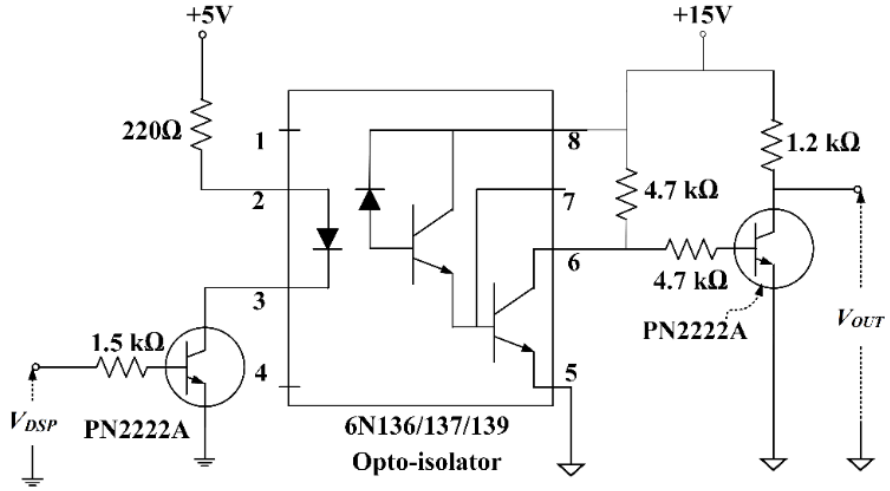

(a)

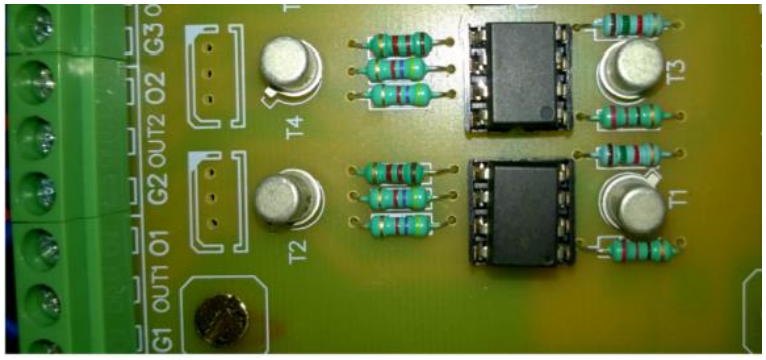

(b)

Fig.3.11. Amplifier and Isolation Circuit: (a) Circuit Diagram; (b) PCB

3.5. SIMULATION STUDIES OF PMSM DRIVE

Field oriented control of PMSM drive is modelled and simulated using MATLAB/Simulink. The performance analysis of field-oriented control of PMSM drive is carried out by using hysteresis current controller and PWM current controller. The dynamic performance of PMSM under constant torque operation for different operating conditions is analysed using the aforesaid two different controllers and the results are compared. For simulation study, the three phase 3.4 kW, 3000 rpm surface mounted PMSM with ratings given in Appendix-1 has been used.

3.5.1. Dynamic Performance of PMSM Drive with HCC for step change in load torque at rated speed operation and speed reversal

Fig.3.12. shows the performance of the drive for a step change in load torque for rated speed operation. The drive is started at rated speed of 314 rad/sec under no load and the motor tracks the speed smoothly. At t = 0.06 sec a load of 11Nm is applied. The motor speed does not change and stator current increases proportional to the load change.

Fig.3.13 shows the simulation results of field-oriented control of PMSM drive based on hysteresis current controller for a step change in speed and load torque along with speed reversal. The drive is started at rated speed of 314rad/sec under no load condition. Motor produces high stator current to develop the required starting torque. When the motor reaches the steady state speed the magnitude of stator current reduces. The load is increased to rated torque of 11 Nm at 0.06 sec. To meet the load requirement, the quadrature axis current increases proportionally as shown in Fig.3.13, with no perturbations in speed. At constant torque operation direct axis current is zero and quadrature axis current is proportional to load

torque. At 0.1 sec speed is changed from 314 rad/sec to -314 rad/sec, the motor tracks the speed without any under or over shoot and there is no change in current at steady state.

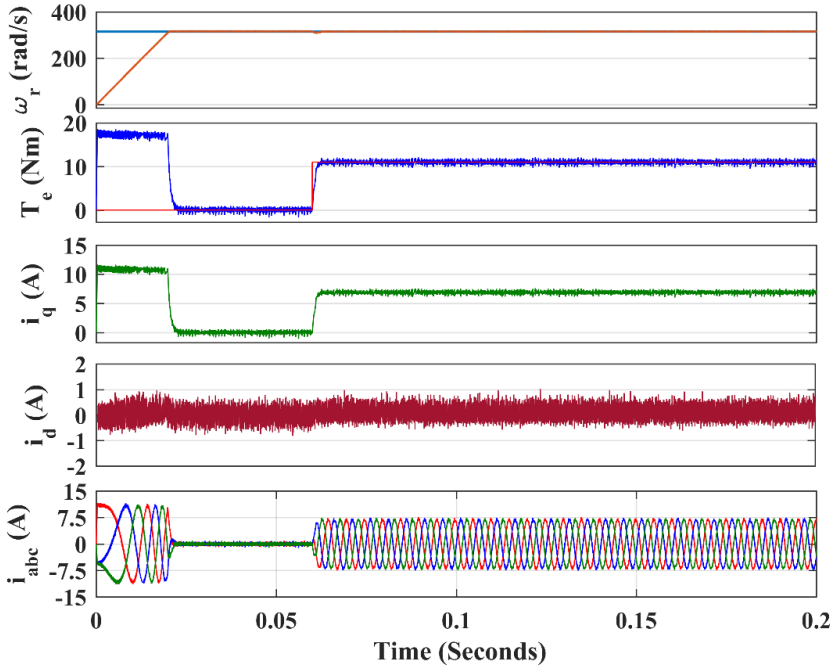

Fig.3.12. FOC of PMSM Drive with HCC for step change in load.

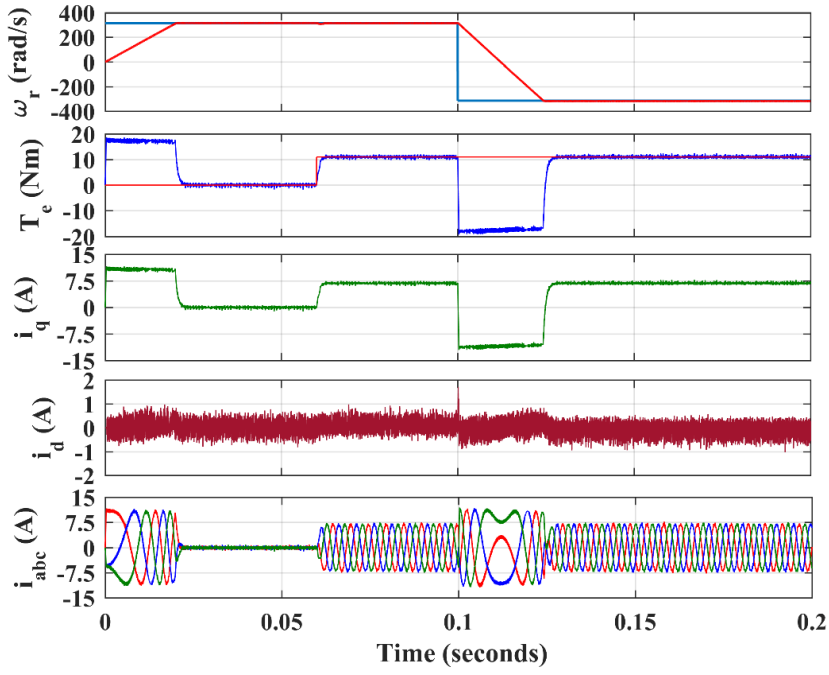

Fig.3.13. FOC of PMSM Drive with HCC for step change in speed and torque.

3.5.2. Dynamic Performance of PMSM Drive with SPWM for step change in load torque at rated speed operation and speed reversal

Fig.3.14, shows the dynamic response of the PMSM Drive with SPWM when speed and load torque is increased suddenly. The drive is started with a reference speed of 314 rad/sec with zero load torque. At t = 0.06 s, when load is increased to 11 Nm, there is no change in the speed. This demonstrates speed regulation features of the drive. Also, the torque developed by the motor increases to 11 Nm, which satisfy the load torque requirement with proportional increase in stator current. This shows complete decoupled control of speed and torque.

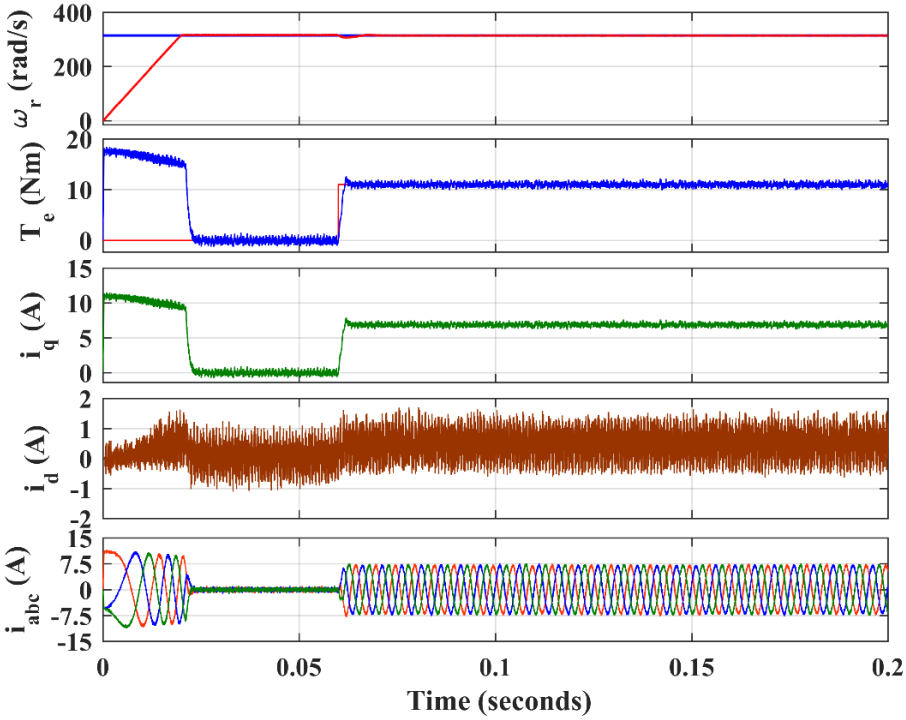

Fig.3.14. FOC of PMSM Drive with SPWM controller for step change in load.

Fig.3.15. shows the simulated dynamic response of the PMSM drive with SPWM for a sudden speed reversal from 314 rad/sec to -314 rad/sec. The actual speed of the motor closely follows the set speed. Initially, the drive is started at rated speed of 314 rad/sec under no load condition. The load is increased to the rated torque o 11 Nm at t =0.06 s but there is no change in speed.

Similarly, when the reference speed is changed from 314 rad/sec to -314 rad/ sec at t = 0.1s with the same constant load of 11 Nm, it is observed that with the change in speed, torque and stator current does not change.

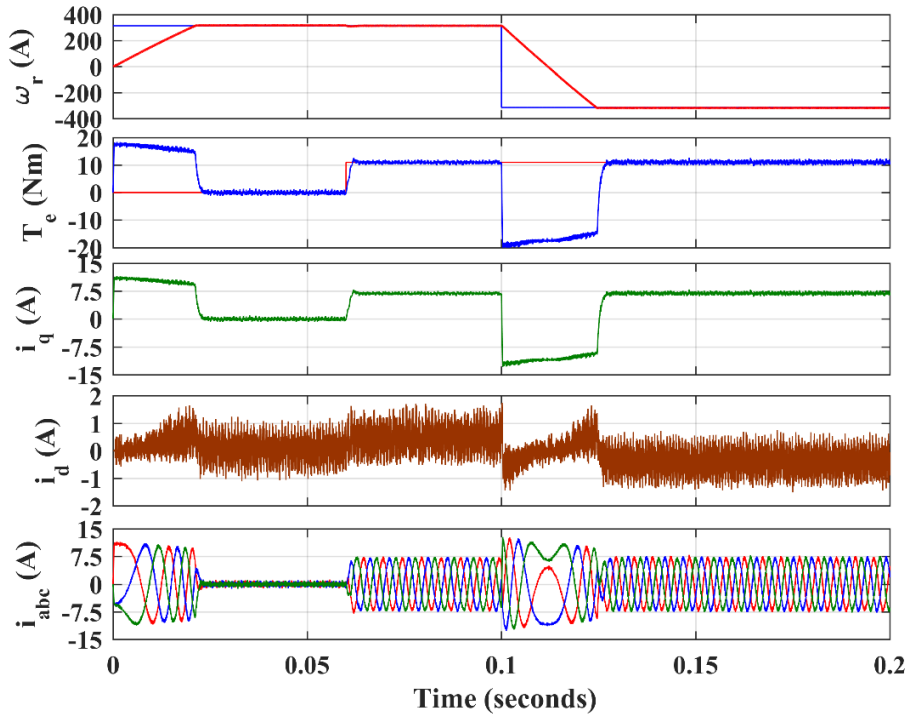

Fig.3.15. FOC of PMSM Drive with SPWM controller for step change in speed and torque.

3.6. EXPERIMENTAL RESULTS

In this section performance of PMSM drive is analysed with experimental study. The output performance of vector control of PMSM drive at no load is presented.

Figs.3.16 (a) and (b) show the steady state waveform of stator currents i_a, i_b, i_c obtained through simulation studies and experimental implementation. It can be seen that the experimental results of stator currents validate simulation studies.

Figs.3.17 (a) and (b) show the steady state characteristics of speed (ω_r), stator current (i_a) and rotor position (θ_r) at speed of 1500 rpm under no load condition obtain through simulation

studies and experimental implementation. The experimental results of drive validate the simulation results effectively.

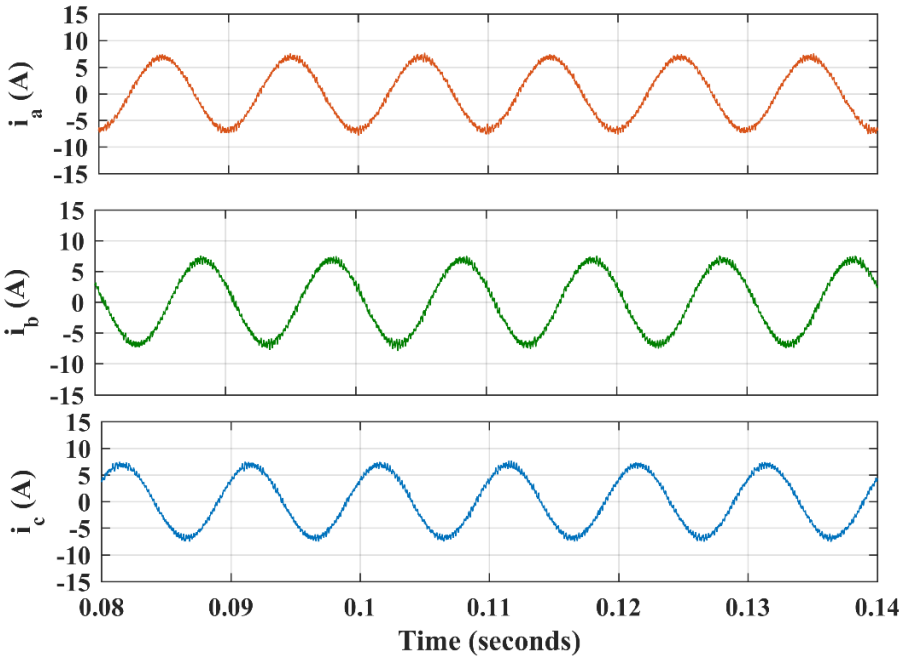

(a)

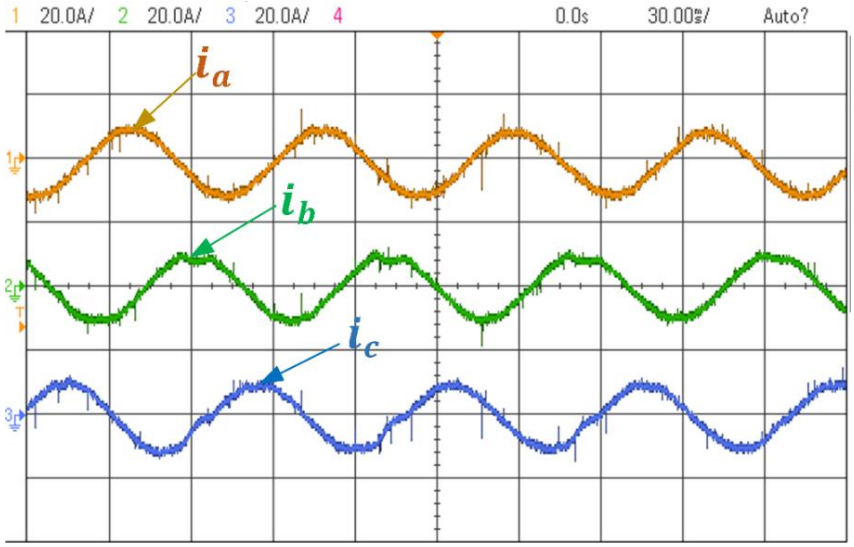

(b)

Fig.3.16. Stator currents of PMSM drives: (a) Simulation Studies (b) Experimental Implementation

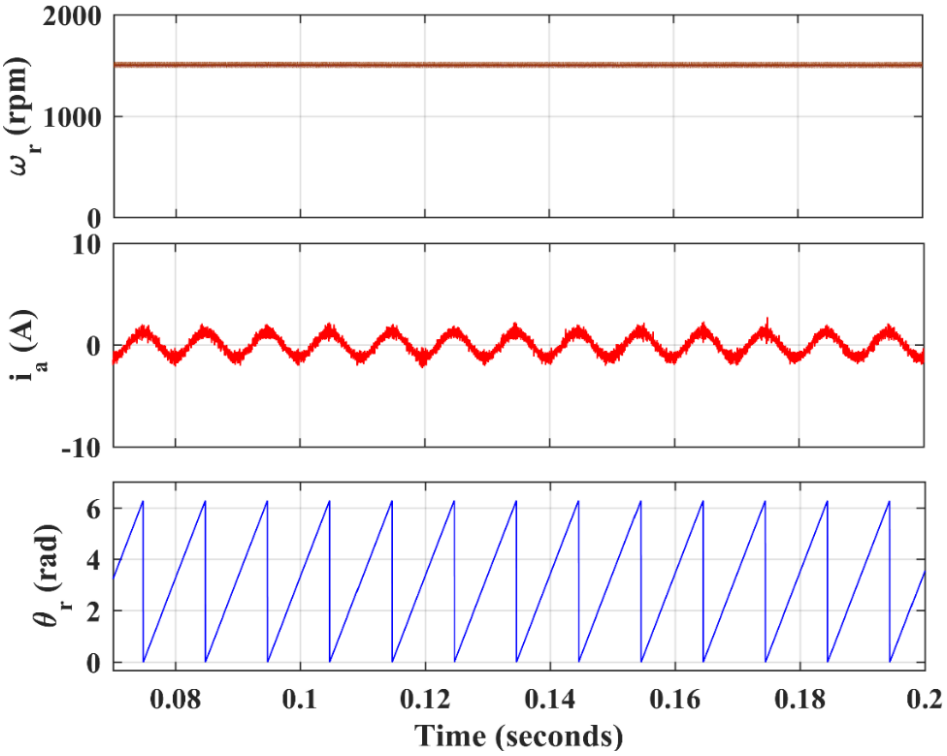

(a)

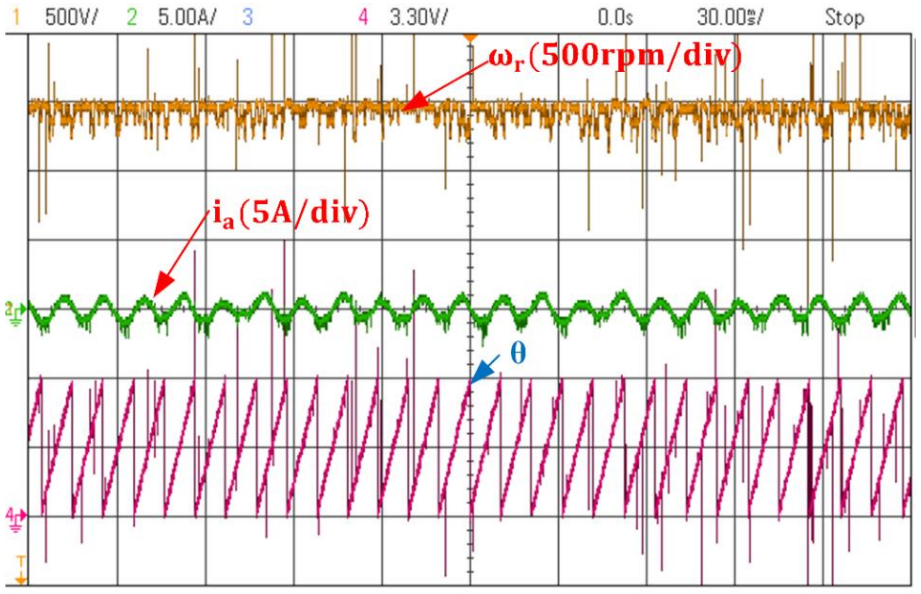

(b)

Fig.3.17. Speed, current and rotor position of PMSM drives at no load: (a) Simulation Studies (b) Experimental implementation

Figs. 3.18 (a) and (b) show steady state characteristics of speed and rotor position at low speed of 300rpm at no load obtain through simulation studies and experimental implementation and it is found that experimental results verify the simulation results.

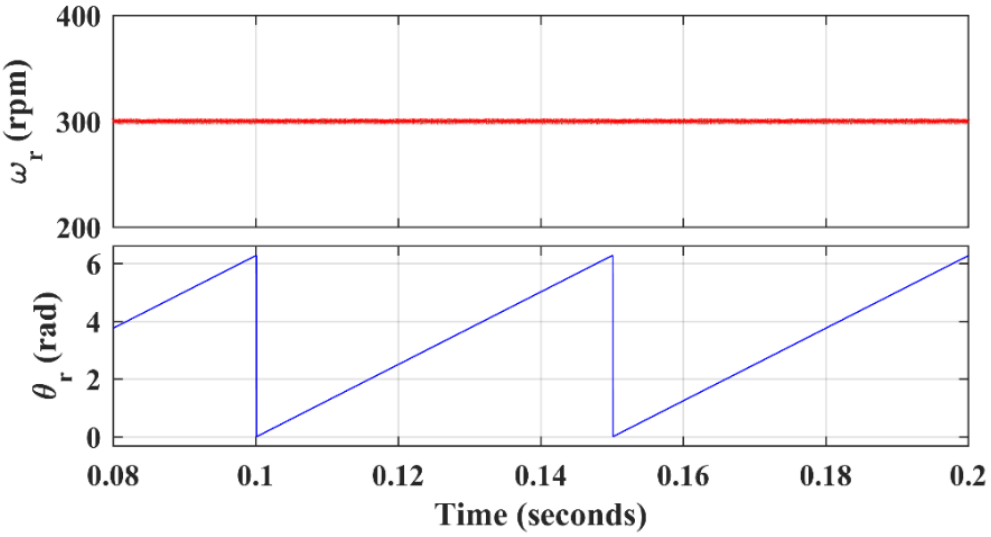

(a)

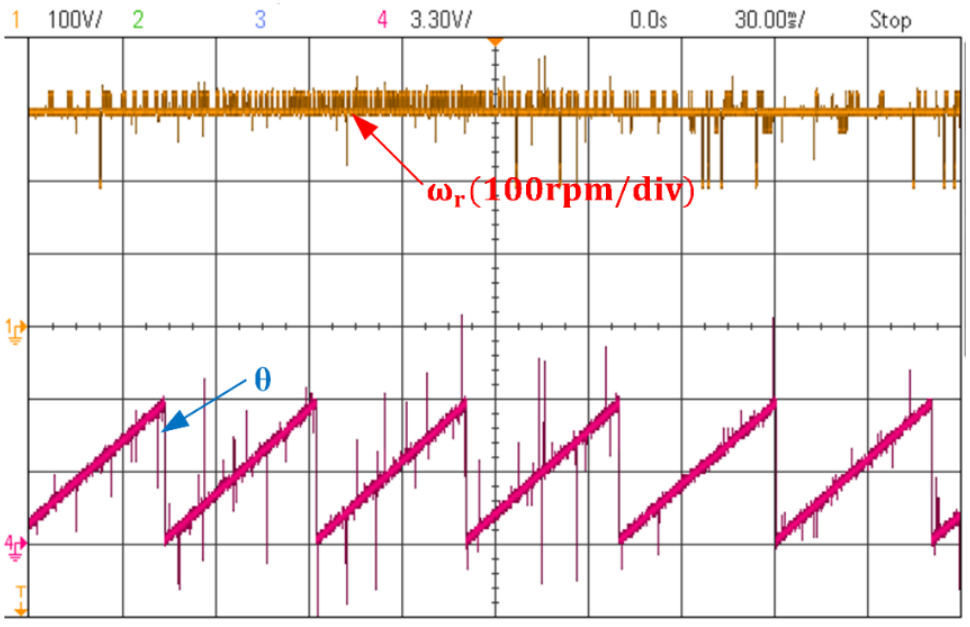

(b)

Fig.3.18. Speed, rotor position waveform of PMSM drive for low-speed operation: (a) simulation studies (b) experimental implementation

Fig.3.19. shows the output voltage waveform of inverter and current i_c. Here it can be seen that current i_c follow its corresponding voltage v_c accurately.

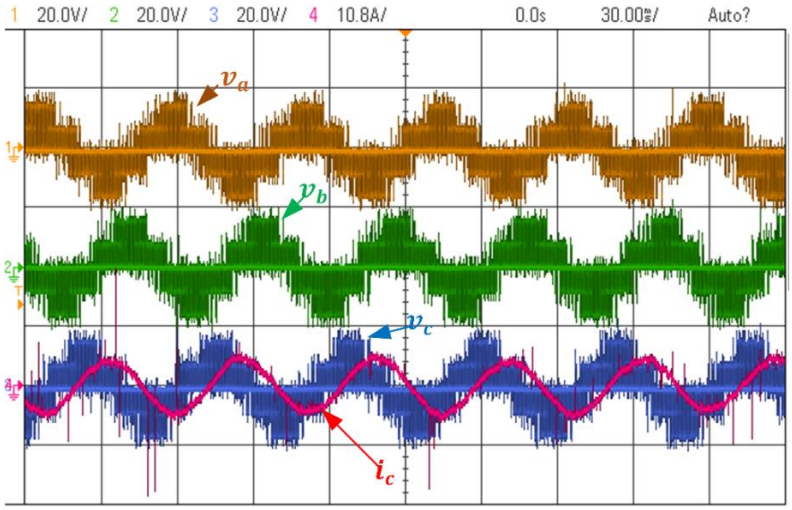

Fig.3.19. Voltage waveform of inverter

3.7. CONCLUSION

In this chapter, the modelling of PMSM is presented in two frames of reference, i.e., stationary frame of reference and rotating frame of reference. The reference frame is chosen according to the requirement of control. FOC of PMSM is developed in MATLAB/Simulink and the performance of PMSM drive is examined using simulation analysis for HCC and SPWM controller at different operating speed with step change in the load torque.

The design and development of laboratory prototype for PMSM drive is also described in this chapter. The control algorithm developed in MATLAB/Simulink are realized in real-time using dSPACE DS1104 controller. The laboratory prototype consisting of three phase auto-transformer, a PMSM with encoder, a three-phase IGBT based inverter, voltage and current sensing circuit and interfacing circuits are designed, developed and integrated with dSPACE. Experimental results are also presented in steady state condition in this chapter to validate the simulation results.

CHAPTER 4

DESIGN AND IMPLEMENTATION OF IMPROVED ANFIS BASED MRAC OBSERVER FOR SENSOR-LESS CONTROL OF PMSM

4.1. GENERAL

Nowadays, AC motors are widely used for industrial, robotic and automobile applications in comparison to DC motors due to their better efficiency, small size for the same power output and low maintenance. However, the control of AC motor is more complex than that of DC motor. IM and PMSM are the most widely used AC motors. PMSMs are preferred in industrial applications over IM, due to their better reliability, compactness, higher power density and higher efficiency [149], [150], [26], [151]. However, for efficient control of PMSM it is essential to know the rotor position, which can either be obtained using resolvers / encoders or estimated using the measured stator currents and back emf. Position sensors like resolver and encoder are mounted on the motor shaft, which results in reduced reliability due to sensitivity to vibration, high temperature, noise. This also in-creases the volume, weight and cost of the machine. These issues can be addressed by estimation of the rotor position rather than using resolvers / encoders. The reported methods for sensor-less control of PMSM drives include: 1) flux linkage and back-emf based estimation of rotor position [152], [153] ; 2) high frequency (HF) signal injection for tracking the rotor saliency [80], [154] and 3) nonlinear state observer-based estimation of rotor position and speed [155]. Based on these categories many established

algorithms are used to estimate the rotor position and motor speed in PMSM drives [156], [157], [158].

The back-EMF based method is generally employed for medium to high-speed operation of the PMSM drive; while HF signal injection method is used for low operation. In HF signal injection method, the position of the rotor is obtained by analysing the injected HF signal. The observer-based sliding mode observer techniques are easy to implement and immune to parametric variations but often results in the chattering problem. MRAC based observer is a direct control approach, which can effectively manage any systems with parametric variations using two models, viz- reference model and adjustable model. An adaptive mechanism is used to adjust the motor parameters continuously. While adjustable model depends on unknown parameter, reference model is not parameter dependent. The error signal of two models is applied to an adaptive mechanism to estimate unknown quantities which tunes the adjustable model. Adaptive control is widely used for both the linear and nonlinear systems. However, the estimation of unknown quantities of the motor in nonlinear system is complex to implement.

In this Chapter[2,3], an improved ANFIS-based MRAC technique is proposed to solve these problems related to uncertain parameters and input saturation [159], [160]. In the proposed method, the adaptive model and mechanism to minimize the stator current error are replaced by ANFIS controller. In the architecture of ANFIS, fuzzy has the ability to handle uncertainties

[2] **Paper Published**: Suryakant, Mini Sreejeth and Madhusudan Singh, 'Improved ANFIS Based MRAC Observer for Sensorless Control of PMSM'. Journal of Intelligent & Fuzzy Systems, vol. Pre-press, No. Pre-press, pp. 1-13, 11 May 2021, DOI: 10.3233/JIFS-189772.

[3] **Paper Published**: Suryakant, M. Sreejeth and M. Singh, "Sensorless control of PMSM Drive with BEMF based MRAC Algorithm," 2019 International Symposium on Advanced Electrical and Communication Technologies (ISAECT),Rome, 2019, pp. 1-6, doi: 10.1109/ISAECT47714.2019.9069705.

and artificial neural network (ANN) has the ability to learn from the process. An adaptive model of PMSM is developed using ANFIS at undefined operating conditions, which automatically compensates for variations in resistance, inductance etc. The PMSM drive is modelled using the rotating reference frame. This mitigates the issues associated with adaptive control in estimating PMSM's rotor position with unknown parameters. The novelties of the proposed improved ANFIS based MRAC observer include: -

- Performance of the proposed observer is improved by using adaptive normalization method to normalize the inputs and output data extracted from the PI controller, which is further applied to reduce the error of two models to fine tune the membership function near the desired speed.
- The PI controller is replaced by an improved ANFIS controller.
- It focuses on the effect of load variation on the speed response in terms of settling time, rise time and overshoot.

The proposed improved ANFIS based MRAC observer is investigated through simulation studies using MATLAB/Simulink for sensor-less speed control of PMSM drive over a wide varying operating condition. The performance of drive with the proposed MRAC is also demonstrated for low-speed operation at low load torque.

4.2. DYNAMIC MODELLING OF PMSM IN D-Q COORDINATES

The modelling equations of PMSM as described in Chapter 3 are used to estimate the rotor position for speed and torque control of the drive. The PMSM is modelled in the d-q rotating reference frame. For easy readability, relevant equations are reproduced herein. The load torque, T_L is defined in terms of T_e , mechanical speed (ω_m) , inertia constant (J) and damping coefficient (B) as:

$$T_L = T_e - B\omega_m - J\frac{d\omega_m}{dt} \quad (4.1)$$

The mechanical speed of the motor is given by

$$\omega_m = \frac{1}{J}\int (T_e - T_L - B\omega_m)dt \quad (4.2)$$

The rotor electrical speed, ω_r and rotor position, θ are:

$$\omega_r = \frac{P}{2}\omega_m \quad (4.3)$$

$$\theta = \int \omega_m \, dt \quad (4.4)$$

Fig.4.1. shows the block diagram of PMSM Drive with improved ANFIS based MRAC observer.

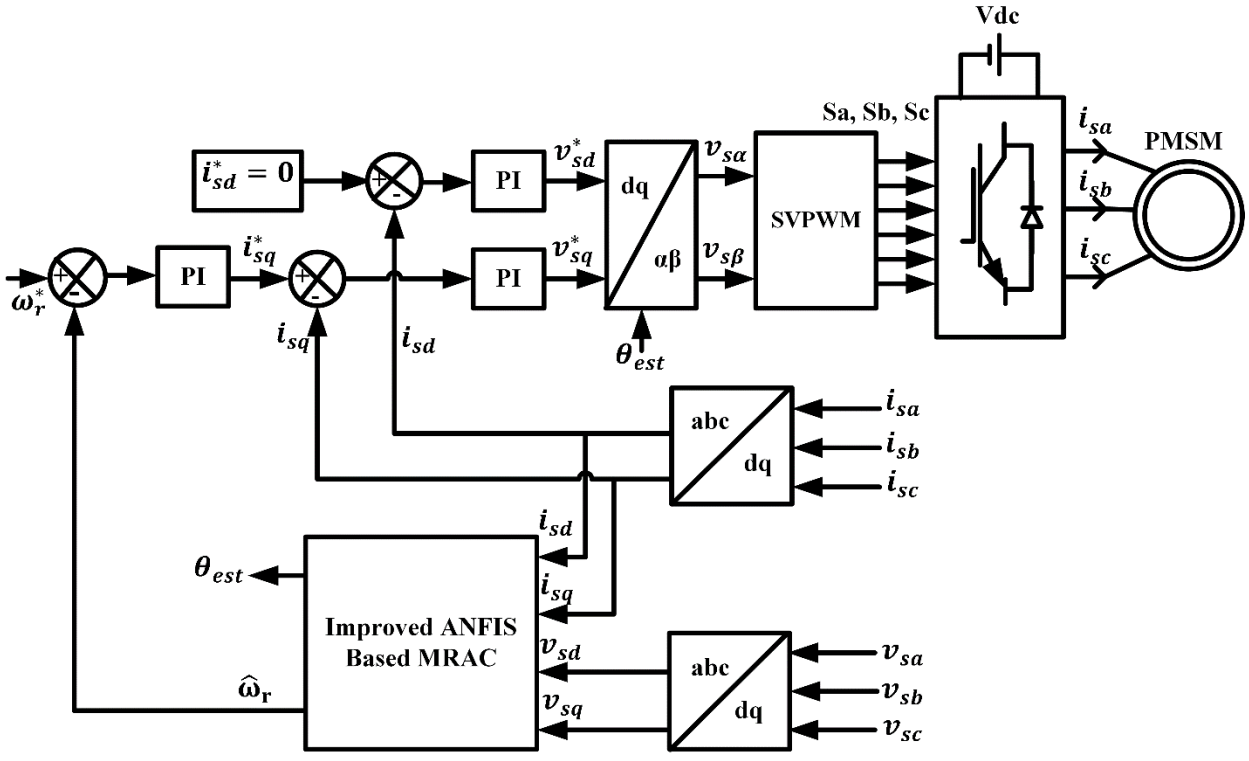

Fig.4.1. Block diagram of PMSM Drive with Improved ANFIS based MRAC Observer

It includes an improved ANFIS based MRAC observer with space vector PWM (SVPWM) and a speed controller in outer loop and two current controllers in inner loop. The speed and

rotor position are estimated through the proposed observer using eqns. (4.2) to (4.4). The measured terminal voltage and current are transformed into the d-q axes using vector transformation. The PWM pulses are generated by SVPWM and fed to VSI which produces the necessary stator voltage for the operation of PMSM.

4.3. DESIGN OF IMPROVED ANFIS BASED MRAC OBSERVER

The rotor position and speed of the PMSM are effectively estimated through MRAC based observer. Figs. 4.2. (a) and (b) show the conventional MRAC based observer and improved ANFIS based MRAC observer used for sensor less control of the PMSM. In MRAC based observers the reference model is derived from PMSM model and adjustable model is derived from stator winding currents, which is regulated by estimated value of speed [161],[162],[163]. In the conventional MRAC adjustable model is regulated by a PI controller used in the adaptive mechanism; while in the proposed method, the adjustable model is regulated by the improved ANFIS based adaptive mechanism.

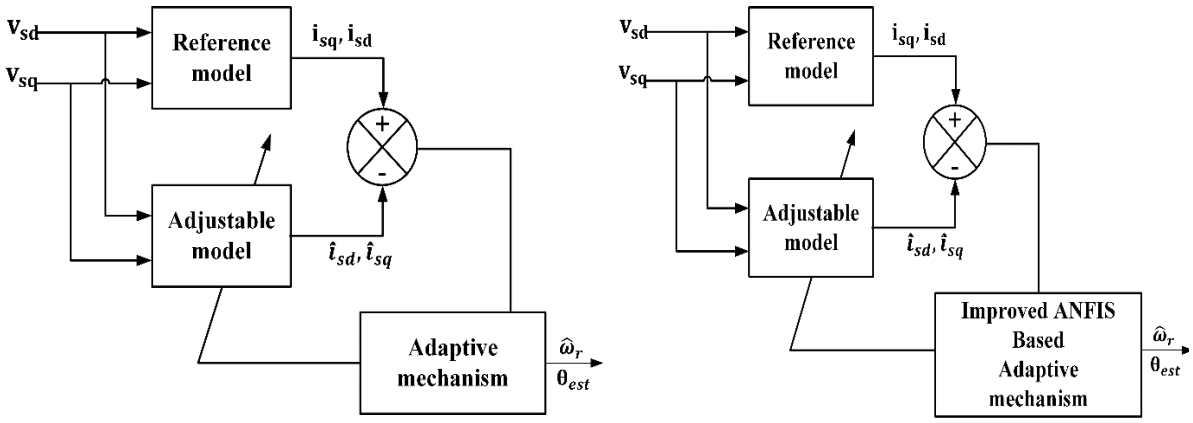

Fig.4.2. Block diagram of: (a) Conventional MRAC (b) Improved ANFIS based MRAC

Adjustable model is derived with the help of stator current equation. Speed error is continuously monitored for negative feedback to ensure system stability.

The stator current equation of PMSM is given as

$$\frac{di_{sd}}{dt} = -\frac{R_s}{L_s} i_{sd} + \omega_r i_{sq} + \frac{v_{sd}}{L_s} \tag{4.5}$$

$$\frac{di_{sq}}{dt} = -\frac{R_s}{L_s} i_{sq} - \omega_r i_{sd} - \frac{\phi_m}{L_s} \omega_r + \frac{v_{sq}}{L_s} \tag{4.6}$$

The equations (4.5) & (4.6) can be expressed as

$$\rho \begin{bmatrix} i'_{sd} \\ i'_{sq} \end{bmatrix} = \begin{bmatrix} -\frac{R_s}{L_s} & \omega_r \\ -\omega_r & -\frac{R_s}{L_s} \end{bmatrix} \begin{bmatrix} i'_{sd} \\ i'_{sq} \end{bmatrix} + \frac{1}{L_s} \begin{bmatrix} v'_{sd} \\ v'_{sq} \end{bmatrix} \tag{4.7}$$

Where $i'_{sd} = i_{sd} + \frac{\phi_m}{L_s}$, $i'_{sq} = i_{sq}$, $v'_{sd} = v_{sd} + \frac{R_s \phi_m}{L_s}$ and $v'_{sq} = v_{sq}$

The speed of the motor is estimated using MRAC with PI controller and expressed as

$$\widehat{\omega}_r = \left(K_p + \frac{K_i}{s}\right) \left[i_{sd} \hat{\imath}_{sq} - i_{sq} \hat{\imath}_{sd} - \frac{\phi_m}{L_s} \left(i_{sq} - \hat{\imath}_{sq} \right) \right] \tag{4.8}$$

Replacing the conventional adjustable model and adaptive mechanism by improved adjustable model and ANFIS based adaptive mechanism mitigates parameter uncertainties. The ANFIS strategy is based of Takagi-Sugeno (TS) system. The rules are defined in linguistic forms hence transitional results can be evaluated and understood easily [164], [165]. The rules can be changed during training and optimization process. The data set required for training of the ANFIS learning is the I/O data pairs of the defined system. The broad outline of the architecture of the ANFIS controller involves the i) defining of fuzzy inference systems; ii) defining of training data set and checking the data sets; iii) defining number of data pairs; iv) defining number of epochs; and v) Learning from the results. The architecture of ANFIS is given in Fig.4.3. It is similar to the fuzzy inference system, expect for the neural network block.

The input of proposed ANFIS controller is given as

$$e(k) = i_s - \hat{i}_s = \begin{bmatrix} i_d - \hat{i}_{sd} \\ i_q - \hat{i}_{sq} \end{bmatrix} \quad (4.9)$$

$$\Delta e(k) = e(k) - e(k-1) \quad (4.10)$$

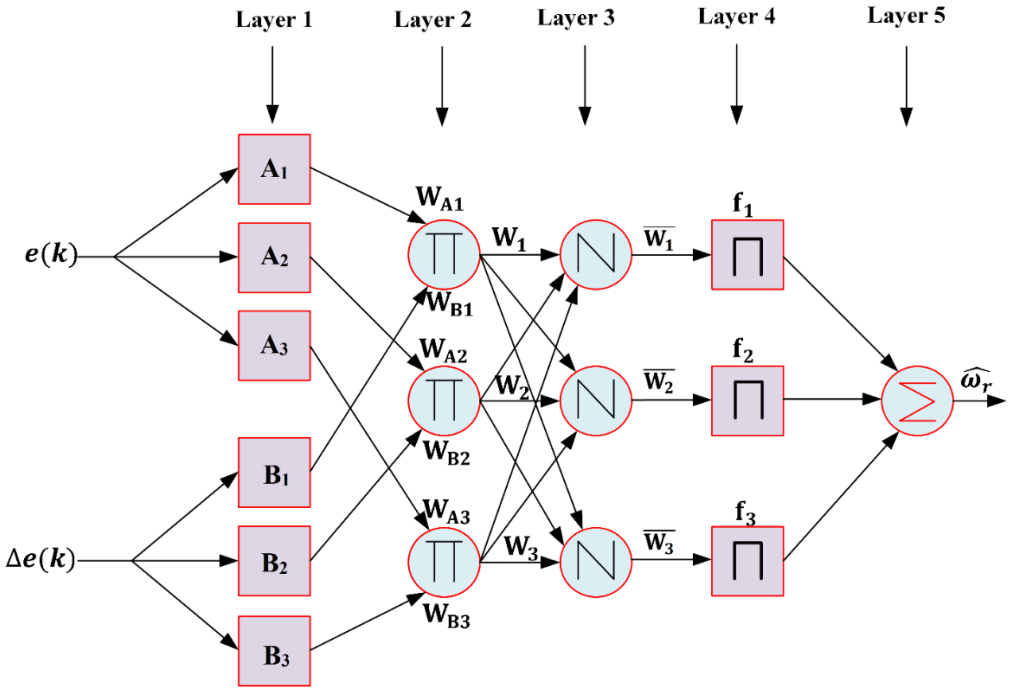

Fig.4.3. Architecture of improved ANFIS

It is structured in five layers linked to each other and termed as follows:

- **Layer 1:** It is defined as the input layer consisting input variables. In this layer triangular membership function are used and input variables are delivered to the next layer at every node.
- **Layer 2:** It is defined as membership function (MF) layer in which the weights of every membership function can be checked. It accepts the input variables from the input layer and determined the MFs for the corresponding input variable's fuzzy sets. It also calculates the membership values in order to identify the degree of the respective input value that is transferred to the next layer to determine the input of that layer.

- **Layer 3:** Every neuron matches the required necessary conditions of fuzzy rules in this layer. The number of layers is equal to number of fuzzy rules and the normalized weights are estimated by each node of these layers. It is called rule layer.
- **Layer 4:** This layer is termed as the defuzzification layer, which generates output values based on application of rules. Links between layers 3 and layer 4 is weighted by the fuzzy singletons that characterizes another set of parameters for the neuro-fuzzy network.
- **Layer 5:** It combines all deliverable inputs from defuzzification layer and converts the fuzzy sets into a crisp value. It is called the output layer.

The improved ANFIS controller employs the backpropagation method, which is automatically adjusted using the least square estimation technique. The gradient descent method is used to update the weight in the backpropagation method, which offers advantages of identifying the global minimum of the cost function, low computing complexity and quick convergence [166], [167].

Fig.4.4. shows the flow chart of proposed MRAC observer, which summarizes how the proposed observer is designed to estimate the motor speed and rotor position.

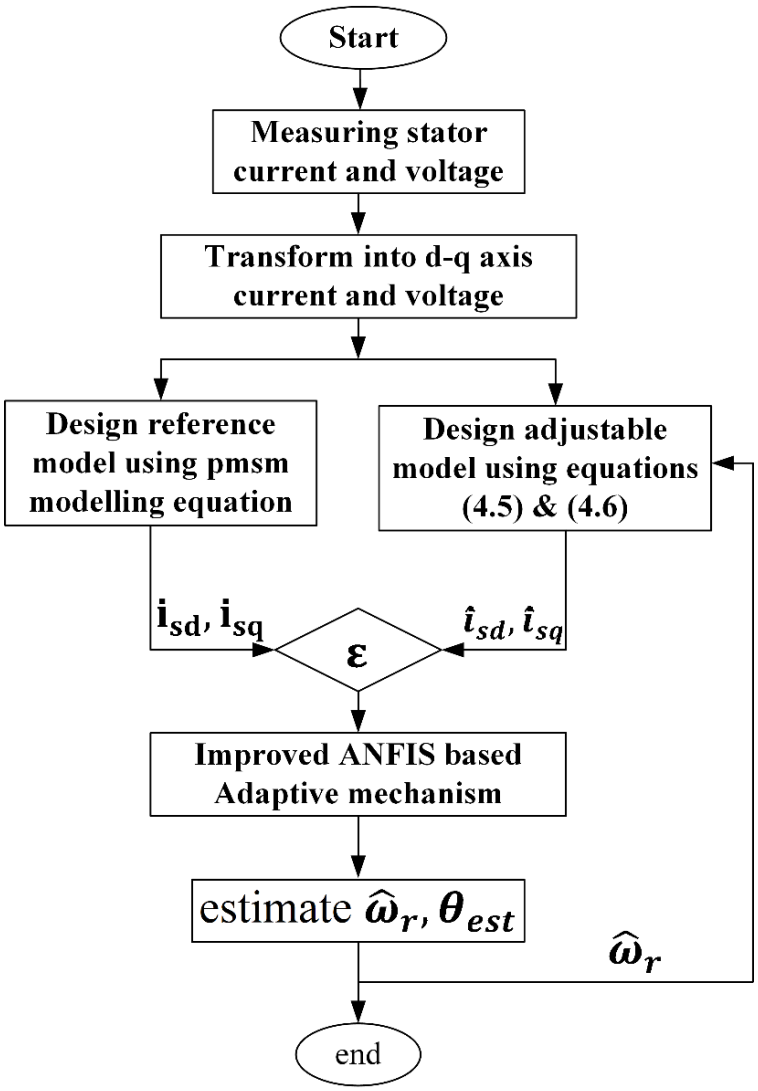

Fig.4.4. Flow chart of proposed Improved ANFIS based MRAC Observer

4.4. BASIC PRINCIPLE OF SVPWM

SVPWM method of PWM generation is the most prevalent among all the methods of PWM generation as it provides better utilization DC voltage, V_{dc} and is easy for implementation in the digital domain [168], [169], [170], [171]. Compared to SPWM, the SVPWM technique has a smaller harmonic present in winding current which reduces the torque ripples. The output voltages of the inverters are represented as space vectors. The spatial position of the three phase voltages (v_{an}, v_{bn} and v_{cn}) fed to the stator windings, determines the magnitude and position

of the space vector, v. The axis and the length of their coordinates define the voltage vectors direction.

$$v = v_{an} + v_{bn} + v_{cn} \tag{4.11}$$

Fig.4.5 shows the block diagram of the VSI. The SVPWM consists of 6 active inverter switching states which are defined as (100) $\overrightarrow{V_1}$, (110) $\overrightarrow{V_2}$, (010) $\overrightarrow{V_3}$, (001) $\overrightarrow{V_4}$, (011) $\overrightarrow{V_5}$, (101) $\overrightarrow{V_6}$ and two null voltage vectors which are defined as (000) $\overrightarrow{V_0}$, (111) $\overrightarrow{V_7}$. When the status is '1', the switch is on and when the status is '0', the switch is off.

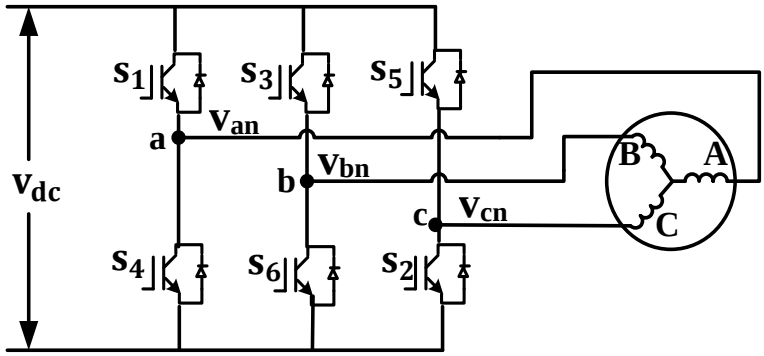

Fig.4.5. Block diagram of a VSI

Fig.4.6 shows the corresponding space vectors. The active voltage vectors are spaced apart with a phase angle of 60° and null vectors are situated at the zero. The required voltage vector can be situated in any of the six sectors, which make a hexagon. The reference voltage vector. V_{ref}, is created by null vector at operating time T_K and adjacent vector at operating times, T_{K+1} , in the sector where V_{ref} resides. At any given sampling instance, the duration of the active vectors and null vectors should follow the volt-sec balance, T_S. The SVPWM input should be in the α-β reference coordinates, so that the voltage components v_{sd}^* and v_{sq}^* can converted into $V_{s\propto}$ and $V_{s\beta}$ using inverse park transformation.

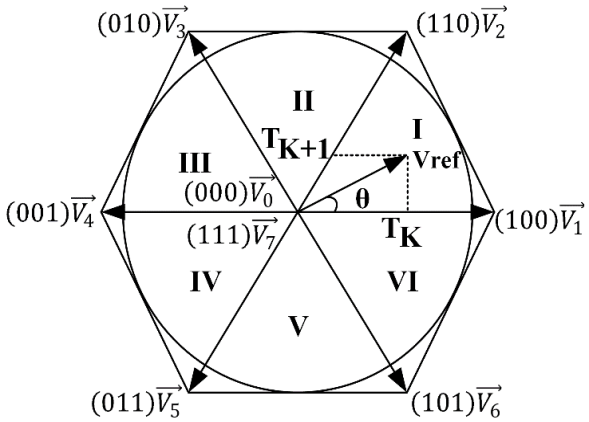

Fig.4.6. Space voltage vectors

This is executed in four steps as given below:

Step-I. Sector selection

The Sector, N, is selected based on the relationship between $V_{\propto}$ and V_{β} in each sector as:

$$\begin{bmatrix} V_{ref1} \\ V_{ref2} \\ V_{ref3} \end{bmatrix} = \frac{1}{2} \begin{bmatrix} 2V_{s\beta} \\ -V_{s\beta} + \sqrt{3}V_{s\alpha} \\ -V_{s\beta} - \sqrt{3}V_{s\alpha} \end{bmatrix} \tag{4.12}$$

$$\begin{cases} V_{ref1} > 0 \; ; \; A = 1 \\ V_{ref2} > 0 \; ; \; B = 1 \\ V_{ref3} > 0 \; ; \; C = 1 \end{cases} \tag{4.13}$$

The sector, N in which the voltage vector lies is determined by the relationship:

$$\mathrm{N} = \mathrm{A} + 2\mathrm{B} + 4\mathrm{C} \tag{4.14}$$

Step-II. Calculation of vector switching time

The operating time, X, Y and Z of respective voltage in current sector $\mathrm{T_K}$ and $\mathrm{T_{K+1}}$ are calculated as follows:

$$\begin{bmatrix} X \\ Y \\ Z \end{bmatrix} = \frac{\sqrt{3}}{2V_{dc}} T \begin{bmatrix} 2V_{s\beta} \\ \left(\sqrt{3}V_{s\alpha} + V_{s\beta}\right) \\ \left(-\sqrt{3}V_{s\alpha} + V_{s\beta}\right) \end{bmatrix} \tag{4.15}$$

where, T is the total switching period. The operating time can be found from Table.4.1.

Table.4.1. Evolution of $\boldsymbol{T_K}$ and $\boldsymbol{T_{K+1}}$

Sector	**I**	**II**	**III**	**IV**	**V**	**VI**
$\boldsymbol{T_K}$	-z	y	x	z	-y	-x
$\boldsymbol{T_{K+1}}$	x	z	-y	-x	-z	y

The mathematical addition of T_K and T_{K+1} should be less than the total switching period T. If the sum is greater than zero, it is revised as:

$$T_K = \frac{T_K\, T}{T_{\mathrm{K}}+T_{K+1}} \tag{4.16}$$

$$T_{\mathrm{K+1}} = \frac{T_{\mathrm{K+1}}\, T}{T_K+T_{\mathrm{K+1}}} \tag{4.17}$$

Step-III. Identifying the vector switching points

By using symmetrical PWM arrangement the voltage vectors are switched and the switching points can be evaluated as below:

$$\begin{bmatrix} T_a \\ T_b \\ T_c \end{bmatrix} = \begin{bmatrix} \frac{1}{4}(T - T_K - T_{K+1}) \\ T_a + \frac{1}{2}T_K \\ T_b + \frac{1}{2}T_{\mathrm{K+1}} \end{bmatrix} \tag{4.18}$$

Table.4.2 defines the switching points T_{sp1} , T_{sp2} and T_{sp3}.

Table.4.2. Vector Switching Points

Vector switching points	Sector I	II	III	IV	V	VI
T_{sp1}	T_a	T_b	T_c	T_c	T_b	T_a
T_{sp2}	T_b	T_a	T_a	T_b	T_c	T_c
T_{sp3}	T_c	T_c	T_b	T_a	T_a	T_b

Step-IV. Generation of the PWM signal

T_{sp1} , T_{sp2} and T_{sp3} are compared with repeating sequence wave with different frequencies to generate the PWM signals PWM_1, PWM_3 and PWM_5. PWM_4, PWM_6 and PWM_2 are the compliments of PWM_1, PWM_3 and PWM_5 respectively.

4.5. RESULTS AND DISCUSSIONS

A 3-phase 3.4kW, 314rad/s vector controlled PMSM drive, with specifications given in Appendix-I, is modelled and simulated in MATLAB/Simulink. The drive performance is studied and examined under various operating conditions using the conventional MRAC observer and the improved ANFIS based MRAC observer. For simulation studies the sampling time is set at 10μ sec.

4.5.1. Dynamic characteristics of PMSM at rated speed operation

Figs. 4.7. (a) and (b) show the dynamic characteristics of sensor less PMSM drive at a rated speed operation with the conventional MRAC observer and the improved ANFIS based MRAC observer.

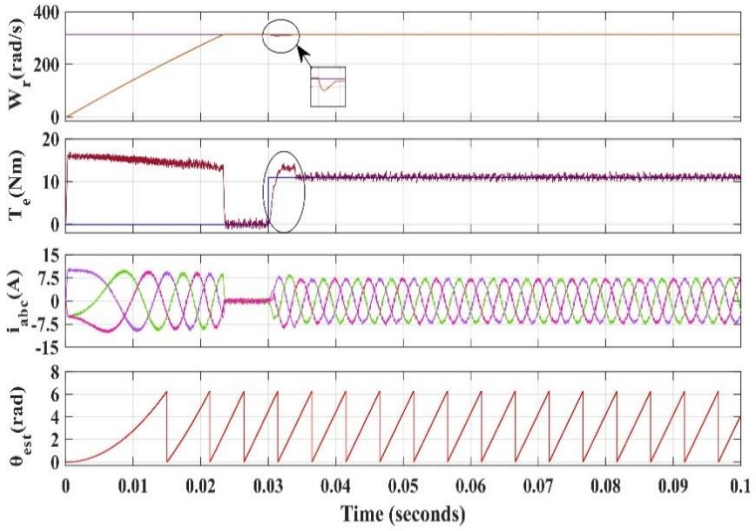

(a)

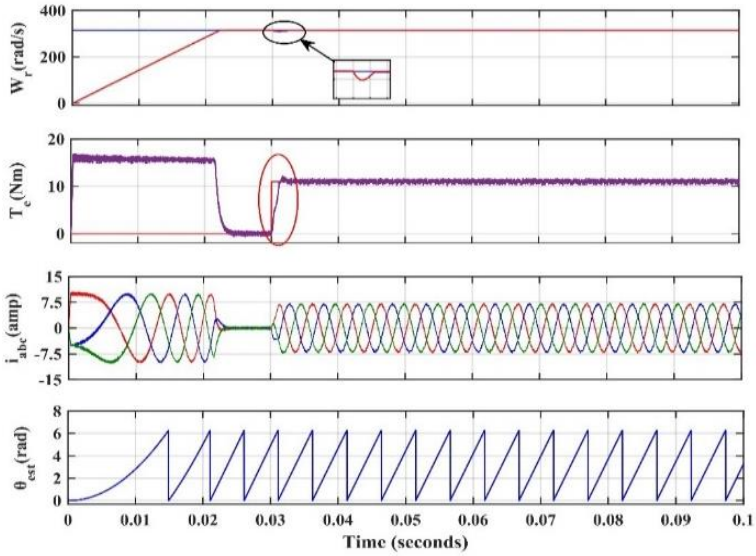

(b)

Fig.4.7. Dynamic characteristics of sensor less PMSM drive at rated speed:

(a) Conventional MRAC, (b) Improved ANFIS based MRAC

The motor is started without any load torque at rated speed of 314 rad/s. At 0.03 sec, when full load is applied to the motor, there is a mild dip in the speed during this transition, however, the motor immediately recovers and follow the commanded speed smoothly. During the starting, the stator current is high, as expected, to provide the required dynamic torque needed to

overcome the motor inertia. No variation is observed in the estimated position of the rotor with change in load torque as observed from Figs. 4.7. (a) and (b). It is also noted that the settling and rise time in improved ANFIS based MRAC is less than the conventional MRAC, hence PMSM response with ANFIS based MRAC is faster.

4.5.2. Dynamic characteristics of PMSM under speed variation

Figs.4.8. (a) and (b) show the dynamic characteristics of sensor less PMSM drive with the conventional MRAC observer and the improved ANFIS based MRAC observer for step change in speed and torque. The motor is started with no-load at half of the rated speed i.e. 157rad/s. At 0.03 sec rated load torque of 11Nm is applied to the motor and the motor is observed to follow the commanded speed smoothly. At 0.05sec the motor speed is increased to rated speed of 314rad/s. It is observed that motor follows the commanded speed smoothly. In the case of the conventional MRAC a mild overshoot in torque is observed during the transition in load, while in the improved ANFIS based MRAC no such overshoot is observed. Thus, improved dynamic torque is achieved with proposed method.

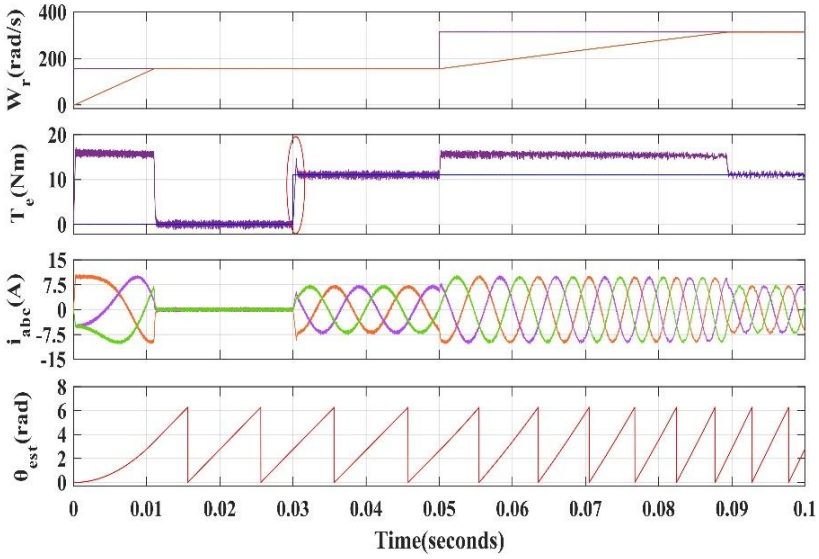

(a)

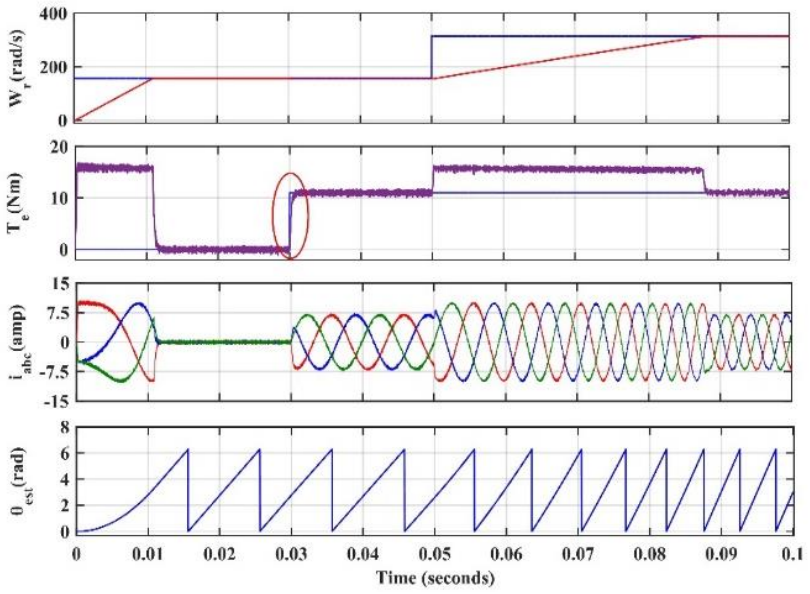

(b)

Fig.4.8. Dynamic characteristics of sensor less PMSM drive under speed variation:

(a) Conventional MRAC, (b) Improved ANFIS based MRAC

4.5.3. Dynamic characteristics of PMSM during speed reversal

Figs. 4.9. (a) and (b) show the dynamic characteristics of sensor less PMSM drive with the conventional MRAC observe and the improved ANFIS based MRAC observer during speed reversal. The motor is running at rated speed of 314 rad/s at no load in starting and the rated load of 11 Nm is applied at 0.03 sec. At 0.05s a speed of the motor is reversed. Some oscillations are observed in the torque response when load torque is applied with the conventional MRAC, while with the proposed method, the load transition is smooth without any oscillations. However, no change is speed is observed during this load transition. During speed reversal, the motor tracks the changed commanded speed smoothly. It is also observed that while achieving steady state speed, there is an overshoot in torque with the conventional MRAC, which is not there in the improved ANFIS based MRAC.

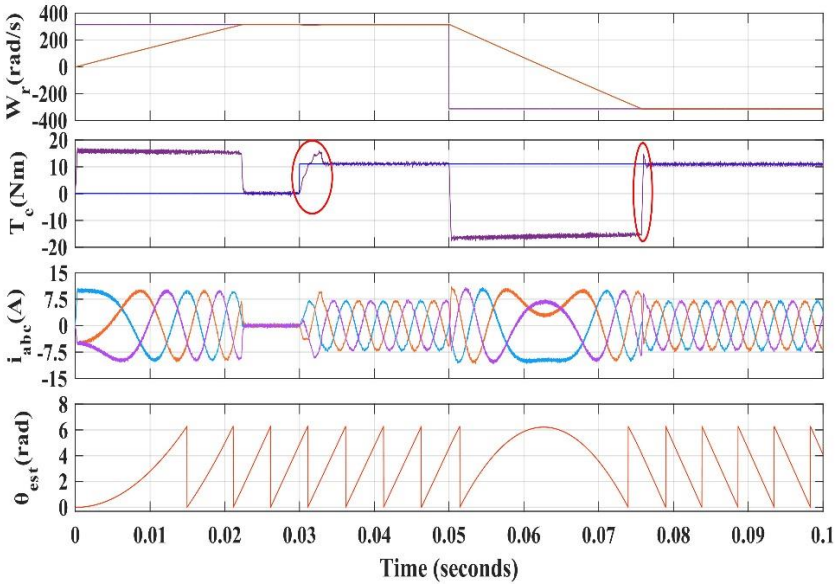

(a)

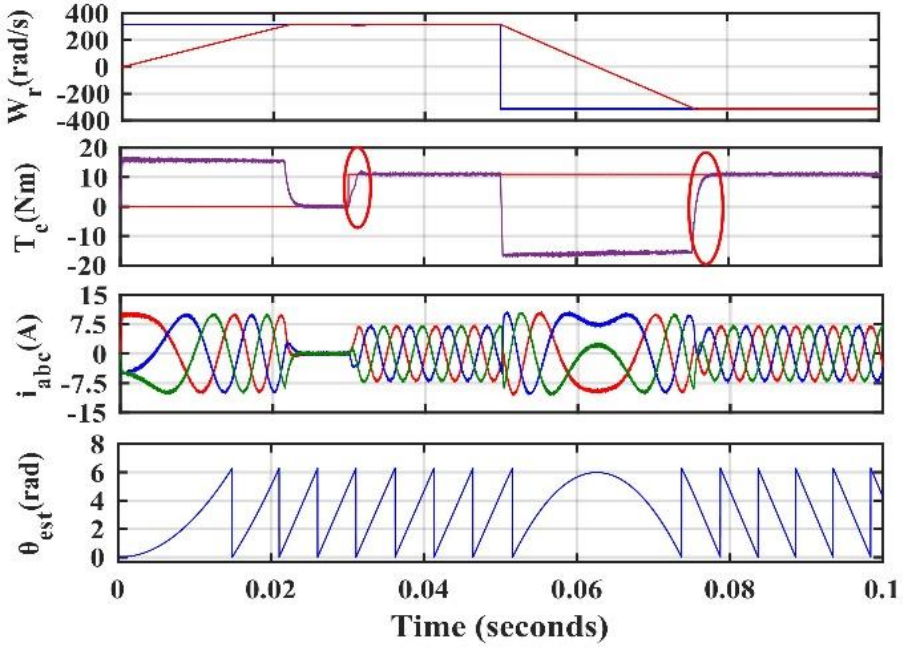

(b)

Fig.4.9. Dynamic characteristics of sensor-less PMSM drive during speed reversal:

(a) Conventional MRAC, (b) Improved ANFIS based MRAC

4.5.4. Dynamic characteristics of PMSM under variations in load

Figs. 4.10. (a) and (b) illustrate the dynamic characteristics of the sensor less PMSM drive with conventional MRAC observer and improved ANFIS based MRAC observer under load variations.

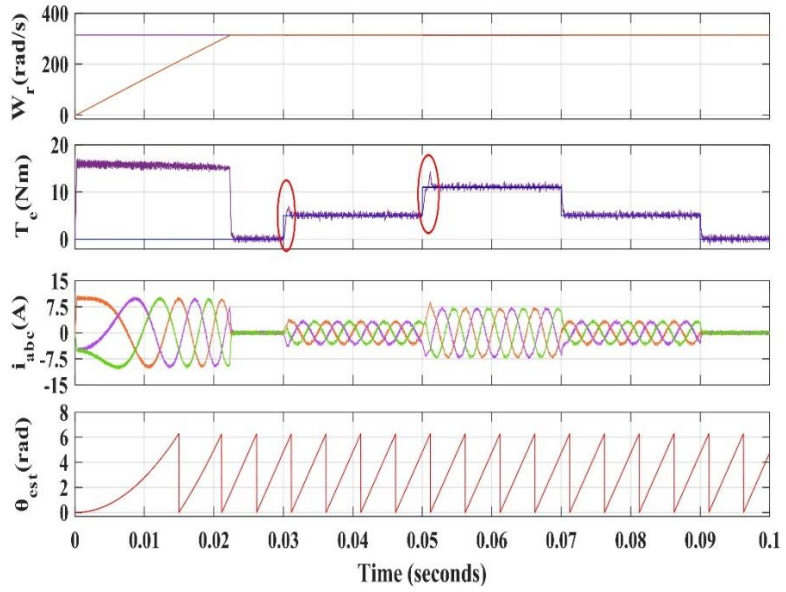

(a)

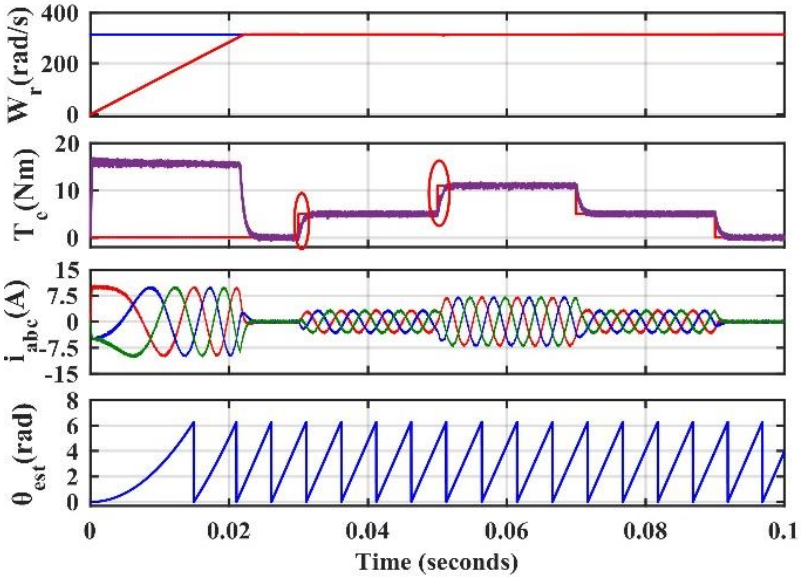

(b)

Fig.4.10. Dynamic characteristics of sensor-less PMSM drive under load variation:

(a) Conventional MRAC, (b) Improved ANFIS based MRAC

The motor is running at no load rated speed condition in starting. At t=0.03 sec a load torque of 5Nm is applied to the rotor and the load torque is increased to 11 Nm at t=0.05 sec.

The load is reduced to 5 Nm at t=0.07 sec followed by a change to no load operation at t= 0.09 sec. During the load transition, some overshoots are observed with the conventional MRAC observer. However, no overshoots are observed with the proposed method and the motor develops the required torque smoothly.

4.5.5. Dynamic characteristics of PMSM at low speed and low load torque operation

Figs. 4.11. (a) and (b) illustrate the dynamic characteristics of the sensor less PMSM drive with the conventional MRAC observer and the improved ANFIS based MRAC observer under low speed operation of 10rad/s with a load torque of 5 Nm.

The motor is started at a commanded speed of 10 rad/sec under no load condition and a load torque of 5Nm is applied at 0.1 sec.

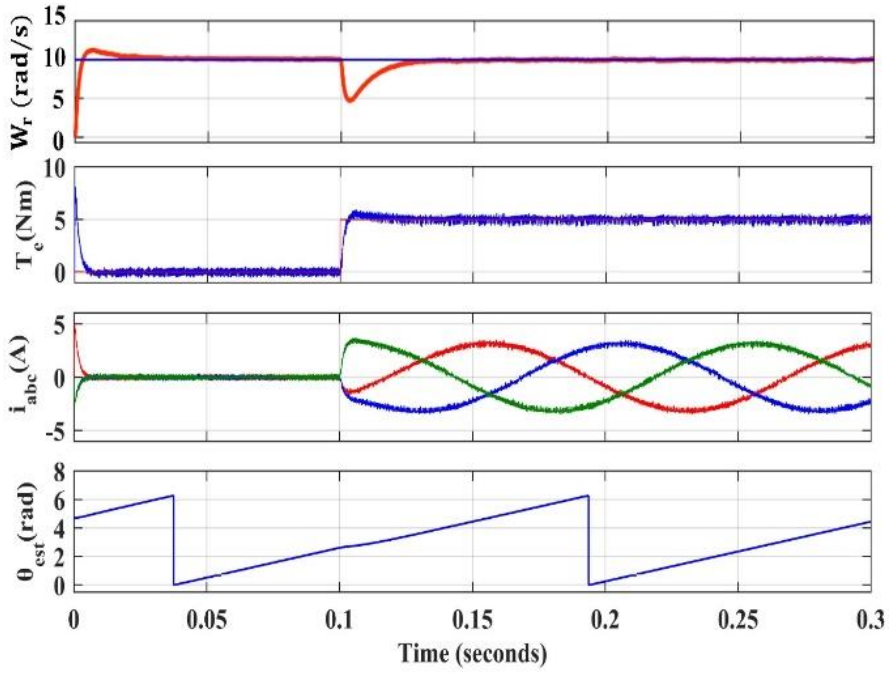

(a)

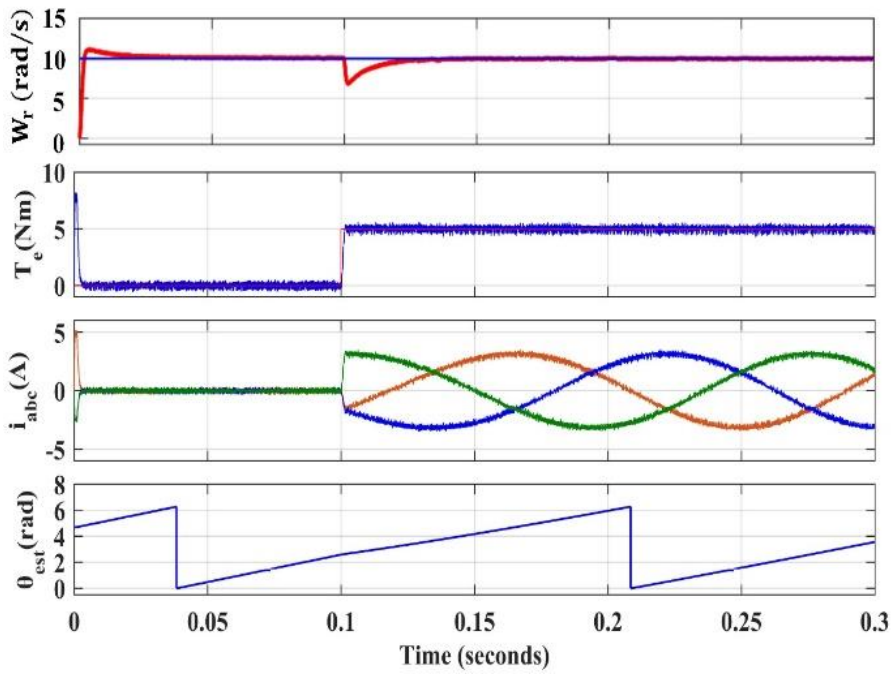

(b)

Fig.4.11. Dynamic characteristics of sensor less PMSM drive at low speed and low torque:

(a) Conventional MRAC, (b) Improved ANFIS based MRAC

It is noted that the motor speed follows the commanded value and the required torque is developed smoothly. The settling and rising times of the speed and torque responses of the improved ANFIS based MRAC observer are observed to be lesser than the conventional MRAC observer.

4.6. CONCLUSION

In this chapter sensor-less field-oriented control of PMSM is described. Different types of sensor-less techniques are presented. An improved ANFIS based MRAC observer is also proposed in this chapter for speed and position estimation in sensor-less control of PMSM drive and its performance is compared with the conventional MRAC observer. The robustness of the proposed observer is demonstrated successfully under various operating conditions like

step change in speed and torque, speed reversal, low speed operation etc. In the proposed MRAC observer, an improved ANFIS based adaptation technique is employed, which estimates the speed of the rotor by minimizing the error of the reference model and adjustable model. The simulation results obtained confirm the improved performance of proposed observer for all operating speeds and different load conditions. The proposed ANFIS based MRAC observer provides improved steady state and dynamic characteristics of the motor at different operating conditions as compared to the conventional MRAC observer.

CHAPTER 5

DESIGN & IMPLEMENTATION OF APCC BASED ON DB CONTROL THEORY FOR THE MINIMIZATION OF STATOR CURRENT & TORQUE RIPPLES IN PMSM DRIVE

5.1. GENERAL

FOC is one of the most popular control algorithms for improving the dynamic performance of PMSM drives [151], [172]. FOC with PI controllers are widely used in industrial applications of PMSM drives due to low ripples in the stator flux and torque, and low stator current THD. However, the use of a PI controller results in a few limitations. (i) Slow dynamic response, as the inner controller regulates the motor currents [173]. (ii) The gains of the PI controllers affect the performance of the drive. (iii) The nonlinear effects of the motor and drive system must be neglected for precise tuning of the PI controller gains. (iv) The optimal tuning of PI controllers is time consuming. To overcome these disadvantages, recent research on AC drives has focused on various controllers like the SMC [174], [175], [176], MRAS [177], IFOC [178], [179], [180], etc. Model predictive controllers (MPCs) [181], [182], [183], are one of the most popular controllers among them. In MPC, a mathematical model of the motor is developed to predict the performance of the motor based on the motor parameters, and an objective function is optimized to choose the best voltage vector(BVV). The selected voltage vector is applied to the motor during the next control cycle. This process is repeated for every control cycle [184]. Generally, MPCs are categorized based on their input sets[185] or available voltage vectors [186] into continuous control set-MPCs (CCS-MPCs) and finite control set-MPCs (FCS-

MPCs) [187]. In FCS-MPCs limited voltage-vectors are used to control the motor without the use of modulation techniques [188], [189], [190]. However, in CCS-MPCs, SVM is normally used to control the motor, due to which any required voltage vector can be produced [191], [192]. Thus, the phase and magnitude of the voltage-vector can be regulated to any required value. Two reported applications of MPC methods include the MPCC method [193] and the model predictive torque control (MPTC) method [194].

In the traditional FCS-MPC, the selected voltage vector is applied to the motor for the entire duration of the control cycle. As a result, the performance variables cannot be controlled with precision, and significant errors exist between the controlled variables and their commanded values. To overcome this drawback, the selected voltage vector is applied to the motor only for a portion of the control cycle [195], [196]. This is achieved by defining the cost function in terms of the error in the stator current and optimizing it to determine the BVV, which is applied as the active voltage vector to the inverter. The duty ratio of the selected BVV is evaluated in such a way that the stator current is controlled according to DB control theory. Thus, only one BVV and one ZVV are applied to the motor. The performance of the controller can be improved by applying two BVVs with one ZVV. However, the computational complexity, computation time and parameter dependence increase as each BVV has to be determined separately. This limitation can be overcome by using an MPCC algorithm based on the current track circle [197] instead of a cost function.

In this Chapter[4], an APCC based on DB control theory is presented. To avoid the complexity associated with selecting two BVVs and the calculation of two different time durations, the

[4] **Published Paper**: Suryakant Shukla, Mini Sreejeth and Madhusudan Singh, "Minimization of ripples in stator current and torque of PMSM drive using advanced predictive current controller based on deadbeat control theory". Journal of Power Electronics 21, 142–152 (2021), available online – https://doi.org/10.1007/s43236-020-00151-2

APCC synthesizes each of the voltage vectors through SVPWM using two voltage components along with one ZVV. The proposed technique reduces the computational complexity and improves the motor performance. The APCC technique is able to achieve improved performance of the PMSM drive under steady state and transient state operations with reduced computational complexity.

In the steady state, the RMS value of the stator current error is computed and used to derive the optimal voltage vector components along with the duration for which it has to be applied during the duty cycle. In the transient condition, the voltage vector having largest magnitude is applied for the entire duration of the control cycle. Furthermore, the phase of the voltage vector is precisely tuned to control the components of the stator current in the DB mode. The MTPA algorithm is used in the proposed APCC for the generation of the reference stator current. This improves the motor efficiency by: (a) reducing the copper losses; (b) reducing ripples in the torque and stator current under steady state; and (c) achieving a fast-dynamic response during transient state.

5.2. DEADBEAT CONTROL THEORY

Deadbeat control is generally implemented in predictive control algorithms. Deadbeat control is referred as a discrete-time model-based control technique that estimates voltages to remove current errors after one cycle using the machine model. The voltages are then synthesized and fed to the machine terminals through a PWM-controlled inverter. The theory of deadbeat control does not require tuning of parameters that's why it is easy and instinctive in comparison to PI controller-based scheme. The switching frequency of inverter is set constant in deadbeat control like as FOC [198]. In contrast to Direct Predictive Control (DPC), which uses a finite number of switching states with variable switching frequency, this allows the design of an

input filter for the PMSM. Furthermore, the deadbeat control technique enables the integration of system limitations and other nonlinearities and it also needs less computational time than DPC.

The pole placement approach, which sets the pole(s) of the controlled discrete system at the origin of the discrete z-plane, is used in conventional deadbeat control [199],[200]. If the system is controlled, allowing any arbitrary poles, then putting them at the origin will remove system dynamics, resulting in a near-perfect response.

In DB control, the error in nonzero vector will be forced to zero during most of the sampling time (n), if the amplitude of the scalar control input $u(k)$ is uncontrolled, where n is defined as the order of the system. Only one design parameter, i.e. the sampling time, exists in DB control. If the sampling time is low, the settling time will be less and the magnitude of control signal $u(k)$ will be very high which creates problem in physical system. As a result, while designing actual deadbeat control, one must consider the compensation between magnitude of control signal and speed response.

5.3. DESIGN OF PROPOSED APCC BASED ON DB CONTROL THEORY

The main objectives of the proposed APCC based on DB control theory are: (a) to reduce the ripples in the stator current and torque under steady state operation and (b) achieve a fast-dynamic response during transient conditions. To effectively implement this technique, it is necessary to obtain the optimum voltage vector components of the BVV along with the duration for which it has to be applied during a control cycle.

5.3.1. Steady-State Operation of PMSM Drive

The modelling equations of the PMSM in the rotor reference frame are

$$v_{sd} = R_s i_{sd} + L_d \frac{d}{dt} i_{sd} - \omega_r L_q i_{sq} \quad (5.1)$$

$$v_{sq} = R_s i_{sq} + L_q \frac{d}{dt} i_{sq} + \omega_r (L_d i_{sd} + \phi_m) \quad (5.2)$$

Where v_{sd} and v_{sq} are stator voltage vectors in d-q axes, i_{sd} and i_{sq} are stator current vectors in d-q axes, R_s is stator resistance, L_d and L_q are stator inductances in d-q axes, ω_r is rotor speed and ϕ_m is magnitude of PM flux. Stator current components are derived from (5.1) and (5.2) as:

$$L_d \frac{d}{dt} i_{sd} = v_{sd} - R_s i_{sd} + \omega_r L_q i_{sq} \quad (5.3)$$

$$L_q \frac{d}{dt} i_{sq} = v_{sq} - R_s i_{sq} - \omega_r (L_d i_{sd} + \phi_m) \quad (5.4)$$

i. Representation of stator current components in discrete time mode:

Stator current components are expressed in discrete time mode for digital implementation of the proposed controller as:

$$\Delta i_{sd} = \frac{\Delta T}{L_d} (v_{sd} - R_s i_{sd} + \omega_r L_q i_{sq}) \quad (5.5)$$

$$\Delta i_{sq} = \frac{\Delta T}{L_q} (v_{sq} - R_s i_{sq} - \omega_r (L_d i_{sd} + \phi_m)) \quad (5.6)$$

Since i_{sd}, i_{sq} and ω_r are measured for every cycle by controlling v_{sd} and v_{sq} in accordance with (5.5) and (5.6), precise control of the stator current components is possible under the assumption that: (a) T_s is the control cycle period, (b) an arbitrary non zero voltage vector $\overrightarrow{v_s^*}$ is applied to the motor for T_k^* where $(T_k^* \leq T_s)$ and (c) a ZVV is applied to the motor in the remaining control cycle. Stator current components of the motor are modified by applying $\overrightarrow{v_s^*}$ and ZVV and are expressed as:

$$\Delta i_{sd0} = S_{d0}(T_s - T_k^*) \tag{5.7}$$

$$\Delta i_{sq0} = S_{q0}(T_s - T_k^*) \tag{5.8}$$

$$\Delta i_{sd1} = \frac{T_k^*}{L_d} v_{sd}^* + S_{d0} T_k^* \tag{5.9}$$

$$\Delta i_{sq1} = \frac{T_k^*}{L_q} v_{sq}^* + S_{q0} T_k^* \tag{5.10}$$

$$S_{d0} = \frac{1}{L_d}(-R_s i_{sd} + \omega_r L_q i_{sq}) \tag{5.11}$$

$$S_{q0} = \frac{1}{L_q}(-R_s i_{sq} - \omega_r (L_d i_{sd} + \phi_m)) \tag{5.12}$$

Where Δi_{sd0} , Δi_{sq0} and Δi_{sd1} , Δi_{sq1} are the modified d – q axes current components when ZVV and $\overrightarrow{v_s^*}$ are applied respectively. For T_s =50μs, all machine parameters remain constant, hence slope S_{d0} and S_{q0} are invariant within one control cycle. Accordingly, the modified stator current in every control cycle is derived as:

$$i_{sd} = \begin{cases} i_{sd}(k) + \left(\frac{1}{L_d} v_{sd}^* + S_{d0}\right) t \;\; 0 \le t \le T_k^* \\ i_{sd}(k) + \frac{T_k^*}{L_d} v_{sd}^* + S_{d0} t \quad T_k^* < t \le T_s \end{cases} \tag{5.13}$$

$$i_{sq} = \begin{cases} i_{sq}(k) + \left(\frac{1}{L_q} v_{sq}^* + S_{q0}\right) t \;\; 0 \le t \le T_k^* \\ i_{sq}(k) + \frac{T_k^*}{L_q} v_{sq}^* + S_{q0} t \quad T_k^* < t \le T_s \end{cases} \tag{5.14}$$

where $i_{sd}(k)$ and $i_{sq}(k)$ are the d – q axes stator current components respectively in the kth control cycle.

ii. Minimization of ripples in stator current components

Generally, the performance of any signal that varies from its reference value is calculated using RMS function[201]. The RMS value of stator current error, $i_{s_{err(RMS)}}$, defined over one control cycle is expressed as

$$\left|i_{s_{err(RMS)}}\right|^2 = \frac{1}{T_s}\int_0^{T_s}\left\{(i_{sd}^* - i_{sd})^2 + \left(i_{sq}^* - i_{sq}\right)^2\right\}dt \tag{5.15}$$

Where i_{sd}^* and i_{sq}^* are reference stator currents in the d-q axes. Using (5.13) and (5.14), (5.15) can be expressed

as:

$$\begin{aligned}\left|i_{s_{err(RMS)}}\right|^2 = \frac{1}{T_s}\int_0^{T_k}\Bigg\{&\left(i_{sd_{err}} - \left(\frac{v_{sd}^*}{L_d} + S_{d0}\right)t\right)^2 \\ &+ \left(i_{sq_{err}} - \left(\frac{v_{sq}^*}{L_d} + S_{q0}\right)t\right)^2\Bigg\}dt \\ &+ \frac{1}{T_s}\int_{T_k}^{T_s}\Bigg\{\left(i_{sd_{err}} - \frac{T_k^*}{L_d}v_{sd}^* - S_{d0}t\right)^2 \\ &+ \left(i_{sq_{err}} - \frac{T_k^*}{L_d}v_{sq}^* - S_{q0}t\right)^2\Bigg\}dt\end{aligned} \tag{5.16}$$

Where

$$i_{sd\_err} = i_{sd}^* - i_{sd}(k) \tag{5.17}$$

$$i_{sq\_err} = i_{sq}^* - i_{sq}(k) \tag{5.18}$$

$\left|i_{s\_err(RMS)}\right|^2$ is used as the objective function with variables T_k^*, v_{sd}^*, v_{sq}^*. An unconstrained optimization problem is introduced in equation (5.16) to reduce stator current ripples and it is solved to obtain the optimal voltage vector components and the optimal time duration as:

$$v_{sd}^{*} = \frac{L_d(i_{sd\_err} - S_{d0}T_s)}{T_s} \tag{5.19}$$

$$v_{sq}^{*} = \frac{L_q(i_{sq\_err} - S_{q0}T_s)}{T_s} \tag{5.20}$$

$$T_k^{*} = \frac{i_{sd\_err} - S_{d0}T_s}{2S_{q1} - S_{q0}} + \frac{i_{sq\_err} - S_{q0}T_s}{2S_{d1} - S_{d0}} \tag{5.21}$$

Where

$$S_{d1} = \frac{1}{L_d}\left(v_{sd}^{*} - R_s i_{sd} + \omega_r L_q i_{sq}\right) \tag{5.22}$$

$$S_{q1} = \frac{1}{L_q}\left(v_{sq}^{*} - R_s i_{sq} + \omega_r L_d i_{sd}\right) \tag{5.23}$$

These calculated values of v_{sd}^{*}, v_{sq}^{*} are transformed into stationary reference frame, i.e. into α-β axes, to obtain the voltage vectors components $v_{s\alpha}^{*}$ and $v_{s\beta}^{*}$. These voltage vector components and T_k^{*} are applied to SVPWM block, which computes the BVV and it is applied to the motor for the duration T_k^{*}. ZVV is applied for the remaining period of the control cycle.

5.3.2. Transient Operation of PMSM Drive

In transient state, the principle of DB control theory is employed, which results in fast dynamic response of the PMSM. At the end of each control cycle the calculated stator current components of the motor track their commanded values. Accordingly, optimal voltage vector components are obtained by solving:

$$\left.\begin{aligned} i_{sd}(k+1) = i_{sd}^{*} = i_{sd}(k) + \frac{T_k^{*}}{L_d}v_{sd}^{*} + S_{d0}T_s \\ i_{sq}(k+1) = i_{sq}^{*} = i_{sq}(k) + \frac{T_k^{*}}{L_q}v_{sq}^{*} + S_{q0}T_s \end{aligned}\right\} \tag{5.24}$$

Using (5.24) the optimal voltage vector components are expressed as

$$v_{sd}^{*} = \frac{L_d}{T_k^{*}}(i_{sd_{err}} - S_{d0}T_s) \tag{5.25}$$

$$v_{sq}^{*} = \frac{L_q}{T_k^{*}}(i_{sq_{err}} - S_{q0}T_s) \tag{5.26}$$

Fast dynamic response under transient state is achieved when voltage vector having largest magnitude computed using equations (5.25) and (5.26) is applied to the motor for the entire duration of the control cycle. i.e. T_k^{*} and $\overrightarrow{v_s^{*}}$ must be adjusted to T_s and V_{max} respectively, where V_{max} is voltage vector with largest magnitude in linear region of SVPWM. Phase of the voltage vector with respect to d-axis of the rotor reference frame is obtained from (5.25) and (5.26) as:

$$\theta_s^{*} = tan^{-1}\left(\frac{L_q(i_{sd\_err} - S_{d0}T_s)}{L_d(i_{sq\_err} - S_{q0}T_s)}\right) \tag{5.27}$$

Applying this voltage vector for the entire duration of control cycle improves the dynamic response of motor appreciably.

5.4. IMPLEMENTATION OF APCC BASED ON DB CONTROL THEORY

The proposed APCC is implemented on a PMSM with specifications as given in Appendix-1. Even though, implementation of over modulation is simpler and it allows better utilization of the DC input voltage, it results in highly distorted non-sinusoidal output voltage and associated high stator current harmonics. Therefore, operation of the SVPWM in the over modulation region has been avoided in the proposed APCC. To avoid operation in over modulation region the magnitude of voltage vector has to be restricted to v_{max} and T_k^{*} has to be restricted to T_s. For the steady state

$$\frac{T_k^{*}\left|\overrightarrow{v_s^{*}}\right|}{T_s} \leq v_{max} \tag{5.28}$$

and for the transient state

$$\frac{T_k^* \left|\overrightarrow{v_s^*}\right|}{T_s} > v_{max} \tag{5.29}$$

Figs.5.1 and 5.2 show the flow chart and the block diagram of the proposed APCC respectively. A PI controller is used to obtain Torque command, T_e^* , which is used by the MTPA block to generate the quadrature and direct axes stator currents, i.e. i_{sd}^* and i_{sq}^*, using the rotor speed. These current components are processed in the APCC to obtain the optimum voltage vector components, v_{sd}^* and v_{sq}^* , which is then transformed to the stationery reference frame before being fed to the SVPWM to produce the required gating pulses for the inverter. MTPA algorithm is used to generate stator reference currents in d-q axes. Maximum torque can be achieved in surface mounted PMSM by using zero d-axis current and q–axis stator current, which is computed using:

$$i_{sd\_mtpa} = 0 \tag{5.30}$$

$$i_{sq\_mtpa} = \frac{T^*}{\frac{3}{2}.P.\phi_m} \tag{5.31}$$

$$i_{sd\_sat} = i_{sd\_mtpa} = 0 \tag{5.32}$$

$$i_{sq\_sat} = sat(i_{sq_{mtpa}}, i_{max}) \tag{5.33}$$

$$i_{max} \geq \sqrt{i_{sd}^2 + i_{sq}^2} \tag{5.34}$$

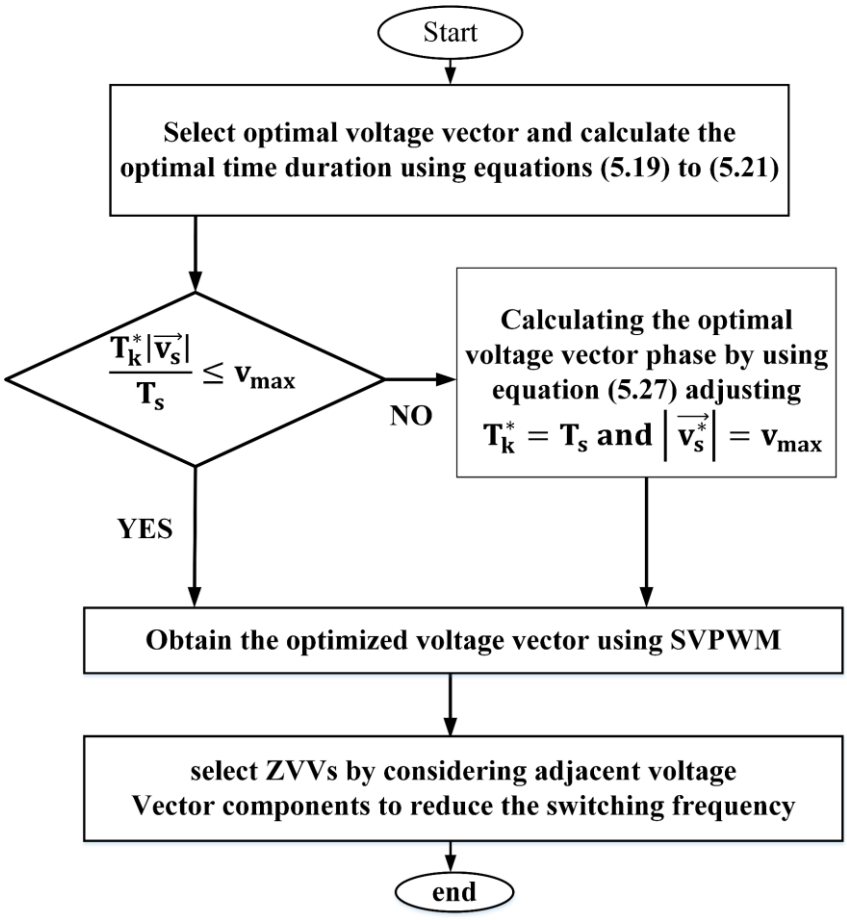

Fig.5.1. Flow Chart of the APCC

Where i_{sd_mtpa}, i_{sq_mtpa} are d-q axes currents corresponding to MTPA, i_{sd_sat}, i_{sq_sat} are d-q axes saturation currents, $i_{\max}$ is maximum phase current and i_{sd}^*, i_{sq}^* are reference currents corresponding to reference torque T*. The stator reference currents in d-q axes are

$$i_{sd}^* = i_{sd\_sat} \tag{5.35}$$

$$i_{sq}^* = i_{sq\_sat} \tag{5.36}$$

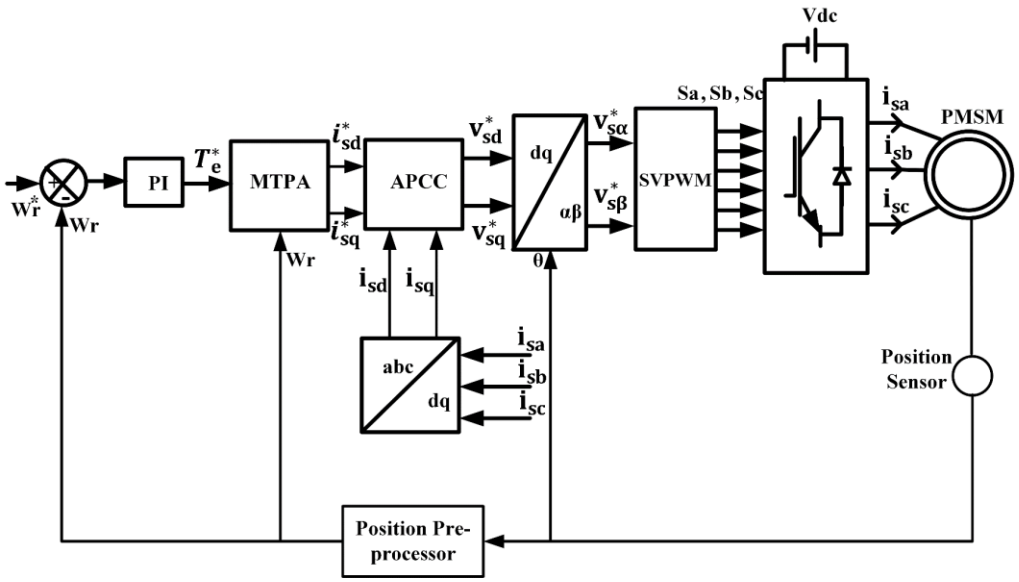

Fig.5.2. Block Diagram of APCC

5.5. COMPARISON OF PROPOSED APCC WITH OTHER RECENT CURRENT CONTROLLERS

The merits and demerits of proposed controller in comparison with the recent controllers implemented in [202] and [203] are briefly discussed in this Section.

5.5.1. Comparison of APCC with Hysteresis based DCC

In DCC [202], cost function is defined by RMS function of torque ripples and control of stator flux is considered as a constraint. The optimization problem to find optimal voltage vector components is solved using Lagrange-Multiplier method. Table.5.1 summarizes the comparison between DCC and the APCC.

Table.5.1. Comparison between DCC and Proposed APCC

Parameter	DCC	APCC
Estimator	Closed loop estimator is employed to estimate stator flux, which increase the computational burden	No estimator is required, hence computational burden is less
Optimization	A constrained optimization problem is solved to find the optimal voltage vector components, which increases complexity	An unconstrained optimization problem is solved, thus reducing the complexity.
Control	Ripples in stator flux cannot be reduced as it is controlled in deadbeat manner	Ripples in stator current and torque can be reduced
Weighing Factor	Weighing factor is required as stator flux is a constraint in the optimization of the objective function to reduce ripples in torque and stator flux.	Weighing factor is not needed as stator current components are controlled directly.
THD and ripples	Higher THD and ripples in stator flux and torque.	Lower THD and ripples in stator flux and torque.

5.5.2. Comparison of APCC with Duty-MPCC

In Duty-MPCC [203], a BVV and ZVV are applied to the PMSM in each control cycle. In this technique BVV is selected by applying two approaches. In the first approach, a cost value of

all accessible voltage vector is defined to find the lowest value of voltage vector and DB control of stator current is attained by defining time duration for the selected voltage vector. In the second approach, theoretical optimum voltage vector is selected through DB control of the stator current and the voltage vector closest to the theoretical optimal voltage vector is selected as the BVV. The error of the selected BVV and theoretical optimum voltage vector is minimized by calculating the time period of voltage vector. Table.5.2 shows the comparison between Duty-MPCC and proposed APCC.

Table.5.2. Comparison between Duty-MPCC and Proposed APCC

Parameters	**Duty-MPCC**	**APCC**
Stator current error	Stator-current error cannot be minimized	Stator-current error can be minimized since SVPWM is used to synthesize the desired voltage vector
Type of control	Same BVV is applied for both steady state and transient operation	The error in stator current under the steady-state is minimized by adopting predictive control and DB control is implemented to acquire a fast-dynamic response under the transient-state.
Computational delay	Cost value of BVV must be calculated for each control cycle.	Only voltage-vector parameters are calculated in each control cycle

5.6. RESULTS AND DISCUSSIONS

The performance of the PMSM drive, with specifications as given in Appendix-I, is investigated using the APCC under different operating conditions through simulation studies. The performance of motor using the proposed controller is also compared with the performance of traditional hysteresis based DCC and Duty-MPCC. Sampling time for the APCC is set at 50μs. In hysteresis based DCC, the bandwidth of hysteresis controller is adjusted to zero to achieve minimum stator current ripples. Only the important characteristics of the control algorithms are considered in the comparative analysis by neglecting non-idealities like dead time in inverter switches, saturation in motor-core etc.

5.6.1. Starting Response of PMSM for Rated Speed Operation

The starting response of PMSM drive at no load and rated speed is shown in Fig.5.3 using DCC, Duty-MPCC and APCC. As a PI controller is used to regulate the speed of PMSM, there is no overshoot.

It is observed that the speed, torque and stator current response for the three controllers are similar without any appreciable steady state error or overshoot in motor speed and torque. The torque response of the drive under rated torque operation is given in Fig.5.4.

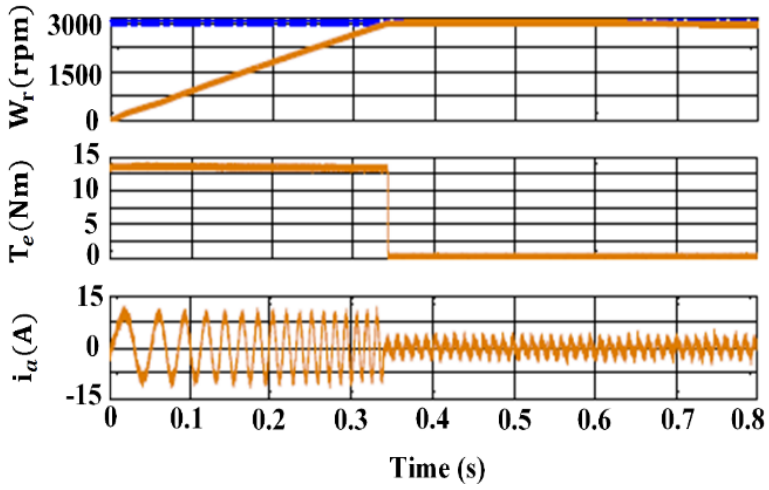

(a)

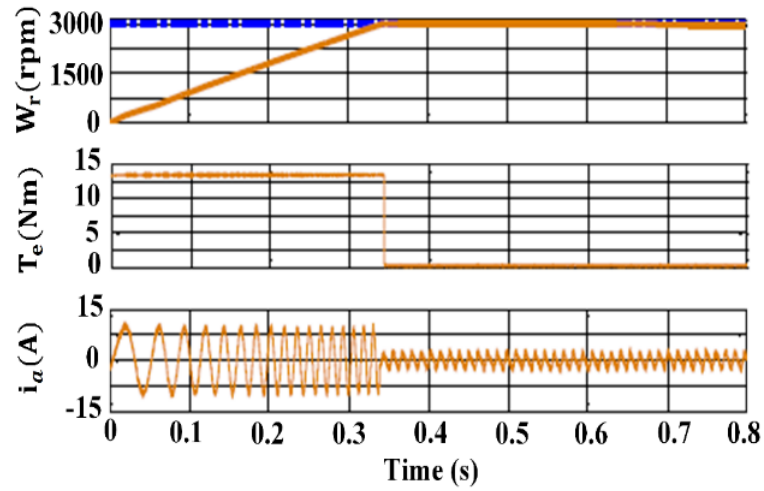

(b)

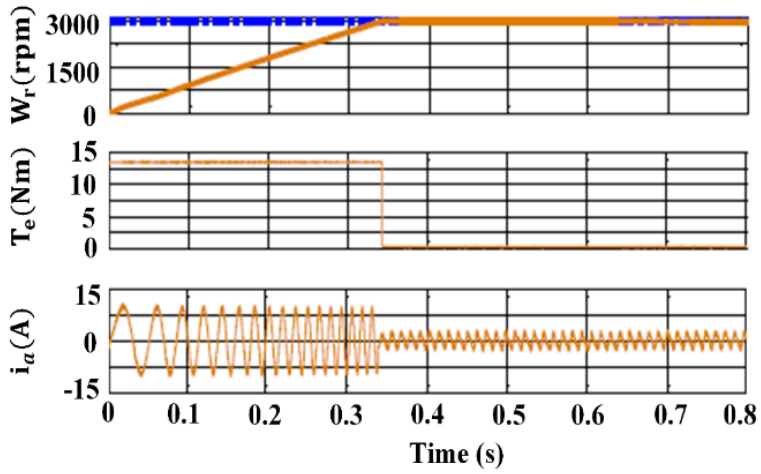

(c)

Fig.5.3. No Load Speed, Torque and Current Characteristics of PMSM: (a) DCC (b) Duty MPCC (c) APCC

It is observed that the dynamic response of the APCC method is faster than the other two methods having minimum settling and rise time as tabulated in Table.5.3.

Table.5.3. Settling and Rising Time of Torque Response

Technique	Settling time (ms)	Rise time (ms)
DCC	3.7	2.9
Duty-MPCC	3.2	3.5
Proposed APCC	2.6	2.19

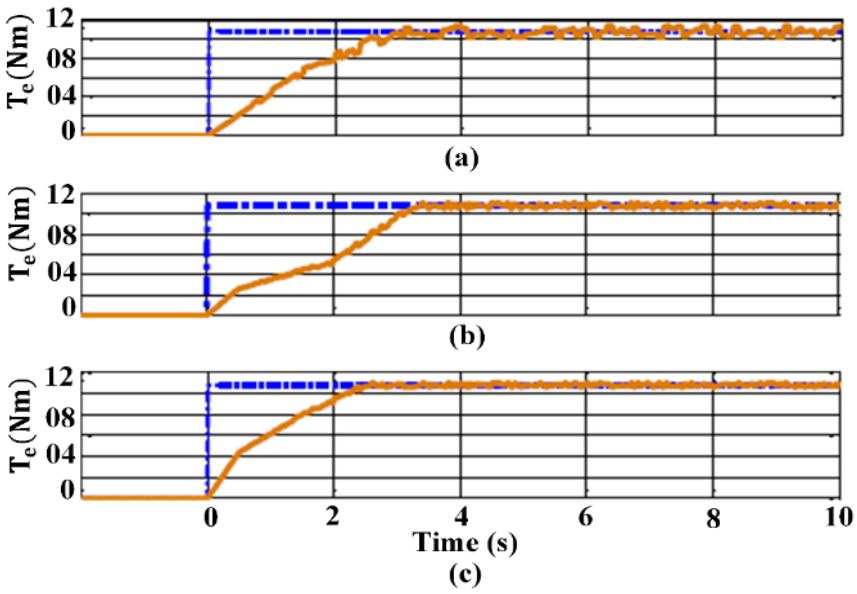

Fig.5.4. Torque Characteristics of PMSM under Rated-torque Operation: (a) DCC (b) Duty-MPCC (c) APCC

5.6.2. THD in Stator Currents

Figs.5.5 and 5.6 represent the harmonic spectrum of stator currents at 3000 rpm and 300 rpm respectively. The stator current ripples and THD will be lower if the switching frequency is high. The average switching frequency for all methods are kept same for comparative analysis.

In simulation analysis average switching frequencies of DCC, Duty-MPCC and proposed APCC are kept constant at 7.5kHz for operating speeds of 3000 rpm and 300 rpm. The THD is analysed up to 6kHz.

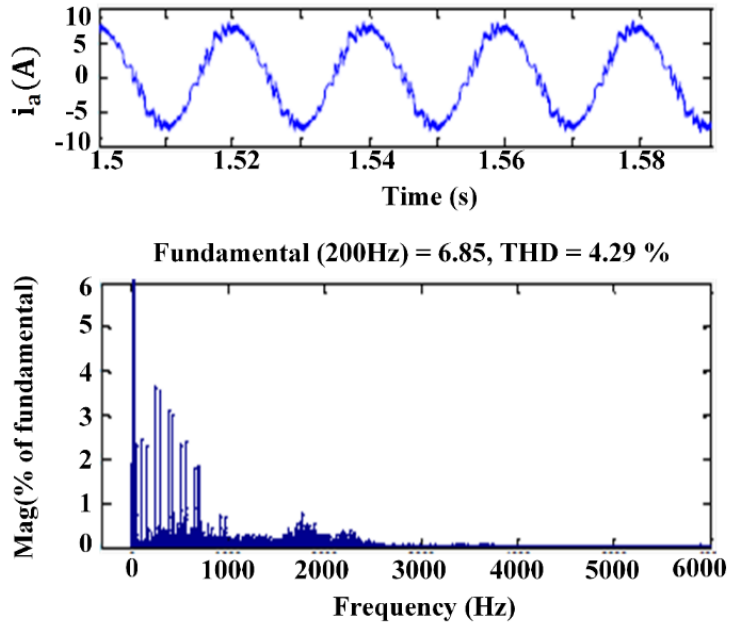

(a)

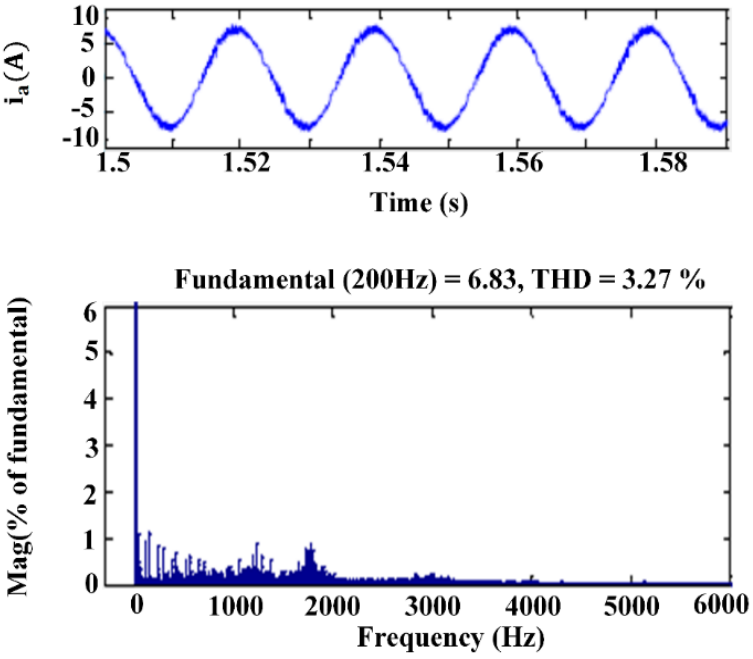

(b)

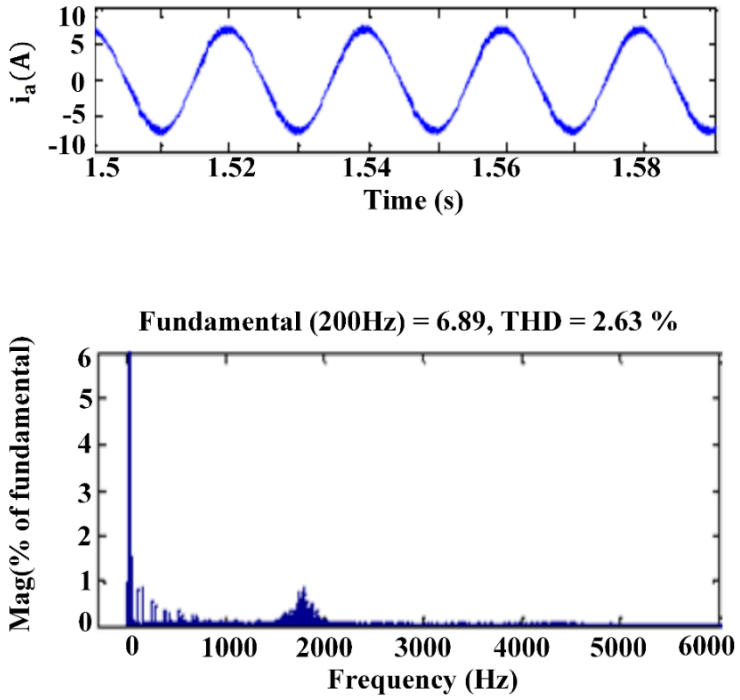

(c)

Fig.5.5. Harmonic Spectrum at 3000rpm: (a) DCC (b) Duty MPCC (c) APCC

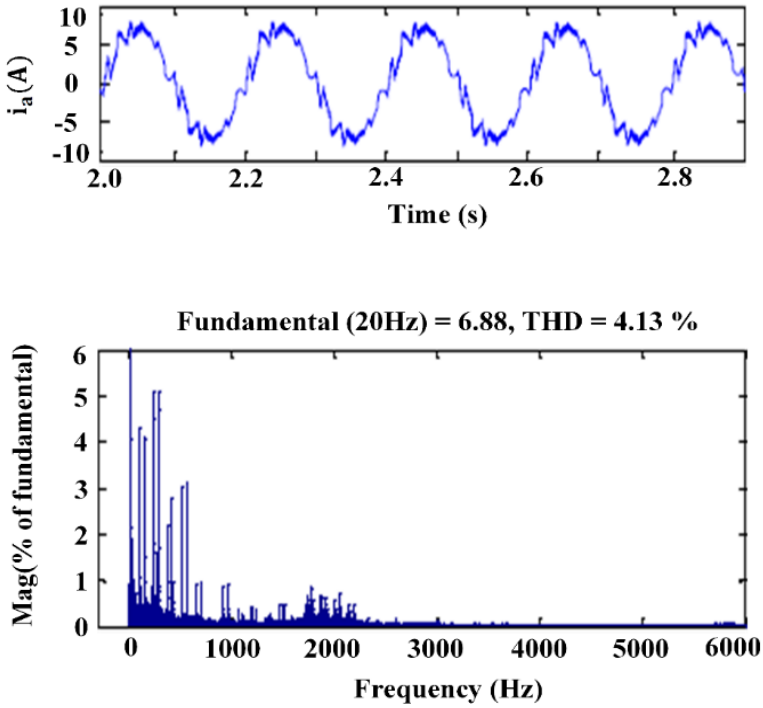

(a)

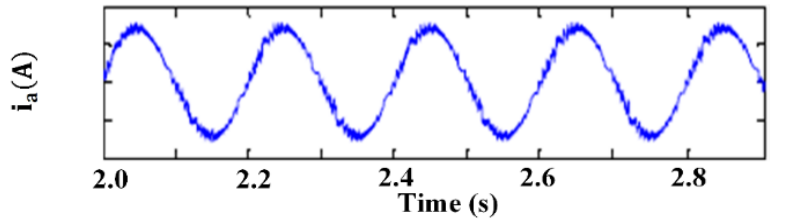

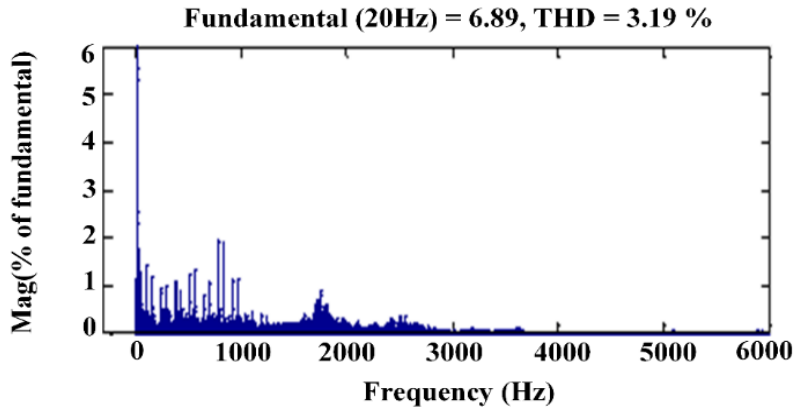

(b)

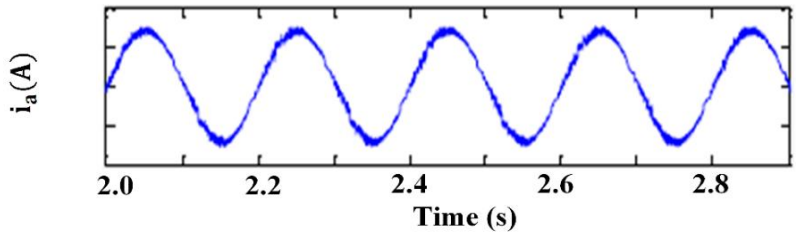

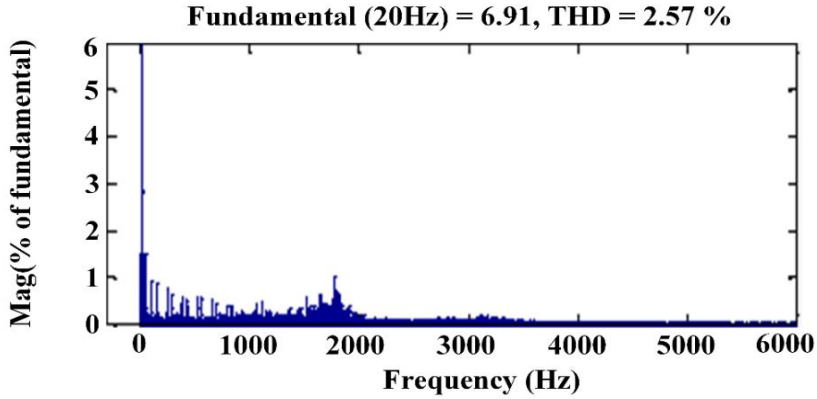

(c)

Fig.5.6. Harmonic Spectrum at 300rpm: (a) DCC (b) Duty MPCC (c) APCC

Fig.5.7. shows the THD in stator current of PMSM using DCC, Duty-MPCC and the APCC at different operating speed of the motor i.e. 300rpm and 3000rpm. It is observed that THD in the stator current with the APCC is 2.63% and the lowest in comparison to DCC and Duty-MPCC.

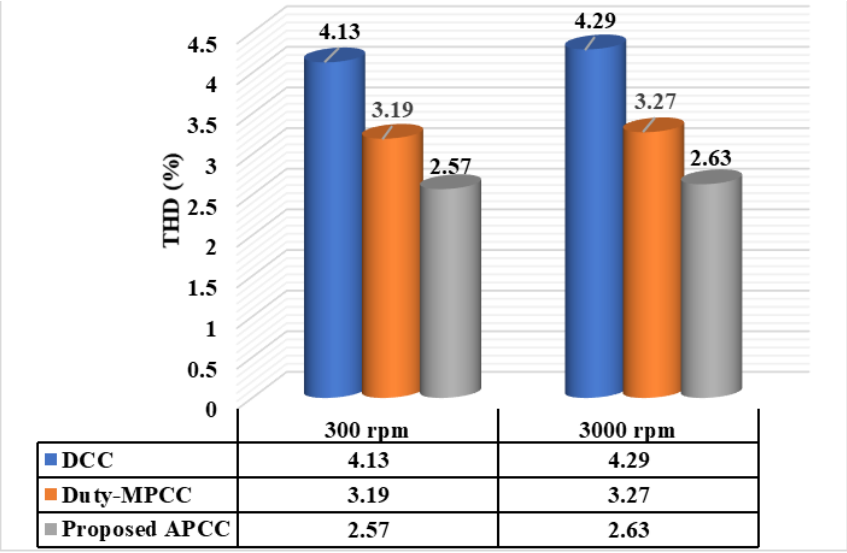

Fig.5.7. Comparison of THD in stator current with DCC, Duty-MPCC & APCC

5.6.3. Steady State Performance of PMSM

The zoomed steady state performance of the motor at rated speed and rated torque operation is shown in Fig.5.8. The stator current ripples are 0.28%, 0.14% and 0.07% in DCC, Duty MPCC and APCC respectively and torque ripples are 0.27%, 0.13% and 0.09% in DCC, Duty MPCC and the APCC respectively.

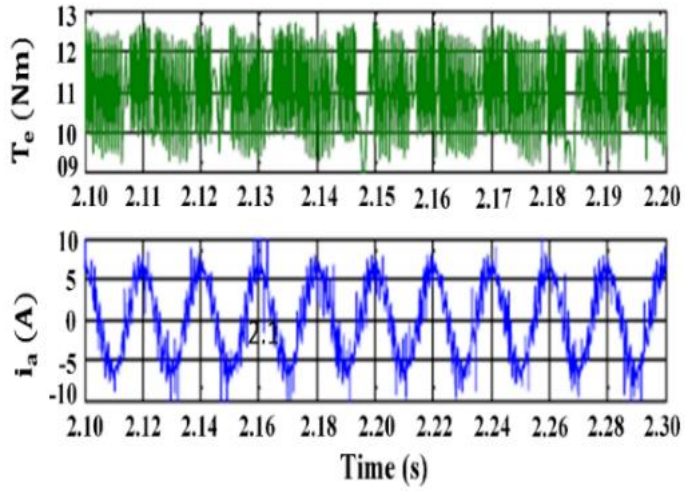

(a)

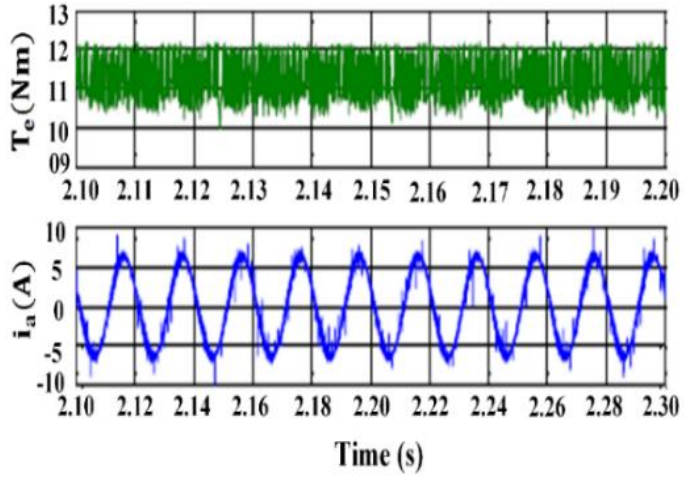

(b)

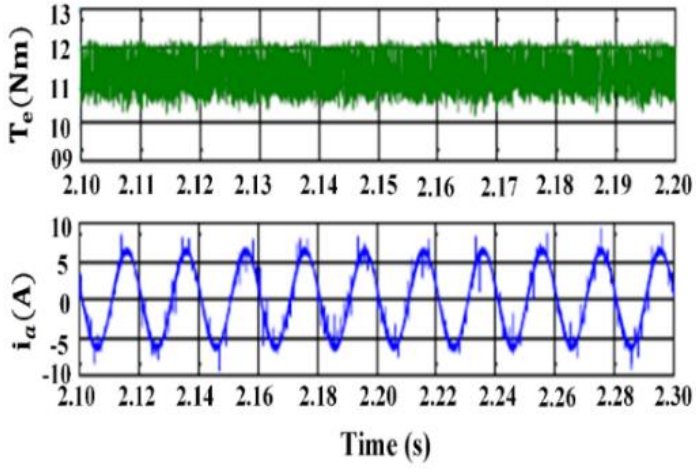

(c)

Fig.5.8. Torque and Stator Current of PMSM at Rated-speed & Rated-torque Operation: (a) DCC (b) Duty MPCC (c) APCC

The lowest torque and stator current ripples are achieved with the APCC. Fig.5.9. shows the comparison of ripples in stator current and torque in PMSM with DCC, Duty-MPCC and APCC. It is noted that the APCC has the lowest stator current and torque ripples.

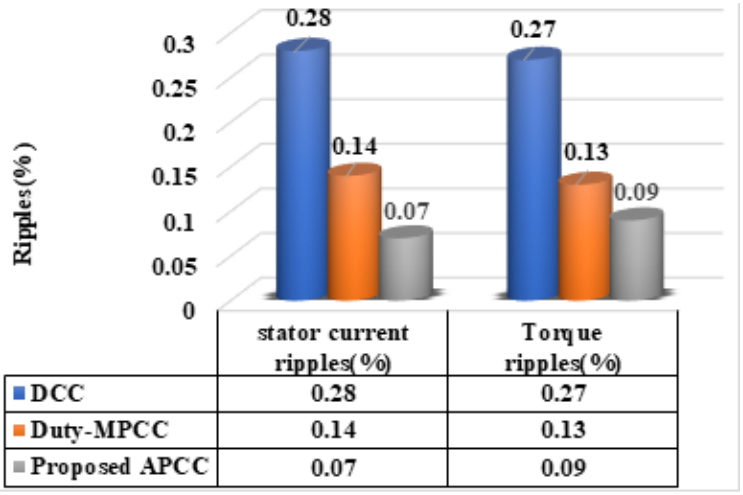

	stator current ripples(%)	Torque ripples(%)
DCC	0.28	0.27
Duty-MPCC	0.14	0.13
Proposed APCC	0.07	0.09

Fig.5.9. Stator Current Ripples and Torque Ripples in PMSM with DCC, Duty-MPCC & APCC

The ripples in stator current and motor torque are calculated as the percentage of the difference of maximum value X_{max} and minimum valueX_{min} compared to average value X_{avg}. Where X can be stator current or motor torque.

5.7. CONCLUSION

In this chapter an advanced predictive current controller based on DB control theory is discussed, which reduces the ripples in the stator current and torque by optimization of the voltage vector components and time for application of this voltage vector to the PMSM Drive. An unconstrained optimization problem is solved, which reduces computational complexity. The proposed method employs a novel approach to calculate the stator current references of the PMSM using MTPA control, which reduces the copper loss. During the transient state, the voltage vector having the largest value is applied to the motor for the complete duration of the

control cycle. The stator current components are controlled in deadbeat manner, whereby at the end of each control cycle phase of the voltage vector component is adjusted in such a way that the stator current error is reduced to zero. Both steady state and transient operations of proposed APCC based on DB control theory are analysed through simulation studies using MATLAB/Simulink. It is observed that in comparison to some of the recently reported predictive current controllers the proposed APCC controller (a) provides better torque dynamics; (b) has significantly less THD in stator current; (c) has less ripples in stator current and torque; and (d) reduced computational complexity. The proposed APCC controller based on DB control theory is a useful alternative to other contemporary predictive current controllers.

CHAPTER 6

DESIGN OF INTELLIGENT HYBRID CONTROLLER TO MINIMIZE THE TORQUE RIPPLES IN PMSM DRIVE

6.1. GENERAL

PMSM has evolved as the most popular motor due to its high-power density, better power factor, enhanced efficiency and superior dynamic performance [204], [205], [206]. PMSM drives are widely used in motion control applications like machine tools, robotics, vehicle propulsion and industrial drives. PM in the rotor of the PMSM enhances the motor efficiency and reduces maintenance requirements due to the elimination of slip rings and brushes. Quick response and fast recovery from instabilities are essential for high performance drives. External disturbances and nonlinear changes in motor parameters affect the performance of the motor. Adaptive control [207], sliding mode control [208], [209], predictive control [210], [211] etc. are used to eliminate the factors which affect nonlinear system uncertainties.

DTC and FOC are the two widely used techniques to control the speed and position of PMSM drives [212]. DTC based drives have superior dynamic response, however it generates high torque and flux ripples. FOC based drives have good steady state performance and use separate PI controllers to control the current, speed and position loops. Inability of these PI controllers to dynamically adapt the controller gains (K_p and K_i) degrade the dynamic performance of the drive. FLC has the ability to overcome this limitation of PI controllers [213]. FLC is designed on the basis of linguistic rules, which is defined by the user [214],[215]. and does not require mathematical modelling. As compared to PI controller, FLC is more complex, computationally

intensive and requires more memory. While PI controller improves steady state performance of the drive [216], [217],[218]. FLC is best suited to meet the transient performance. An intelligent hybrid controller [219], [220] can be designed to achieve the merits of both PI controller and FLC.

Torque ripples caused due to spatial harmonics of the magnetic field, time harmonics of the armature current, cogging torque etc. reduce the useful life of the machine. Torque ripples can be controlled either through improvement in machine design or through suitable motor control strategies. In the perspective of machine design methods, optimizing the winding distribution to improve spatial magnetic field is commonly employed. Designing stators using fractional slot and skewed slot techniques have proved to be valid in weakening the cogging torque [221][22]. Machine control approaches optimize the excitation current, which remove torque ripples and produce a smooth torque output [222], [223], [118]. The performance of drive is affected by the choice of the controller in the outer speed loop.

This Chapter[5] presents an IHC designed and developed, based on a novel torque estimation technique, with major focus on reducing torque ripples. In the outer speed loop, speed error is processed by the IHC to generate the reference torque, which is compared with the estimated torque. Torque is estimated using measured currents, DC link voltage and the status information of the VSI switches. The estimated torque is compared with the reference torque and the error signal thus generated is fed to the current controller to produce the torque producing *q-axis* current.

[5] **Paper Communicated:** Suryakant, Mini Sreejeth and Madhusudan Singh, "Minimization of Torque ripples in PMSM using Intelligent Hybrid Controller", Arabian Journal of Science & Engineering, Springer.

Thus, the IHC employed in the outer loop helps to generate reference torque, which reduces the torque ripples.

The proposed IHC incorporates both FLC and PI controller with a switching unit capable of intelligently switching to the FLC during transient operations and the PI controller under steady state operation. The membership functions for FLC are tuned based on the variation in input / output variables. Novelty has been achieved in the design of FLC through optimization of universe of discourse by fine-tuning the membership functions at the centre to provide greater sensitivity in the region around rated speed. Enhancement in performance of the drive is also achieved through fine tuning of the membership functions in accordance with the variations in input and output variables. The dynamic performance of the PMSM drive using the IHC is investigated and compared with the classical PI controller.

6.2. PRINCIPLE OF SPEED CONTROL OF SPMSM THROUGH TORQUE ESTIMATION

To ensure decoupled control of rotor flux and stator current, the SPMSM is modelled in the α-β stationary reference frame as described herein.

6.2.1. Torque Estimation using Stationary Reference Frame

The stator voltages, $\mathbf{v_{s\alpha}}$, $\mathbf{v_{s\beta}}$ in the α-β axes are:

$$v_{s\alpha} = R_s i_{s\alpha} + \frac{d\phi_{s\alpha}}{dt} \tag{6.1}$$

$$v_{s\beta} = R_s i_{s\beta} + \frac{d\phi_{s\beta}}{dt} \tag{6.2}$$

the stator flux in the α-β axes is represented as

$$\phi_{s\alpha} = \int (v_{s\alpha} - i_{s\alpha} R_s) dt \tag{6.3}$$

$$\phi_{s\beta} = \int \left(v_{s\beta} - i_{s\beta} R_s\right) dt \tag{6.4}$$

The stator voltages in the α-β axes can be represented in terms of the DC link voltage, $\mathbf{V_{dc}}$ and the status of the inverter switches as

$$v_{s\alpha} = \frac{V_{dc}}{3}(2S_a - S_b - S_c) \tag{6.5}$$

$$v_{s\beta} = \frac{V_{dc}}{3}\left[\sqrt{3}\,(S_b - S_c)\right] \tag{6.6}$$

where $\mathbf{S_a}$, $\mathbf{S_b}$ and $\mathbf{S_c}$ correspond to the positions of the switches of the VSI, the value being 1 when the switch is off and 0 when the switch is on. Similarly, the stator currents are expressed as

$$i_{s\alpha} = i_{sa} \tag{6.7}$$

$$i_{s\beta} = \frac{1}{\sqrt{3}}(i_{sb} - i_{sc}) \tag{6.8}$$

The estimated Torque, $\mathbf{T_{est}}$ is represented as

$$T_{est} = \left(\frac{3}{2}\right)\left(\frac{P}{2}\right)\left(\phi_{s\alpha} i_{s\beta} - \phi_{s\beta} i_{s\alpha}\right) \tag{6.9}$$

The proposed torque estimator is modeled using equations (6.1) to (6.9) and is shown in Fig.6.1.

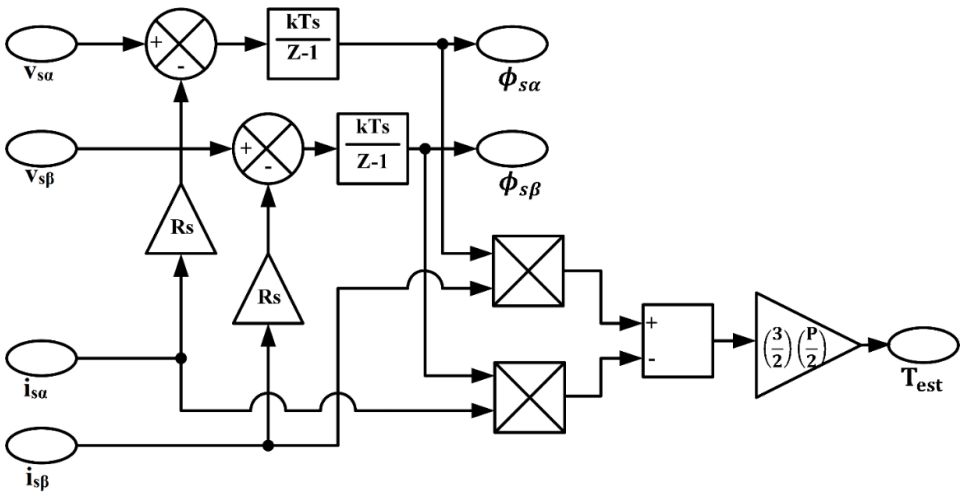

Fig.6.1. Torque Estimator

6.2.2. PI Speed and Current Controllers

The block diagram of the PI controller is shown in Fig.6.2. The time domain output of the PI Controller, $\mathbf{e_0(k)}$, is defined as:

$$e_0(k) = K_p e(k) + K_i \int_0^k e(k)dt \qquad (6.10)$$

The speed error e(k) , which generates reference torque at the Kth instance, $\mathbf{T_e^*(K)}$, using PI controller is defined by the expressions

$$e(k) = \omega_r^* - \omega_r \qquad (6.11)$$

$$T_e^*(K) = \left(K_{p\omega s} + \frac{K_{i\omega s}}{S}\right) e(K) \qquad (6.12)$$

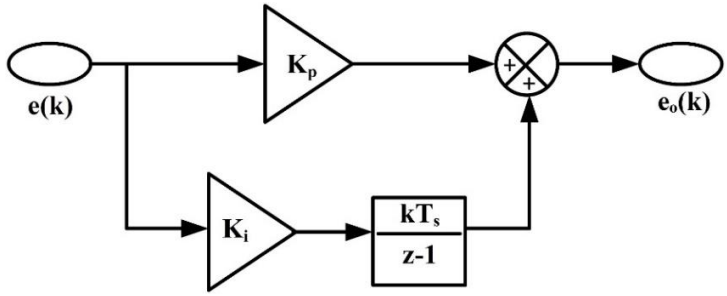

Fig.6.2. PI Controller

The torque error, $\mathbf{T_{e_{err}}}$, between the reference torque, $\mathbf{T_e^*}$, and estimated torque, $\mathbf{T_{est}}$, is used to generate the q-axis stator current, $\mathbf{i_{sq}^*(K)}$ using PI controller which is expressed as

$$T_{e_{err}} = T_e^* - T_{est} \qquad (6.12)$$

$$i_{sq}^*(K) = \left(K_{pqs} + \frac{K_{iqs}}{S}\right) T_{e_{err}}(K) \qquad (6.13)$$

6.3. DESIGN OF INTELLIGENT HYBRID CONTROLLER

Performance limitations of conventional methods employed for controlling the speed of PMSM drive, which depend on precise mathematical models, can be overcome by using soft-computing techniques [224], [225]. While the desired dynamic performance of PMSM drive may not be achieved by using only the PI controller, use of simple FLC is plagued by

difficulties in eliminating steady-state errors due to the missing integral action [167]. As compared to PI controller, FLC is more complex, computationally intensive and requires more memory. While PI controller improves steady state performance of the drive, FLC is best suited to meet the transient performance. To mitigate these problems, it is therefore prudent to design and employ a dual approach controller, which can gainfully utilize the advantages of both PI controller and FLC. The developed intelligent hybrid controller combines the speed deviation and specific set value for comparison. The FLC operates when the set value is less than the deviation and PI controller operates when the deviation is less than the set value. Fig.6.3. shows the developed intelligent hybrid controller.

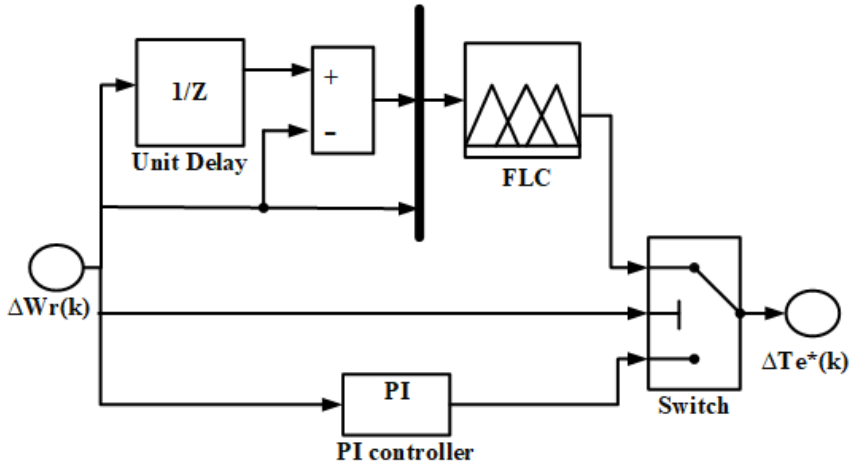

Fig.6.3. Intelligent hybrid controller

The designed IHC integrates both the PI controller and FLC with intelligent switching capability to use the FLC during transient operating conditions and the PI controller under steady state operation of the PMSM drive. The switching decision of the developed IHC is based on overshoots, undershoots and oscillations observed in the system. FLC is designed on the basis of linguistic rules, which is defined by the user and does not require mathematical modelling. The FLC algorithm designed for the speed control of PMSM drive is given below:

(i) Determine input and output variable.

(ii) Select membership function and state.

(iii) Define possible inference with membership functions and control rules.

(iv) Convert the fuzzy set into crisp set.

(v) Regulate the input and output gains appropriately to get the desired performance.

Speed error, $e(k)$ and change in speed error, $\Delta e(k)$, are the input crisp variables of the FLC and are defined as:

$$e(k) = \omega_r^*(k) - \omega_r(k) \tag{6.14}$$

$$\Delta e(k) = e(k) - e(k-1) \tag{6.15}$$

Output of the FLC is the reference torque component, which is defined as

$$\Delta T_e^*(k) = \Delta T_e^*(k-1) + \mu.\Delta T_e^*(k) \tag{6.16}$$

where $\Delta T_e^*(k)$ is reference torque inferred by FLC at the k^{th} sampling time and μ is the gain factor of FLC. The operation of the FLC can be described using three major steps: viz. fuzzyfication, rule execution, and defuzzyfication. In first step triangular membership functions of input and output convert crisp variables into fuzzy variables. Figs. 6.4 and 6.5 show the membership functions of the two inputs i.e. $\Delta e(k)$, $e(k)$.

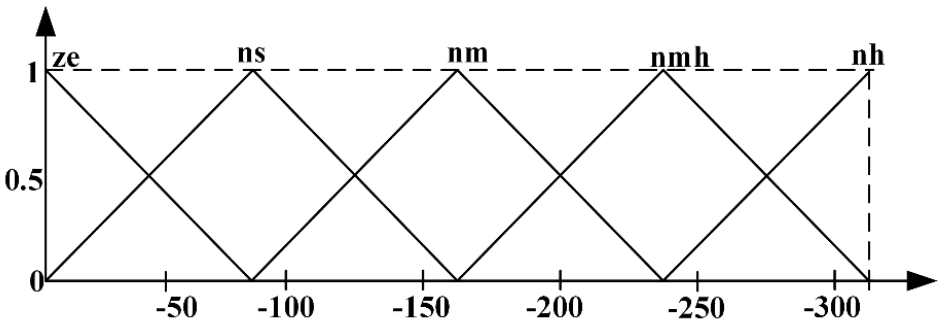

Fig.6.4. Membership Functions of Input 1, $\Delta e(k)$

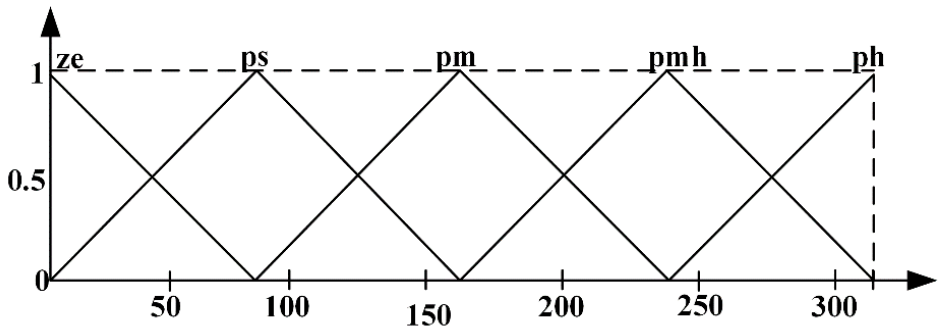

Fig.6.5. Membership functions of input 2, $\boldsymbol{e(k)}$

In the developed IHC fifteen linguistic variables are defined for input and output variables. The five linguistic variables for the 1st input, $\Delta e(k)$ are zero(***ze***), negative small(***ns***), negative medium(***nm***), negative medium high(***nmh***) and negative high(***nh***). Similarly, the five linguistic variables for the 2nd input, $\Delta\omega_r(k)$ are ***ze***, positive small(***ps***), positive medium(***pm***), positive medium high(***pmh***) and positive high(***ph***). Accordingly, the five output linguistic variables are ***ze***, ***ps***, ***pm***, ***pmh*** and ***ph***.

In second step a set of control rules are defined and executed using fuzzy variables from knowledge of expert. Each rule is expressed in the form

Rule: IF $e(k)$ is A and $\Delta e(k)$ is B, THEN $\Delta T_e^*(k)$ is C

where A, B and C are fuzzy sets.

Table.6.1. Fuzzy Rule Base of IHC

$\Delta T_e^*(k)$		$\Delta e(k)$				
		ze	**ns**	**nm**	**nmh**	**nh**
$e(k)$	**ze**	ze	ps	pmh	pmh	ph
	ps	ps	ze	ps	pmh	ph

	pm	pmh	ps	ze	ps	pmh
	pmh	pm	pmh	ps	ps	ps
	ph	ph	pm	pmh	ps	ze

In the third step, called defuzzyfication, fuzzy variables are converted into crisp variables to obtain computable outcomes in fuzzy logic, fuzzy sets and membership function. Various methods of defuzzyfication include use of center-of-sets defuzzifier, center-of-sums defuzzifier, centroid defuzzifier and height defuzzifier. The developed FLC uses centroid defuzzifier method for defuzzyfication because of less computational time and better dynamic behavior. The matrix of fuzzy base rules used in the IHC is tabulated in Table.6.1.

6.4. CONTROL OF PMSM DRIVE WITH PROPOSED IHC

In vector control, space vectors of flux, current, and voltage are controlled using field-oriented approach [226], [227], [228]. Fig.6.6. shows the block diagram of PMSM drive system with the developed IHC.

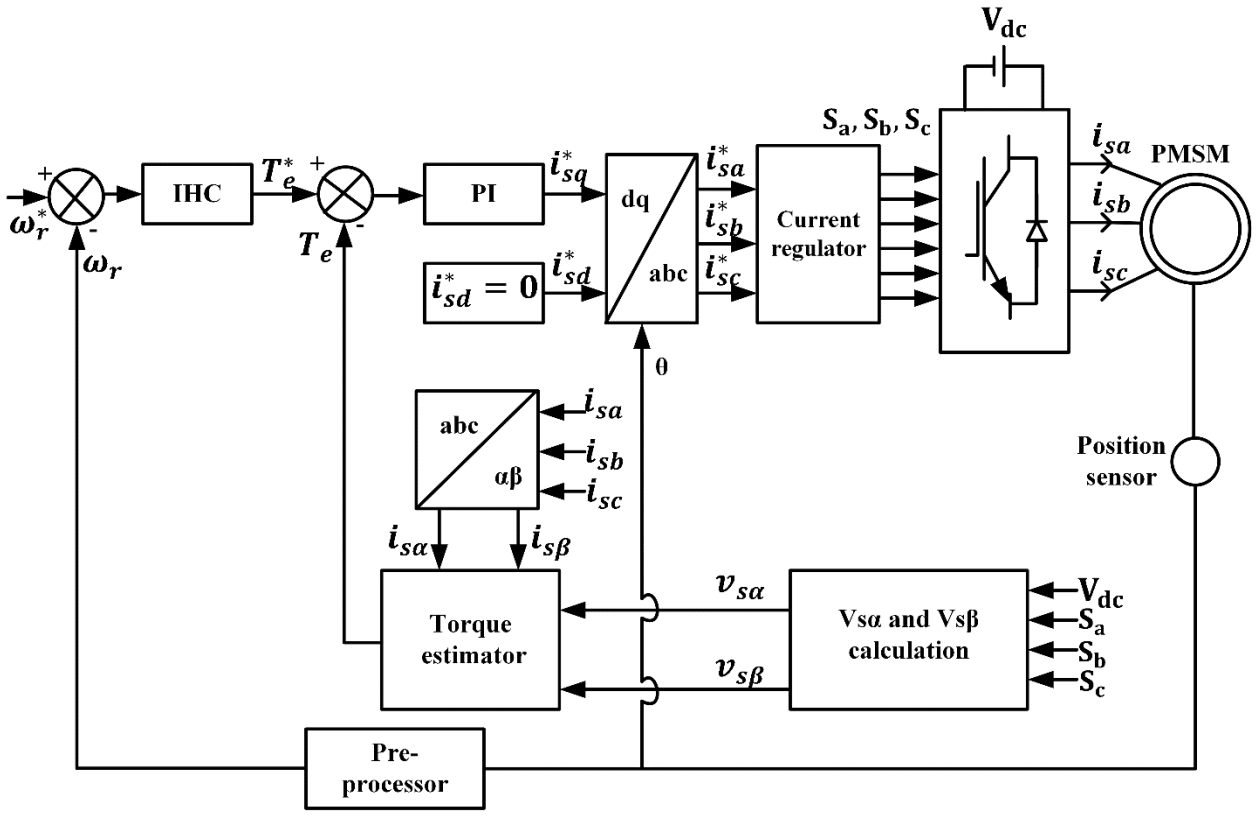

Fig.6.6. Block Diagram of PMSM Drive with IHC

In high performance drives inner loop having high bandwidth is required to track current accurately, reduce the transient period and to ensure that VSI can be used as a current source amplifier [172] .

In the outer speed loop, speed error is processed by the IHC to generate the reference torque command, which is compared with the estimated torque. The torque is estimated using the DC link voltage, measured currents (i_{sa} , i_{sb} and i_c) and the status of the switches (S_a, S_b and S_c) of the VSI generated using the pulses from current regulator as discussed earlier. This estimated torque is compared with the reference torque and the error signal thus generated is fed to the current controller to produce the torque producing quadrature axis current, i_{sq}^* .

6.5. RESULTS AND DISCUSSIONS

A 3-phase 3.4kW, 314 rad/s vector controlled PMSM drive with parameters as given in Appendix-I is modeled and simulated using MATLAB/Simulink. The performance of the drive is studied and analyzed under various operating conditions using the conventional PI controller and the developed IHC. For simulation studies the sampling time is set at $\mathbf{10}\boldsymbol{\mu}$ sec.

6.5.1. Performance of PMSM Drive at Rated Speed Operation

Figs.6.7 (a) and (b), show the dynamic response of speed, torque and stator currents of PMSM drive using PI controller and IHC respectively for rated speed operation i.e. 314rad/sec. The motor is started under no-load condition at rated speed and it tracks the reference speed smoothly. When rated-load is applied at 0.03 sec, a momentary dip is observed in speed response after which the drive tracks the reference speed smoothly.

From the torque response in Figs.6.7 (a) and (b), it is noted that ripples in torque of the motor is considerably reduced by using IHC as compared to the conventional PI controller.

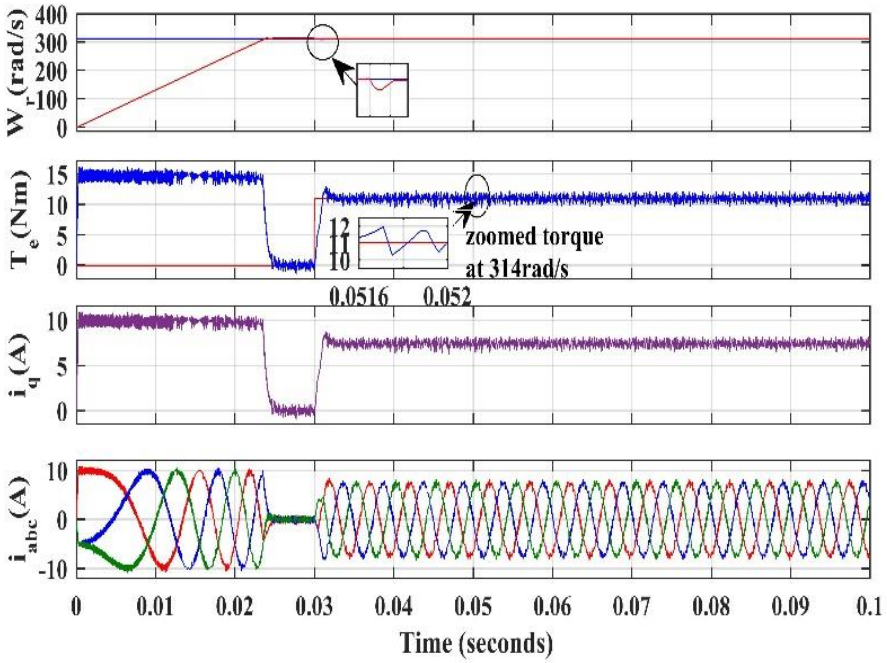

(a)

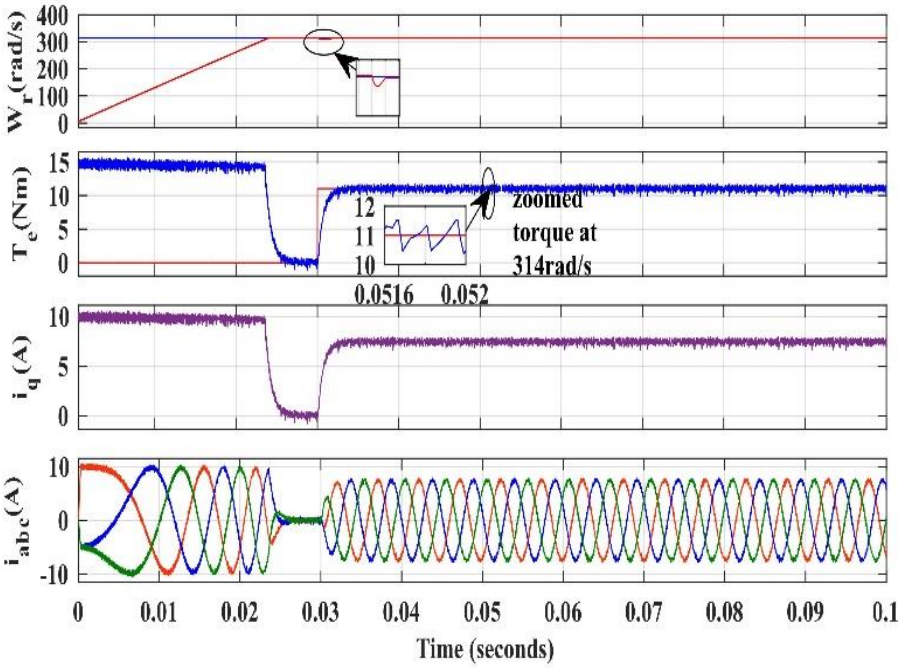

(b)

Fig.6.7. Dynamic Performance of PMSM Drive for Rated Speed Operation:

(a)using PI Controller, (b)using IHC

6.5.2. Performance of the PMSM Drive for step change in speed

Figs.6.8 (a) and (b), show the dynamic response of speed, torque and stator currents of the PMSM drive with PI controller and IHC respectively for a step change in speed from 157 rad/sec to 314rad/sec.

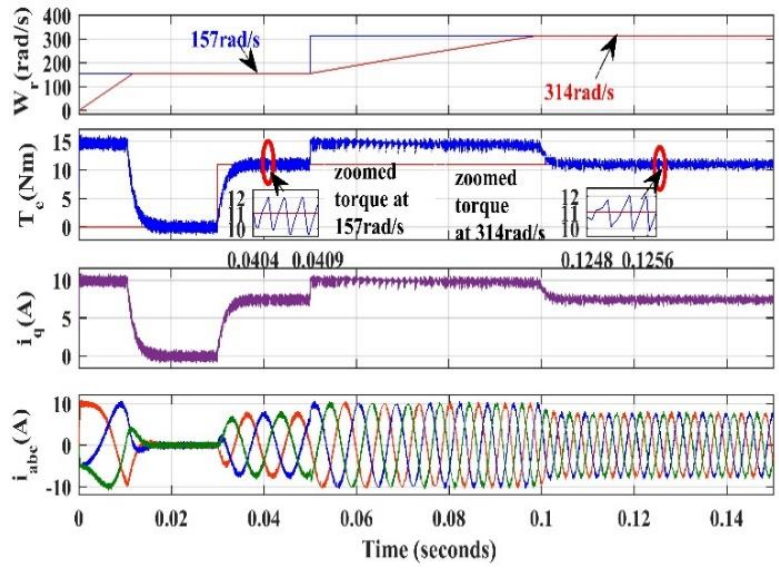

(a)

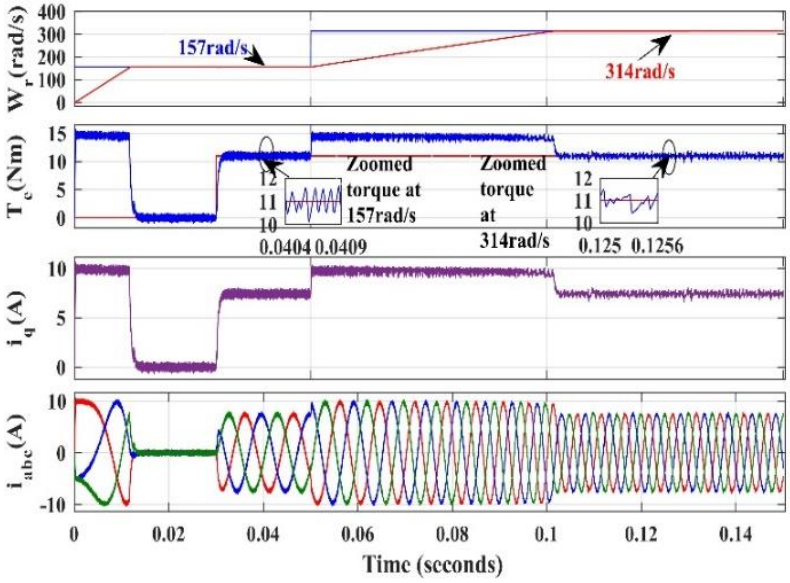

(b)

Fig.6.8. Dynamic Performance of PMSM Drive for Step Change in Speed

(a) using PI Controller, (b) using IHC

The motor is started under no-load condition at half rated speed. At 0.03 sec, rated load is applied to the motor and it is observed that the motor developed the required torque without any delay. At 0.05 sec, when the speed is changed from 50% of rated speed (157rad/sec) to rated speed (314rad/sec), it is found that the speed and torque of the motor follow their reference

values. Analysis of the torque response of the motor shows that toque ripples are significantly reduced by employing the IHC.

6.5.3. Performance of the PMSM Drive for Speed Reversal

The performance of the PMSM drive is analysed for speed reversal at rated–speed–rated–torque condition. Figs.6.9 (a) and (b), show the dynamic response of speed, torque and stator currents of the drive using PI controller and IHC respectively during reversal of speed from 314 rad/sec to –314 rad/sec. When the motor is running at rated speed, rated torque condition, a speed reversal command is given at 0.05 sec. It is observed that the speed and torque of the motor track their reference values smoothly. Torque responses of the motor under speed reversal at rated–speed–rated–torque condition also show that torque ripples are less with IHC as compared to the PI controller.

6.5.4. Comparison of Estimated Torque and Developed Torque under Steady State Operation

Figs. 6.10 and 6.11 show the comparison between developed torque and estimated torque of the PMSM drive with PI controller and IHC under steady state operation. The developed torque (T_e) is 11Nm at rated speed of 314rad/s and the estimated torque output (T_{est}) from estimator is 10.9Nm. The average error between actual torque output and estimated torque output is observed to be 0.1Nm.

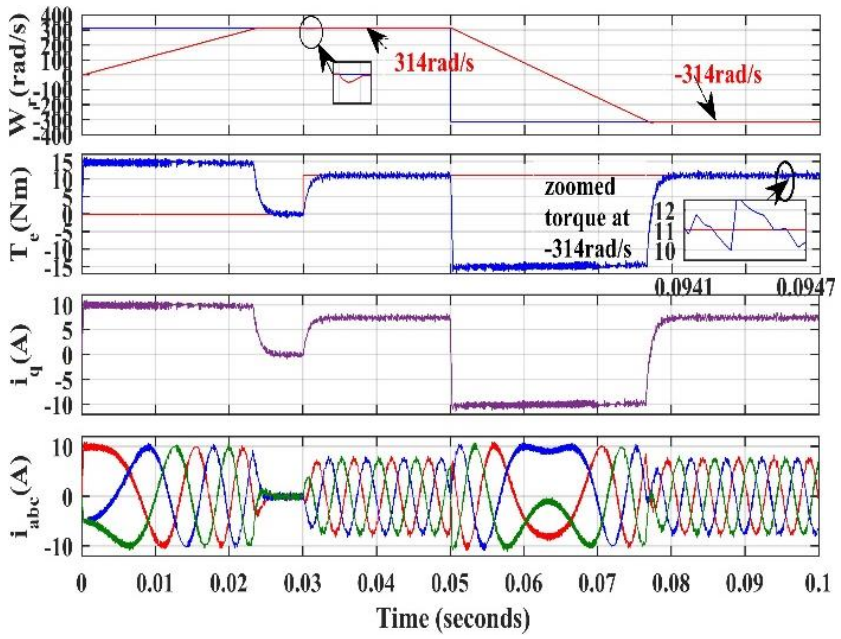

(a)

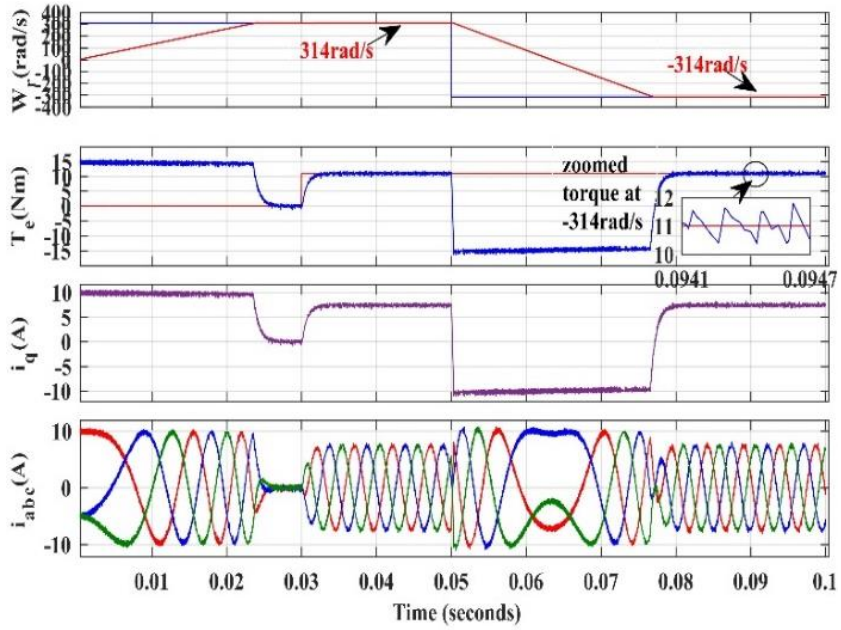

(b)

Fig.6.9. Dynamic Performance of PMSM Drive during Speed Reversal

(a) using PI Controller, (b) using IHC

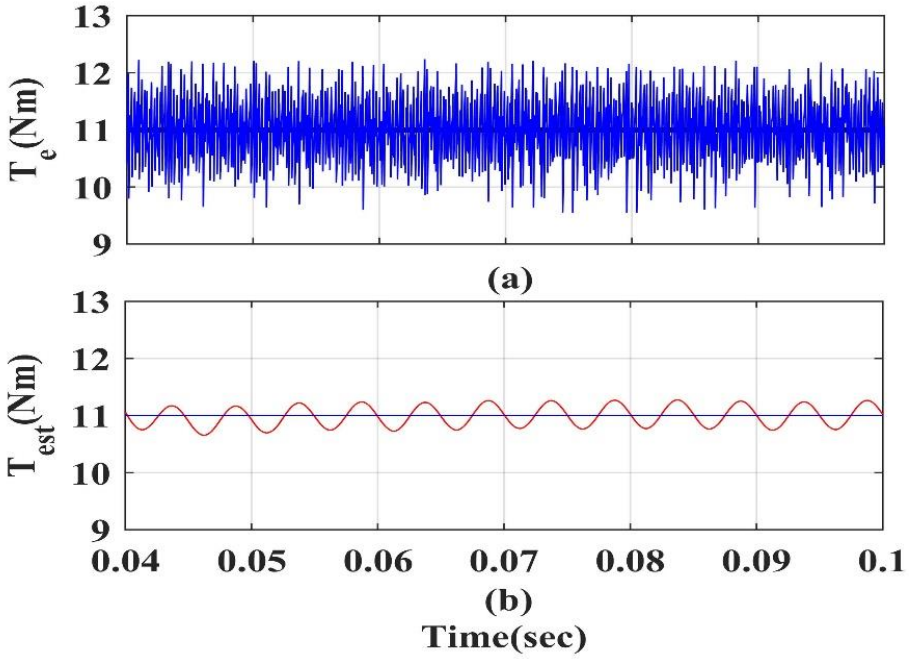

Fig.6.10. Torque Responses of PMSM Drive with PI Controller:

(a) Developed Torque, (b) Estimated Torque

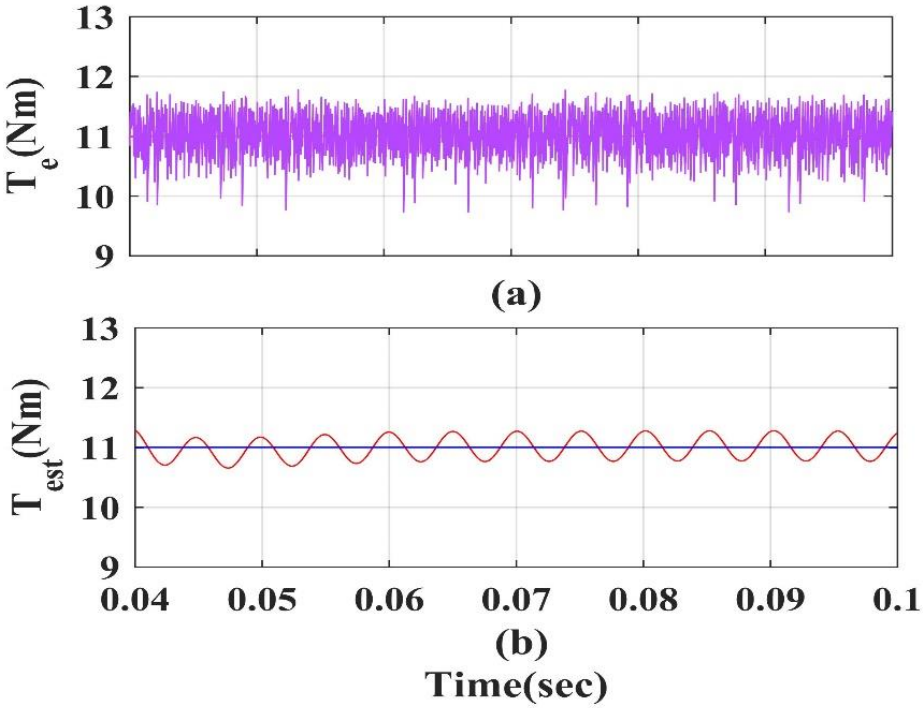

Fig.6.11. Torque Responses of PMSM Drive with IHC:

(a) Developed Torque, (b) Estimated Torque

6.5.5. Torque ripple Analysis

Torque ripple is expressed as the percentage of the difference between the maximum torque, T_{max} and the minimum torque, T_{min} compared to the rated torque, T_e [229], [230] as given below:

$$\text{Torque ripple (\%)} = \frac{T_{max} - T_{min}}{T_e} \times 100 \qquad (6.17)$$

T_{max}, T_{min} are obtained from the given torque responses. Figure.6.12. shows the comparative analysis of torque ripples in vector controlled PMSM drive at different operating speeds with PI controller and IHC. It is observed that ripples are considerably reduced by using IHC as speed controller as compared to the PI controller.

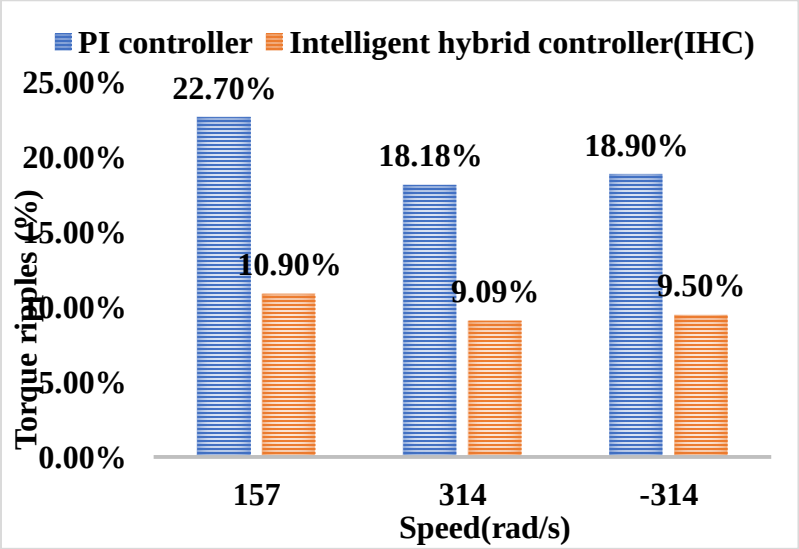

Fig.6.12. Comparative Analysis of Torque Ripples in PMSM at different Operating Speeds with PI Controller and IHC

6.5.6. THD analysis

Figs.6.13(a) and (b) show the harmonic spectrum of stator current at rated speed operation of the drive with PI controller and IHC respectively. THD with PI controller is 5.8% while that

with IHC is observed to be 4.6%. Figs.6.14(a) and (b) show the harmonic spectrum of stator current at half rated speed operation (157 rad/sec) of the drive with PI controller and IHC.

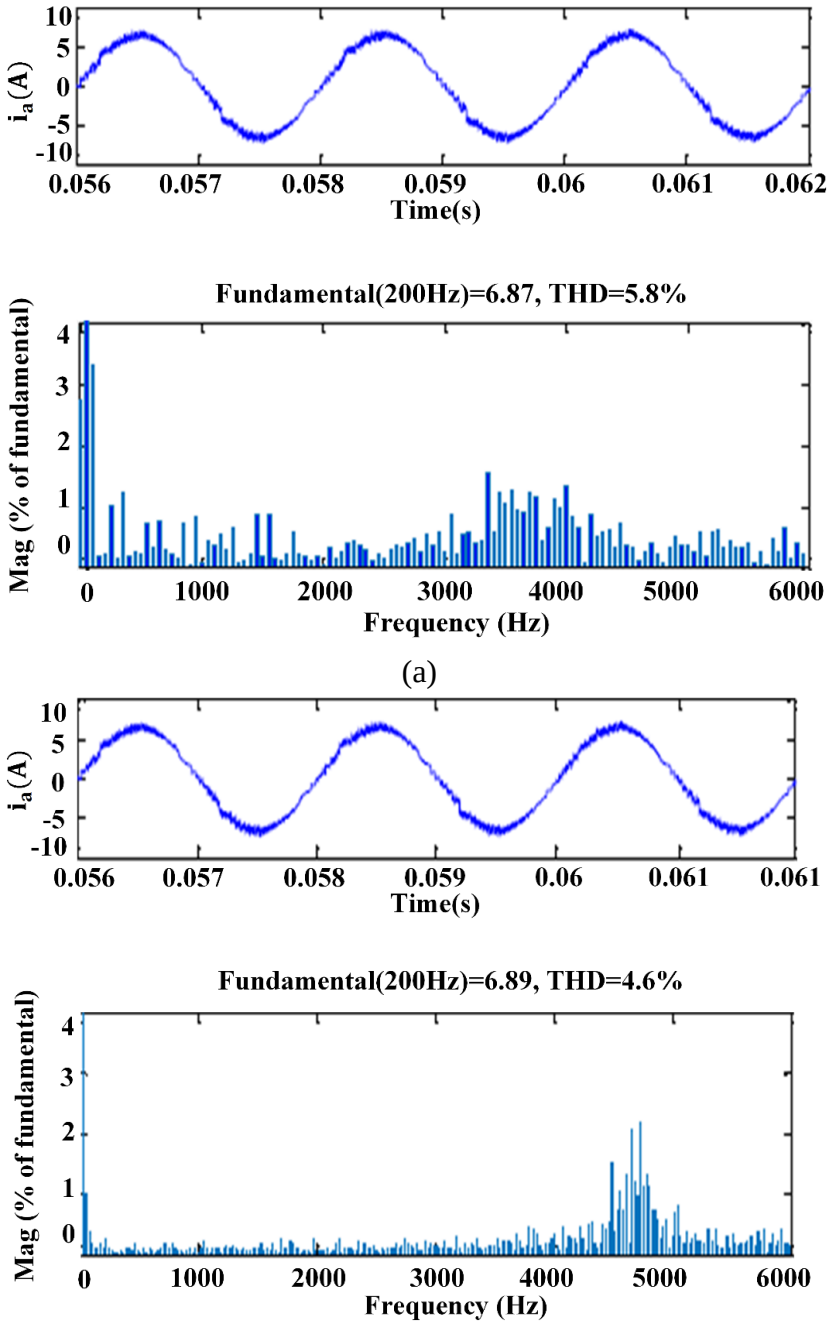

Fig.6.13. THD of Stator Current of the PMSM Drive at Rated Speed:

(a) using PI Controller, (b) using IHC

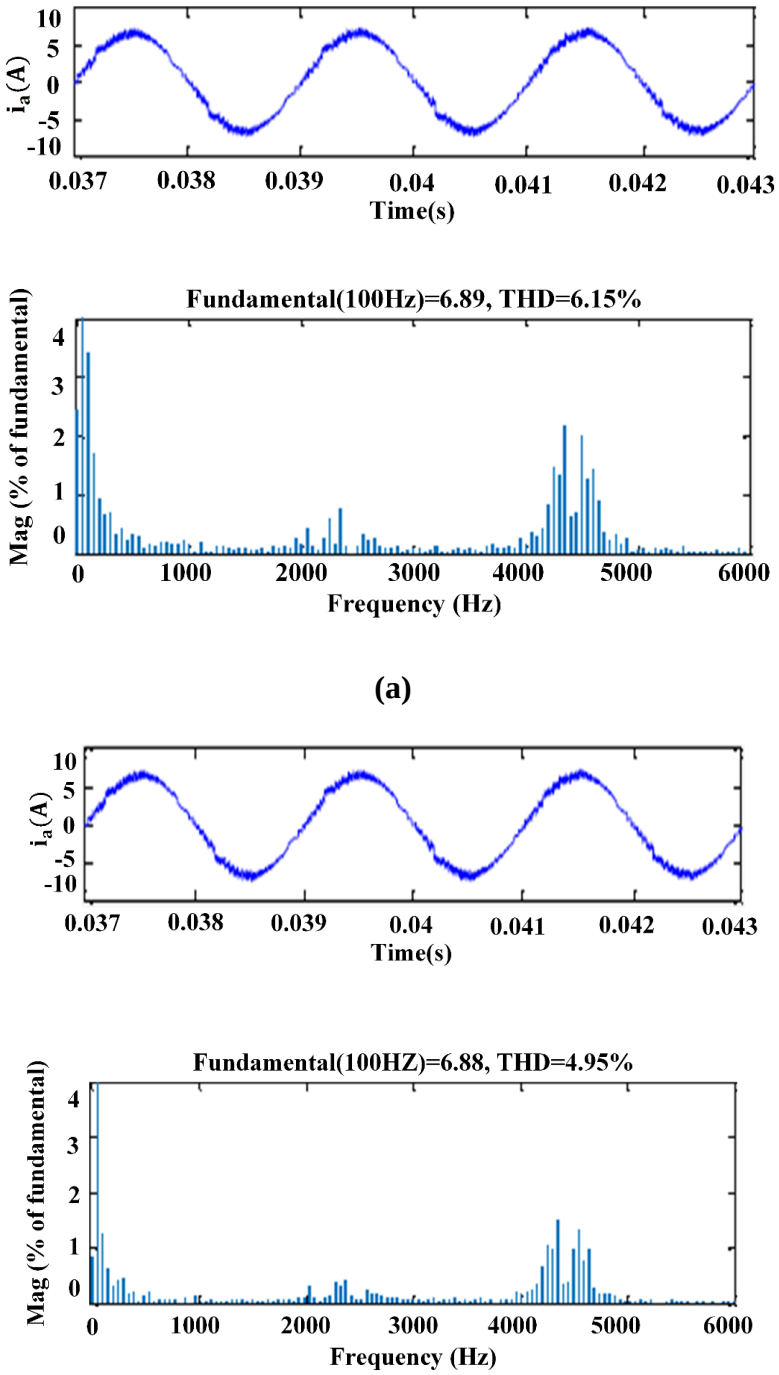

Fig.6.14. THD of Stator Current of the PMSM Drive at half of the Rated Speed:

(a) using PI Controller, (b) using IHC

Figs.6.14(a) and (b) show the harmonic spectrum of stator current at half rated speed operation (157 rad/sec) of the drive with PI controller and IHC. THD with PI controller is 6.15% while

that with IHC is observed to be 4.95%. For comparative analysis the average switching frequency for all methods is kept same. For simulation studies the average switching frequencies of both methods are kept same at 7.5 kHz for rated speed of operation. THD is analyzed up to 6kHz and it is observed that THD in stator current of PMSM drive with Intelligent Hybrid Controller is lower as compared to that of PI controller.

6.6. CONCLUSION

To overcome the limitations of conventional PI controller and FLC, an IHC is designed and developed for a vector controlled PMSM drive. The designed IHC integrates both the PI controller and FLC with intelligent switching capability to use the FLC during transient operating conditions and the PI controller under steady state operation of the PMSM drive. The proposed controller thus gainfully utilizes the advantages of both PI and FLC. In this hybrid control scheme, the torque is estimated using measured current and DC link voltages and compared with the reference torque generated by the IHC employed in the speed loop to generate the reference q-axis stator current, thereby reducing the torque ripples. Simulation studies are carried out for a vector controlled PMSM drive with PI controller and IHC as speed controller. The effectiveness of PMSM drive with IHC controller is investigated under different operating conditions viz rated-speed-rated-torque operation, step change in speed and reversal of speed. The performance of the IHC based PMSM is compared with the performance of the PMSM with conventional PI controller. It is found that the IHC gives improved dynamic performance of PMSM and also reduces THD in stator current of the motor. It is also observed that torque ripples are less when IHC is employed as speed controller instead of the conventional PI controller.

CHAPTER 7

DESIGN AND IMPLEMENTATION OF PI-RES CONTROLLER FOR TORQUE RIPPLE MINIMIZATION IN MPC BASED PMSM DRIVE

7.1. GENERAL

PMSMs have been commonly used in variable speed drives for industrial applications, due to their high efficiency, low volume, high torque density and wide range of speed of operation. PMSM has a few inherent limitations, such as machine design imperfectness, pulsating torque resulting from effect of dead time, error in current measurement and other uncertainties, especially when motor is used for low-speed operations [231]. The ripples in motor torque can produce speed ripples in the motor, which is not desirable for servo application such as machine tools etc.

Torque dynamics can be improved through use of appropriate control technique. Predictive control is one of the most admired techniques amongst them. PMSM can achieve good control performance when the real time three-phase current is measured accurately. However, error in measuring the current can produce speed ripples in PMSM drive. Current measurement errors are usually caused by the hall sensor units, the signal processing circuit, A/D converter and filter circuits[232]. Torque ripples produced due to error in current measurement can be reduced by compensation of the torque generating current. This technique depends on motor variables of machine and is difficult to realize for practical applications.

Speed ripples in motor can be reduced by employing suitable control approach based on principle of internal mode such as repetitive controller [233], [234] and resonant controllers [125], [235], [236]. Repetitive controller has limitation relating to adapting the frequency as it requires variable sampling frequency. Resonant controllers can achieve precise reference tracking and disturbance rejection while producing infinite gain at the unbalanced frequency. This Chapter[6] elucidates the design and implementation of a PI-RES speed controller for minimisation of torque ripples in MPC based PMSM drive. The PI-RES controller is designed by connecting a frequency variable resonant controller with PI controller in parallel. The PI-RES controller produces the reference current for MPC of PMSM. The proposed controller produces the reference torque current and is able to reduce ripples by generating compensation torque current from resonant controller along with the main reference current. Simulation studies were carried out to compare the performance of the developed PI-RES controller and the classical PI controller for MPC of PMSM drive.

7.2. BASIC PRINCIPLE OF MPC FOR PMSM DRIVE

MPC has developed as an effective technique for controlling PMSM drives and power converters for high performance applications [237], [238]. MPC has several advantages such as simple handling of multivariable cases, the ability to adapt to dead times and ease of handling nonlinearities [239]. In MPC an objective function is defined as the selection criteria, which selects the optimal switching states fed to the VSI. The estimated values of the variables to be monitored are used to determine the objective function. The switching states are calculated by predicting the value of these variables and only the switching states that can

[6] **Paper Communicated:** Suryakant, Mini Sreejeth, Madhusudan Singh, "Minimization of Torque Ripples in PMSM Drive using PI Resonant Controller based Model Predictive Control", Electrical Engineering, Springer.

minimize the objective function are chosen. The proposed MPC involves the following three steps: -

(1) Define the objective function.

(2) Build predictive model of inverter and find out its optimal switching states.

(3) Create a prediction model of load.

PMSM being the load on the VSI, a discrete time PMSM model is needed to predict the behaviour of variables (such as load current) assessed by the objective functions. The block diagram of MPC algorithm applied in current control method of PMSM drive is presented in Fig.7.1. The stator reference current, i_k^* is obtained from the outer speed loop of PI-RES controller and i_k is measured. For each of the different voltage vectors, the motor's modelling equations are used to predict the value of i_k in the next sampling period (i_{k+1}). The objective function measures the error of predicted and reference currents for the next sampling time. The voltage which produces the minimum value of current error is chosen and applied to the load. The flow chart of the algorithm for implementation of MPC of PMSM is shown as Fig.7.2.

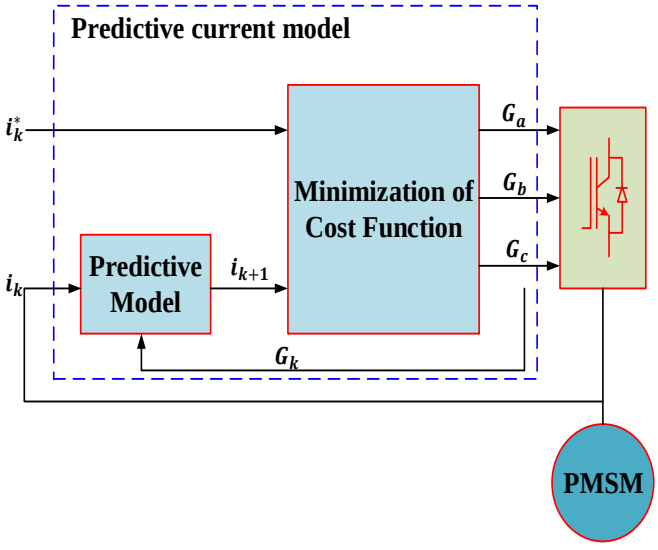

Fig.7.1. Scheme for MPC of PMSM

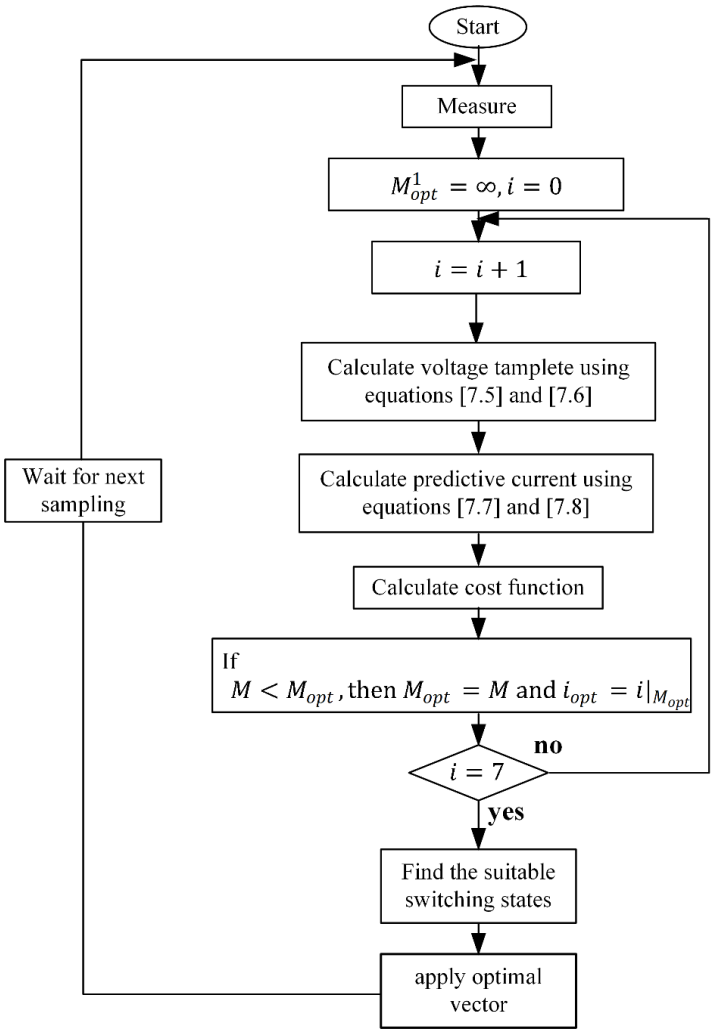

Fig.7.2. Flow Chart of MPC for PMSM drive

The states of the switching are defined by the equations:

$$G = \frac{2}{3}(G_a + aG_b + a^2G_c) \tag{7.1}$$

where G_a, G_b, G_c are the pulses given to the inverter and $a = e^{j2\pi/3}$. The output of inverter is

$$G = \frac{2}{3}(v_{an} + av_{bn} + a^2v_{cn}) \tag{7.2}$$

The current vector, i, and back-EMF, e, of the PMSM is expressed as

$$i = \frac{2}{3}(i_{sa} + ai_{sb} + a^2i_{sc}) \tag{7.3}$$

$$e = \frac{2}{3}(e_{sa} + ae_{sb} + a^2 e_{sc}) \tag{7.4}$$

From the modelling equations of PMSM in d-q axis the predictive model is derived as

$$v_{sq}(k) = R_s i_{sq}(k) + \frac{L}{T_s}\left[i_{sq}(k+1) - i_{sq}(k)\right] + L\omega_r i_{sd}(k) - \varphi_m \omega_r \tag{7.5}$$

$$v_{sd}(k) = R_s i_{sd}(k) + \frac{L}{T_s}[i_{sd}(k+1) - i_{sd}(k)] - L\omega_r i_{sq}(k) \tag{7.6}$$

$$i_{sq}(k+1) = i_{sq}(k) + \frac{T_s}{L}\left[v_{sq}(k) - R_s i_{sq}(k) - L\omega_r i_{sd}(k) - \varphi_m \omega_r\right] \tag{7.8}$$

$$i_{sd}(k+1) = i_{sd}(k) + \frac{T_s}{L}\left[v_{sd}(k) - R_s i_{sd}(k) + L\omega_r i_{sq}(k)\right] \tag{7.9}$$

The objective function, M, for the model predictive control is defined as

$$M = \left|i_{sq_{ref}} - i_{sq}(k+1)\right| + \left|i_{sd_{ref}} - i_{sd}(k+1)\right| \tag{7.10}$$

7.3. DESIGN OF PROPOSED PI-RES CONTROLLER

The outer loop of the PMSM drive with classical PI controller is presented in Fig.7.3, where T_d is the inner loop delay. The expression of proportional resonant (PR) controller to track AC signal in s-domain is [236], [240].

$$G(s)_{PR} = K_p + \frac{2K_{ir}\omega_c s}{S^2 + 2\omega_c s + \omega^2} \tag{7.11}$$

where, ω is the regulated signal frequency, ω_c is cut off frequency and K_{ir} is the resonance coefficient. The damping coefficient contributes to increasing the bandwidth of centre frequency of ω as well as expand the phase margin of control system. $G(s)_{PR}$ gives the open loop infinite gain at resonant frequency ω, that promises accurate tracing for oscillating variables at ω when applied in closed loop, similar to the $G(s)_{PI}$ applied in rotational reference

frame of ω. The $G(s)_{PI-res}$ is designed by connecting $G(s)_{PI}$ and $G(s)_{PR}$ in parallel. In this controller only one gain i.e. K_p is required to be tuned [241]

$$G(s)_{PI} = K_p + \frac{K_i}{s} \tag{7.12}$$

$$G(s)_{PI-res} = K_p + \frac{K_i}{s} + \frac{2K_{ir}\omega_c s}{S^2+2\omega_c s+\omega^2} \tag{7.13}$$

Here PI controller is used to calculate the error between reference speed, ω_r^* and measured speed, ω_r and to minimize the steady state error of speed. Motion control systems commonly employ PI controllers. A proportional gain provides an output proportionate to the input error, whereas an integral gain minimizes the steady state error to zero for a step change in the input.

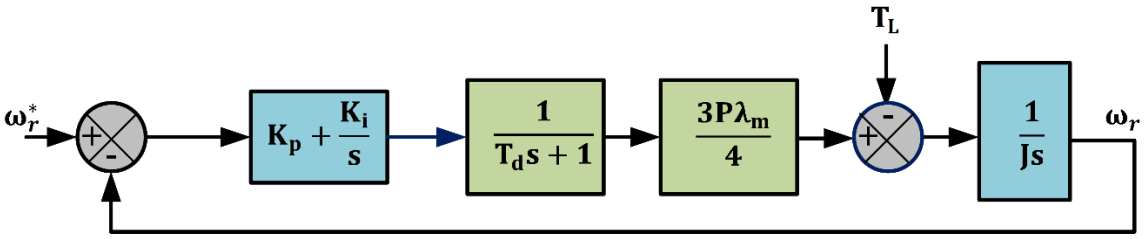

Fig.7.3. Outer loop of PMSM Drive with classical PI speed controller

Fig.7.4 shows the outer loop of PMSM with proposed PI-RES speed controller. Since the controlling perturbation is repeated and with twice the sinusoidal rotor frequency, the proposed PI-RES controller is created by combining a PR controller with a classical PI controller. The proposed controller has good ability to control the harmonics as compared to classical PI controller. Here the resonance word addresses the rotor frequency of second harmonic, that is acquired from position sensors or through sensor-less control techniques. By combining the compensating torque current produced by the resonant controller and reference current generated by the PI controller, the speed ripples are minimized. PI-RES controller generates the reference of pulsating torque current that counter the ripples in load torque.

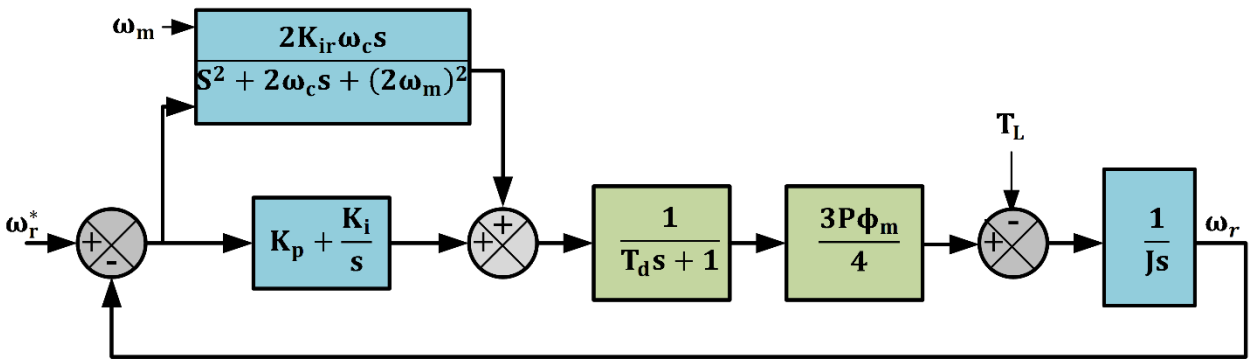

Fig.7.4. Outer loop of PMSM Drive with PI-RES speed controller

The motor speed is generally obtained by differentiating the rotor position; however, in this process high frequency noise is produced in discrete systems. A low-pass filter of 500 Hz frequency is employed to reduce this noise in the speed signal. When the PI-RES controller is employed in the speed loop, the dynamic performance is controlled by K_p, while K_i and K_{ir} remove the error in steady state condition. The phase margin of the speed loop is almost 90° when $K_i = K_{ir} = 0$ and the system will be stable. The system behaves like a second order system if K_i and K_{ir} are neglected and the speed loop transfer function is expressed as:

$$G_s(s) = K_p.\frac{1}{Js}.\frac{1}{T_d\,s+1}.\frac{3P\phi_m}{4} \tag{7.4}$$

$$T_d = \frac{1}{B_i} + \tau_{LPF} \tag{q2(7.5)}$$

The proportional constant of the speed loop, K_p is:

$$K_p = \frac{1}{4\delta^2 T_d}\frac{4J}{3P\phi_m} \tag{7.6}$$

where, δ is the damping gain, T_d is delay time, τ_{LPF} is time constant and B_i is bandwidth of deference in ω.

7.4. CONTROL OF PMSM DRIVE WITH PROPOSED PI-RES CONTROLLER

FOC technique is used to control space vectors of flux, current, and voltage in vector controlled PMSM drive [242],[226]. The block diagram for MPC of a PMSM drive with a PI-RES controller is presented in Fig.7.5.

The PI-RES controller is used in the speed outer loop to generate reference current depending on the error in reference and motor speeds. MPC is employed to generate the ideal voltage vector and supplied to inverter. The voltage is chosen and fed to inverter in such a way that the error between reference and predicted current is minimized. Using the observed voltage and current from the inverter, the predicted current for the k^{th} sampling is determined.

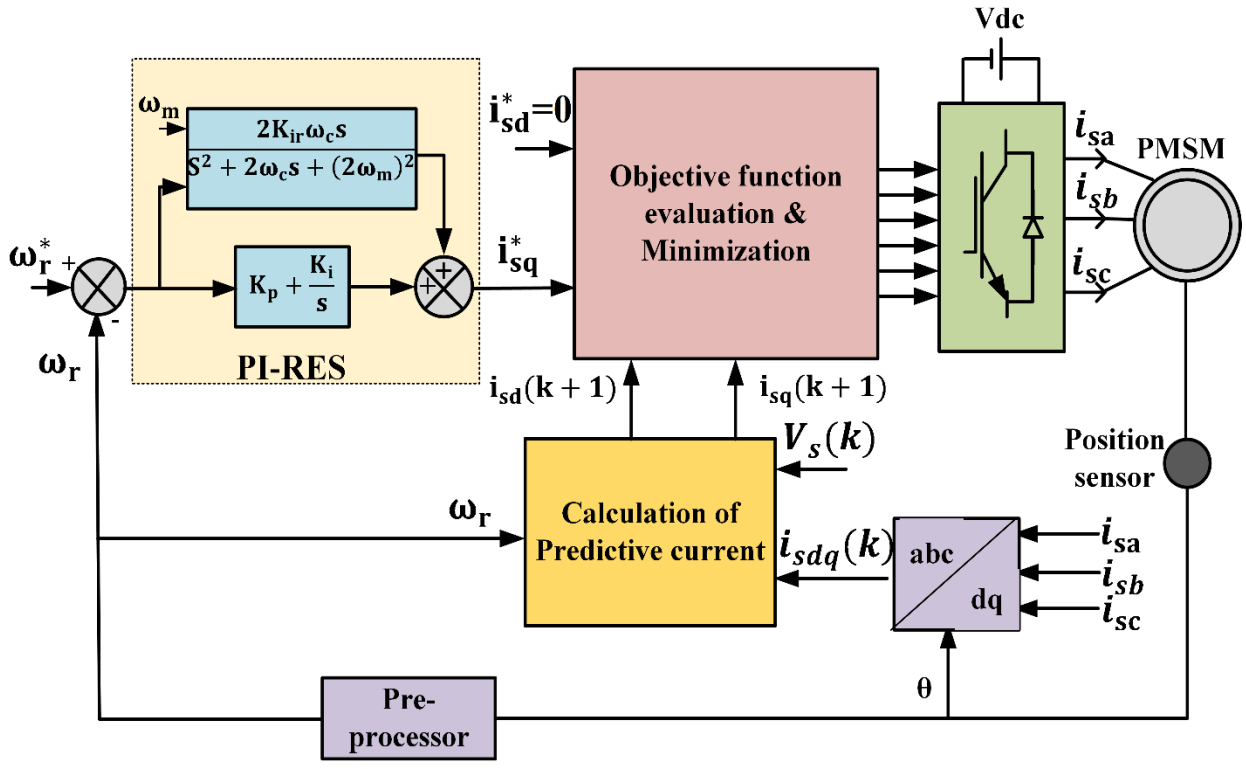

Fig.7.5. PMSM Drive with PI-RES Speed Controller

7.5. RESULTS AND DISCUSSIONS

The performance of classical PI controller and proposed PI-RES controller for speed control for MPC of PMSM drive are investigated through simulation studies using MATLAB/ Simulink, for the motor with specifications as given in Appendix-I. Load variation, low speed operation, torque ripple analysis and THD analysis at sampling time of 10μs are considered for testing of the proposed controller.

7.5.1. Starting characteristics of PMSM Drive

The starting characteristics of PMSM drive at no-load and rated-speed operation are presented in Figs.7.6. (a) and (b) using PI and proposed PI-RES controller, respectively. Some overshoot and distortion in speed, torque and stator current are observed when PI controller is used as speed controller; while PI-RES controller regulates the speed of the motor without overshoot and gives fast and smooth response.

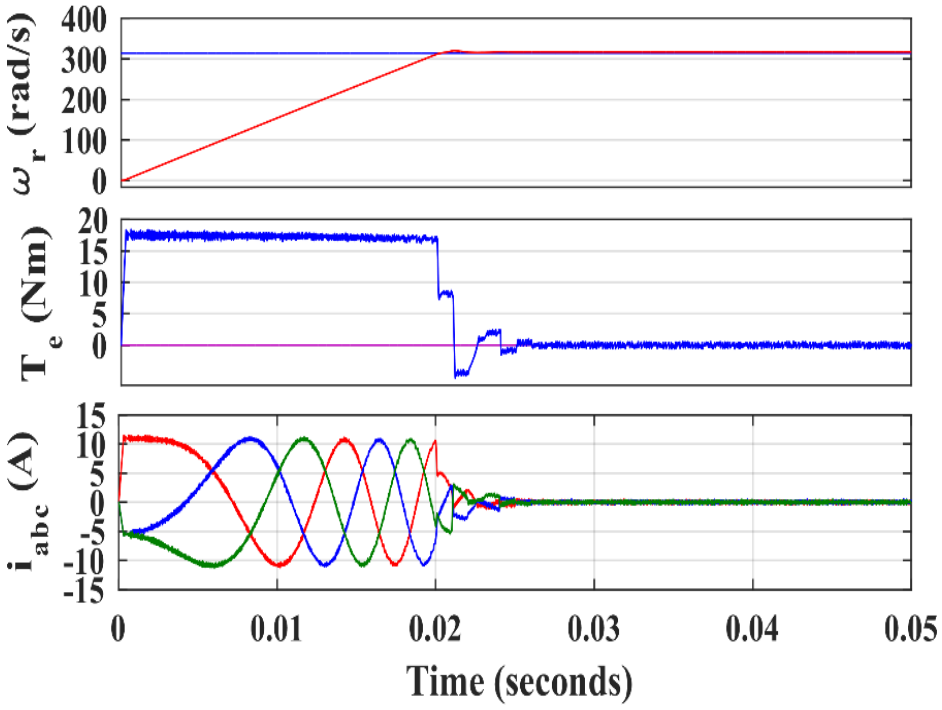

(a)

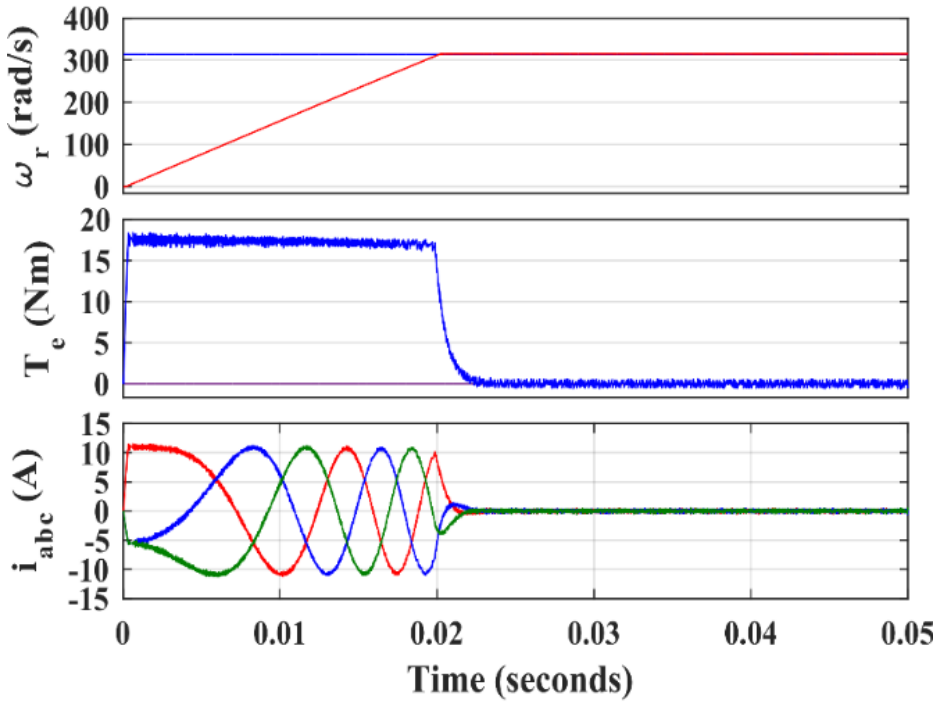

(b)

Fig.7.6. Starting characteristics for MPC of PMSM drive at rated operation with: (a) PI Controller (b) PI-RES Controller

7.5.2. Dynamic response of PMSM Drive during sudden change of load torque

Figs. 7.7 (a) and (b) shows the zoomed dynamic response of the drive during torque transition at rated speed operation of the motor. The rising time and settling time are also observed to be less with PI-RES controller in comparison to PI controller, which makes the response of the drive faster.

Fig.7.8. shows the transient characteristics of MPC of PMSM drive at rated speed with PI controller and PI-RES controller, respectively. During starting with no load, some overshoot and undershoot are observed with the PI controller; while PI-RES gives smooth speed characteristics.

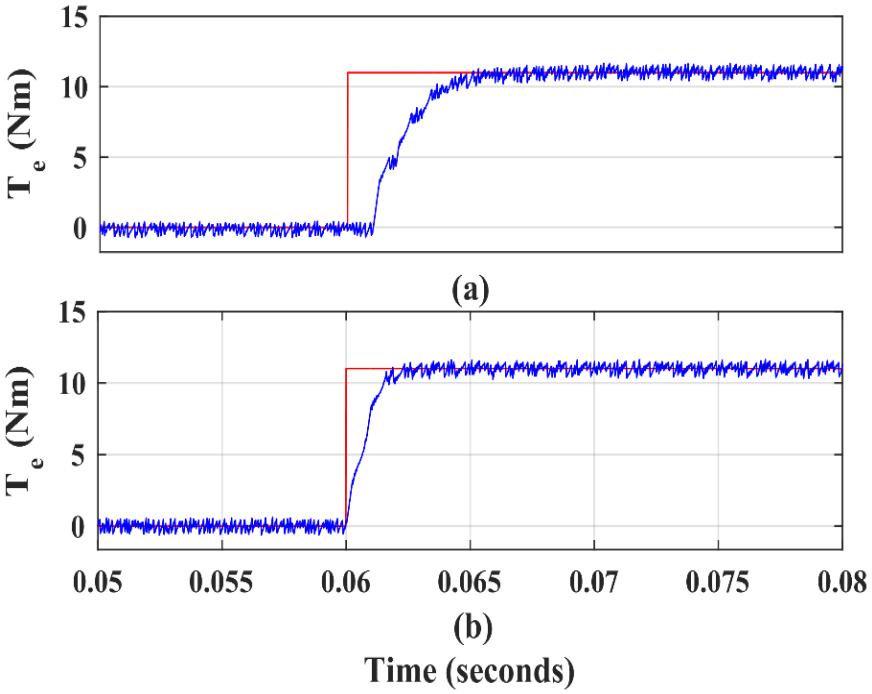

Fig.7.7. Torque dynamics for MPC of PMSM during torque transition at rated speed operation: (a) PI Controller (b) PI-RES Controller

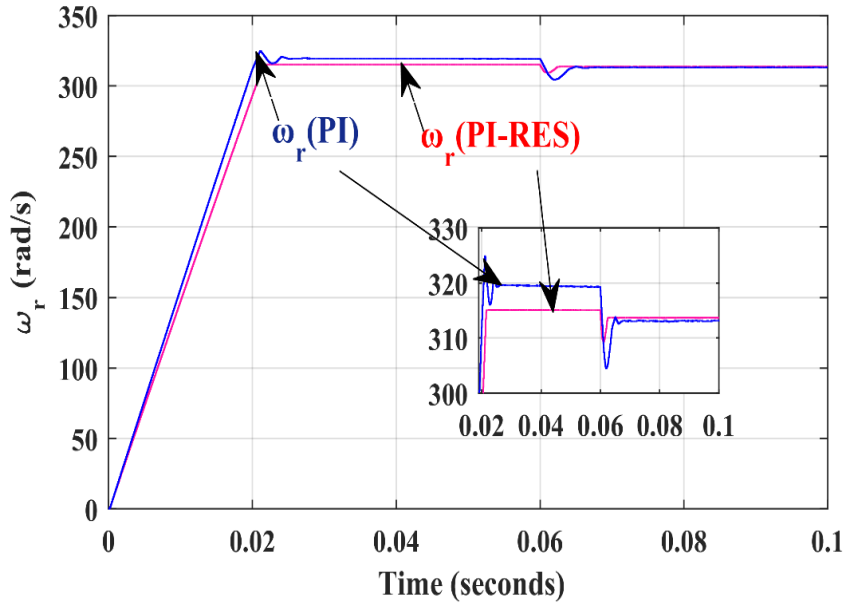

Fig.7.8. Transient characteristics of model predictive control of PMSM Drive at rated speed with: (a) PI Controller (b) PI-RES Controller

When the full load is applied at t=0.06s, speed of the motor settled to the commanded value earlier with PI-RES controller as compared to the PI controller. During the torque transition, the speed perturbation is less in the PI-RES controller.

7.5.3. Dynamic performance of PMSM Drive at low-speed operation

Figs. 7.9 (a) and (b) present the speed, torque and stator current characteristics for MPC of PMSM drive with PI controller and PI-RES controller, respectively, for low-speed (10% of rated-speed) operation.

Fig.7.10. presents the zoomed speed characteristics during torque transition for this operating speed. The proposed PI-RES controller reduces the overshoot and undershoot of speed when load torque is applied. In addition, the settling time of motor speed to its reference speed with PI-RES speed controller is faster than that of conventional PI speed controller.

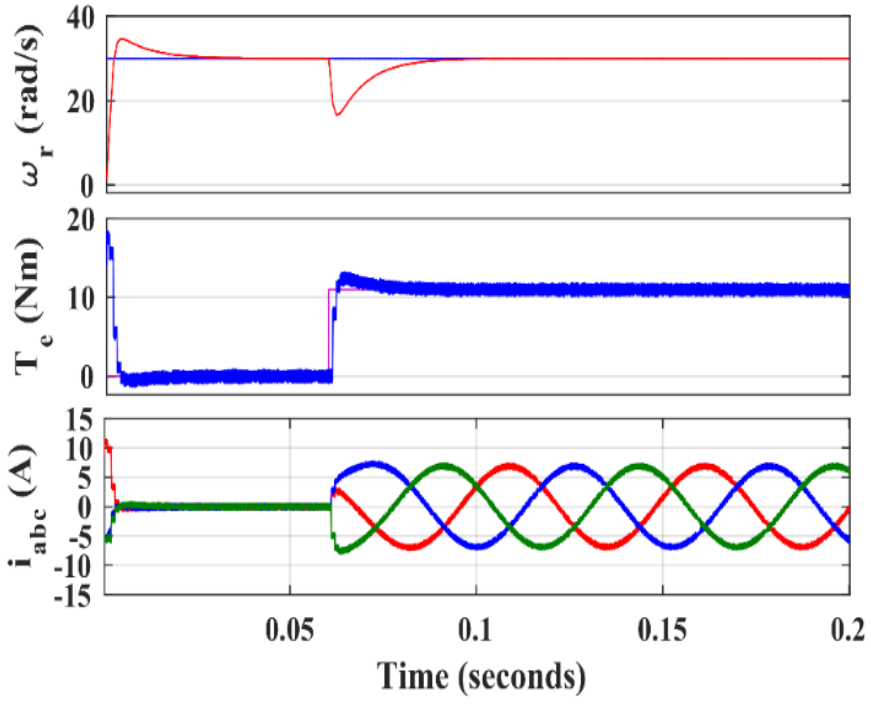

(a)

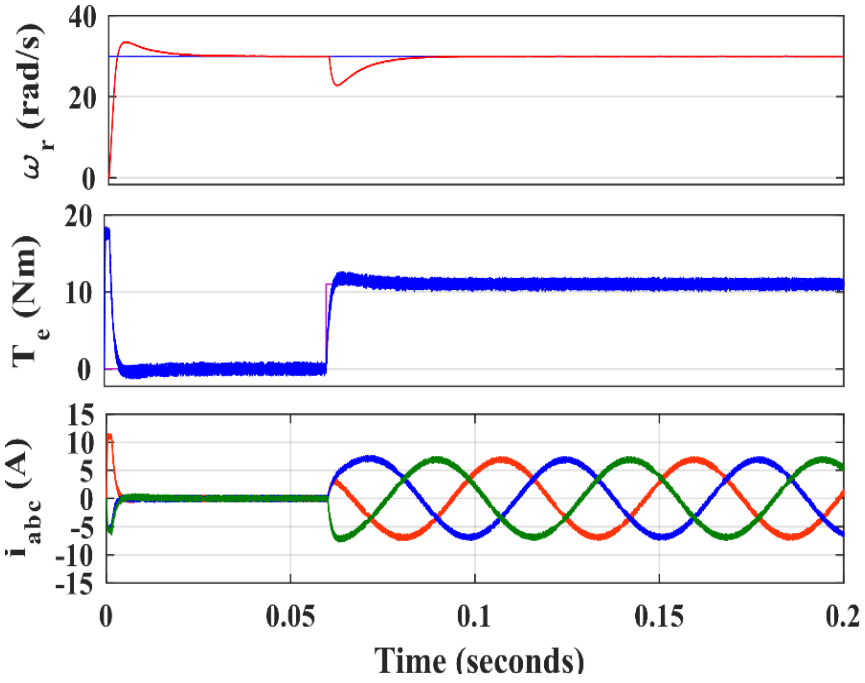

(b)

Fig.7.9. Dynamic performance for MPC of PMSM at 10% of rated-speed operation with: (a) PI Controller (b) PI-RES Controller

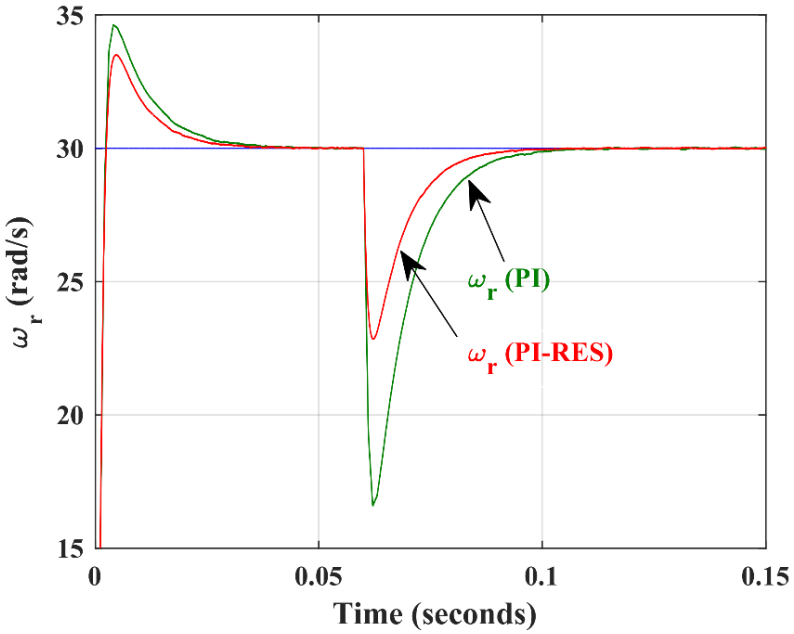

Fig.7.10. Zoomed speed-response during torque transition for MPC of PMSM at 10% of rated-speed operation with: (a) PI Controller (b) PI-RES Controller

7.5.4. Steady State characteristics of PMSM Drive

The steady state characteristics for MPC of PMSM drive with PI controller and PI–RES controller are shown in Figs. 7.11 (a) and (b) respectively.

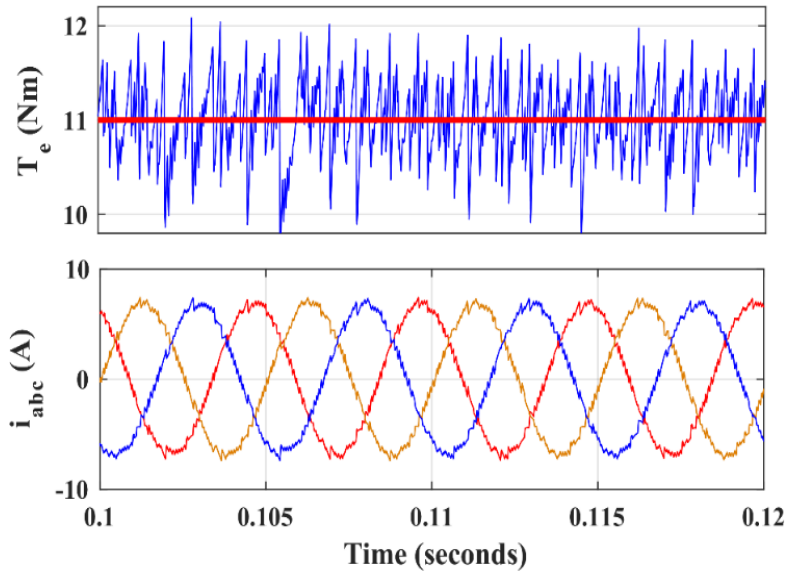

(a)

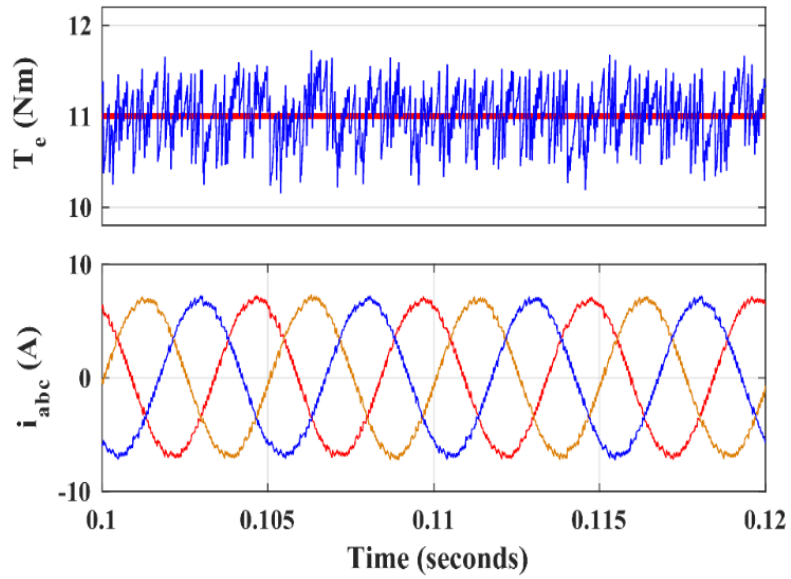

(b)

Fig.7.11. Steady state characteristics for MPC of PMSM at rated torque operation with: (a) PI Controller (b) PI-RES Controller

Some torque ripples are observed in the steady state characteristics. The ripples in motor torque are 27.2% and 9.1% for MPC of PMSM drive with PI controller and proposed PI-RES controller respectively. Thus, it is evident that the use of PI-RES for MPC of PMSM achieves better torque characteristics, with less ripples during steady state condition, as compared to classical PI controller.

7.5.5. THD in stator current of PMSM

Figs.7.12 (a) and (b) present the harmonics spectrum of stator current at full load with PI controller and PI-RES controller, respectively. Figs.7.13 (a) and (b) present the harmonics spectrum of stator current at 50% of rated load with PI controller and PI-RES controller, respectively. The ripples in stator current of the motor will low when the switching frequency is high. The average frequencies of switching in both methods i.e. PI and PI-RES are set similar for the comparative analysis. The THD is analysed unto 6kHz for the motor fundamental frequency of 200Hz. The stator current is selected up to 2 cycles for THD analysis.

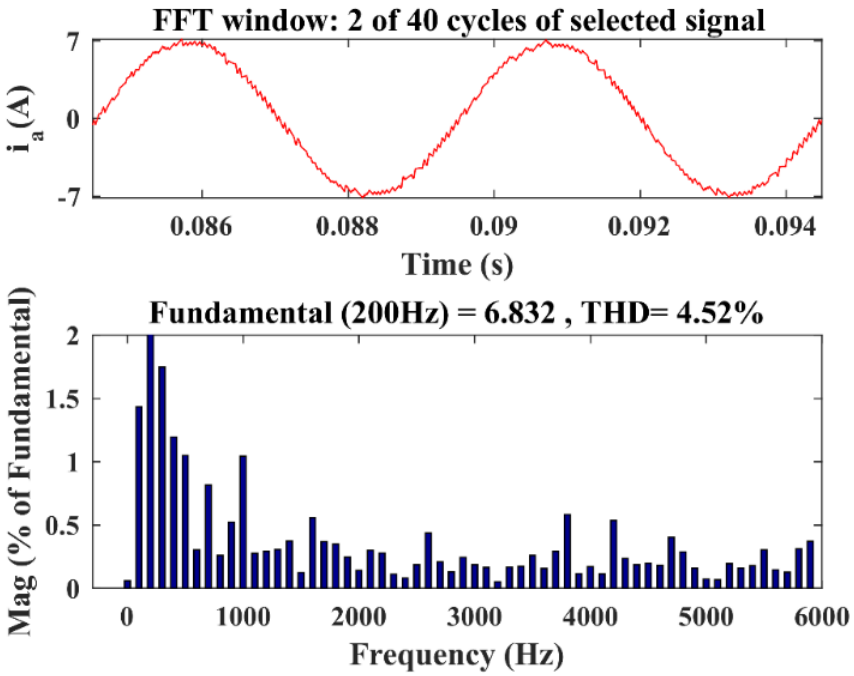

(a)

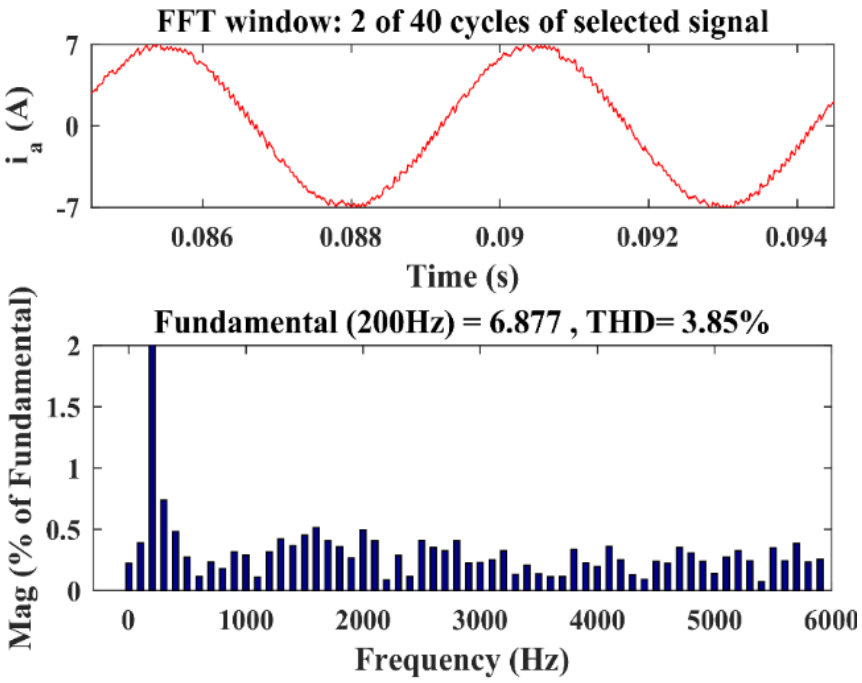

(b)

Fig.7.12. THD in stator current during rated-load operation with: (a) PI Controller (b) PI-RES Controller

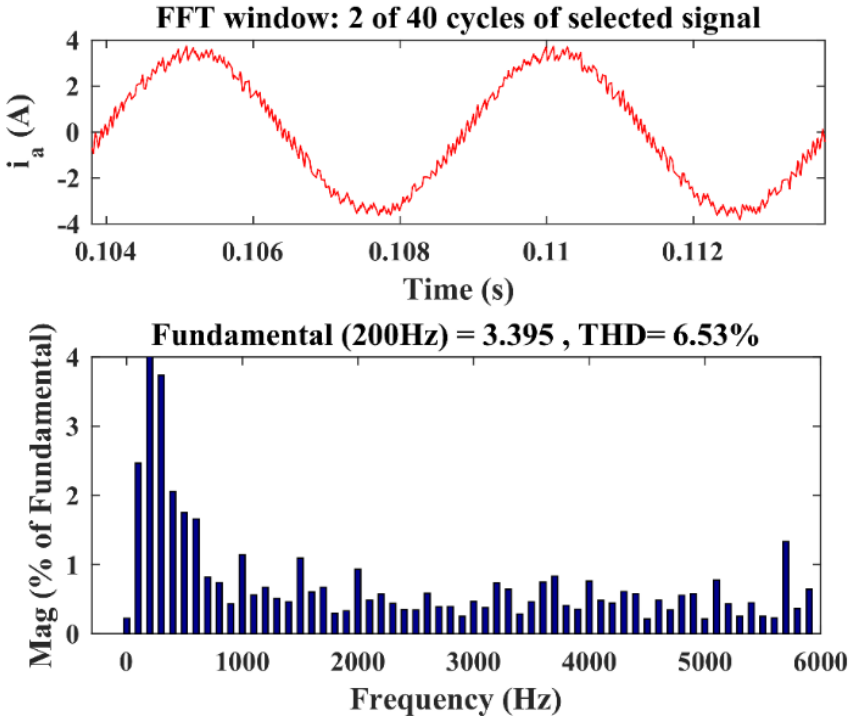

(a)

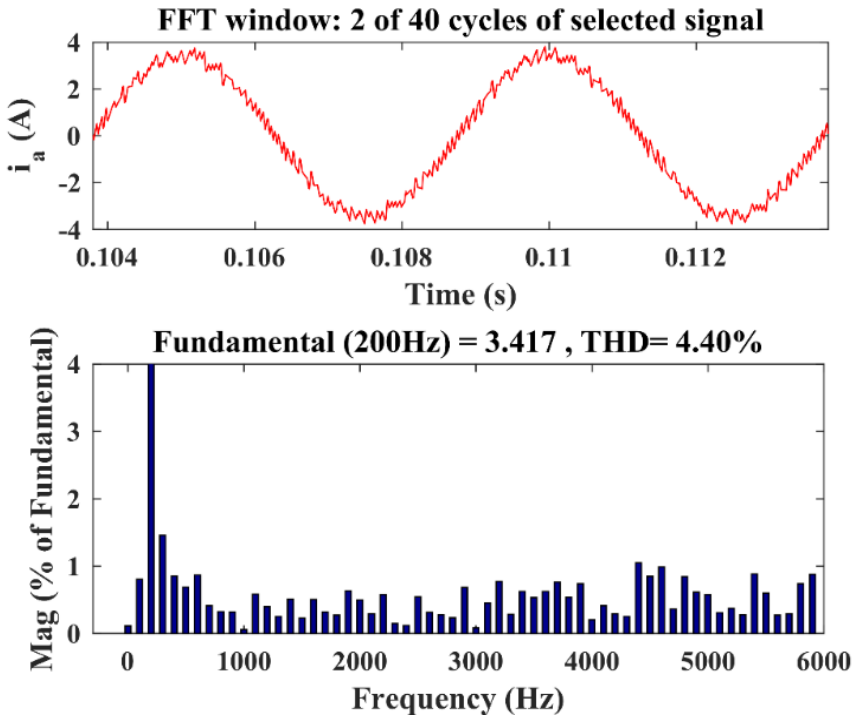

(b)

Fig.7.13. THD in current during operation at 50% of rated-load with: (a) PI Controller (b) PI-RES Controller

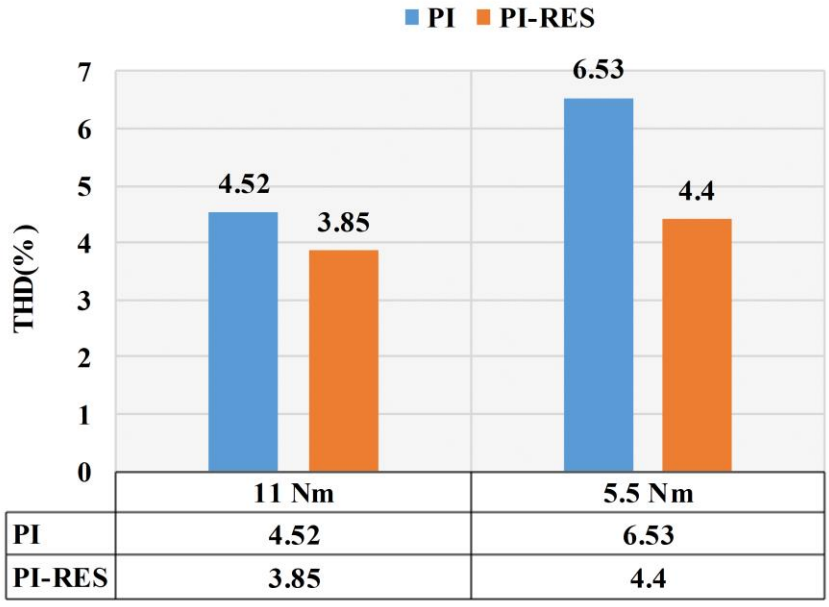

	11 Nm	5.5 Nm
PI	4.52	6.53
PI-RES	3.85	4.4

Fig.7.14. Comparison of THD in stator current for loads of 11Nm and 5.5 Nm

Fig.7.14. shows the comparative results of THD in stator current for load torques of 11Nm and 5.5Nm. It is observed that THD in stator current using PI-RES is lower in comparison with that of PI controller.

7.6. CONCLUSION

A PI-RES controller is designed and implemented for MPC of PMSM drive to regulate the speed and minimize the torque ripples. The performance of proposed controller is validated by comparing it with classical PI controller. The results of simulation studies verified that the proposed controller provides superior dynamic performance in comparisons to the conventional PI controller in terms of starting characteristics, low speed operation, and transient characteristics. The proposed PI-RES controller is also able to achieve faster dynamics as it has less rising time and settling time. It can be summarised that the implementation of PI-RES controller in MPC of PMSM drive gives smooth and faster torque response with minimum ripples and less THD in the stator current of the motor as compared to classical PI controller.

CHAPTER 8

CONCLUSIONS AND FUTURE SCOPE OF WORK

8.1. MAIN CONCLUSION

This research endeavour was started with an aim to analyse and propose different control techniques to minimize torque ripples and enhance the performance of PMSM drives. The proposed control methods were analysed through simulation study and their effects on reducing the torque ripples in PMSM compared to previously reported control techniques. Accordingly, this dissertation presents a detailed review of the reported literature on modelling of PMSM, FOC of PMSM, sensor-less control techniques for PMSM and torque ripple minimization in PMSM. Strategies for minimizing torque ripples in PMSM, which has been reported in literature, can be broadly classified into – a) techniques based on appropriate motor design, b) methods based on control techniques or c) a combination of the two.

Precise mathematical modelling of PMSM drive is required for accurate analysis and develop most of effective implementation of control techniques. Modelling of PMSM drive in both stationary and rotating reference frame are presented for FOC of PMSM using HCC and SPWM controller in MATLAB/Simulink. The efficacy of the performance of the controllers are evaluated through analysis of dynamic response, TRF analysis and THD analysis.

The control algorithm developed in MATLAB/Simulink are tested on the developed laboratory prototype drive system. The laboratory prototype includes a PMSM with encoders, a three-phase IGBT based inverter, voltage and current sensing circuit and interfacing circuits

designed and a dSPACE DS1104 controller. Experimental results are presented in steady state condition to validate the simulation results.

An improved ANFIS based MRAC observer is designed and implemented for speed and position estimation for sensor-less control of PMSM drive and its performance compared with the conventional MRAC observer for FOC of PMSM drive. The improved ANFIS based adaptation technique employed in proposed MRAC observer, estimates the speed of the rotor by minimizing the error of the reference model and adjustable model. The robustness of the proposed observer is demonstrated successfully under various operating conditions like step change in speed and torque, speed reversal, low speed operation etc. Simulation studies confirm the improved performance of the proposed ANFIS based MRAC observer under steady state and transient operating condition of the motor at different operating speed with variation in load torque as compared to the conventional MRAC observer based control of drive.

An APCC based on DB control theory is designed and developed, which reduces the ripples in the stator current and torque by optimization of the voltage vector components and time for application of this voltage vector to the PMSM. An unconstrained optimization problem is solved, which reduces computational complexity. The proposed method employs a novel approach to calculate the stator current references of the PMSM using MTPA control, which reduces the copper loss. During the transient state, the voltage vector having the largest value is applied to the motor for the complete duration of the control cycle. The stator current components are controlled in DB manner, whereby at the end of each control cycle phase of the voltage vector component is adjusted in such a way that the stator current error is reduced to zero. Steady state and transient operations of proposed APCC based on DB control theory

are analysed through simulation studies. It is observed that in comparison to some of the recently reported predictive current controllers the proposed APCC controller (a) provides better torque dynamics; (b) has significantly less THD in stator current; (c) has less ripples in stator current and torque; and (d) reduced computational complexity. The proposed APCC controller based on DB control theory is a useful alternative to other contemporary predictive current controllers.

To mitigate the limitations of conventional PI controller and FLC, an IHC is designed and developed for a vector controlled PMSM drive. The designed IHC integrates both the PI controller and FLC with an intelligent switching capability to use the FLC during transient operating conditions and the PI controller under steady state operation of the PMSM drive. The proposed controller thus gainfully utilizes the advantages of both PI and FLC. In addition, the torque is estimated using measured current and DC link voltages and compared with the reference torque generated by the IHC employed in the speed loop to generate the reference q-axis stator current, thereby reducing the torque ripples. Simulation studies are carried out for a vector controlled PMSM drive with PI controller and IHC as speed controller. The effectiveness of PMSM drive with IHC controller is investigated under different operating conditions viz rated-speed-rated-torque operation, step change in speed and reversal of speed. It is demonstrated that the IHC gives improved dynamic performance of PMSM, with reduced THD in stator current and less torque ripples of the motor in comparison with the performance of the PMSM with conventional PI controller.

A PI-RES controller is also designed and implemented for MPC of PMSM drive to regulate the speed and minimize the torque ripples. The proposed controller is validated by comparing it with classical PI controller. The results of simulation studies show that the proposed

controller provides superior dynamic performance in comparisons to the conventional PI controller in terms of starting characteristics, low speed operation, and transient characteristics. The proposed PI-RES controller is also able to achieve faster dynamic response as it has less rising and settling time for speed. The implementation of PI-RES controller in MPC of PMSM drive gives smooth and faster torque response with minimum torque ripples and less THD in the stator current of the motor as compared to classical PI controller.

8.2. FUTURE SCOPE OF WORK

Even though the objective set for this research work has been achieved, it is opined that as an extension of the current research work, the following areas may be investigated as a future scope of work: -

(1) Explore the possibility of using adaptable virtual voltage vector injection techniques for minimisation of torque ripples.

(2) New optimization method may be explored and implemented to minimize the cost function in predictive control techniques.

(3) The detection, diagnosis, and remediation techniques of faults in the converters and PMSM can be considered as a key research topic.

(4) Due to the limitations imposed by the COVID-19 pandemic, all the proposed topologies and control techniques designed and developed through simulation studies could not be verified on the developed laboratory prototype. These topologies may be validated on an experimental platform in the future.

REFERENCES

[1] Ion Boldea and Syed A. Nasar, *Electric Drives*, 3rd ed. CRC Press, 2016.

[2] Morris Brenna; Federica Foiadelli; Dario Zaninelli, "AC Motor Drives," in *Electrical Railway Transportation Systems*, IEEE, 2018, pp. 423–504.

[3] Bimal K. Bose, "Electrical machines for drives," in *Power Electronics and Variable Frequency Drives: Technology and Applications*, no. 1, IEEE, 1997, pp. 36–79.

[4] T. H. Blair, "Variable Frequency Drive Systems," in *Energy Production Systems Engineering*, IEEE, 2017, pp. 441–466.

[5] R. Dobra, D. Pasculescu, and M. Risteiu, *Variable frequency drive (VFD): AC motor control*, no. May. Editura UNIVERSITAS, 2019.

[6] M. Tuna, C. B. Fidan, S. Kocabey, and S. Görgülü, "Effective and reliable speed control of permanent magnet DC (PMDC) motor under variable loads," *J. Electr. Eng. Technol.*, vol. 10, no. 5, pp. 2170–2178, 2015, doi: 10.5370/JEET.2015.10.5.2170.

[7] A. Senthil Kumar, T. Prasath Vijay Raj, A. Tharagesh, and V. Prasanna, "Design and Analysis of a Permanent Magnet DC Motor," *Lect. Notes Electr. Eng.*, vol. 442, pp. 237–249, 2018, doi: 10.1007/978-981-10-4762-6_22.

[8] R. Krishnan, *Permanent Magnet Synchronous and Brushless DC Motor Drives*. 2017.

[9] I. Petrov and J. Pyrhonen, "Performance of low-cost permanent magnet material in PM synchronous machines," *IEEE Trans. Ind. Electron.*, vol. 60, no. 6, pp. 2131–2138, 2013, doi: 10.1109/TIE.2012.2191757.

[10] L. Dosiek and P. Pillay, "Cogging Torque Reduction in Permanent Magnet Machines," *IEEE Trans. Ind. Appl.*, vol. 43, no. 6, pp. 1565–1571, 2007.

[11] R. Islam, I. Husain, A. Fardoun, and K. McLaughlin, "Permanent-magnet synchronous

motor magnet designs with skewing for torque ripple and cogging torque reduction," *IEEE Trans. Ind. Appl.*, vol. 45, no. 1, pp. 152–160, 2009, doi: 10.1109/TIA.2008.2009653.

[12] S. Urbanek, R. Keuter, E. Peter, and B. Ponick, "Effects of continuous rotor skewing in additively manufactured permanent magnet rotors," *2020 Int. Symp. Power Electron. Electr. Drives, Autom. Motion, SPEEDAM 2020*, pp. 662–669, 2020, doi: 10.1109/SPEEDAM48782.2020.9161932.

[13] T. M. Jahns and W. L. Soong, "Pulsating torque minimization techniques for permanent magnet AC motor drives - A review," *IEEE Trans. Ind. Electron.*, vol. 43, no. 2, pp. 321–330, 1996, doi: 10.1109/41.491356.

[14] D. Wang, X. Wang, and S. Y. Jung, "Cogging torque minimization and torque ripple suppression in surface-mounted permanent magnet synchronous machines using different magnet widths," *IEEE Trans. Magn.*, vol. 49, no. 5, pp. 2295–2298, 2013, doi: 10.1109/TMAG.2013.2242454.

[15] L. Alberti, M. Barcaro, N. Bianchi, and S. Member, "Design of a Low-Torque-Ripple Fractional-Slot Interior Permanent-Magnet Motor," *IEEE Trans. Ind. Appl.*, vol. 50, no. 3, pp. 1801–1808, 2014.

[16] A. M. E.-R. and K. H. P. B. Reddy, "Effect of Number of Layers on Performance of Fractional-Slot Concentrated-Windings Interior Permanent Magnet Machines," *IEEE Trans. Power Electron.*, vol. 30, no. 4, pp. 2205–2218, 2015.

[17] M. Kiuchi, T. Ohnishi, H. Hagiwara, and Y. Yasuda, "V/F control of permanent magnet synchronous motors suitable for home appliances by DC-link peak current control method," in *2010 International Power Electronics Conference - ECCE Asia -, IPEC*

2010, 2010, pp. 567–573.

[18] S. F. Rabbi, M. P. Halloran, T. Ledrew, A. Matchem, and M. A. Rahman, "Modeling and V/F Control of a Hysteresis Interior Permanent-Magnet Motor," *IEEE Trans. Ind. Appl.*, vol. 52, no. 2, pp. 1891–1901, 2016.

[19] N. P. Quang and J.-A. Dittrich, *Vector Control of Three-Phase AC Machines*, 1st ed. Springer-Verlag Berlin Heidelberg, 2008.

[20] J. W. Finch and D. Giaouris, "Controlled AC electrical drives," *IEEE Trans. Ind. Electron.*, vol. 55, no. 2, pp. 481–491, 2008.

[21] D. Xu, B. Wang, G. Zhang, G. Wang, and Y. Yu, "A review of sensorless control methods for AC motor drives," *CES Trans. Electr. Mach. Syst.*, vol. 2, no. 1, pp. 104–115, 2020.

[22] Y. Zhang, W. Cao, S. McLoone, and J. Morrow, "Design and Flux-Weakening Control of an Interior Permanent Magnet Synchronous Motor for Electric Vehicles," *IEEE Trans. Appl. Supercond.*, vol. 26, no. 7, pp. 1–6, 2016.

[23] Z. Zhang, C. Wang, M. Zhou, and X. You, "Flux-Weakening in PMSM Drives: Analysis of Voltage Angle Control and the Single Current Controller Design," *IEEE J. Emerg. Sel. Top. Power Electron.*, vol. 7, no. 1, pp. 437–445, 2019.

[24] C. Wang and Z. Q. Zhu, "Fuzzy Logic Speed Control of Permanent Magnet Synchronous Machine and Feedback Voltage Ripple Reduction in Flux-Weakening Operation Region," *IEEE Trans. Ind. Appl.*, vol. 56, no. 2, pp. 1505–1517, 2020.

[25] T. Sebastian and G. R. Sl-n, "Modelling of permanent magnet synchronous motors," *IEEE Trans. Magn.*, vol. 22, no. 5, pp. 1069–1071, 1986.

[26] P. Pillay and R. Krishnan, "Modeling, simulation, and analysis of permanent-magnet

motor drives. I. The permanent-magnet synchronous motor drive," *IEEE Trans. Ind. Appl.*, vol. 25, no. 2, pp. 265–273, 1989.

[27] A. H. Wijenayake and P. B. Schmidt, "Modeling and analysis of permanent magnet synchronous motor by taking saturation and core loss into account," *Proc. Int. Conf. Power Electron. Drive Syst.*, vol. 2, pp. 530–534, 1997.

[28] B. K. Bose, *Modern power electronics and AC drives*. Prentice Hall, 2001.

[29] B. Cui, J. Zhou, and Z. Ren, "Modeling and simulation of permanent magnet synchronous motor drives," in *ICEMS 2001 - Proceedings of the 5th International Conference on Electrical Machines and Systems*, 2001, pp. 905–908.

[30] K. Gulez and A. A. Adam, "High-frequency common-mode modeling of permanent magnet synchronous motors," *IEEE Trans. Electromagn. Compat.*, vol. 50, no. 2, pp. 423–426, 2008.

[31] S. Bolognani, L. Peretti, M. Zigliotto, and E. Bertotto, "Commissioning of electromechanical conversion models for high dynamic PMSM drives," *IEEE Trans. Ind. Electron.*, vol. 57, no. 3, pp. 986–993, 2010.

[32] P. Rasilo, M. A. Lemesle, A. Belahcen, A. Arkkio, and M. Hinkkanen, "Comparison of finite-element-based state-space models for PM synchronous machines," *IEEE Trans. Energy Convers.*, vol. 29, no. 2, pp. 535–543, 2014.

[33] W. Zheng, Y. Luo, Y. Chen, and Y. Pi, "Fractional-order modeling of permanent magnet synchronous motor speed servo system," *JVC/Journal Vib. Control*, vol. 22, no. 9, pp. 2255–2280, 2016.

[34] A. J. Pina, P. Pramod, R. Islam, R. Mitra, and L. Xu, "Modeling and experimental verification of torque transients in interior permanent magnet synchronous motors by

including harmonics in d- and q-axes flux linkages," pp. 398–404, 2016.

[35] A. Gebregergis, M. H. Chowdhury, M. S. Islam, and T. Sebastian, "Modeling of permanent-magnet synchronous machine including torque ripple effects," *IEEE Trans. Ind. Appl.*, vol. 51, no. 1, pp. 232–239, 2015, doi: 10.1109/TIA.2014.2334733.

[36] G. Luo, R. Zhang, Z. Chen, W. Tu, S. Zhang, and R. Kennel, "A Novel Nonlinear Modeling Method for Permanent-Magnet Synchronous Motors," *IEEE Trans. Ind. Electron.*, vol. 63, no. 10, pp. 6490–6498, 2016, doi: 10.1109/TIE.2016.2578839.

[37] S. Zarate, G. Almandoz, G. Ugalde, J. Poza, and A. J. Escalada, "Extended DQ model of a Permanent Magnet Synchronous Machine by including magnetic saturation and torque ripple effects," *Proc. 2017 IEEE Int. Work. Electron. Control. Meas. Signals their Appl. to Mechatronics, ECMSM 2017*, 2017, doi: 10.1109/ECMSM.2017.7945881.

[38] Roger A. Ordonez and Cesar Hernandez, "Modeling and Control of a PMSM Motor," *J. Eng. Appl. Sci.*, vol. 12, pp. 4514–4525, 2017.

[39] F. Blaschke, "The Principle of Field Orientation as Applied to the NEW Transvector Closed-Loop System for Rotating-Field Machines," *Siemens Rev.*, vol. 34, no. 3, pp. 217–220, 1972.

[40] A. De Doncker, R. W., Pulle, D. W. J., & Veltman, *Advanced Electrical Drives Analysis, Modeling, Control*. Springer, 2011.

[41] J. L. T. and J. C. A. A. Benchaib, S. Poullain, "Discrete-Time Field-Oriented Control for SM-PMSM Including Voltage and Current Constraints," in *IEEE International Electric Machines and Drives Conference, IEMDC'03*, 2003, pp. 999–1005.

[42] M. Rashed, P. F. A. MacConnell, A. F. Stronach, and P. Acarnley, "Sensorless indirect-

rotor-field-orientation speed control of a permanent-magnet synchronous motor with stator-resistance estimation," *IEEE Trans. Ind. Electron.*, vol. 54, no. 3, pp. 1664–1675, 2007, doi: 10.1109/TIE.2007.895136.

[43] C. Y. and C. C. C. Wonhee Kim, "Design and Implementation of Simple Field-Oriented Control for Permanent Magnet Stepper Motors Without DQ Transformation," *IEEE Trans. Magn.*, vol. 47, no. 10, pp. 4231–4234, 2011.

[44] D. V. Lukichev and G. L. Demidova, "Features of tuning strategy for field oriented control of PMSM position drive system with two-mass load," *Int. J. Circuits, Syst. Signal Process.*, vol. 10, no. 1, pp. 88–94, 2016.

[45] Z. Wang, J. Chen, M. Cheng, and K. T. Chau, "Field-oriented control and direct torque control for paralleled VSIs Fed PMSM drives with variable switching frequencies," *IEEE Trans. Power Electron.*, vol. 31, no. 3, pp. 2417–2428, 2016, doi: 10.1109/TPEL.2015.2437893.

[46] P. Kumar, S. Dhundhara, and R. Makin, "Performance analysis of PMSM drive based on FOC technique with and without MRAS method," *2016 Int. Conf. Recent Adv. Innov. Eng. ICRAIE 2016*, pp. 6–11, 2016, doi: 10.1109/ICRAIE.2016.7939492.

[47] P. Zhang and W. Zhang, "Comparative Study of Field-Oriented Control in Different Coordin ate Systems for DTP-PMSM," in *International Conference on Electrical Machines and Systems*, 2013, pp. 1015–1019.

[48] J. Lara, J. Xu, and A. Chandra, "Effects of Rotor Position Error in the Performance of Field-Oriented-Controlled PMSM Drives for Electric Vehicle Traction Applications," *IEEE Trans. Ind. Electron.*, vol. 63, no. 8, pp. 4738–4751, 2016, doi: 10.1109/TIE.2016.2549983.

[49] M. F. Moussa, A. Helal, Y. Gaber, and H. A. Youssef, “Unity power factor control of permanent magnet motor drive system,” *2008 12th Int. Middle East Power Syst. Conf. MEPCON 2008*, pp. 360–367, 2008, doi: 10.1109/MEPCON.2008.4562309.

[50] F. Wu, S. M. Wan, and S. H. Huang, “Unity power factor control for PMSM position sensorless drive,” *Proc. 11th Int. Conf. Electr. Mach. Syst. ICEMS 2008*, pp. 1618–1620, 2008.

[51] J. Agrawal and S. Bodkhe, “Steady-state analysis and comparison of control strategies for PMSM,” *Model. Simul. Eng.*, vol. 2015, 2015, doi: 10.1155/2015/306787.

[52] S. Choi and W. J. Lee, “Maximum Torque per Ampere Control of a Single-Phase Permanent Magnet Synchronous Motor, Part 1: Maximum Torque Capability Analysis,” *J. Electr. Eng. Technol.*, vol. 15, no. 6, pp. 2617–2625, 2020, doi: 10.1007/s42835-020-00517-3.

[53] S. Choi and W. J. Lee, “Maximum Torque Per Ampere Control of a Single-Phase Permanent Magnet Synchronous Motor, Part 2: Variable Speed Control Method,” *J. Electr. Eng. Technol.*, vol. 15, no. 6, pp. 2609–2616, 2020, doi: 10.1007/s42835-020-00514-6.

[54] K. Li and Y. Wang, “Maximum Torque per Ampere (MTPA) Control for IPMSM Drives Using Signal Injection and an MTPA Control Law,” *IEEE Trans. Ind. Informatics*, vol. 15, no. 10, pp. 5588–5598, 2019, doi: 10.1109/TII.2019.2905929.

[55] K.Dutta, P. P. Puthra, and P. K. Das, “Constant torque angle controlled permanent magnet synchronous motor drive using hysteresis band current controller,” in *7th India International Conference on Power Electronics (IICPE)*, 2016, pp. 1–5.

[56] D. Lin, P. Zhou, and Z. J. Cendes, “In-depth study of the torque constant for permanent-

magnet machines," *IEEE Trans. Magn.*, vol. 45, no. 12, pp. 5383–5387, 2009, doi: 10.1109/TMAG.2009.2026043.

[57] P. P. Acarnley and J. F. Watson, "Review of position-sensorless operation of brushless permanent-magnet machines," *IEEE Trans. Ind. Electron.*, vol. 53, no. 2, pp. 352–362, 2006, doi: 10.1109/TIE.2006.870868.

[58] S. K. Sul and S. Kim, "Sensorless control of IPMSM: Past, present, and future," *IEEJ J. Ind. Appl.*, vol. 1, no. 1, pp. 15–23, 2012.

[59] G. Wang, M. Valla, and J. Solsona, "Position sensorless permanent magnet synchronous machine drives - A review," *IEEE Trans. Ind. Electron.*, vol. 67, no. 7, pp. 5830–5842, 2020.

[60] S. Bolognani, L. Ortombina, F. Tinazzi, and M. Zigliotto, "Model Sensitivity of Fundamental-Frequency-Based Position Estimators for Sensorless PM and Reluctance Synchronous Motor Drives," *IEEE Trans. Ind. Electron.*, vol. 65, no. 1, pp. 77–85, 2018, doi: 10.1109/TIE.2017.2716902.

[61] Y. Lee and S. K. Sul, "Model-Based Sensorless Control of an IPMSM with Enhanced Robustness Against Load Disturbances Based on Position and Speed Estimator Using a Speed Error," *IEEE Trans. Ind. Appl.*, vol. 54, no. 2, pp. 1448–1459, 2018, doi: 10.1109/TIA.2017.2777390.

[62] Y. Lee, Y. C. Kwon, and S. K. Sul, "Comparison of rotor position estimation performance in fundamental-model-based sensorless control of PMSM," *2015 IEEE Energy Convers. Congr. Expo. ECCE 2015*, pp. 5624–5633, 2015, doi: 10.1109/ECCE.2015.7310451.

[63] Y. Zhao, Z. Zhang, W. Qiao, and L. Wu, "An Extended Flux Model-Based Rotor

Position Estimator for Sensorless Control of Salient-Pole Permanent-Magnet Synchronous Machines," *IEEE Trans. Power Electron.*, vol. 30, no. 8, pp. 4412–4422, 2015, doi: 10.1109/TPEL.2014.2358621.

[64] T. Aas, J. S. Åsrud, and H. Van Khang, "Parameter sensitivity of flux-linkage based sensorless control for permanent magnet synchronous motors," *2017 20th Int. Conf. Electr. Mach. Syst. ICEMS 2017*, pp. 1–5, 2017.

[65] J. Lee, J. Hong, K. Nam, R. Ortega, L. Praly, and A. Astolfi, "Sensorless control of surface-mount permanent-magnet synchronous motors based on a nonlinear observer," *IEEE Trans. Power Electron.*, vol. 25, no. 2, pp. 290–297, 2010, doi: 10.1109/TPEL.2009.2025276.

[66] S. C. Yang and R. D. Lorenz, "Surface permanent-magnet machine self-sensing at zero and low speeds using improved observer for position, velocity, and disturbance torque estimation," *IEEE Trans. Ind. Appl.*, vol. 48, no. 1, pp. 151–160, 2012, doi: 10.1109/TIA.2011.2175472.

[67] T. Wang *et al.*, "An EMF Observer for PMSM Sensorless Drives Adaptive to Stator Resistance and Rotor Flux Linkage," *IEEE J. Emerg. Sel. Top. Power Electron.*, vol. 7, no. 3, pp. 1899–1913, 2019.

[68] F. Briz, M. W. Degner, P. García, and R. D. Lorenz, "Comparison of saliency-based sensorless control techniques for AC machines," *IEEE Trans. Ind. Appl.*, vol. 40, no. 4, pp. 1107–1115, 2004, doi: 10.1109/TIA.2004.830768.

[69] G. Scarcella, G. Scelba, and A. Testa, "High performance sensorless controls based on HF excitation: A viable solution for future AC motor drives?," *Proc. - 2015 IEEE Work. Electr. Mach. Des. Control Diagnosis, WEMDCD 2015*, pp. 178–187, 2015, doi:

10.1109/WEMDCD.2015.7194527.

[70] X. Zhang, H. Li, S. Yang, and M. Ma, “Improved Initial Rotor Position Estimation for PMSM Drives Based on HF Pulsating Voltage Signal Injection,” *IEEE Trans. Ind. Electron.*, vol. 65, no. 6, pp. 4702–4713, 2018, doi: 10.1109/TIE.2017.2772204.

[71] G. Zhang, G. Wang, and D. Xu, “Saliency-based position sensorless control methods for PMSM drives - A review,” *Chinese J. Electr. Eng.*, vol. 3, no. 2, pp. 14–23, 2019, doi: 10.23919/cjee.2017.8048408.

[72] N. Bianchi and S. Bolognani, “Influence of rotor geometry of an IPM motor on sensorless control feasibility,” *IEEE Trans. Ind. Appl.*, vol. 43, no. 1, pp. 87–96, 2007, doi: 10.1109/TIA.2006.887317.

[73] J. H. Jang, S. K. Sul, J. I. Ha, K. Ide, and M. Sawamura, “Sensorless Drive of Surface-Mounted Permanent-Magnet Motor by High-Frequency Signal Injection Based on Magnetic Saliency,” *IEEE Trans. Ind. Appl.*, vol. 39, no. 4, pp. 1031–1039, 2003, doi: 10.1109/TIA.2003.813734.

[74] Q. Tang, A. Shen, X. Luo, and J. Xu, “PMSM Sensorless Control by Injecting HF Pulsating Carrier Signal into ABC Frame,” *IEEE Trans. Power Electron.*, vol. 32, no. 5, pp. 3767–3776, 2017, doi: 10.1109/TPEL.2016.2583787.

[75] Y. D. Yoon, S. K. Sul, S. Morimoto, and K. Ide, “High bandwidth sensorless algorithm for AC machines based on square-wave type voltage injection,” *2009 IEEE Energy Convers. Congr. Expo. ECCE 2009*, pp. 2123–2130, 2009, doi: 10.1109/ECCE.2009.5316256.

[76] N. C. Park and S. H. Kim, “Simple sensorless algorithm for interior permanent magnet synchronous motors based on high-frequency voltage injection method,” *IET Electr.*

Power Appl., vol. 8, no. 2, pp. 68–75, 2014, doi: 10.1049/iet-epa.2013.0221.

[77] Z. Chen, F. Wang, G. Luo, Z. Zhang, and R. Kennel, "Secondary Saliency Tracking-Based Sensorless Control for Concentrated Winding SPMSM," *IEEE Trans. Ind. Informatics*, vol. 12, no. 1, pp. 201–210, 2016.

[78] P. L. Jansen and R. D. Lorenz, "Transducerless Position and Velocity Estimation in Induction and Salient AC Machines," *IEEE Trans. Ind. Appl.*, vol. 31, no. 2, pp. 240–247, 1995.

[79] D. Raca, P. García, D. D. Reigosa, F. Briz, and R. D. Lorenz, "Carrier-signal selection for sensorless control of PM synchronous machines at zero and very low speeds," *IEEE Trans. Ind. Appl.*, vol. 46, no. 1, pp. 167–178, 2010, doi: 10.1109/TIA.2009.2036551.

[80] X. Luo, Q. Tang, A. Shen, and Q. Zhang, "PMSM Sensorless Control by Injecting HF Pulsating Carrier Signal into Estimated Fixed-Frequency Rotating Reference Frame," *IEEE Trans. Ind. Electron.*, vol. 63, no. 4, pp. 2294–2303, 2016.

[81] C. H. Choi and J. K. I. Seok, "Pulsating signal injection-based sensorless control of PMSM using injection axis switching scheme without additional offline commissioning test," *Conf. Rec. - IAS Annu. Meet. (IEEE Ind. Appl. Soc.*, pp. 2365–2370, 2007.

[82] H. Wang, K. Lu, D. Wang, and F. Blaabjerg, "Pulse-Injection-Based Sensorless Control Method with Improved Dynamic Current Response for PMSM," *2018 Int. Power Electron. Conf. IPEC-Niigata - ECCE Asia 2018*, pp. 1183–1188, 2018.

[83] J. M. Liu and Z. Q. Zhu, "Novel Sensorless Control Strategy With Injection of High-Frequency Pulsating Carrier Signal Into Stationary Reference Frame," *IEEE Trans. Ind. Appl.*, vol. 50, no. 4, pp. 2574–2583, 2014.

[84] M. Schroedl, "Operation of the permanent magnet synchronous machine without a

mechanical sensor," 1990.

[85] E. Robeischl and M. Schroedl, "Optimized INFORM-measurement sequence for sensorless PM synchronous motor drives with respect to minimum current distortion," *IEEE Trans. Ind. Appl.*, vol. 40, no. 2, pp. 92–98, 2004.

[86] S. K. Panda, J. X. Xu, and W. Qian, "Review of torque ripple minimization in PM synchronous motor drives," *IEEE Power Energy Soc. 2008 Gen. Meet. Convers. Deliv. Electr. Energy 21st Century, PES*, pp. 1–6, 2008.

[87] L. Jia, M. Lin, W. Le, N. Li, and Y. Kong, "Dual-Skew Magnet for Cogging Torque Minimization of Axial Flux PMSM with Segmented Stator," *IEEE Trans. Magn.*, vol. 56, no. 2, 2020, doi: 10.1109/TMAG.2019.2951704.

[88] N. Bianchi and S. Bolognani, "Design techniques for reducing the cogging torque in surface-mounted PM motors," *IEEE Trans. Ind. Appl.*, vol. 38, no. 5, pp. 1259–1265, 2002.

[89] N. Levin, S. Orlova, V. Pugachov, B. Ose-Zala, and E. Jakobsons, "Methods to reduce the cogging torque in permanent magnet synchronous machines," *Elektron. ir Elektrotechnika*, vol. 19, no. 1, pp. 23–26, 2013, doi: 10.5755/j01.eee.19.1.3248.

[90] C. S. Koh, B. K. Kang, J. S. Ryu, and J. S. Seol, "The effects of the distribution of residual magnetization on the cogging torque and switching signals in permanent magnet (PM) motors," *IEEE Trans. Magn.*, vol. 38, no. 2 I, pp. 1217–1220, 2002.

[91] Z. Q. Zhu and D. Howe, "Influence of design parameters on cogging torque in permanent magnet machines," *IEEE Trans. Energy Convers.*, vol. 15, no. 4, pp. 407–412, 2000.

[92] M. Aydin and M. Gulec, "Reduction of cogging torque in double-rotor axial-flux

permanent-magnet disk motors: A review of cost-effective magnet-skewing techniques with experimental verification," *IEEE Trans. Ind. Electron.*, vol. 61, no. 9, pp. 5025–5034, 2014, doi: 10.1109/TIE.2013.2276777.

[93] K. S. Seo, Y. J. Kim, and S. Y. Jung, "Stator teeth shape design for torque ripple reduction in surface-mounted permanent magnet synchronous motor," in *2014 17th International Conference on Electrical Machines and Systems, ICEMS 2014*, 2014, pp. 387–390.

[94] L. Hao, M. Lin, D. Xu, N. Li, and W. Zhang, "Analysis of Cogging Torque Reduction Techniques in Axial-Field Flux-Switching Permanent-Magnet Machine," *IEEE Trans. Appl. Supercond.*, vol. 26, no. 4, 2016, doi: 10.1109/TASC.2016.2516920.

[95] X. Wang, Y. Yang, and D. Fu, "Study of cogging torque in surface-mounted permanent magnet motors with energy method," *J. Magn. Magn. Mater.*, vol. 267, no. 1, pp. 80–85, 2003, doi: 10.1016/S0304-8853(03)00324-X.

[96] L. Zhu, S. Z. Jiang, Z. Q. Zhu, and C. C. Chan, "Analytical methods for minimizing cogging torque in permanent-magnet machines," *IEEE Trans. Magn.*, vol. 45, no. 4, pp. 2023–2031, 2009, doi: 10.1109/TMAG.2008.2011363.

[97] S. H. Han, T. M. Jahns, W. L. Soong, M. K. Güven, and M. S. Illindala, "Torque ripple reduction in interior permanent magnet synchronous machines using stators with odd number of slots per pole pair," *IEEE Trans. Energy Convers.*, vol. 25, no. 1, pp. 118–127, 2010.

[98] W. Fei and P. C. K. Luk, "A new technique of cogging torque suppression in direct-drive permanent-magnet brushless machines," *IEEE Trans. Ind. Appl.*, vol. 46, no. 4, pp. 1332–1340, 2010, doi: 10.1109/TIA.2010.2049551.

[99] R. Dutta, A. Pouramin, and M. F. Rahman, "A Novel Rotor Topology for High-Performance Fractional Slot Concentrated Winding Interior Permanent Magnet Machine," *IEEE Trans. Energy Convers.*, vol. 36, no. 2, pp. 658–670, 2020, doi: 10.1109/tec.2020.3030302.

[100] Y. H. Jung, M. S. Lim, M. H. Yoon, J. S. Jeong, and J. P. Hong, "Torque Ripple Reduction of IPMSM Applying Asymmetric Rotor Shape under Certain Load Condition," *IEEE Trans. Energy Convers.*, vol. 33, no. 1, pp. 333–340, 2018.

[101] Z. S. Du and T. A. Lipo, "Reducing Torque Ripple Using Axial Pole Shaping in Interior Permanent Magnet Machines," *IEEE Trans. Ind. Appl.*, vol. 56, no. 1, pp. 148–157, 2020.

[102] V. Petrovic, R. Ortega, A. M. Stankovic, and G. Tadmor, "Design and Implementation of an Adaptive Controller for Torque Ripple Minimization in PM Synchronous Motors," *IEEE Trans. POWE Electron.*, vol. 15, no. 5, pp. 871–880, 2000.

[103] B. Grčar, P. Cafuta, G. Štumberger, and A. M. Stanković, "Control-based reduction of pulsating torque for PMAC machines," *IEEE Trans. Energy Convers.*, vol. 17, no. 2, pp. 169–175, 2002, doi: 10.1109/TEC.2002.1009464.

[104] K. Gulez, A. A. Adam, I. E. Buzcu, and H. Pastaci, "Using passive filters to minimize torque pulsations and noises in surface PMSM derived field oriented control," *Simul. Model. Pract. Theory*, vol. 15, no. 8, pp. 989–1001, 2007.

[105] N. Nakao and K. Akatsu, "A new control method for torque ripple compensation of permanent magnet motors," *2010 Int. Power Electron. Conf. - ECCE Asia -, IPEC 2010*, pp. 1421–1427, 2010.

[106] Y. Yan, W. Li, W. Deng, G. Zhang, and C. Xia, "Torque ripple minimization of PMSM

using PI type iterative learning control," *IECON Proc. (Industrial Electron. Conf.*, pp. 925–931, 2014.

[107] Z. Zeng, C. Zhu, X. Jin, W. Shi, and R. Zhao, "Hybrid Space Vector Modulation Strategy for Torque Ripple Minimization in Three-Phase Four-Switch Inverter-Fed PMSM Drives," *IEEE Trans. Ind. Electron.*, vol. 64, no. 3, pp. 2122–2134, 2017.

[108] J. Liu, H. Li, and Y. Deng, "Torque Ripple Minimization of PMSM Based on Robust ILC Via Adaptive Sliding Mode Control," *IEEE Trans. Power Electron.*, vol. 33, no. 4, pp. 3655–3671, 2018, doi: 10.1109/TPEL.2017.2711098.

[109] J. Kang, X. Li, Y. Liu, S. Mu, and S. Wang, "Predictive Current Control with Torque Ripple Minimization for PMSM of Electric Vehicles," *Proc. - 2018 IEEE Int. Power Electron. Appl. Conf. Expo. PEAC 2018*, pp. 1–6, 2018.

[110] Z. Zhou, C. Xia, Y. Yan, Z. Wang, and T. Shi, "Torque Ripple Minimization of Predictive Torque Control for PMSM with Extended Control Set," *IEEE Trans. Ind. Electron.*, vol. 64, no. 9, pp. 6930–6939, 2017, doi: 10.1109/TIE.2017.2686320.

[111] H. Zhu, X. Xiao, and Y. Li, "Torque ripple reduction of the torque predictive control scheme for permanent-magnet synchronous motors," *IEEE Trans. Ind. Electron.*, vol. 59, no. 2, pp. 871–877, 2012, doi: 10.1109/TIE.2011.2157278.

[112] J.-H. Lee, J.-W. Ahn, and D.-H. Lee, "Advanced PID scheme for low torque ripple PMSM drive," in *IEEE Vehicle Power and Propulsion Conference*, 2012, pp. 148–153.

[113] J. Kim, S. W. Ryu, M. S. Rafaq, H. H. Choi, and J. W. Jung, "Improved Torque Ripple Minimization Technique with Enhanced Efficiency for Surface- Mounted PMSM Drives," *IEEE Access*, vol. 8, no. Ilc, pp. 115017–115027, 2020, doi: 10.1109/ACCESS.2020.3004042.

[114] G. Feng, C. Lai, J. Tian, and N. C. Kar, “Multiple Reference Frame Based Torque Ripple Minimization for PMSM Drive under Both Steady-State and Transient Conditions,” *IEEE Trans. Power Electron.*, vol. 34, no. 7, pp. 6685–6696, 2019, doi: 10.1109/TPEL.2018.2876607.

[115] A. Ebrahimi, “A Novel Harmonic Current Control Algorithm for Torque Ripple Reduction of Permanent Magnet Synchronous Motors for Traction Application,” in *2018 IEEE International Conference on Electrical Systems for Aircraft, Railway, Ship Propulsion and Road Vehicles and International Transportation Electrification Conference, ESARS-ITEC 2018*, 2019, pp. 1–5.

[116] S. F. Toloue, S. H. Kamali, and M. Moallem, “Torque Ripple Minimization and Control of a Permanent Magnet Synchronous Motor Using Multiobjective Extremum Seeking,” *IEEE/ASME Trans. Mechatronics*, vol. 24, no. 5, pp. 2151–2160, 2019, doi: 10.1109/TMECH.2019.2929390.

[117] P. Mattavelli, L. Tubiana, and M. Zigliotto, “Torque-ripple reduction in PM synchronous motor drives using repetitive current control,” *IEEE Trans. Power Electron.*, vol. 20, no. 6, pp. 1423–1431, 2005, doi: 10.1109/TPEL.2005.857559.

[118] G. Feng, C. Lai, and N. C. Kar, “A Closed-Loop Fuzzy-Logic-Based Current Controller for PMSM Torque Ripple Minimization Using the Magnitude of Speed Harmonic as the Feedback Control Signal,” *IEEE Trans. Ind. Electron.*, vol. 64, no. 4, pp. 2642–2653, 2017, doi: 10.1109/TIE.2016.2631524.

[119] Y. Cho, K. B. Lee, J. H. Song, and Y. Il Lee, “Torque-ripple minimization and fast dynamic scheme for torque predictive control of permanent-magnet synchronous motors,” *IEEE Trans. Power Electron.*, vol. 30, no. 4, pp. 2182–2190, 2015, doi:

10.1109/TPEL.2014.2326192.

[120] H. Mahmoudi, M. Aleenejad, and R. Ahmadi, “Torque Ripple Minimization for a Permanent Magnet Synchronous Motor Using a Modified Quasi-Z-Source Inverter,” *IEEE Trans. Power Electron.*, vol. 34, no. 4, pp. 3819–3830, 2019.

[121] L. A. Adase, I. M. Alsofyani, and K. B. Lee, “Predictive Torque Control with Simple Duty-Ratio Regulator of PMSM for Minimizing Torque and Flux Ripples,” *IEEE Access*, vol. 8, pp. 2373–2381, 2020, doi: 10.1109/ACCESS.2019.2961935.

[122] L. Chen, G. Gotting, and I. Hahn, “DC-Link Current and Torque Ripple Optimized Self-Sensing Control of Interior Permanent-Magnet Synchronous Machines for Hybrid and Electrical Vehicles,” *IEEE Trans. Ind. Appl.*, vol. 53, no. 5, pp. 4536–4546, 2017, doi: 10.1109/TIA.2017.2708032.

[123] K. Gulez, A. A. Adam, and H. Pastaci, “Torque ripple and EMI noise minimization in PMSM using active filter topology and field-oriented control,” *IEEE Trans. Ind. Electron.*, vol. 55, no. 1, pp. 251–257, 2008, doi: 10.1109/TIE.2007.896295.

[124] A. M. Bozorgi, M. Farasat, and S. Jafarishiadeh, “Model predictive current control of surface-mounted permanent magnet synchronous motor with low torque and current ripple,” *IET Power Electron.*, vol. 10, no. 10, pp. 1120–1128, 2017, doi: 10.1049/iet-pel.2016.0850.

[125] J. Gao, X. Wu, S. Huang, W. J. Zhang, and L. Xiao, “Torque ripple minimisation of permanent magnet synchronous motor using a new proportional resonant controller,” *IET Power Electron.*, vol. 10, no. 2, pp. 208–214, 2017, doi: 10.1049/iet-pel.2015.0946.

[126] M. Tang, A. Formentini, S. A. Odhano, and P. Zanchetta, “Torque Ripple Reduction of PMSMs Using a Novel Angle-Based Repetitive Observer,” *IEEE Trans. Ind. Electron.*,

vol. 67, no. 4, pp. 2689–2699, 2020, doi: 10.1109/TIE.2019.2912798.

[127] M. Huang, Y. Deng, H. Li, and J. Wang, “Torque ripple suppression of PMSM using fractionalorder vector resonant and robust internal model control,” *IEEE Trans. Transp. Electrif.*, vol. 7782, no. c, 2021, doi: 10.1109/TTE.2021.3053063.

[128] Z. Song, X. Ma, and R. Zhang, “Enhanced Finite-Control-Set Model Predictive Flux Control of Permanent Magnet Synchronous Machines With Minimum Torque Ripples,” *IEEE Trans. Ind. Electron.*, vol. 68, no. 9, pp. 7804–7813, 2020.

[129] G. Feng, C. Lai, and N. C. Kar, “Speed Harmonic Based Decoupled Torque Ripple Minimization Control for Permanent Magnet Synchronous Machine with Minimized Loss,” *IEEE Trans. Energy Convers.*, vol. 35, no. 4, pp. 1796–1805, 2020, doi: 10.1109/TEC.2020.2992487.

[130] W. Zhang, B. Cao, N. Nan, M. Li, and Y. Q. Chen, “An adaptive PID-type sliding mode learning compensation of torque ripple in PMSM position servo systems towards energy efficiency,” *ISA Trans.*, vol. 110, pp. 258–270, 2021, doi: 10.1016/j.isatra.2020.10.045.

[131] Dakai Hu, “IMPROVEMENT OF TORQUE AND SPEED CONTROL OF PERMANENT MAGNET SYNCHRONOUS MACHINES IN THE FLUX-WEAKENING REGION,” The Ohio State University, 2014.

[132] L. W. Matsch and J. D. Morgan, *Electromagnetic and Electromechanical Machine*, 3rd editio. HARPER & ROW, PUBLISHERS, New York, 1986.

[133] Sergey Edward Lyshevski, *Electromechanical Systems, Electric Machines, and Applied Mechatronics*, 1st editio. CRC Press, 2000.

[134] W. C. Duesterhoeft, M. W. Schulz, and E. Clarke, “Determination of Instantaneous Currents and Voltages by Means of Alpha, Beta, and Zero Components,” *Trans. Am.*

Inst. Electr. Eng., vol. 70, no. 2, pp. 1248–1255, 1951.

[135] R. H. PARK, "Two-Reaction Theory of Synchronous Machines: Generalized Method of Analysis-Part I," *Trans. Am. Inst. Electr. Eng.*, vol. 48, no. 3, pp. 716–727, 1929.

[136] M. F. Oettmeier, "Stator-Flux-Oriented Control and Real-Time Emulation Techniques for Permanent-Magnet Synchronous Machines," the Faculty of Electrical and Computer Engineering of Ruhr-University Bochum, 2012.

[137] A. Tripathi and P. C. Sen, "Comparative Analysis of Fixed and Sinusoidal Band Hysteresis Current Controllers for Voltage Source Inverters," *IEEE Trans. Ind. Electron.*, vol. 39, no. 1, pp. 63–73, 1992.

[138] B. J. Kang and C. M. Liaw, "A robust hysteresis current-controlled PWM inverter for linear PMSM driven magnetic suspended positioning system," *IEEE Trans. Ind. Electron.*, vol. 48, no. 5, pp. 956–967, 2001, doi: 10.1109/41.954560.

[139] A. Naik, B. Chitti Babu, and A. K. Panda, "Improved performance of adaptive hysteresis current controller based vector control of PMSM drive system," in *Proceeding of the 2011 IEEE Students' Technology Symposium*, 2011, pp. 303–309.

[140] M. K. Waghmare and S. V. Patil, "Speed Control Strategy of Permanent Magnet Synchronous Motor Drive Using SPWM Technique," in *2019 4th IEEE International Conference on Recent Trends on Electronics, Information, Communication and Technology, RTEICT 2019 - Proceedings*, 2019, no. 1, pp. 1328–1332.

[141] R. Shanthi, S. Kalyani, and R. Thangasankaran, "Performance analysis of speed control of PMSM drive with sinusoidal PWM and space vector pwm fed voltage source inverters," in *IEEE International Conference on Innovations in Green Energy and Healthcare Technologies - 2017, IGEHT 2017*, 2017, pp. 1–10.

[142] A. Consoli, F. Gennaro, V. John, and T. A. Lipo, “Effects of the internal layout on the performance of IGBT power modules,” *Brazilian Power Electron. Conf.*, no. June, pp. 1–10, 1999.

[143] Semikron, “IGBT Modules SKM 150GB 12V.” https://www.semikron.com/dl/servicesupport/downloads/download/semikrondatasheet - skm150gb12v-22892043.

[144] “LEM Voltage Transducer LV 20-P.” https://media.digikey.com/pdf/data sheets/lem usa pdfs/lv 20-p.pdf .

[145] “Texas Instruments LF353 Wide-Bandwidth JFET-Input Dual Operational Amplifier.” http://www.ti.com/lit/ds/symlink/lf353.pdf.

[146] “LEM Current Transducer LA 55-P.” http://www.lem.com/docs/products/la_55-p_e.pdf.

[147] “Fairchild Semiconductor 6N136 High Speed Transistor Optocouplers.” http://www.farnell.com/datasheets/94979.pdf .

[148] “ST Microelectronics PN2222A Small Signal NPN Transistor.” http://pdf.datasheetcatalog.com/datasheet/stmicroelectronics/8869.pdf.

[149] P. C._Krause, O. Wasynczuk, and S. D.Sudhof, *Analysis of Electric Machinary and Drive System*, Second. IEEE Press, 2002.

[150] B.K. Bose, *Power electronics and variable frequency drives*. IEEE Press, 1997.

[151] M. Sreejeth, M. Singh, and P. Kumar, “Particle swarm optimisation in efficiency improvement of vector controlled surface mounted permanent magnet synchronous motor drive,” *IET Power Electron.*, vol. 8, no. 5, pp. 760–769, 2015.

[152] F. Genduso, R. Miceli, C. Rando, and G. R. Galluzzo, “Back EMF sensorless-control

algorithm for high-dynamic performance PMSM," *IEEE Trans. Ind. Electron.*, vol. 57, no. 6, pp. 2092–2100, 2010.

[153] K. Schuhmacher, E. Grasso, and M. Nienhaus, "Improved rotor position determination for a sensorless star-connected PMSM drive using Direct Flux Control," *J. Eng.*, vol. 2019, no. 17, pp. 3749–3753, 2019.

[154] S. Wang, K. Yang, and K. Chen, "An Improved Position-Sensorless Control Method at Low Speed for PMSM Based on High-Frequency Signal Injection into a Rotating Reference Frame," *IEEE Access*, vol. 7, pp. 86510–86521, 2019.

[155] G. Zhu, A. Kaddouri, L. A. Dessaint, and O. Akhrif, "A nonlinear state observer for the sensorless control of a permanent-magnet AC machine," *IEEE Trans. Ind. Electron.*, vol. 48, no. 6, pp. 1098–1108, 2001.

[156] L. Yongdong and Z. Hao, "Sensorless control of permanent magnet synchronous motor - A survey," *2008 IEEE Veh. Power Propuls. Conf. VPPC 2008*, pp. 1–7, 2008.

[157] M. S. Rafaq, F. Mwasilu, J. Kim, H. H. Choi, and J. W. Jung, "Online Parameter Identification for Model-Based Sensorless Control of Interior Permanent Magnet Synchronous Machine," *IEEE Trans. Power Electron.*, vol. 32, no. 6, pp. 4631–4643, 2017.

[158] Y. Zhao, C. Wei, Z. Zhang, and W. Qiao, "A Review on Position/Speed Sensorless Control for Permanent-Magnet Synchronous Machine-Based Wind Energy Conversion Systems," *IEEE J. Emerg. Sel. Top. Power Electron.*, vol. 1, no. 4, pp. 1–14, 2013.

[159] A. Kusagur, S. F. Kodad, and B. V. S. Ram, "Modeling, Design and Simulation of an Adaptive Neuro-Fuzzy Inference System (ANFIS) for Speed Control of Induction Motor," *Int. J. Comput. Appl.*, vol. 6, no. 12, pp. 29–44, 2010.

[160] M. Singh and A. Chandra, "Application of adaptive network-based fuzzy inference system for sensorless control of PMSG-based wind turbine with nonlinear-load-compensation capabilities," *IEEE Trans. Power Electron.*, vol. 26, no. 1, pp. 165–175, 2011.

[161] S. Maiti, C. Chakraborty, and S. Sengupta, "Simulation studies on model reference adaptive controller based speed estimation technique for the vector controlled permanent magnet synchronous motor drive," *Simul. Model. Pract. Theory*, vol. 17, no. 4, pp. 585–596, 2009, doi: 10.1016/j.simpat.2008.08.017.

[162] J. Xu, T. Wu, W. Gu, Y. Wang, and R. Chen, "A Position Observer Design for Interior Permanent Magnet Synchronous Motor Based on Fuzzy PI Model Reference Adaptive Control," *Proc. 30th Chinese Control Decis. Conf. CCDC 2018*, pp. 4798–4803, 2018, doi: 10.1109/CCDC.2018.8407961.

[163] A. T. Nguyen, M. S. Rafaq, H. H. Choi, and J. W. Jung, "A model reference adaptive control based speed controller for a surface-mounted permanent magnet synchronous motor drive," *IEEE Trans. Ind. Electron.*, vol. 65, no. 12, pp. 9399–9409, 2018, doi: 10.1109/TIE.2018.2826480.

[164] J. S. R. Jang, "ANFIS: Adaptive-Network-Based Fuzzy Inference System," *IEEE Trans. Syst. Man Cybern.*, vol. 23, no. 3, pp. 665–685, 1993, doi: 10.1109/21.256541.

[165] A. G. Aissaoui, M. Abid, A. Tahour, and A. C. Megherbi, "Synchronous motor speed control based on ANFIS methodology and sliding mode observer," *Int. J. Artif. Intell. Soft Comput.*, vol. 5, no. 1, p. 3, 2015.

[166] G. Durgasukumar and M. K. Pathak, "Comparison of adaptive Neuro-Fuzzy-based space-vector modulation for two-level inverter," *Int. J. Electr. Power Energy Syst.*, vol.

38, no. 1, pp. 9–19, 2012, [Online]. Available: http://dx.doi.org/10.1016/j.ijepes.2011.10.017.

[167] N. V. Naik, J. Thankachan, and S. P. Singh, “A neuro-fuzzy direct torque control using bus-clamped space vector modulation,” *IETE Tech. Rev. (Institution Electron. Telecommun. Eng. India)*, vol. 33, no. 2, pp. 205–217, 2016.

[168] W. Srirattanawichaikul, “A generalized switching function-based discontinuous space vector modulation technique for unbalanced two-phase three-leg inverters,” *Turkish J. Electr. Eng. Comput. Sci.*, vol. 27, no. 2, pp. 1157–1171, 2019.

[169] M. M. Hasan, S. Mekhilef, T. Messikh, and M. Ahmed, “Three-phase multilevel inverter with high value of resolution per switch employing a space vector modulation control scheme,” *Turkish J. Electr. Eng. Comput. Sci.*, vol. 24, no. 4, pp. 1993–2009, 2016.

[170] M. Abassi, A. Khlaief, O. Saadaoui, A. Chaari, and M. Boussak, “Performance analysis of FOC and DTC for PMSM drives using SVPWM technique,” *16th Int. Conf. Sci. Tech. Autom. Control Comput. Eng. STA 2015*, pp. 228–233, 2016.

[171] S. Singh and A. N. Tiwari, “Analysis and simulation of vector controlled PMSM drive using SVPWM inverter,” *2017 2nd Int. Conf. Converg. Technol. I2CT 2017*, pp. 709–714, 2017.

[172] Suryakant, M. Sreejeth, and M. Singh, “Performance Analysis of PMSM Drive using Hysteresis Current Controller and PWM Current Controller,” *2018 IEEE Int. Students’ Conf. Electr. Electron. Comput. Sci. SCEECS 2018*, no. 1, pp. 1–5, 2018.

[173] D. Casadei, F. Profumo, G. Serra, and A. Tani, “FOC and DTC: Two viable schemes for induction motors torque control,” *IEEE Trans. Power Electron.*, vol. 17, no. 5, pp. 779–787, 2002.

[174] Z. Zhang, H. Xu, L. Xu, and L. E. Heilman, “Sensorless direct field-oriented control of three-phase induction motors based on ‘sliding mode’ for washing-machine drive applications,” *IEEE Trans. Ind. Appl.*, vol. 42, no. 3, pp. 694–701, 2006.

[175] J. Ye, P. Malysz, and A. Emadi, “A fixed-switching-frequency integral sliding mode current controller for switched reluctance motor drives,” *IEEE J. Emerg. Sel. Top. Power Electron.*, vol. 3, no. 2, pp. 381–394, 2015.

[176] O. Aydogmus, E. Deniz, and K. Kayisli, “PMSM Drive Fed by Sliding Mode Controlled PFC Boost Converter,” *Arab. J. Sci. Eng.*, vol. 39, no. 6, pp. 4765–4773, 2014.

[177] H. Ben Azza, N. Zaidi, M. Jemli, and M. Boussak, “Development and Experimental Evaluation of a Sensorless Speed Control of SPIM Using Adaptive Sliding Mode-MRAS Strategy,” *IEEE J. Emerg. Sel. Top. Power Electron.*, vol. 2, no. 2, pp. 319–328, 2014.

[178] L. Amezquita-Brooks, J. Liceaga-Castro, and E. Liceaga-Castro, “Speed and position controllers using indirect field-oriented control: A classical control approach,” *IEEE Trans. Ind. Electron.*, vol. 61, no. 4, pp. 1928–1943, 2014.

[179] G. K. Singh, D. K. P. Singh, K. Nam, and S. K. Lim, “A simple indirect field-oriented control scheme for multiconverter-fed induction motor,” *IEEE Trans. Ind. Electron.*, vol. 52, no. 6, pp. 1653–1659, 2005.

[180] M. Masiala, B. Vafakhah, J. Salmon, and A. Knight, “Fuzzy self-tuning speed control of an indirect field-oriented control induction motor drive,” *Conf. Rec. - IAS Annu. Meet. (IEEE Ind. Appl. Soc.*, pp. 1008–1014, 2007.

[181] Y. Wang *et al.*, “Deadbeat Model-Predictive Torque Control with Discrete Space-Vector Modulation for PMSM Drives,” *IEEE Trans. Ind. Electron.*, vol. 64, no. 5, pp.

3537–3547, 2017.

[182] M. Preindl, E. Schaltz, and P. Thøgersen, “Switching frequency reduction using model predictive direct current control for high-power voltage source inverters,” *IEEE Trans. Ind. Electron.*, vol. 58, no. 7, pp. 2826–2835, 2011.

[183] M. B. Shadmand, M. Mosa, R. S. Balog, and H. Abu-Rub, “Model predictive control of a capacitorless matrix converter-based STATCOM,” *IEEE J. Emerg. Sel. Top. Power Electron.*, vol. 5, no. 2, pp. 796–808, 2017.

[184] C. K. Lin, T. H. Liu, J. Te Yu, L. C. Fu, and C. F. Hsiao, “Model-free predictive current control for interior permanent-magnet synchronous motor drives based on current difference detection technique,” *IEEE Trans. Ind. Electron.*, vol. 61, no. 2, pp. 667–681, 2014.

[185] J. B. Rawlings and Mayne David Q, *Model Predictive Control: Theory and Design*. Nob Hill Pub, 2009.

[186] F. Morel, X. Lin-Shi, J. M. Rétif, B. Allard, and C. Buttay, “A comparative study of predictive current control schemes for a permanent-magnet synchronous machine drive,” *IEEE Trans. Ind. Electron.*, vol. 56, no. 7, pp. 2715–2728, 2009.

[187] Y. Zhang, S. Gao, and W. Xu, “An improved model predictive current control of permanent magnet synchronous motor drives,” *Conf. Proc. - IEEE Appl. Power Electron. Conf. Expo. - APEC*, pp. 2868–2874, 2016.

[188] P. Karamanakos, P. Stolze, R. M. Kennel, S. Manias, and H. Du Toit Mouton, “Variable Switching Point Predictive Torque Control of Induction Machines,” *IEEE J. Emerg. Sel. Top. Power Electron.*, vol. 2, no. 2, pp. 285–295, 2014.

[189] V. Yaramasu, M. Rivera, B. Wu, and J. Rodriguez, “Model predictive current control

of two-level four-leg inverters -Part i: Concept, algorithm, and simulation analysis," *IEEE Trans. Power Electron.*, vol. 28, no. 7, pp. 3459–3468, 2013.

[190] V. Yaramasu, W. Bin, M. Rivera, and J. Rodriguez, "A new power conversion system for megawatt pmsg wind turbines using four-level converters and a simple control scheme based on two-step model predictive strategy - Part i: Modeling and theoretical analysis," *IEEE J. Emerg. Sel. Top. Power Electron.*, vol. 2, no. 1, pp. 3–13, 2014.

[191] M. H. Vafaie, B. M. Dehkordi, P. Moallem, and A. Kiyoumarsi, "Improving the steady-state and transient-state performances of PMSM through an advanced deadbeat direct torque and flux control system," *IEEE Trans. Power Electron.*, vol. 32, no. 4, pp. 2964–2975, 2017.

[192] M. H. Vafaie, B. M. Dehkordi, P. Moallem, and A. Kiyoumarsi, "A New Predictive Direct Torque Control Method for Improving Both Steady-State and Transient-State Operations of the PMSM," *IEEE Trans. Power Electron.*, vol. 31, no. 5, pp. 3738–3753, 2016.

[193] X. Zhang, L. Zhang, and Y. Zhang, "Model predictive current control for PMSM drives with parameter robustness improvement," *IEEE Trans. Power Electron.*, vol. 34, no. 2, pp. 1645–1657, 2019.

[194] X. Sun *et al.*, "MPTC for PMSMs of EVs with Multi-Motor Driven System Considering Optimal Energy Allocation," *IEEE Trans. Magn.*, vol. 55, no. 7, pp. 1–6, 2019.

[195] Y. Zhang, J. Zhu, W. Xu, and Y. Guo, "A simple method to reduce torque ripple in direct torque-controlled permanent-magnet synchronous motor by using vectors with variable amplitude and angle," *IEEE Trans. Ind. Electron.*, vol. 58, no. 7, pp. 2848–2859, 2011, doi: 10.1109/TIE.2010.2076413.

[196] X. Zhang and B. Hou, “Double Vectors Model Predictive Torque Control Without Weighting Factor Based on Voltage Tracking Error,” *IEEE Trans. Power Electron.*, vol. 33, no. 3, pp. 2368–2380, 2018, doi: 10.1109/TPEL.2017.2691776.

[197] X. Sun, M. Wu, G. Lei, Y. Guo, and J. Zhu, “An Improved Model Predictive Current Control for PMSM Drives Based on Current Track Circle,” *IEEE Trans. Ind. Electron.*, vol. 68, no. 5, pp. 3782–3793, 2021, doi: 10.1109/TIE.2020.2984433.

[198] A. D. Alexandrou, N. K. Adamopoulos, and A. G. Kladas, “Development of a Constant Switching Frequency Deadbeat Predictive Control Technique for Field-Oriented Synchronous Permanent-Magnet Motor Drive,” *IEEE Trans. Ind. Electron.*, vol. 63, no. 8, pp. 5167–5175, 2016, doi: 10.1109/TIE.2016.2559419.

[199] Jose Rodriguez and P. Cortes, *Predictive Control of Power Converters and Electrical Drives*. Wiley-IEEE Press, 2012.

[200] L. Niu, M. Yang, and D. G. Xu, “Deadbeat predictive current control for pmsm,” *15th Int. Power Electron. Motion Control Conf. Expo. EPE-PEMC 2012 ECCE Eur.*, no. 1, pp. 1–6, 2012.

[201] K. K. Shyu, J. K. Lin, V. T. Pham, M. J. Yang, and T. W. Wang, “Global minimum torque ripple design for direct torque control of induction motor drives,” *IEEE Trans. Ind. Electron.*, vol. 57, no. 9, pp. 3148–3156, 2010.

[202] M. H. Vafaie, B. Mirzaeian Dehkordi, P. Moallem, and A. Kiyoumarsi, “Minimizing Torque and Flux Ripples and Improving Dynamic Response of PMSM Using a Voltage Vector with Optimal Parameters,” *IEEE Trans. Ind. Electron.*, vol. 63, no. 6, pp. 3876–3888, 2016.

[203] Y. Zhang, D. Xu, J. Liu, S. Gao, and W. Xu, “Performance Improvement of Model-

Predictive Current Control of Permanent Magnet Synchronous Motor Drives," *IEEE Trans. Ind. Appl.*, vol. 53, no. 4, pp. 3683–3695, 2017.

[204] K. H. Harib, E. A. Khousa, and A. Ismail, "Field oriented motion control of a 3-phase permanent magnet synchronous motor," *2011 2nd Int. Conf. Electr. Power Energy Convers. Syst. EPECS 2011*, pp. 1–7, 2011.

[205] M. N. Uddin, T. S. Radwan, G. H. George, and M. A. Rahman, "Performance of current controllers for VSI-fed IPMSM drive," *IEEE Trans. Ind. Appl.*, vol. 36, no. 6, pp. 1531–1538, 2000.

[206] R. Dhaouadi and N. Mohan, "Analysis of current-regulated voltage-source inverters fur permanenet magnet synchronous mutor drives in normal and extended speed ranges," *IEEE Trans. Energy Convers.*, vol. 5, no. 1, pp. 137–144, 1990.

[207] R. J. Wai, M. W. Chen, and Y. K. Liu, "Design of adaptive control and fuzzy neural network control for single-stage boost inverter," *IEEE Trans. Ind. Electron.*, vol. 62, no. 9, pp. 5434–5445, 2015.

[208] Z. Qiao, T. Shi, Y. Wang, Y. Yan, C. Xia, and X. He, "New sliding-mode observer for position sensorless control of permanent-magnet synchronous motor," *IEEE Trans. Ind. Electron.*, vol. 60, no. 2, pp. 710–719, 2013.

[209] P. Mani, R. Rajan, L. Shanmugam, and Y. H. Joo, "Adaptive fractional fuzzy integral sliding mode control for PMSM model," *IEEE Trans. Fuzzy Syst.*, vol. 27, no. 8, pp. 1674–1686, 2019.

[210] A. Abbaszadeh, D. Arab Khaburi, and J. Rodríguez, "Predictive control of permanent magnet synchronous motor with non-sinusoidal flux distribution for torque ripple minimisation using the recursive least square identification method," *IET Electr. Power*

Appl., vol. 11, no. 5, pp. 847–856, 2017.

[211] T. Turker, U. Buyukkeles, and A. F. Bakan, "A Robust Predictive Current Controller for PMSM Drives," *IEEE Trans. Ind. Electron.*, vol. 63, no. 6, pp. 3906–3914, 2016.

[212] M. S. Merzoug and F. Naceri, "Comparison of Field-Oriented Control and Direct Torque Control for Permanent Magnet Synchronous Motor (PMSM)," *Int. J. Electr. Comput. Eng.*, vol. 2, no. 9, pp. 1797–1802, 2008.

[213] H. Asgharpour-Alamdari, Y. Alinejad-Beromi, and H. Yaghobi, "A fuzzy-based speed controller for improvement of induction motor's drive performance," *Iran. J. Fuzzy Syst.*, vol. 13, no. 2, pp. 61–70, 2016, doi: 10.22111/ijfs.2016.2359.

[214] M. N. Uddin and M. A. Rahman, "Fuzzy logic based speed control of an IPM synchronous motor drive," *Can. Conf. Electr. Comput. Eng.*, vol. 3, pp. 1259–1264, 1999, doi: 10.20965/jaciii.2000.p0212.

[215] M. N. Uddin and M. M. I. Chy, "A novel fuzzy-logic-controller-based torque and flux controls of IPM synchronous motor," *IEEE Trans. Ind. Appl.*, vol. 46, no. 3, pp. 1220–1229, 2010, doi: 10.1109/TIA.2010.2045334.

[216] A. V. Sant, "PM synchronous motor speed control using hybrid fuzzy-PI with novel switching functions," *IEEE Trans. Magn.*, vol. 45, no. 10, pp. 4672–4675, 2009, doi: 10.1109/TMAG.2009.2022191.

[217] A. V. Sant, K. R. Rajagopal, and N. K. Sheth, "Permanent magnet synchronous motor drive using hybrid PI speed controller with inherent and noninherent switching functions," *IEEE Trans. Magn.*, vol. 47, no. 10, pp. 4088–4091, 2011.

[218] M. Zerikat and S. Chekroun, "Design and Implementation of a Hybrid Fuzzy Controller for a High-Performance Induction Motor," *World Acad. Sci. Eng. Technol.*, vol. 26, no.

2, pp. 263–269, 2007.

[219] A. Rubaai, D. Ricketts, and M. D. Kankam, “Experimental verification of a hybrid fuzzy control strategy for a high-performance brushless dc drive system,” *IEEE Trans. Ind. Appl.*, vol. 37, no. 2, pp. 503–512, 2001, doi: 10.1109/28.913715.

[220] B. Singh, B. P. Singh, and S. Dwivedi, “DSP based implementation of hybrid fuzzy PI speed controller for direct torque controlled permanent magnet synchronous motor drive,” *Int. J. Emerg. Electr. Power Syst.*, vol. 8, no. 2, 2007, doi: 10.2202/1553-779X.1246.

[221] N. Nakao and K. Akatsu, “Suppressing pulsating torques: Torque ripple control for synchronous motors,” *IEEE Ind. Appl. Mag.*, vol. 20, no. 6, pp. 33–44, 2014, doi: 10.1109/MIAS.2013.2288383.

[222] P. H. Truong, D. Flieller, N. K. Nguyen, J. Mercklé, and G. Sturtzer, “Torque ripple minimization in non-sinusoidal synchronous reluctance motors based on artificial neural networks,” *Electr. Power Syst. Res.*, vol. 140, pp. 37–45, 2016, [Online]. Available: http://dx.doi.org/10.1016/j.epsr.2016.06.045.

[223] D. Flieller, N. K. Nguyen, P. Wira, G. Sturtzer, D. O. Abdeslam, and J. Mercklé, “A self-learning solution for torque ripple reduction for nonsinusoidal permanent-magnet motor drives based on artificial neural networks,” *IEEE Trans. Ind. Electron.*, vol. 61, no. 2, pp. 655–666, 2014, doi: 10.1109/TIE.2013.2257136.

[224] H. Chaoui and P. Sicard, “Adaptive fuzzy logic control of permanent magnet synchronous machines with nonlinear friction,” *IEEE Trans. Ind. Electron.*, vol. 59, no. 2, pp. 1123–1133, 2012, doi: 10.1109/TIE.2011.2148678.

[225] J. S. Yu, S. H. Kim, B. K. Lee, C. Y. Won, and J. Hur, “Fuzzy-logic-based vector control

scheme for permanent-magnet synchronous motors in elevator drive applications," *IEEE Trans. Ind. Electron.*, vol. 54, no. 4, pp. 2190–2200, 2007, doi: 10.1109/TIE.2007.894692.

[226] M. Lajoie-Mazenc, C. Villanueva, and J. Hector, "Study and Implementation of Hysteresis Controlled Inverter on a Permanent Magnet Synchronous Machine.," *IEEE Trans. Ind. Appl.*, vol. IA-21, no. 2, pp. 408–413, 1985, doi: 10.1109/TIA.1985.349662.

[227] M. Aner, N. Benaifa, and E. Nowicki, "A PMSM drive design with inverter-stage soft-switching hysteresis current control and space vector modulation for two-level operation of a very sparse matrix converter," *2009 IEEE Electr. Power Energy Conf. EPEC 2009*, 2009, doi: 10.1109/EPEC.2009.5420980.

[228] H. Rayd and N. Zahid, "Robust emerged artificial intelligence speed controller for PMSM drive," in *2014 Second World Conference on Complex Systems (WCCS)*, 2014, pp. 1–8.

[229] G. Heins, M. Thiele, and T. Brown, "Accurate torque ripple measurement for PMSM," *IEEE Trans. Instrum. Meas.*, vol. 60, no. 12, pp. 3868–3874, 2011.

[230] C. Jedryczka, D. Danielczyk, and W. Szelag, "Torque Ripple Minimization of the Permanent Magnet Synchronous Machine by Modulation of the Phase Currents," *Sensors*, vol. 20, no. 2406, pp. 1–11, 2020.

[231] K. W. Lee and S. Il Kim, "Dynamic Performance Improvement of a Current Offset Error Compensator in Current Vector-Controlled SPMSM Drives," *IEEE Trans. Ind. Electron.*, vol. 66, no. 9, pp. 6727–6736, 2019.

[232] G. P. Myers and M. W. Degner, "Compensation method for current-sensor gain errors," US6998811[P]., 2006.

[233] K. Zhou, Y. Yang, F. Blaabjerg, and D. Wang, "Optimal selective harmonic control for power harmonics mitigation," *IEEE Trans. Ind. Electron.*, vol. 62, no. 2, pp. 1220–1230, 2015, doi: 10.1109/TIE.2014.2336629.

[234] P. Cui, Q. Wang, G. Zhang, and Q. Gao, "Hybrid Fractional Repetitive Control for Magnetically Suspended Rotor Systems," *IEEE Trans. Ind. Electron.*, vol. 65, no. 4, pp. 3491–3498, 2018, doi: 10.1109/TIE.2017.2752119.

[235] Z. Zhou, C. Xia, Y. Yan, Zhiqiang Wang, and Tingna Shi, "Disturbances Attenuation of Permanent Magnet Synchronous Motor Drives Using Cascaded Predictive-Integral-Resonant Controllers," *IEEE Trans. Power Electron.*, vol. 33, no. 2, pp. 1514–1527, 2018.

[236] Q. Zhang *et al.*, "An adaptive proportional-integral-resonant controller for speed ripple suppression of PMSM drive due to current measurement error," *International Journal of Electrical Power and Energy Systems*, vol. 129. 2021, doi: 10.1016/j.ijepes.2021.106866.

[237] Y. Zhang and S. Gao, "Simultaneous optimization of voltage vector and duty cycle in model predictive torque control of PMSM drives," *2014 17th Int. Conf. Electr. Mach. Syst. ICEMS 2014*, pp. 3338–3344, 2014.

[238] S. Chai, L. Wang, and E. Rogers, "Model predictive control of a permanent magnet synchronous motor with experimental validation," *Control Eng. Pract.*, vol. 21, no. 11, pp. 1584–1593,2013, [Online]. Available: http://dx.doi.org/10.1016/j.conengprac.2013.07.008.

[239] S. Kamat and R. K. Junnuri, "Model Predictive Control Approaches for Permanent Magnet Synchronous Motor in Virtual Environment," in *1st IEEE International*

Conference on Power Electronics. Intelligent Control and Energy Systems (ICPEICES-2016), 2016, pp. 1–6.

[240] C. Xia, B. Ji, and Y. Yan, "Smooth Speed Control for Low-Speed High-Torque Permanent-Magnet Synchronous Motor Using Proportional-Integral-Resonant Controller," *IEEE Trans. Ind. Electron.*, vol. 62, no. 4, pp. 2123–2134, 2015, doi: 10.1109/TIE.2014.2354593.

[241] A. G. Yepes, F. D. Freijedo, Ó. López, and J. Doval-Gandoy, "High-performance digital resonant controllers implemented with two integrators," *IEEE Trans. Power Electron.*, vol. 26, no. 2, pp. 563–576, 2011, doi: 10.1109/TPEL.2010.2066290.

[242] R. Krishnan and A. J. Beutler, "Performance and design of an axial field permanent magnet synchronous motor servo drive," in *In Proc. IEEE IAS Annu. Meeting*, 1985, pp. 634–640.

LIST OF PUBLICTIONS

Journals(SCI/SCIE)

- Suryakant Shukla, Mini Sreejeth, Madhusudan Singh, “Minimization of Ripples in Stator Current and Torque of PMSM Drive using Advanced Predictive Current Controller based on Deadbeat Control Theory”, Journal of Power Electronics, Springer, Vol.21, Issue. 1, 2021, pp. 142-152, (SCIE- IF: 1.114).
- Suryakant, Mini Sreejeth, Madhusudan Singh, “Improved ANFIS based MRAC observer for Sensorless control of PMSM”, Journal of Intelligent & Fuzzy Systems, IOS press, vol. Pre-press, no. Pre-press, pp. 1-13, 2021, (SCIE- IF: 1.8).
- Suryakant, Mini Sreejeth, Madhusudan Singh, “Minimization of Torque ripples in PMSM using Intelligent Hybrid Controller”, Arabian Journal of Science & Engineering, Springer (Communicated).
- Suryakant, Mini Sreejeth, Madhusudan Singh, “Minimization of Torque Ripples in PMSM Drive using PI Resonant Controller based Model Predictive Control", Electrical Engineering (Communicated).

International Conferences:

- Suryakant, Mini Sreejeth, Madhusudan Singh, “Performance Analysis of PMSM Drive using Hysteresis Current Controller and PWM Current Controller”, 2018 IEEE International Students' Conference on Electrical, Electronics and Computer Science (SCEECS), MANIT, Bhopal, 24^{th} – 25^{th} Feb, 2018, pp. 1-5.
- Suryakant, M. Sreejeth and M. Singh, "Sensorless control of PMSM Drive with BEMF based MRAC Algorithm," International Symposium on Advanced Electrical and

APPENDIX-I

Rated Parameters of PMSM

Rated Parameters of PMSM used in this research work are tabulated as

Parameter	**Value**	**Parameter**	**Value**
Voltage, V	380V	Current, I	6.9 A
Rated output power	3.4kW	Maximum current	13.8A
Rated Speed, N	3000 rpm	No. of poles, P	8
Stator Resistance, $\boldsymbol{R_s}$	1.93 Ω	Torque, T	11 Nm
Q-axis inductance, $\boldsymbol{L_q}$	0.0114 H	D-axis inductance, L_d	0.0114 H
PM Flux linkage, $\boldsymbol{\phi_m}$	0.265 Wb	Motor Inertia, J	0.11kgm^2
Torque constant, K_t	1.6 Nm/A	Voltage constant, K_e	193.07 volt-sec/rad
DC link voltage, V_{dc}	600V	Fundamental Frequency, f	200Hz
Maximum Torque	33 Nm		

AUTHOR'S BIOGRAPHY

Suryakant was born in Uttar Pradesh, India, in 1989. He received the B.Tech. degree in Electrical and Electronics Engineering from Uttar Pradesh Technical University, Lucknow, India in 2010. He received M. Tech. degree in Condition Monitoring (Electrical Engineering) from National Institute of Technology, Himachal Pradesh, India in 2012. From August 2012 to July 2016, he worked as Assistant Professor in HMR Institute of Technology & Management, Delhi, India. He completed his PhD from Electrical Engineering Department, Delhi Technological University (DTU), New Delhi, India in 2021. His research interests are control system, electric machine drives and power electronics.